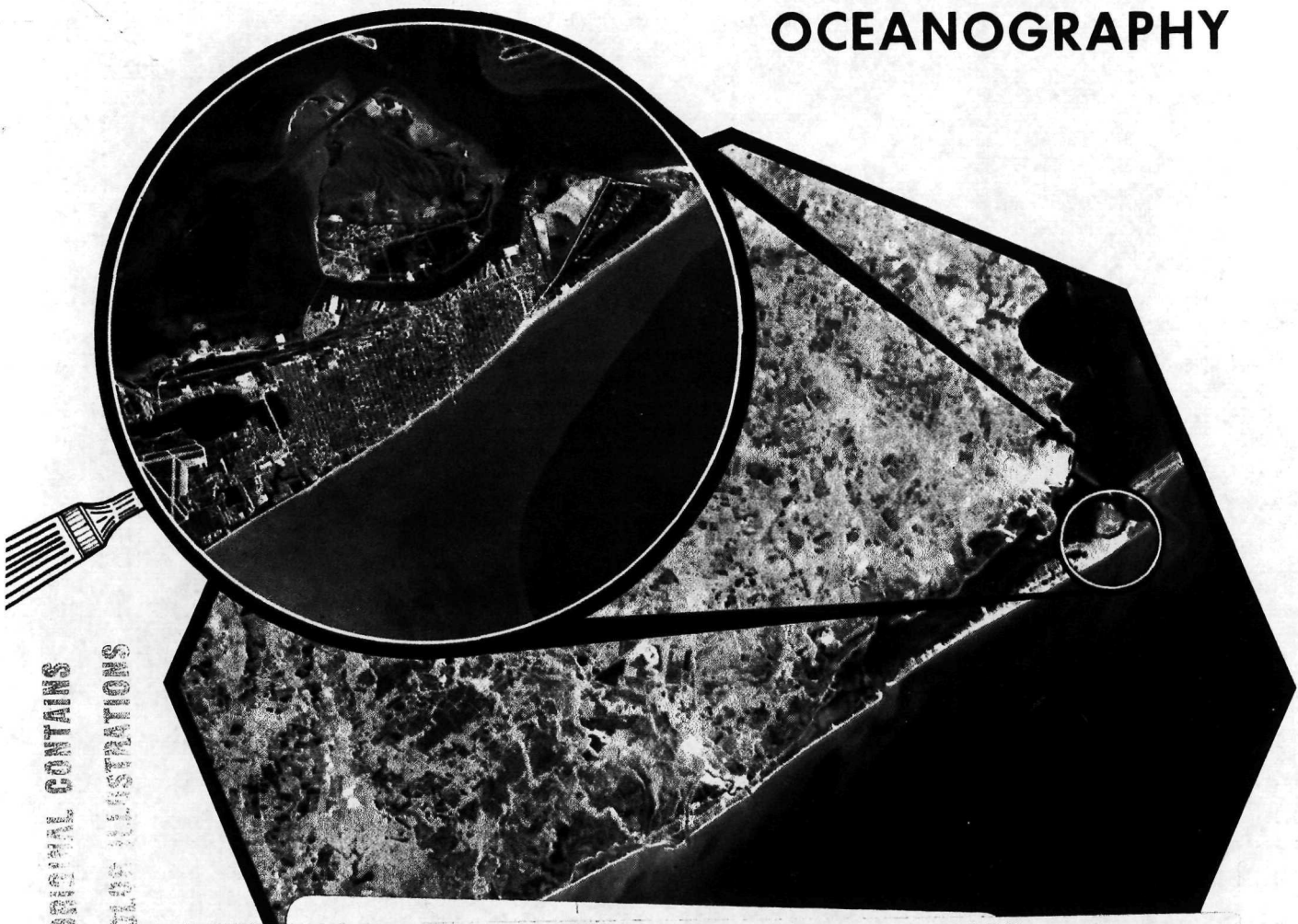


THIRD ANNUAL EARTH RESOURCES PROGRAM REVIEW

VOLUME III HYDROLOGY AND OCEANOGRAPHY



CONTAINS
CONTAINS

N72-12295 (NASA-TM-X-67405) THIRD ANNUAL EARTH
 thru RESOURCES PROGRAM REVIEW. VOLUME 3:
 N72-12319 HYDROLOGY AND OCEANOGRAPHY (NASA) 1970
 Unclas 351 p CSCL 08C
 09159

G3/13

(CATEGORY)

Presented at the
NASA Manned Spacecraft Center
Houston, Texas



Reproduced by
**NATIONAL TECHNICAL
 INFORMATION SERVICE**
 Springfield, Va. 22151

December 1 to 3, 1970

i

N O T I C E

THIS DOCUMENT HAS BEEN REPRODUCED FROM THE BEST COPY FURNISHED US BY THE SPONSORING AGENCY. ALTHOUGH IT IS RECOGNIZED THAT CERTAIN PORTIONS ARE ILLEGIBLE, IT IS BEING RELEASED IN THE INTEREST OF MAKING AVAILABLE AS MUCH INFORMATION AS POSSIBLE.

FOREWORD

A review of various aspects of the Earth Resources Program was held at the Manned Spacecraft Center, Houston, Texas, December 1, 2, and 3, 1970. Particular emphasis was placed on the results of analysis of data obtained with the Manned Spacecraft Center and other aircraft which have contributed data to the program.

The review was divided into the disciplinary areas of Geology, Geography, Hydrology, Agriculture, Forestry, and Oceanography. Program investigators presented the results of their work in each of these areas. The material presented is published in three volumes:

VOLUME I -- GEOLOGY AND GEOGRAPHY

VOLUME II -- AGRICULTURE, FORESTRY, AND SENSOR
STUDIES

VOLUME III -- HYDROLOGY AND OCEANOGRAPHY

The review provided a current assessment of the program for both management and technical personnel. Note that the material presented represented the current status of ongoing programs and complete technical analyses will be available at a later date.

Where papers were not submitted for publication or were not received in time for printing, abstracts are used.

PRECEDING PAGE BLANK NOT FILMED

CONTENTS OF VOLUME I

Section		Page
	FOREWORD	iii
1	INTRODUCTORY COMMENTS ON THE USGS GEOGRAPHIC APPLICATIONS PROGRAM	1-1
	By Arch C. Gerlach	
2	CENSUS CITIES PROJECT AND ATLAS OF URBAN AND REGIONAL CHANGE	2-1
	By James R. Wray	
3	THE APPLICATION OF REMOTE SENSING TECHNIQUES TO SELECTED INTER AND INTRA URBAN DATA ACQUISITION PROBLEMS	3-1
	By Frank E. Horton	
4	CLIMATOLOGY OF URBAN-REGIONAL SYSTEMS	4-1
	By Robert W. Pease	
5	REGIONAL LAND USE STUDIES	5-1
	By John L. Place	
6	ENVIRONMENTAL APPLICATION OF REMOTE SENSING METHODS TO COASTAL ZONE LAND USE AND MARINE RESOURCES MANAGEMENT	6-1
	By H. G. Goodell	
7	EXPERIMENTAL APPLICATIONS OF MULTISPECTRAL DATA TO NATURAL RESOURCE INVENTORY AND SURVEY	7-1
	By Harry J. Mallon	
8	SPECIAL PROJECTS OF THE GEOGRAPHIC APPLICATIONS PROGRAM	8-1
	By Gary W. North	
9	GEOGRAPHY PROGRAM, DESIGN, STRUCTURE, AND OPERATIONAL STRATEGY	9-1
	By Robert H. Alexander	

Section		Page
10	PROCESSING OF MULTISPECTRAL DATA AND SIMULATION OF ERTS DATA CHANNELS TO MAKE COMPUTER TERRAIN MAPS OF A YELLOWSTONE NATIONAL PARK TEST SITE	10-1
	By Harry W. Smedes, Margaret M. Spencer, and Frederick J. Thomson	
11	LINEAR GEOLOGIC STRUCTURE AND MAFIC ROCK DISCRIMINATION AS DETERMINED FROM INFRARED DATA	11-1
	By T. W. Offield, L. C. Rowan, and R. D. Watson	
12	MULTISPECTRAL ANALYSIS OF LIMESTONE, DOLOMITE, AND GRANITE, MILL CREEK, OKLAHOMA	12-1
	By L. C. Rowan and Kenneth Watson	
13	A THERMAL MODEL FOR ANALYSIS OF INFRARED IMAGES	13-1
	By Kenneth Watson	
14	A STUDY OF PASSIVE MICROWAVE TECHNIQUES APPLIED TO GEOLOGIC PROBLEMS	14-1
	By A. T. Edgerton	
15	GEOLOGIC INTERPRETATION OF APOLLO 6 STEREOPHO- TOGRAPHY FROM BAJA CALIFORNIA TO WEST TEXAS	15-1
	By Stephen J. Gawarecki	
16	GEOLOGIC TERRAIN MAPPING FROM EARTH-SATELLITE AND ULTRA-HIGH AERIAL PHOTOGRAPHS	16-1
	By R. B. Morrison	
17	REMOTE SENSING IN MARINE GEOLOGY: ARTIC TO CARIBBEAN	17-1
	By Paul R. Carlson	
18	RELATIONSHIP BETWEEN VEGETATION REFLECTANCE SPECTRA AND SOIL GEOCHEMISTRY: NEW DATA FROM CATHEART MOUNTAIN, MAINE	18-1
	By F. C. Canney, Sondra Wenderoth, and Edward Yost	

Section		Page
19	GROUND TRUTH VERSUS NO GROUND TRUTH	19-1
	By Grover B. Torbert	
20	A REVIEW OF APPLICATION STUDIES ON INDIAN LANDS USING NASA AEROSPACE IMAGERY	20-1
	By Arthur M. Woll	

CONTENTS OF VOLUME II

Section		Page
21	CARTOGRAPHY By Alden P. Colvocoresses	21-1
22	AUTOMATIC CARTOGRAPHY TECHNIQUES FOR EARTH RESOURCES RESEARCH By Dean T. Edson	22-1
23	SPECTRAL REFLECTANCE FROM PLANT CANOPIES AND OPTIMUM SPECTRAL CHANNELS IN THE NEAR INFRARED By William A. Allen, Harold W. Gausman, and Craig L. Wiegand	23-1
24	AERIAL PHOTOGRAPHY FOR SENSING PLANT ANOMALIES By H. W. Gausman, R. Cardenas, and W. G. Hart	24-1
25	REMOTE SENSING FOR DETECTION OF SOIL LIMITATIONS IN AGRICULTURAL AREAS By C. J. Frazee, R. D. Heil, and F. C. Westin	25-1
26	RECOGNITION OF CROPS AND SOILS BY SPOT DENSITY MEASUREMENTS OF IMAGERY By Gerald D. Nelson	26-1
27	THERMAL SCANNER DATA FOR STUDYING FREEZE CONDITIONS AND FOR AIDING IRRIGATION SCHEDULING By Jon F. Bartholic, Craig L. Wiegand, Ross W. Leamer, and Leo N. Namken	27-1

Section		Page
28	COMPUTER DISCRIMINATION PROCEDURES APPLICABLE TO AERIAL AND ERTS MULTISPECTRAL DATA	28-1
	By Arthur J. Richardson, Robert J. Torline, and William A. Allen	
29	THE APPLICATIONS OF REMOTE SENSING TO CORN BLIGHT DETECTION AND CROP YIELD FORECASTING	29-1
	By R. B. MacDonald	
30	A SEMI-OPERATIONAL AGRICULTURAL INVENTORY USING SMALL-SCALE AERIAL PHOTOGRAPHY	30-1
	By William C. Draeger and Lawrence R. Pettinger	
31	IMAGE RESOLUTION: ITS SIGNIFICANCE IN A WILDLAND AREA	31-1
	By Donald T. Lauer and Randolph R. Thaman	
32	IDENTIFICATION AND MEASUREMENT OF SHRUB-TYPE VEGETATION ON LARGE-SCALE AERIAL PHOTOGRAPHS	32-1
	By Richard S. Driscoll	
33	A VEGETATIONAL INVENTORY AND ECOLOGICAL RESOURCE ANALYSIS FROM SPACE AND HIGH-FLIGHT PHOTOGRAPHY	33-1
	By Charles E. Poulton, David P. Faulkner, and Barry J. Schrupf	
34	REMOTE DETECTION OF INSECT EPIDEMICS IN CONIFERS	34-1
	By Robert C. Heller	
35	MULTISPECTRAL SENSING OF MOISTURE STRESS	35-1
	By Charles E. Olson Jr. and Wayne G. Rohde	

Section		Page
36	CLASSIFYING FOREST AND NONFOREST LAND ON SPACE PHOTOGRAPHS	36-1
	By Robert C. Aldrich	
37	SUMMARY OF MICHIGAN MULTISPECTRAL INVESTIGATIONS PROGRAM	37-1
	By Richard R. Legault	
38	USER ORIENTED DATA PROCESSING AT THE UNIVERSITY OF MICHIGAN	38-1
	By Frederick J. Thomson	
39	THE APPLICATION OF AUTOMATIC RECOGNITION TECHNIQUES IN THE APOLLO IX SO-65 EXPERIMENT	39-1
	By R. B. MacDonald	
40	THE DEVELOPMENT OF MACHINE TECHNOLOGY PROCESSING FOR EARTH RESOURCE SURVEY	40-1
	By D. A. Landgrebe	
41	REMOTE SENSING AT THE UNIVERSITY OF KANSAS IN RADAR SYSTEMS	41-1
	By Richard K. Moore	
42	DATA PROCESSING AT THE UNIVERSITY OF KANSAS	42-1
	By G. L. Kelly	
43	RECENT ADVANCES IN RADAR APPLICATIONS TO AGRICULTURE	43-1
	By Stanley A. Morain	
44	INTERACTIVE DISPLAY/GRAPHICS SYSTEMS FOR REMOTE SENSOR DATA ANALYSIS	44-1
	By W. G. Eppler, D. L. Loe, E. L. Wilson, S. L. Whitley, and R. J. Sachen	

Section		Page
45	RESULTS OF SCATTEROMETER SYSTEMS ANALYSIS FOR NASA/MSC EARTH OBSERVATION SENSOR EVALUATION PROGRAM	45-1
	By K. Krishen, N. Vlahos, O. Brandt, and G. Graybeal	
46	PHENOMENOLOGICAL APPROACH TO SCATTER- OMETER DATA INTERPRETATION	46-1
	By F. E. Alzofon	

CONTENTS OF VOLUME III

Section		Page	
47	DETECTION AND IDENTIFICATION OF BENTHIC COMMUNITIES AND SHORELINE FEATURES IN BISCAYNE BAY USING MULTIBAND IMAGERY	47-1	✓
	By Milton C. Kolipinski and Aaron L. Higer		
48	REMOTE SENSING FOR DEFINING AQUIFERS IN GLACIAL DRIFT	48-1	✓
	By Victor I. Myers		
49	SUMMARY -- REMOTE SENSING SOIL MOISTURE RESEARCH	49-1	✓
	By Fred A. Schmer, Hal D. Werner, and Fred A. Waltz		
50	MEASUREMENT OF PLANT COMMUNITY COVER FROM AERIAL PHOTOGRAPHS USING EKTACHROME INFRARED AERO FILM	50-1	✓
	By Raymond M. Turner		
51	EMMISSION CHARACTERISTICS OF SNOW AND ICE IN THE MICROWAVE RANGE	51-1	✓
	By Mark F. Meier and A. T. Edgerton		
52	MANAGEMENT APPLICATIONS FOR THERMAL IR IMAGERY OF LAKE PROCESSES	52-1	✓
	By J. M. Whipple and R. B. Haynes		
53	SPECTRAL REFLECTANCE CHARACTERISTICS AND AUTOMATED DATA REDUCTION TECHNIQUES WHICH IDENTIFY WETLAND AND WATER QUALITY CONDITIONS IN THE CHESAPEAKE BAY	53-1	✓
	By Dr. Richard R. Anderson		

Section		Page
54	DATA RELAY SYSTEM SPECIFICATIONS FOR ERTS IMAGE INTERPRETATION	54-1 ✓
	By James F. Daniel	
55	THE ROLE OF REMOTELY SENSED AND RELAYED DATA IN THE DELAWARE RIVER BASIN	55-1 ✓
	By Richard W. Paulson	
56	NOAA's OCEANOGRAPHY STUDIES UNDER THE EARTH RESOURCES SURVEY PROGRAM	56-1 ✓
	By E. Paul McClain	
57	NOAA's HYDROLOGY STUDIES UNDER THE EARTH RESOURCES SURVEY PROGRAM	57-1 ✓
	By E. Paul McClain	
58	REMOTE SENSING AND THE PELAGIC FISHERIES ENVIRONMENT OFF OREGON	58-1 ✓
	By William G. Percy	
59	REMOTE SENSING OF OCEAN COLOR FROM AIRCRAFT	59-1 ✓
	By G. L. Clarke and G. C. Ewing	
60	THE REMOTE SENSING NEEDS OF ARTIC GEOPHYSICS	60-1 ✓
	By William J. Campbell	
61	MEASUREMENT OF WATER DEPTH BY MULTISPECTRAL RATIO TECHNIQUES	61-1 ✓
	By F. C. Polcyn	
62	RADAR MONITORING OF OIL POLLUTION	62-1 ✓
	By N. W. Guinard	
63	VISIBLE REGION REMOTE SPECTROSCOPY OF POLLUTED WATER	63-1 ✓
	By Peter G. White	

Section		Page	
64	LASER OBSERVATIONS OF WAVE GROWTH AND FOAM DENSITY FOR FETCH-LIMITED 25M/SEC WINDS	64-1	✓
	By Duncan B. Ross and Vincent Cardone		
65	WHITECAP COVERAGE FROM AERIAL PHOTOGRAPHY	65-1	✓
	By Roswell W. Austin		
66	ON THE USE OF A SINGLE BLUE BAND IN OCEANOGRAPHY	66-1	✓
	By John W. Sherman III		
67	THE VARIATION OF RADAR CROSS SECTION WITH WIND	67-1	✓
	By N. W. Guinard		
68	NANOSECOND RADAR OBSERVATIONS OF THE OCEAN SURFACE FROM A STABLE PLATFORM	68-1	✓
	By B. S. Yaplee, A. Shapiro, D. L. Hammond, and E. A. Uliana		
69	PASSIVE MICROWAVE STUDIES	69-1	✓
	By James P. Hollinger		
70	THE INTEGRATION OF REMOTE SENSING DATA INTO GLOBAL WEATHER PREDICTION, WAVE FORECASTING, AND OCEAN CIRCULATION COMPUTER BASED SYSTEMS	70-1	✓
	By Willard J. Pierson, Jr.		

TABLES

Table		Page
48-1	SIMPLE CORRELATION COEFFICIENTS USED TO RELATE VARIABLES TO OPTICAL DENSITY OF NEGATIVE THERMAL FILM	48-16
53-1	TYPES AND QUALITY OF DATA RECEIVED FROM MISSIONS 103 AND 104, CHESAPEAKE BAY TEST SITE, SEPTEMBER 1969	53-16
53-2	RELATIONSHIP BETWEEN SPECTRAL REFLECTANCE AND TONAL SIGNATURE ON COLOR IR FILM OF SELECTED MARSH PLANT SPECIES	53-17
54-1	EROS DCS NETWORKS FOR ERTS EXPERIMENTATION	54-8
56-1	COMPOSITE MINIMUM BRIGHTNESS (CMB) VALUES FOR VARIOUS ICE CONCENTRATIONS AND CONDITIONS	56-8
64-1	A COMPARISON OF WINDS OBTAINED FROM THE NASA CV990 OVER THE NORTH SEA AND 20-METER LEVEL WINDS REDUCED FROM GEOSTROPHIC WINDS BASED UPON THE ANALYSIS SHOWN IN FIGURE 64-3	64-13

FIGURES

Figure		Page
47-1	Location map of areas covered by optical-mechanical scanner from an overflight on March 10, 1970	47-7
47-2	Location map of the 19 sea and ground truth sites in South Biscayne Bay	47-8
47-3	The Florida Regional Ecological Test Site is a multidisciplinary experiment established to test and evaluate remote sensor applications to resource problems from space, aircraft, and ground platforms	47-9
47-4	Location map of Biscayne National Monument in South Biscayne Bay	47-10
47-5	Schematic of multispectral scanner operation over study area in South Biscayne Bay	47-11
47-6	Block diagram of multispectral scanner imagery processing operations for benthic communities	47-12
47-7	Comparison of spectral ranges of various film-filter combinations with ERTS-A imagery bands and an optical-mechanical scanner system	47-13
47-8	Color composite recognition map of benthic communities in South Biscayne Bay	47-14
47-9	Generalized cross section through South Biscayne Bay showing biogeologic features	47-15
47-10	Color composite recognition map of surface water temperatures in South Biscayne Bay on March 10, 1970	47-16

Figure		Page
48-1	Portion of Beadle County, South Dakota showing thickness of water-saturated material in surficial deposits and location of predawn flight lines on August 5, 1970	48-17
48-2	Thermograms of sections of flight lines shown in figure 48-1	48-18
48-3	Enlarged thermogram of area shown in figure 48-2	48-19
48-4	Color encoded map of figure 48-3	48-20
49-1	Experimental ground setup for remote sensing soil moisture research under cultivated cropping conditions	49-7
49-2	South Dakota State University Cottonwood Range Field Station, Cottonwood, South Dakota	49-8
49-3	Six summer pastures on South Dakota State University Cottonwood Range Field Station	49-9
50-1	Seasonal variation of adjusted red transmittances obtained from Ektachrome IR images of a saltcedar forest, Gila River, Arizona	50-6
50-2	Comparison of adjusted red transmittances and foliar cover in four plant communities	50-7
50-3	Comparison of evapotranspiration and adjusted red transmittance in three plant communities on three dates in 1969	50-8
51-1	Microwave measurements of snow	
	a. Microwave measurements of soil before constructing a snowpack	51-6
	b. Microwave measurements of artificial snowpack constructed layer by layer over bare soil	51-7

Figure		Page
51-2	Measured brightness temperature as a function of snow mass per unit area (water equivalent), for cold, dry snow	51-8
51-3	Numerical simulation of brightness temperature at 0.811-cm wavelength as a function of snow depth	51-9
51-4	Numerical simulation of brightness temperature at 0.319-cm wavelength as a function of snow density	51-10
51-5	Brightness temperature as a function of viewing angle, wavelength 1.55-cm, dry snow, Mount Rainier	51-11
51-6	Brightness temperature and surface free water changes during the warming of a cold snow-pack	51-12
51-7	Numerical simulation of brightness temperature as a function of free water contact in snow	51-13
51-8	Measured brightness temperature as a function of snow mass per unit area (water equivalent) for wet snow	51-14
52-1	Study area, Lake Ontario Basin	52-7
52-2	Overview of Onondaga Lake, IR imagery	52-8
52-3	Northern end of Onondaga Lake, IR imagery	52-9
52-4	Southern end of Onondaga Lake, IR imagery	52-10
52-5	Oswego Harbor, March, IR imagery	52-11
52-6	Oswego Harbor, summer, IR imagery	52-12
52-7	Nuclear power plant, Lake Ontario, IR imagery	52-13
53-1	Map of the Chesapeake Bay showing extent of study area and status of thermal electric power plant development	53-18

Figure		Page
53-2	Low altitude photograph of Baltimore Harbor showing one of several industrial effluents	53-19
53-3	High altitude photograph of the Potomac River near Washington, D.C., showing severe algae blooms in the water	53-20
53-4	Low and high altitude photographs illustrating only slight loss of information in wetland going from low to high altitude analysis	53-21
53-5	Compares spectral reflectance characteristics in the 0.4 to 1.3 micrometer range of <u>Zizania aquatica</u> (wild rice), <u>Nuphar advenum</u> (water lily), and <u>Juncus</u> sp. (block rush)	53-22
53-6	Color IR photograph showing tonal quality of important wetland species	53-23
53-7	Spectral reflectance curves for <u>Phragmites communis</u> between 0.4 and 1.35 microns	53-24
53-8	Spring and fall photographs of a wetland area showing seasonal change in reflectance of plant species	53-25
53-9	Datacolor image showing possible analysis of sediment discharge with this system	53-26
53-10	Datacolor image and black and white photograph from which image was generated	53-27
53-11	High altitude photograph of a wetland showing distinctive features of high and low marshes	53-28
53-12	Datacolor image of wetland showing high and low marshes and shallow water	53-29
55-1	Map showing location of U.S. Geological Survey water quality monitors in the Delaware River Basin	55-11

Figure		Page
55-2	A computer listing of hourly value data for 1 month	55-12
55-3	A computer listing of daily statistics data and deviations from Delaware River Basin Commission stream quality objectives for 1 month	55-13
55-4	A daily teletype release of Delaware River estuary water quality data	55-14
55-5	A graph of estimated periods of mutual visibility of a Delaware River Basin hydrologic station and the National Aeronautics and Space Administration's Goddard Space Flight Center from a typical orbital pattern of the Earth Resources Technology Satellite	55-15
55-6	A computer summary of dissolved oxygen concentration data	55-16
55-7	A computer summary of temperature data	55-17
55-8	Computer summaries	
	a. Specific conductance data	55-18
	b. Specific conductance data	55-19
56-1	Three-day composite chart of a sea surface temperature derived statistically from all satellite infrared measurements falling within 280-km grid areas	56-9
56-2	Image derived from satellite infrared measurements (10.5 to 12.5-m wavelength) on October 19, 1970, at 09:00 G.m.t.	56-10
56-3	Sea-surface isotherms analyzed from scan-spot listings of satellite infrared measurements for the same time and for a portion of the same area as in figure 56-2	56-11
56-4	Seasonal variation of composite minimum bright- ness (CMB) values for several sea-ice areas in the North American Arctic	56-12

Figure		Page
57-1	Results of field measurements of microwave brightness temperature at three levels of soil moisture	57-6
57-2	Comparison of satellite and aerial survey measurements of spring decrease in snow extent (percent of basin covered)	57-7
57-3	Seasonal variation of composite minimum brightness (CMB) values for snowy areas in northern Canada having different vegetative cover or topography	57-8
57-4	Comparison of aircraft and satellite surveys of surface water temperature	57-9
58-1	Sea surface temperature from airborne PRT-5 radiometer survey, August 12, 1969	58-8
58-2	Sea surface temperature from airborne PRT-5 radiometer survey, July 13, 1969	58-9
58-3	Catches of albacore tuna by Loran blocks and sea surface temperature	58-10
58-4	Sea surface temperature from airborne PRT-5 radiometer survey, July 29, 1970	58-11
58-5	Sea surface temperature from airborne PRT-5 radiometer survey, July 30, 1970	58-12
59-1	Examples of reflectance spectra from ocean waters containing different concentrations of chlorophyll	59-5
59-2	Spectra obtained at 500-foot altitude across a transition from ocean water containing chlorophyll	59-6
59-3	Spectra obtained across transition at 1000-foot altitude	59-7
59-4	Spectra obtained across transition at 2000-foot altitude	59-8

Figure		Page
59-5	Spectra obtained across transition at 5000-foot altitude	59-9
59-6	Spectra obtained across transition at 10 000-foot altitude	59-10
59-7	Difference of spectra across a transition in ocean color at flight altitudes shown	59-11
59-8	Contrast ratio of light differences to total light across transition	59-12
60-1	Drift track of ice island T-3 from April 1952 until September 1970	60-9
60-2	Lead in multi-year sea ice	60-10
60-3	Polynya in multi-year sea ice with three successive layers of new sea ice	60-11
60-4	Large ridge, approximately five meters high, in multi-year sea ice	60-12
60-5	Finger ice between multi-year ice floes	60-13
60-6	Side looking airborne radar (SLAR) image of a group of polynyas in the Beaufort Sea	60-14
60-7	Passive microwave image of multi-year sea ice with polynyas	60-15
61-1	Multispectral comparison of light penetration in water	61-5
61-2	Equation developed to compute water depth by ratio technique	61-6
61-3	Lake Michigan water depth curves a. Generated from shallow water parameters b. Generated from deep water parameters	61-7 61-8
61-4	Digital printout of depth chart, before averaging	61-9

Figure		Page
61-5	Digital printout of water depth, with averaging	61-10
61-6	Depth chart printout for Ceasar Creek area, Florida Keys	61-11
63-1	Spectral regions suitable for remote polluted measurements	63-5
63-2	Northern portion of test area showing spectrometer scan locations and surface truth points	63-6
63-3	Thermal image of northern portion of test area	63-7
63-4	Typical spectral reflectance signatures	63-8
63-5	Complete test area	63-9
63-6	Map of test area showing measurement locations	63-10
63-7	Parameter K_1 versus Secchi depth	63-11
63-8	Parameter K_2 versus Secchi depth	63-12
63-9	Parameter K_3 versus Secchi depth	63-13
63-10	Spectral reflectance of water containing two concentrations of algae	63-14
63-11	Parameter K_4 versus Secchi depth	63-15
64-1	Geodolite 3A laser profilometer	64-14
64-2	Geodolite block diagram	64-15
64-3	Comparison of laser and wave-staff recordings of surface waves from a fixed ocean platform	64-16
64-4	Comparison of wave-energy spectra derived from laser and wave-staff recordings of surface waves	64-17

Figure		Page
64-5	Airborne laser profiles of surface waves obtained in conjunction with simultaneous continuous strip photography	64-18
64-6	Comparison of wave-power spectra obtained with the laser profiles aboard a U.S. Navy aircraft with that obtained from an in situ wave staff	64-19
64-7	Aircraft heave displacement spectrum showing energy contribution in surface wave pass band	64-20
64-8	Ship reports in the North Sea, March 14, 1969	64-21
64-9	Observations of significant wave height as a function of fetch	64-22
64-10	Wind speeds reported by the German beacon ship LHHT on March 14, 1969	64-23
64-11	Contours of equal spectral density on a frequency-fetch diagram	64-24
64-12	Plots of spectral density versus fetch for selected frequencies	64-25
64-13	An example of the computation of percent white caps	64-26
64-14	25 m/sec windspeed	64-27
64-15	12 m/sec windspeed	64-27
65-1	Canvas grey scale deployed next to runway	65-8
65-2	Scanning microdensitometer	65-8
65-3	Visibility laboratory interactive image manipulation computer facility	65-8

Figure		Page
65-4	Typical film characteristic curve with gray scale data superimposed	65-9
65-5	Frame taken by RC8 camera on Mission 88, Flight 6, on March 1969, at an altitude of 1500 feet with surface winds of 48 to 50 knots	65-9
65-6	Cumulative areas (as percent of total area scanned) versus film density for the four regions outlined in figure 65-5	65-10
65-7	Cumulative areas for three frames of photography taken about 10 seconds apart (no overlap) showing variation occurring in independent areas in the same wind field	65-10
65-8	White water coverage versus wind speed as obtained from earlier studies	65-11
66-1	Spectral contrast ratio as a function of wavelength and altitude	66-5
66-2	Spectral contrast ratio of chlorophyll- enriched water to sterile water	66-6
66-3	Analysis of single bandpass channel for chlorophyll discrimination	66-7
66-4	Relationship between maximum SCR, preferred filter-center wavelength, and the filter bandwidth	66-8
66-5	Altitude effects on the maximum spectral contrast ratio	66-9
66-6	Altitude effects on the preferred blue channel	66-10
68-1	Radar system	68-4
68-2	Chesapeake light tower	68-5
68-3	Antenna mounting on catwalk	68-6

Figure		Page
68-4	Wave pole and corner reflector	68-7
68-5	Computer plot of radar data	68-8
68-6	Computer plot of radar data	68-9
68-7	Power spectra of radar and wave poles	68-10
68-8	Power spectra of radar and wave poles	68-11
68-9	Reflected power versus wave depth	68-12
68-10	Reflected power versus wave depth	68-13
68-11	Equivalent impulse response	68-14
68-12	Equivalent impulse response	68-15
69-1	The vertical and horizontal components of the brightness temperature of the sea	69-11
69-2	Individual measurements at 1.41, 8.36, and 19.34 GHz of the vertical and horizontal components of brightness temperature and the percentage polarization	69-12
69-3	The slopes of linear least-square solutions fitted to the measurements of the vertical and horizontal com- ponents of the brightness temperature and the percentage polarization	69-13
69-4	The solid curves are calculations of the differential change in horizontal brightness temperature	69-14
70-1	ATS image showing fronts and low centers near spiral cloud bands over the North Atlantic and South Atlantic Oceans	70-15
70-2	Computer grid system covering the North Atlantic Ocean	70-16
70-3	Computer grid system covering the eastern half of the North Pacific Ocean	70-17
70-4	Computer grid system covering the western half of the North Pacific Ocean	70-18

Figure		Page
70-5	Computer grid system covering the western North Pacific Ocean	70-19
70-6	Computer grid system covering the western North Pacific Ocean	70-20
70-7	Computer grid system covering the western North Pacific Ocean	70-21
70-8	Computer grid system covering the western North Pacific Ocean	70-22
70-9	The computation of the whitecap production index	70-23
70-10	Land-sea table for wave hindcasts	70-24
70-11	Land-sea table for wave hindcasts	70-25
70-12	Initialization significant wave heights for North Pacific Ocean	70-26
70-13	Pressure field analysis based on ships and windspeed information	70-27

COLOR ILLUSTRATIONS

SECTION 47

Hydrology

DETECTION AND IDENTIFICATION OF BENTHIC COMMUNITIES
AND SHORELINE FEATURES IN BISCAYNE BAY
USING MULTIBAND IMAGERY^{1/}

Milton C. Kolipinski and Aaron L. Higer^{2/}

INTRODUCTION

Progress has been made in the development of a technique for identifying and delineating benthic and shoreline communities using multispectral imagery. Heretofore, manual mapping from aerial photographs or on-site surveys were the only feasible methods to inventory benthic features in large, shallow bodies of water (refs. 1, 2 and 3). Images were collected on March 10, 1970, with the University of Michigan's multispectral scanner systems mounted in a C-47 aircraft. The overflight covered south Biscayne Bay, Florida and adjacent shoreline (fig. 1), including a region affected by heated water from an electrical power plant. Concurrent with the overflight, ecological ground-and sea-truth information was collected at 19 sites in the bay and on the shore (fig. 2). South Biscayne Bay is a study area within the Florida Regional Ecological Test Site (fig. 3).

The work reported herein was sponsored by the National Aeronautics and Space Administration. The authors gratefully acknowledge Fred Thomson, Infrared and Optical Sensor Laboratory of Willow Run Laboratories, University of Michigan, for conducting the multispectral processing.

Also, the authors express appreciation to the scientists and engineers that assisted in the sea-truth operations and experiments conducted in south Biscayne Bay during March 2-13, 1970. Although many persons contributed their efforts, the following individuals and agencies deserve special credit: U.S. Environmental Protection Agency - John Hagan, Sanitary Engineer; Lee Purkerson, Microbiologist; Reginald Rogers, Aquatic Biologist; Douglas Lair, Operation Engineer; Michael Polito, Chemist;

^{1/}Publication authorized by the Director, U.S. Geological Survey.

^{2/}Aquatic Biologist and Hydrologist, respectively. U.S. Geological Survey, Miami, Florida.

Don Lawton, Science Technician. U.S. National Park Service - Dr. Bill Robertson, Research Biologist; John Ogden, Research Biologist; Richard Klukas, Management Biologist; James Stewart, Ranger; Frank Nix, Hydraulic Engineer. U.S. Bureau of Sport Fisheries and Wildlife - John Billinger, Aquatic Biologist. University of Michigan - Norma Thomson, Research Ecologist; Dr. Fabian Polycyn, Physicist. University of Miami - Dr. Howard Gordon, Physicist; Peter Schroeder, Research Biologist; Thomas McKinney, Research Biologist; Peter Rhodes, Research Biologist; Dr. Robert Pope, Research Biologist; Dr. Jay Zieman, Marine Biologist; Robert Sterns, Marine Scientist. North American Rockwell Corp. - Dave Hodder, Research Scientist; Phillip Chandler, Research Scientist. Fairchild Gardens, Miami - Dr. Malcolm Gill, Botanist.

Biscayne Bay, along the Atlantic shoreline, is a shallow semi-enclosed estuary that includes the Biscayne National Monument (fig. 4). The detailed interpretation of the character of the bottom is important for species identification in ecological studies. The bottom flora provides shelter and food for juvenile sport and game fish, shrimp, and other commercial species. The occurrence and distribution of plants can serve as an index of pollution by indicating the state of biological well-being of the estuary. The pollutants range from pesticides to heated water. Increased water temperature caused by the heated effluent from electric generating plants, especially those powered by nuclear energy, are a potential problem in Florida and other states. One such plant is under construction in south Biscayne Bay. Another problem in the bay results from turbidity caused by dredge and fill operations. Either excessive temperature or turbidity can destroy plankton, attached vegetation, and sessile animals. It may even diminish or destroy natural communities and the commercial and sport fisheries of an area.

Fresh water enters the bay by runoff and ground-water discharge. In places, the discharge emerges in sufficient strength to form springs, subcircular depressions a few feet in diameter. Thermal contrasts between the upwelling water and the surrounding bay water were sensed remotely.

In many instances, the zonation of plants in the coastal marshes and forests of south Biscayne Bay indicates the extent and duration of tidal inundation. The typical zonation pattern is red mangrove (Rhizophora mangle) through the intertidal zone, black mangrove (Avicennia nitida) in the upper tidal reaches, and buttonwood (Conocarpus erectus) in the supratidal region. The delineation and mapping of these species can be valuable to those concerned in planning and in settling problems relating to the legal definitions of shorelines or mean high-water lines that concern ownership or the seaward limit allowable for landfill and bulkhead lines.

DESCRIPTION OF APARATUS AND METHOD OF ANALYSIS

The multispectral data collector consists of an optical-mechanical scanner mounted in an aircraft. As the aircraft flies over the terrain to be mapped, a rotating mirror scans the field of view of a parabolic-mirror telescope across the ground perpendicular to the direction of flight. This action, in conjunction with the aircraft motion, covers a strip of terrain centered under the aircraft with a continuous scan (fig. 5). Two telescopes and one double-sided rotating mirror (the two sides are rotated 90° with respect to each other) constitute the scanner. Two scanners are employed in the C-47 aircraft operated by the University of Michigan. Filtered detectors convert the radiation from the ground into electrical signals, which are amplified and recorded on magnetic tape along with synchronizing signals necessary to reconstruct the images (ref. 4).

The processing of scanner data depends upon the automatic recognition of objects by their spectral signatures (fig. 6). Essentially, the processing procedure consists of four steps:

- (1) Selection of a decision rule which states in mathematical terms the criteria to be used in determining the nature of the scanned objects.
- (2) Training of the digital computer by presenting it with a sample of data from the object (biological community) to be mapped - a training set. The parameters of the decision rule are adjusted to this set to optimize the detection process.
- (3) Presenting the analog computer with unknown data and asking it to recognize all objects similar to those in the training sets.
- (4) Preparing a community recognition map with a film-strip printer.

A detailed theoretical discussion of data processing is presented by Higer and others, 1970 (ref. 4) Voss and others, 1969 (ref. 5). Two new digital programs (F. Thomson, University of Michigan, oral communication, 1970) were developed for processing the Biscayne Bay data; one corrects for sun glint, and the other corrects for geometric distortion of features induced by the scanner (fig. 6).

Results and Discussion

Preliminary processing of the scanner imagery with a CDC 1604 digital computer provided the optimum channels for discernment among different underwater and coastal objects. The following six spectrometer bands were used for discrimination of underwater features:

Multispectral data Channel <u>Number in Figure 7</u>	Wavelength Interval, <u>Micrometers</u>	Approximate Subjective <u>Color</u>
2	0.430-0.455	Violet
4	0.485-0.500	Blue-Green
5	0.500-0.520	Blue-Green
6	0.520-0.545	Green
8	0.580-0.630	Light Red
9	0.630-0.680	Deep Red

Recognition maps of benthic community types were provided by electronically processing combinations of video signals in the six spectral bands. The computer was trained to identify each community type from the intertidal zone to a depth of 3 meters to compensate for variations of reflectivity due to such factors as light scattering and extinction as a function of water depth.

Computer maps were printed in different colors and superposed to provide a color-composite map of recognized community types in the study area (fig. 8). The plant and animal communities in south Biscayne Bay and Card Sound are varied and rich in species; a list for Biscayne National Monument contains about 1,400 different marine species (ref. 5). Several pertinent reports contain detailed discussions of the communities in south Biscayne Bay and neighboring areas (refs. 6, 7, 8 and 9). The identification of benthic communities using remote sensing techniques shows them to be large, sessile, and common. Communities are characterized from the air by species composition, organism density, and nature of substrata or bottom. Bottom composition is a major factor in the reflectivity from a benthic community, especially where attached organisms are sparse. Two distinct composition types occur in the bay: soft bottom that is dark in color and contains sand, calcitic mud, and organic sediments ranging from 0.5 to about 4 meters deep; and hard bottom that is light in color and contains materials such as carbonate and quartz sand and shell hash that have accumulated in shallow layers as thick as a few centimeters. Sea grasses characterize the soft bottom community; macro-algae and sponges characterize the hard bottom community (fig. 9).

The dominant plants of the soft bottom community (color coded red in fig. 8) are turtle grass (Thalassia testudinum), manatee grass (Syringodium filiforme), and Diplanthera wrightii. These grasses often form dense mats on the bottom. In some regions the grasses are sparse and are invaded by algae such as Laurencia, Penicillus, Canlespa, and Halimeda. In a few small regions of the bay the soft bottom lacks attached vegetation. The bare soft bottom adjacent to West Arsenicker Key and mapped in figure 8 (color coded dark yellow) becomes emergent at low tide.

Hard bottom community (color coded green in fig. 8) covers much of the deeper part of the bay. The largest common forms within this community designation are sponges, notably the vase sponge (Ircinia campana) and the loggerhead sponge (Spheciospongia vesparia). Also abundant are sponges of the genera Hippiospongia and Spongia. The formerly mentioned algae that invade the soft-bottom community are common in the hard-bottom community. Corals of the genera Porites, Solenastrea and Siderastrea and sea feathers of the genera Plexaurella and Pterogoria occur regularly in the hard-bottom sites.

The hard- and soft-bottom communities are intermixed over large parts of the study area (color coded dark blue in fig. 8). In these regions the biological components and substrate of both communities are present. The recognition map was color coded light blue for regions where the mixed hard- and soft-bottom community is sparsely inhabited by grasses, algae, corals, and sea feathers. White areas on the color-composite recognition map are those that failed to receive a community designation during computer processing. Additional training sets would need to be established for these areas.

The accuracy of the boundaries of the delineated communities has not yet been established, but detailed spot checks indicate excellent agreement between mapped and observed community types.

A computer map of surface-water temperatures overlying the mapped bay-bottom communities was produced in which temperature intervals of 2 and 3° F are assigned different roles (fig. 10). The mapped temperatures ranged from 64.9 to 83.8° F. The accuracy of the temperature profiles lies within ±1.5° F (F. Thomson, oral commun., 1970).

Automatic mapping of the benthic plants by multiband imagery and the mapping of isotherms and hydrodynamic parameters by digital model coupled together can become an effective predictive ecological tool. Using the two systems, it appears possible to predict conditions that could adversely affect the benthic communities. With the advent of the ERTS satellites and space platforms, imagery data of south Biscayne Bay could be obtained which, when used in conjunction with water-level and meteorological data, would provide for continuous ecological monitoring.

References

1. Kumpf, H. E., and Randall, H. A., 1961, Charting the marine environments of St. John, U.S. Virgin Islands: Bull. Marine Sci. Gulf and Caribbean, v. 4.
2. Kelly, G., 1969, Applications of remote photography to the study of coastal ecology in Biscayne Bay, Florida: Univ. of Miami, Coral Gables, 24 p.
3. Brown, W. L., Thomson, N., and Thomson, F., 1970, Selection of optimum channels for recognition of underwater features in Biscayne Bay: Univ. of Michigan, Ann Arbor, 11 p.
4. Higer, A. L., Thomson, N. S., Thomson, F. J., and Kolipinski, M. C., 1970, Applications of multispectral remote sensing techniques to hydrobiological investigations in Everglades National Park: Univ. of Michigan, Ann Arbor, 25 p.
5. Voss, G. L., Bayer, F. M., Robins, C. R., Gomon, M., and LaRoe, E. T., 1969, The marine ecology of the Biscayne National Monument: Univ. of Miami, Coral Gables, 128 p.
6. Stephenson, T. A., and Stephenson, A., 1950, Life between tidemarks in North America. I. The Florida Keys: Jour. Ecology, v. 38, no. 2, p. 354-402.
7. Voss, G. L., and Voss, N. A., 1955, An ecological survey of Soldier Key, Biscayne Bay, Florida: Bull. Marine Sci. Gulf and Caribbean, v. 5, no. 3.
8. McNulty, J. K., Work, R. C., and Moore, H. B., 1962, Level sea bottom communities in Biscayne Bay and neighboring areas: Bull. Marine Sci. Gulf and Caribbean, v. 12, no. 2, p. 204-233.
9. Kohout, F. A., and Kolipinski, M. C., 1964, Biological zonation related to groundwater discharge along the shore of Biscayne Bay, Florida, in Lauff, G. H., Estuaries: Amer. Assoc. Adv. Sci., Publ. 83, p. 488-499.

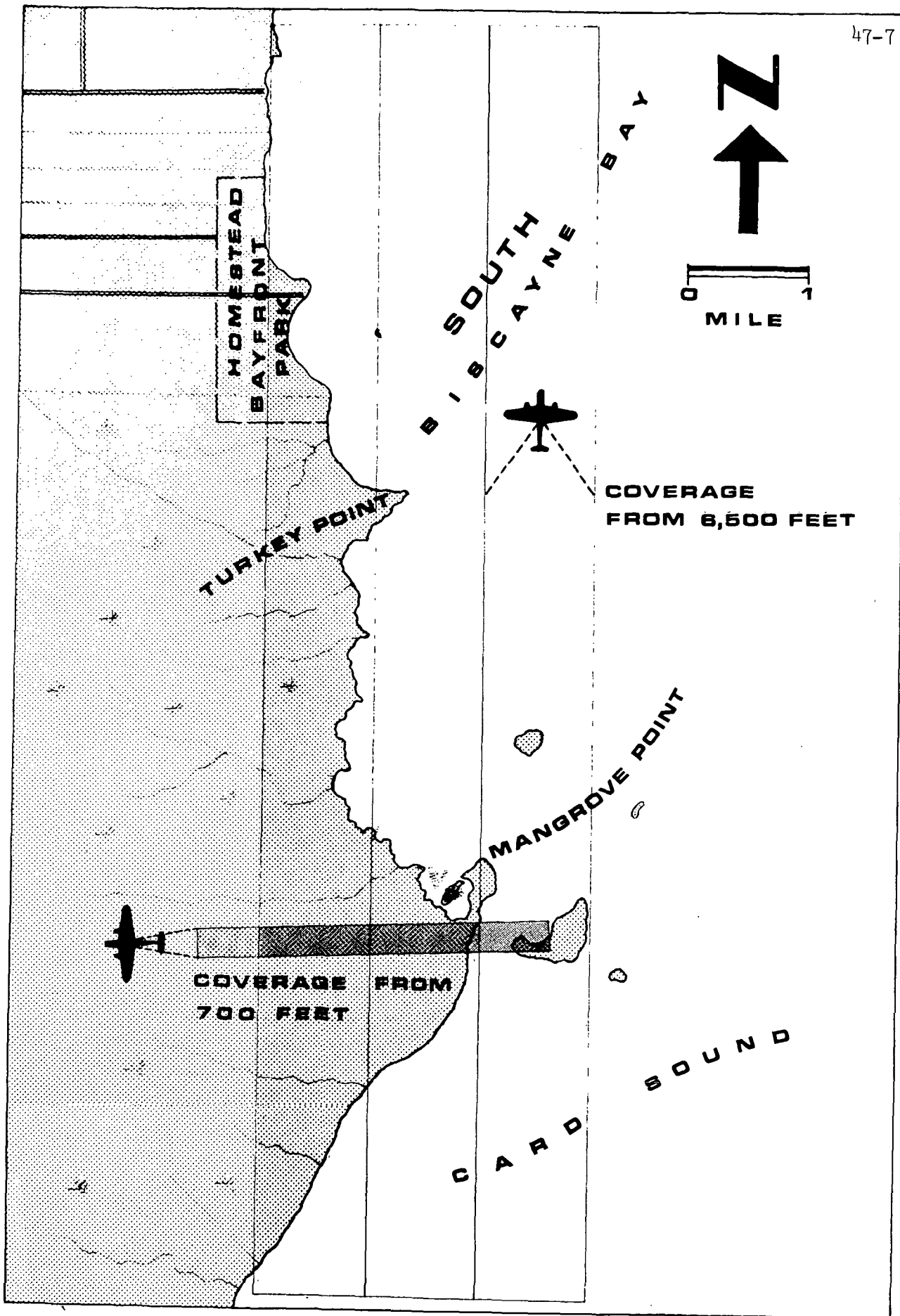
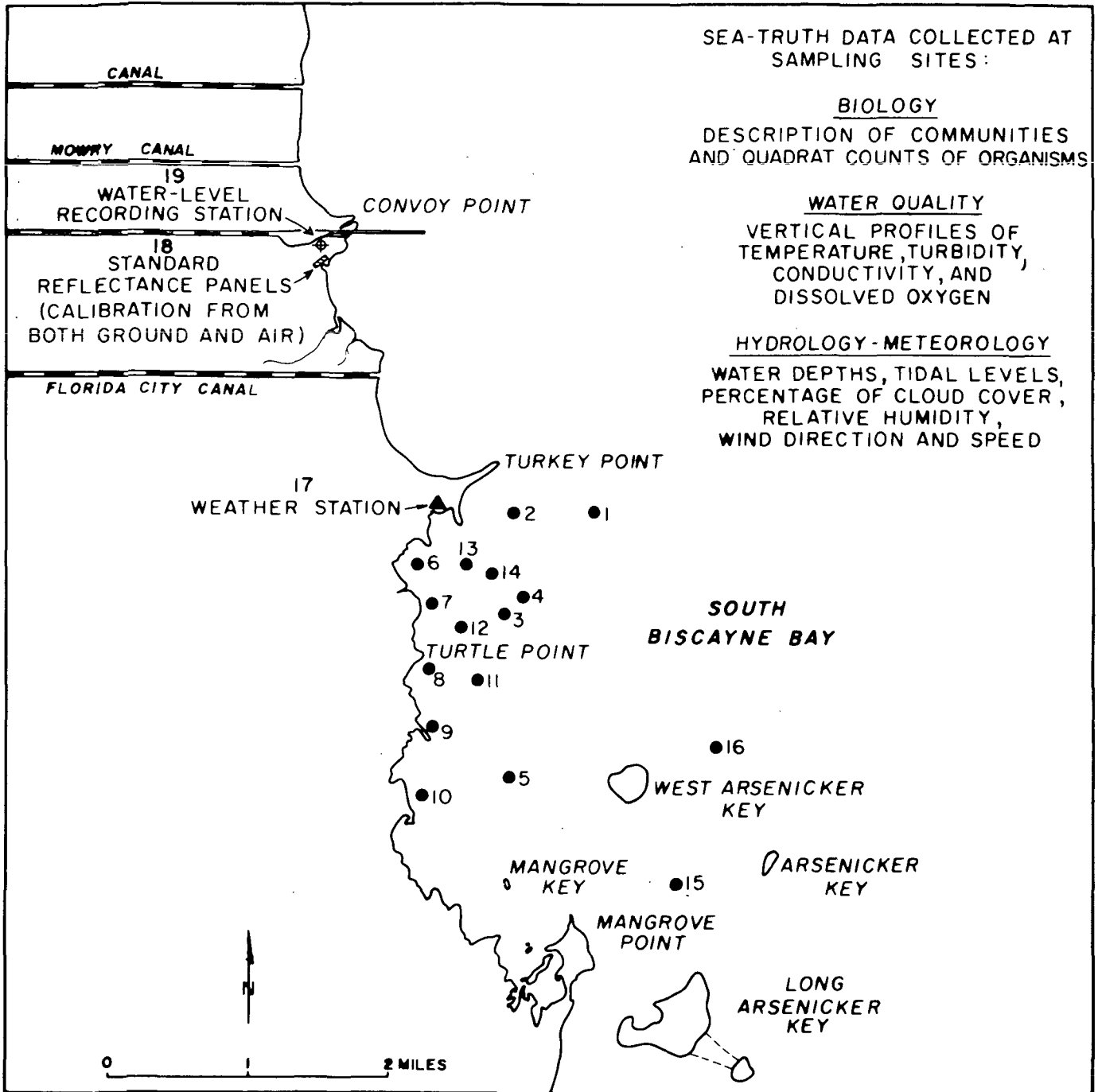


Figure 1.- Location map of areas covered by optical-mechanical scanner from an overflight on March 10, 1970.



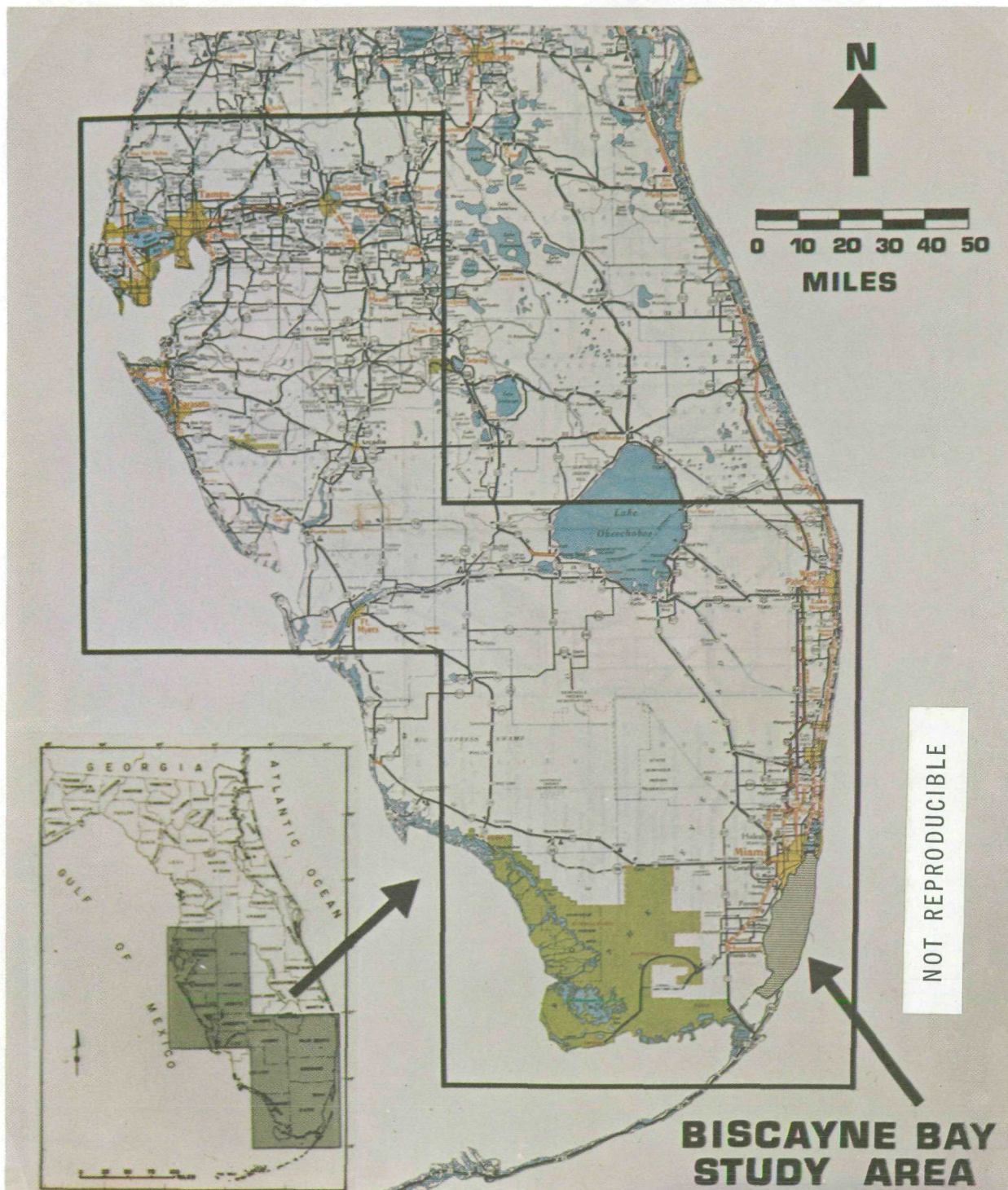


Figure 3.- The Florida Regional Ecological Test Site is a multidisciplinary experiment, established to test and evaluate remote sensor applications to resource problems from space, aircraft and ground platforms.

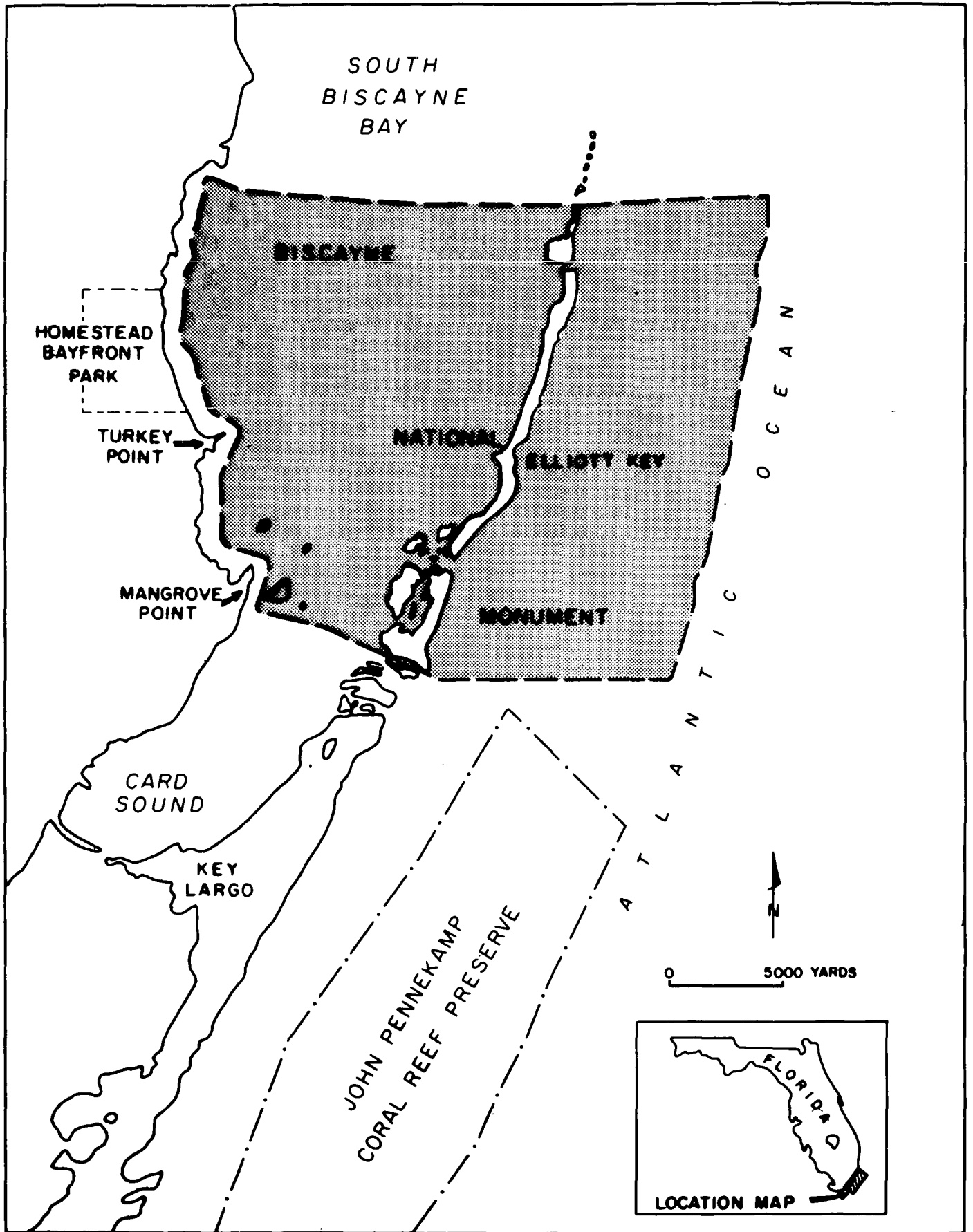


Figure 4.- Location map of Biscayne National Monument in south Biscayne Bay.

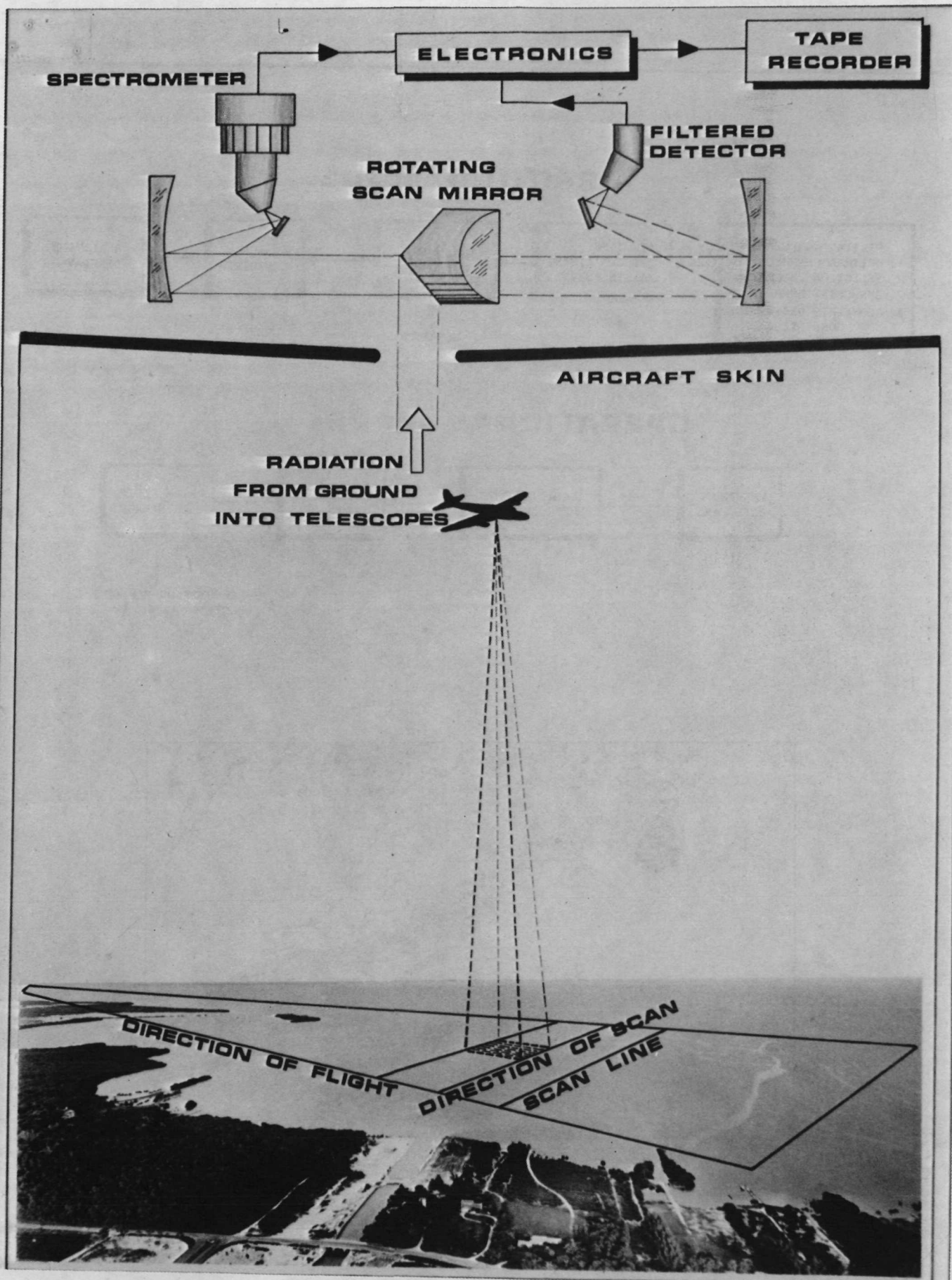
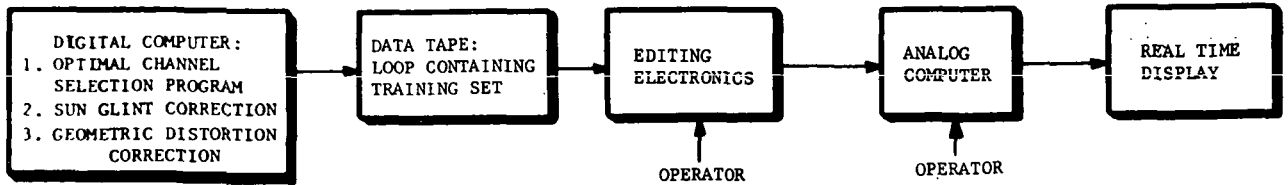


Figure 5.- Schematic of multispectral scanner operation over study area in south Biscayne Bay.

TRAINING MODE



OPERATIONAL MODE

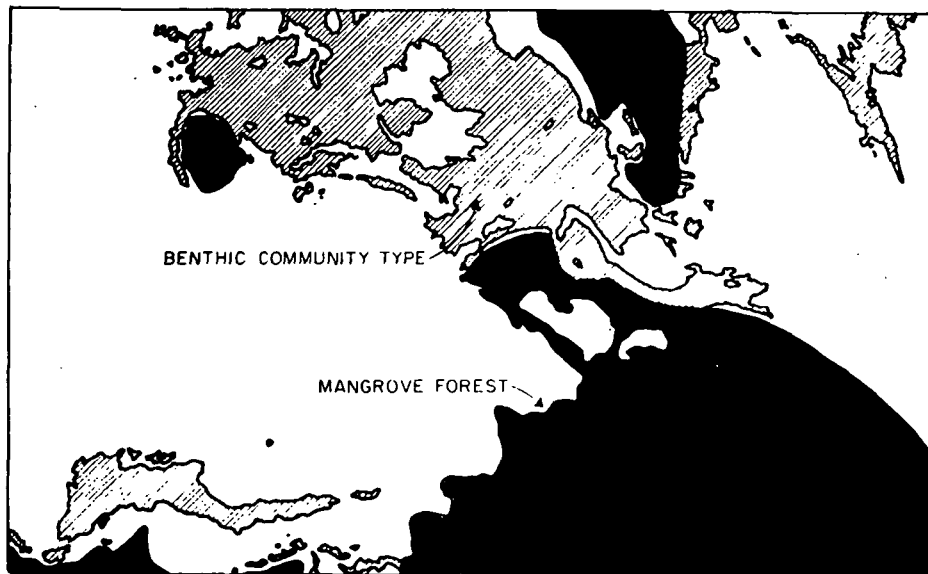
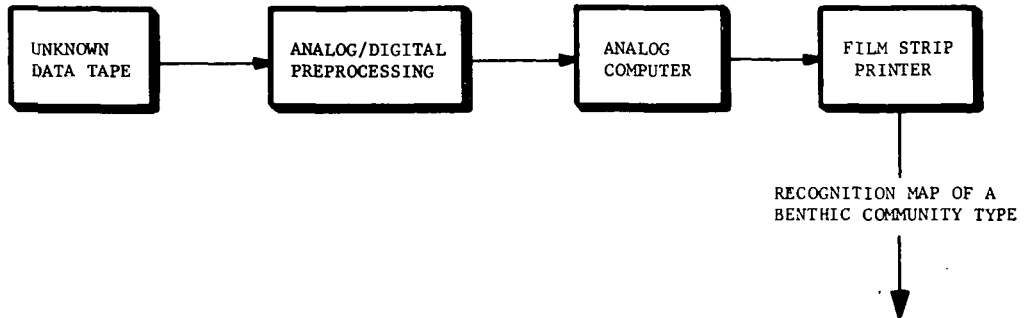


Figure 6.- Block diagram of multispectral-scanner-imagery processing operations for benthic communities. The spectral characteristics of targets and background objects are analyzed to determine how to electronically process spectral information from a scene using both digital and analog techniques. Each recognition map with its assigned color is superposed to provide an imagery mosaic of the benthic communities of the study area.

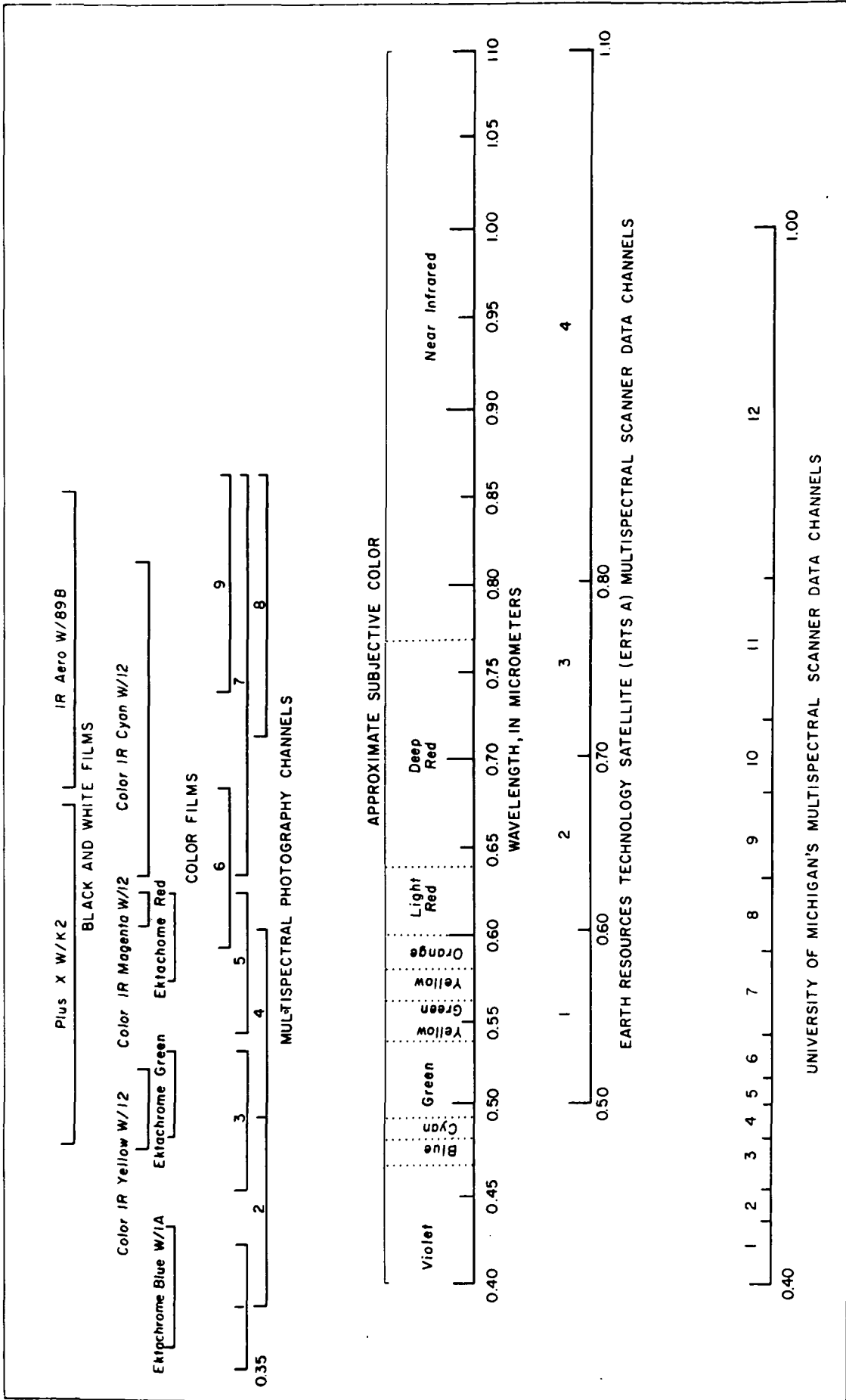


Figure 7.- Comparison of spectral ranges of various film-filter combinations with ERTS-A imagery bands and an optical-mechanical-scanner system.

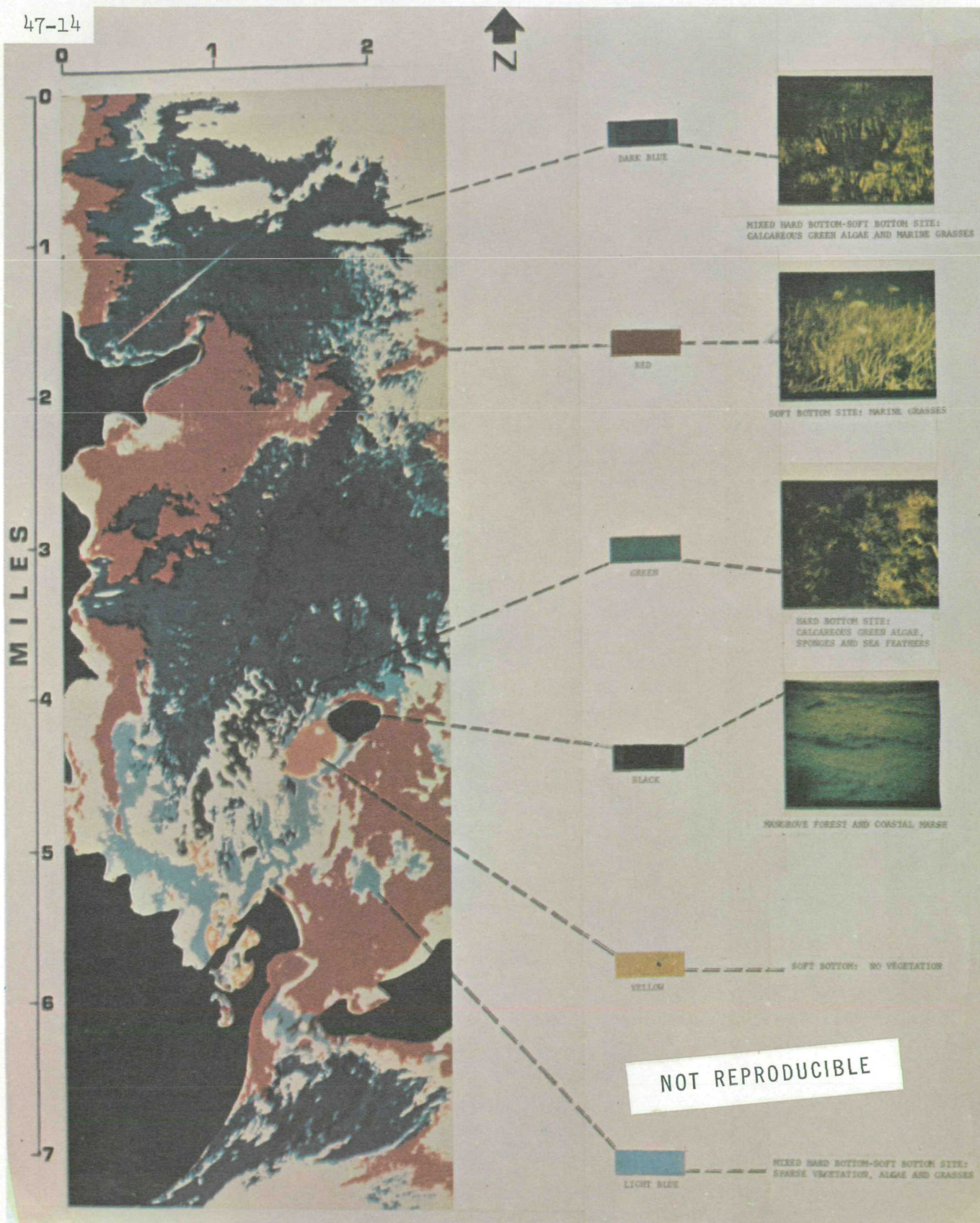


Figure 8.- Color-composite recognition map of benthic communities in south Biscayne Bay. Underwater photographs illustrate dominant community types. Water depths in the mapped area ranged from 0 to 3 meters during the overflight.

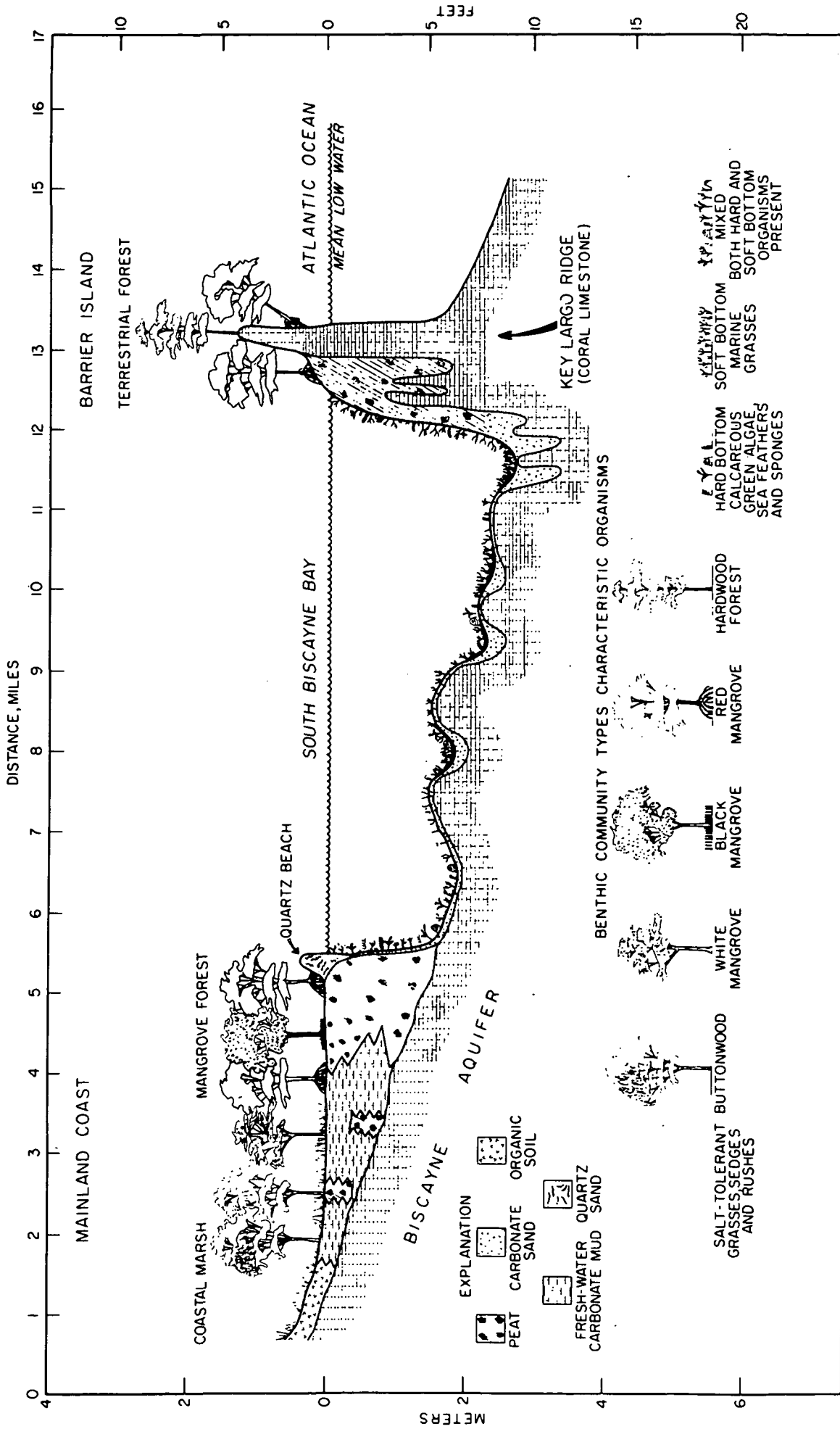


Figure 9.- Generalized cross section through south Biscayne Bay showing biogeologic features. Adapted from Wanless, 1969, (ref. 3). Vertical scale exaggerated 1000x.

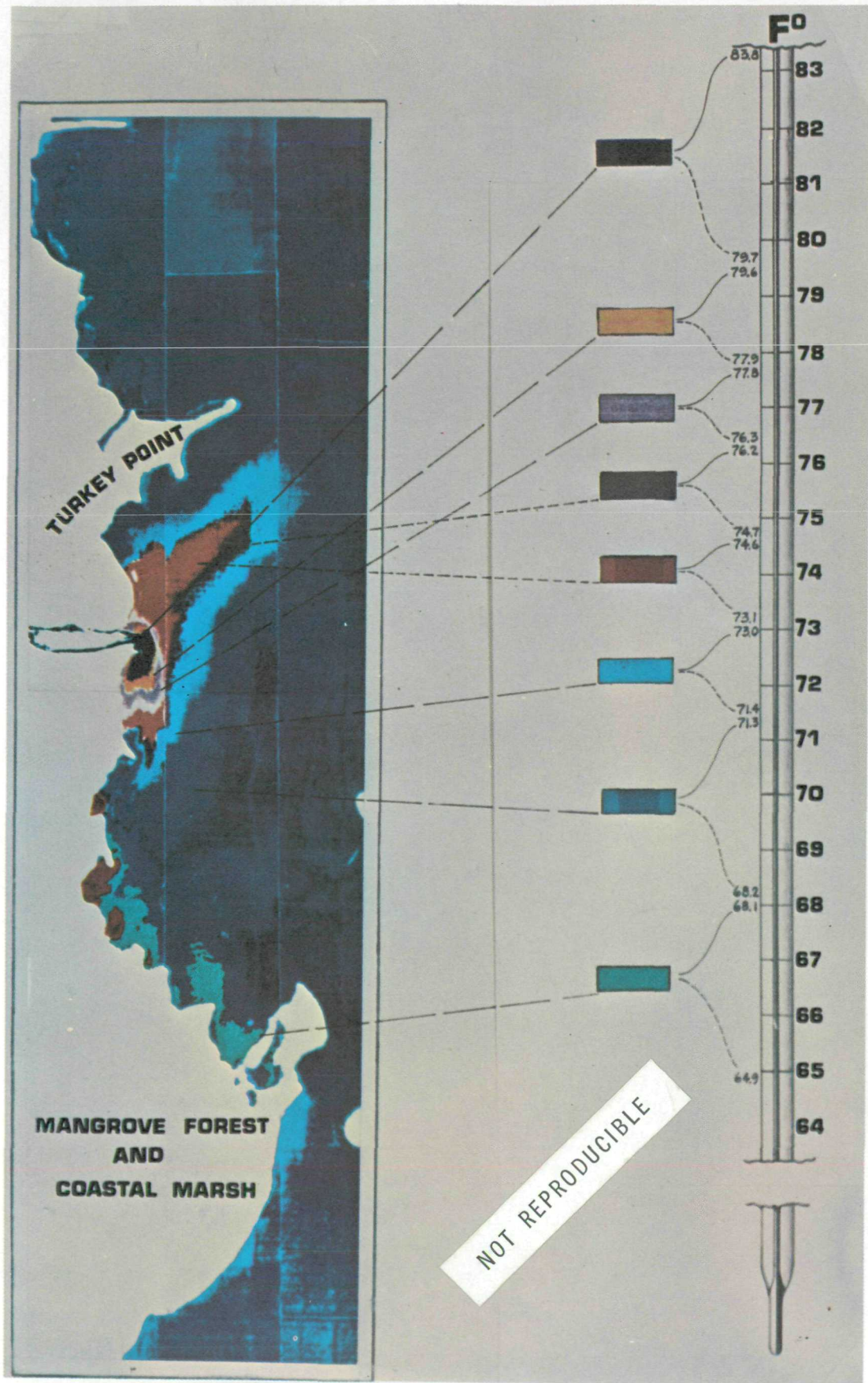


Figure 10.- Color composite recognition-map of surface water temperatures in south Biscayne Bay on March 10, 1970, between 10:08 and 10:56 a.m. Temperature distributions were derived from scanner imagery (8-13.5 μ m) that was calibrated with a network of manual thermometers and recording thermographs.

REMOTE SENSING FOR DEFINING AQUIFERS IN GLACIAL DRIFT

By

Victor I. Myers
Remote Sensing Institute (RSI)
South Dakota State University
Brookings, South Dakota

INTRODUCTION

The economy of much of the glaciated portion of the middle western states is greatly influenced by the availability of ground water. Shallow aquifers, which contain extensive ground-water reserves and are continually replenished to some degree, occur throughout the region.

The bottom of many shallow aquifers in glacial drift is less than 100 feet (30.5 meters) below the surface. Thickness of these outwash sands and gravels may vary from only a few feet to as much as 80 feet (24 meters) or more. Quality of water is generally good. Present plans for mapping these aquifers extend many years into the future because of tedious standard investigation procedures. Remote sensing may provide part of the information required to speed up these ground-water surveys.

Aquifers can seldom be detected directly by using remote sensing, but there are certain properties of aquifers, and a number of associated features and conditions which influence reflected and emitted radiant energy. Features that appear on imagery that aid in identifying aquifers are land forms, glacial outwash patterns, stream patterns, vegetative type and condition, soil moisture, and snow melt patterns. Also, thermodynamic considerations show that a shallow aquifer might form a heat sink that influences and modifies the temperature effects of heat originating at the land surface and within the crust [2] [3].

The objectives of this study are to determine the properties of shallow aquifers and related features that influence electromagnetic energy, to determine how these properties can be detected remotely, and to establish remote sensing procedures for aiding in ground-water mapping.

This research effort is underway in areas of South Dakota where intensive geology and water resources investigations have been conducted. Thus a great deal of data are readily available for correlation with remote sensing imagery. Upon successful completion of the studies in areas of known aquifers, the effort will be expanded to a pilot study in an area where a ground-water investigation is in its early stages. Procedures developed under the known conditions will be used to predict the occurrence of aquifers.

This progress report deals specifically with the thermal infrared phase of aquifer mapping; in particular the direct influence of aquifer characteristics on surface thermal contrasts. The related photographic and thermal studies involving soil moisture and other conditions and features as they relate to the occurrence of aquifers are still underway.

The research work reported in part herein is expected to yield ground-water maps of shallow aquifers in glacial drift. The maps should be useful in detailed investigations for determining the location for drilling explorations. It is expected that detailed explorations can be made faster and at a reduced cost with the availability of aquifer maps produced from remote sensing imagery.

The project is jointly supported by the U. S. Geological Survey and the National Aeronautics and Space Administration. The District Office of USGS at Huron, South Dakota, the South Dakota State Geological Survey, and the U. S. Bureau of Reclamation furnished the well logs and historical information used in the studies and gave valuable advice in setting up the studies. Dr. Fred Schmer of RSI was helpful in providing advice and consultation. Dr. Fred Waltz and Mrs. Josephine Parikh of RSI conducted the statistical studies.

DESCRIPTION AND LOCATION OF STUDY AREA

The geology and hydrology of Beadle County, South Dakota, where these studies were conducted, were investigated and reported by Hedges [5] and by Howells and Stephens [6]. Brief sections from those reports are reproduced here to give the reader an insight into the ground water potential and investigation problems.

"Most surficial deposits in Beadle County are the result of glaciation and collectively are called drift. Along water courses and in sloughs and lakes the drift is covered by deposits of alluvium; locally the drift is covered by windblown sand and silt. Alluvium in the county consists of poorly sorted, poorly stratified, thin, discontinuous layers of material that range in grain size from clay to boulders.

"Drift in Beadle County can be divided into two major types, till and outwash. Till, which was deposited directly from or by glacial ice, is a heterogeneous mixture of silt, sand, gravel, and boulders in a matrix of clay. It is the most abundant glacial deposit in the county. Outwash, which was deposited from or by meltwater streams beyond the margin of active glacial ice, consists primarily of layers of clayey or silty sand and sandy gravel interbedded with layers of sandy and gravelly silt or clay. Beds of well-sorted sand and gravel are contained in the outwash but generally are small or discontinuous.

"About 62 percent of the area of Beadle County is underlain by 10 feet (3.05 meters) or more of aquifer material in surficial deposits. Water levels in the aquifers fluctuate in response to recharge and discharge; in Beadle County, average water levels generally have been stable or rising slightly during the past 10 years, indicating that recharge is equal to or slightly in excess of discharge.

"More than 5 million acre-feet of water (616×10^7 cubic meters) is stored in three aquifers in surficial deposits in Beadle County. The greatest potential for development of high-capacity wells is in areas where the major aquifers are more than 25 feet (7.6 meters) thick. The aquifers are recharged by infiltration of precipitation in Beadle County and by underflow from adjacent areas."

Two areas are being studied having contrasting aquifer conditions. Shallow aquifers in the James River Basin are intermittent with intermingled layering of sands and gravels and finer materials. The aquifers in the Sioux River Basin, on the other hand, consist of fairly coarse, unconsolidated

materials in well-defined layers. This report is concerned only with investigations in Beadle County in the James Basin. A later report will deal with the Sioux Basin.

PROCEDURE

Flight lines labeled as J-J' and H-H' in Figure 1, were located to provide maximum data relative to diverse aquifer conditions, and number of well logs.

Aircraft missions which provided data reported in this study were flown by the South Dakota State University (SDSU) RC45J Remote Sensing Institute (RSI) aircraft. Ideal conditions for conducting predawn flights to obtain thermal imagery for identifying aquifers are rare in areas away from arid deserts, and cannot be predicted more than a few hours prior to flight time. It is thus desirable to have an aircraft available on a basis of "quick alert" to obtain a successful predawn mission.

Photographic imagery was taken by the NASA RB-57F aircraft at an altitude of 60,000 feet (18,300 meters) on November 9, 1970. The high altitude imagery covered an extensive area, including Beadle County, and will be useful in this study as an aid in ground-water mapping by evaluating surface conditions related to the occurrence of aquifers.

Remote sensing instrumentation aboard the RSI aircraft includes the following:

1. Four 70mm format Hasselblad 500 EL cameras, 50mm focal length for multispectral photography.
2. Framing cameras, 9 1/2-inch (24.1cm) film format, 6-inch (15.2cm) and 12-inch (30.4cm) focal lengths (used alternately with the Hasselblad cameras).
3. Thermal infrared scanner with sensitivity in the 4.5 to 5.5 μm wavelength band.
4. Precision radiometer, PRT-5, 2° field of view, for calibration of thermal scanner data.
5. Sol-a-Meters -- one on top of the aircraft with 180° field of view to measure incoming radiation and three on the bottom of the aircraft to measure reflected radiation. Purpose of the Sol-a-Meters is to provide continuous data for correction of imagery adversely affected by attenuation of the solar beam.

The PRT-5 radiometer is used as a basic sensor for thermal infrared mapping flights. The radiometric data are used to calibrate the infrared scanner imagery when the instruments are both used. When the PRT is used alone, the tracking data, plotted on a strip chart recorder, are related to known ground conditions. Several predawn missions were flown with the PRT providing the only temperature record, during periods when the scanner was not available.

Three cameras in the multispectral array were provided with film-filter combinations to correspond as closely as possible to the bandwidths in the ERTS-A spacecraft.

All processing of imagery from the RSI aircraft is done in the RSI laboratory for purposes of achieving quality control. Local processing also provides rapid turn-around for quick checking against field conditions. A color-encoding television densitometer was used in this study for producing color maps that separate the range of optical densities into narrow density bands. If appropriate, boundaries of areas representing real conditions can be closely approximated or inferred by visually manipulating the color slices to create the desired density contrasts.

Missions were flown diurnally and seasonally to take advantage of time-dependent phenomena that may help define aquifer and related soil moisture conditions. Flights were timed to assess theoretical considerations concerning maximum temperature gradients between the land surface and aquifers. Since heat is conducted from warm to cool materials, the direction of heat transfer at various times of the year can be inferred. In the spring and fall, the orientation of isotherms is nearly vertical, which means that the vertical heat movement is reduced to nearly zero. The steepest temperature gradients occur during the warmest and coldest parts of the year.

Summer missions, with multispectral cameras and thermal scanner, were flown to test the heat exchange hypothesis where little or no vegetation existed, and where plant cover was profuse, to indirectly measure soil moisture by plant temperature sensing. Plants without adequate soil moisture are warmer since their transpirational cooling mechanism is inhibited.

Diurnal flights were made at three times [7]; (1) predawn for soil moisture and thermal characteristics of aquifers and recharge areas, (2) after sundown for shallow subsoil thermal

characteristics, and (3) between the hours of 2-4 pm during periods of maximum transpiration, for thermal characteristics of plants and ground water conditions.

Flight lines were generally laid out for convenience in gathering ground truth so that their centers coincided with roads. Also, exploration wells are most frequently drilled along roadways. However, actual flights must pass about 1/8 mile (0.20 kilometer) on either side of the centerline road so that radiance detected by the calibration PRT-5 can be associated with uniform soil and vegetation conditions that are identifiable on the thermal imagery.

To aid in nighttime navigation, rotating beacons were laid out along flight lines. Under clear conditions it was found that beacons placed 5 to 8 miles (8 to 13 kilometers) apart were adequate.

By far, the most valuable ground truth data available were the published results of geology and water resources investigations, along with profile data contained in well logs. Ground truth data gathered at the time of overflights included the following: temperature and depth to water table in selected observation wells, vegetation and soil type and condition, soil moisture, soil temperature, snow depth and water content, and climatological information. Detailed descriptions of procedures used in gathering ground truth are included for only those measurements used in this report.

A temperature log has been recorded monthly by USGS District Office Personnel in a 500-foot (155 meters) depth artesian well near the center of flight line H-H'. The temperature profile measurement is made to monitor changes in water temperature with depth, as the season changes. Since the well remains capped between measurements, it is likely that water profile temperatures are very close to soil profile temperatures. The artesian well flows very slowly, when uncapped, during periods of measurement.

A substantial number of remote sensing aircraft missions have been flown for this project to determine the optimum conditions for conducting such missions, to obtain good data. Careful recording of meteorological data related to successful missions has resulted in the accumulation of recommended conditions for conducting such missions. Optimum daytime flight conditions are not difficult to determine. On the other hand, predawn flight conditions for assessing aquifers are very difficult to determine.

Data from a predawn mission flown August 5, 1970 were used in the studies reported here. The locations of logged exploration wells were plotted on thermal imagery and optical densities (D) measured at the plotted points with a Macbeth spot densitometer. Values of optical density were then statistically correlated with data taken from the well logs. Simple linear correlation techniques were used to determine the degree of dependence of surface temperature on the independent variables. The dependent variable used in this analysis was optical density (D) of the thermal film. [optical density (D) was used instead of temperature (T) of the ground since there is a linear relationship between (D) and (T)]. The independent variables used in the analyses are:

- X₂ - Depth to water table
- X₃ - Depth to top of aquifer
- X₄ - Thickness of aquifer
- X₅ - Estimated thermal diffusivity coefficient
- X₆ - Topography (departure from average surface elevation in area)
- X₇ - Depth to bedrock
- X₈ - Type of bedrock material.

An explanation of the variables listed is given below.

The depth to water table was recorded in more recent logs but was not recorded in most earlier logs. Shallow aquifers in the area are usually saturated; however, water tables fluctuate seasonally, and with years depending on recharge. Where no figure appeared in the well log, the depth to top of shallowest aquifer was used. This may be inaccurate since artesian pressures in the area frequently result in a water table above the shallowest aquifer.

Depth to top of aquifer was considered to be the depth to the shallowest water-bearing material.

Aquifer thickness was the sum of the thicknesses of all material with water-bearing capabilities.

Estimated thermal diffusivity was based on published values for saturated aquifer materials [1] [2].

Depth to bedrock was the figure recorded in the well logs. Data were recorded as missing where the well did not extend to bedrock.

Topography was recorded as the positive or negative departure of ground surface from average surface elevation in the near vicinity of the well.

Type of bedrock material was recorded in the well logs where the well extended to bedrock.

RESULTS AND DISCUSSION

The area in which these studies were conducted, and the specific flightlines for the predawn August 5, 1970 flight are shown in Figure 1. The three sections of thermal imagery that appear in Figure 2 are referenced for location in Figure 1.

Three sections of thermal imagery from along flightlines J-J' and H-H' are shown in Figure 2. Circled numbers on the imagery refer to apparent or proven locations of shallow aquifers. Imagery described as Sections A and B covers all portions of flightline J-J' from which well log data were used. Section C imagery covers only the part of the total H-H' flight line for which well log data are available, but is typical of the entire flightline.

The following discussions of numbered locations pertain to the numbers that appear on the three sections of imagery in Figure 2.

Location 1 is a highly-explored aquifer with 16 vertical profile logs available. Averaging the log data for the 16 holes shows an average depth to aquifer of 28 feet (8.5 meters) and an average aquifer thickness of 73 feet (22 meters).

Location 2 indicates a possible aquifer of limited thickness, suggested by the cooler surface temperature in the general area. The water resources map of Figure 1 does not show there being an aquifer in this immediate area.

Location 3, with very cool surface temperatures, indicates a possible aquifer for considerable thickness. No well logs are available, except for one slightly beyond the periphery of the area. Figure 1 does not show there being an aquifer in this area.

Location 4 lies in an area which is a part of a major aquifer, shown in Figure 1, and is indicated by the triangular

shaped cool area in Figure 2. Most of the logs available in this area are from a location off the lower edge of the imagery. However, they do verify the existence of the aquifer.

Location 5 is in an area of a proven water-bearing aquifer. It coincides with the location of an extensive aquifer shown in Figure 1. Sixteen well logs in the immediate area show an average depth to aquifer of 34 feet (10.4 meters) and an average aquifer thickness of 55 feet (16.7 meters).

Location 6 has the appearance of an area underlain by a shallow aquifer. Five well logs show an average depth to aquifer of 36 feet (11 meters) and an average aquifer thickness of 50 feet (15.2 meters).

The area in Section C, represented by two numerals 7, is a broad, flat glacial outwash plain with shallow water-bearing materials under the entire area. Twenty-one well logs represented by Section C, and in the remainder of 'J-J' to the south, show an average depth to aquifer of 28 feet (8.5 meters) and an average aquifer thickness of 30 feet (9.2 meters).

With reference to the thermal infrared imagery shown in Figure 2, dark areas on the imagery are coolest, and light areas are warmest. Theoretical considerations indicate that the darker or cool areas that appear on predawn imagery flown during summer months are associated with shallow aquifers. Optical densities, D , of thermal film were used for correlations rather than ground temperatures, T . Densities are easier to obtain and their use avoids the extra step of relating D to T . The relation between D and T for a particular flightline is likely to be different for each mission.

Simple correlation coefficients were computed to relate the seven independent variables shown in the procedure section to optical density, D , of the negative thermal film. It must be remembered that optical density of the negative film yields values that are low for cool areas and high for warm areas. Some of the data were missing from well logs which resulted in unequal numbers of paired calculations. The numbers of observations for each variable are given as follows:

<u>Variable</u>	<u>No. of Observations</u>
X ₂	50
X ₃	45
X ₄	47
X ₅	44
X ₆	50
X ₇	35
X ₈	33

Standard methods for testing the significance of correlation coefficients were used [4]. Table I shows the results of the statistical correlations.

Variable X₄, thickness of aquifer, is the best index of soil surface temperature for the conditions of this mission. Factors which tend to reduce the statistical correlation are, (1) aquifers frequently extend to depths beyond which the annual cycle of heat exchange is completely damped out, (2) shallow aquifers are not necessarily continuous with depth, and (3) aquifers occur at varying depths below the surface. The depth of the stratum of constant temperature is deeper in higher latitudes. Although the depth of damping has not yet been determined for conditions in the study area, methods are being devised for computing it.

Variable X₃, depth to aquifer, is not significant in the analyses involving both flightlines. X₃ was significant when computed for line J-J' only, where there was a considerable variation in depths to aquifers. The range of X₃ data for line H-H' was less which would tend to lower the correlation coefficient in this case.

Variable X₂, depth to water table, is not significant. However, as pointed out earlier, many of the well logs did not have depth to water table recorded. Where X₂ data were not available, a figure was used equal to X₃. In most cases where an X₂ figure appeared in a well log, it indicated a water table above the aquifer. It is known that artesian conditions exist in the area, and that water tables are generally above the top of the water-bearing formation. In calculation of X₃ and X₂ coefficients for line J-J' alone, X₃ was significant but X₂ was not, suggesting that aquifer depth has a greater influence on surface temperature than does the depth to water table.

Variable X₅ is highly significant. Establishing a measure of validity for estimated thermal diffusivity coefficients will be useful in later heat flux computations.

Variable X_6 , topography, is not significant. In connection with predawn flights, the assumption could be made that cold air drainage into low areas could result in cooling the ground surface. Since exploration wells were drilled in high, low, and level areas, the fact that X_6 lacks significance is strong evidence that air drainage was not a factor for this particular mission.

Variable X_7 , depth to bedrock, is highly significantly correlated with density of the film. It is likely that the correlation results from the association of thicker aquifers with greater depth to bedrock. Since aquifer thickness is highly correlated with surface temperature, so is depth to bedrock, since they increase and decrease somewhat in unison.

Figure 3 is an enlargement of a thermogram of the area shown as 1 in section A of Figure 2. The imagery in Figure 3 was obtained on a north-south flightline about one hour later than when J-J' was flown.

Figure 4 is a color-encoded map of the thermogram shown in Figure 3. It was produced with the color-encoding equipment described earlier. The potential of the color-encoding system is obvious when one considers that it offers a means for automatic delineation of classes of information related to optical density. In this case the stratifications are aquifer thickness.

The maximum and minimum temperatures measured by the PRT radiometer in the airplane during this mission were 14.2°C and 17.8°C , respectively. The radiometer has a 2° field of view and integrates an area about 175 feet (53.4 meters) in diameter at an altitude of 5,000 feet (1525 meters).

Information derived from well logs for correlating with surface temperatures has certain deficiencies which is not surprising in view of the fact that the explorations extended over a period of more than 30 years, involving a number of individuals and several organizations. Also, the data were not gathered with remote sensing studies in mind.

The timing of flights, the antecedent weather conditions, and those occurring during the mission are critical factors. The optimum timing and conditions are:

1. A flight date in late winter or early spring for maximum upward, and late summer or early fall for maximum downward temperature gradients.

2. A period of low temperatures in winter and high temperatures in summer for several days, with minimum cloud cover, prior to and during the mission to create larger temperature gradients, and greater surface contrasts.
3. Clear weather with low humidity, and a minimum of haze, aerosols, etc. When the sky is cloudy the amount of solar radiation is sharply reduced. Thus there is less energy available to heat the soil during the day. The base of a cloud radiates with nearly black-body intensity for its temperature. During the night hours, this return flux from the cloud reduces to almost zero the net radiation loss from the ground surface and thus reduces the fall of air and soil temperature below that expected on a clear night.
4. Very little or no snow cover over aquifers. Snow, because of its low heat conductivity, acts as an insulator and reduces to almost zero the amplitude of the temperature fluctuations in the soil. During periods of extremely cold air temperatures, the soil is kept much warmer than it would otherwise be by this insulating blanket. When the air temperature is at or above the melting point of ice, much of the heat energy of the air and radiant energy of sun and sky are used to melt and evaporate the snow, and thus are unavailable to warm and thaw the upper soil layers [1].
5. Very little antecedent rainfall. Rain can be expected to reduce or completely obliterate temperature anomalies produced by shallow aquifers. The downward movement of water of uniform temperature will erase the anomaly temporarily, or reduce it to a size that is almost indistinguishable. Generally, the more permeable the soil, the more easily the anomaly is lost by infiltration of rain water, and the less precipitation necessary to erase the anomaly.
6. Surface wind velocity of less than 5 to 7 knots if possible. Temperature anomalies associated with shallow aquifers are of the order of no

more than 2 or 3° C. Convection and conductance of heat caused by air turbulence can be expected to eliminate temperature anomalies of that magnitude.

7. A difference of more than 3 or 4° C between ambient temperature and dew point temperature at flight time, to avoid the possibility of dew, frost or fog.

The many important factors to consider in scheduling remote sensing aircraft to obtain usable data for this particular remote sensing application are obvious from the foregoing.

SUMMARY

This continuing remote sensing study of shallow aquifers leads to these conclusions for late summer, predawn missions.

1. Dynamic thermal changes near the earth's surface can be used for thermal infrared sensing for detection of shallow aquifers in glacial drift.
2. Surface soil temperatures along the flightlines varied between 14.2° C to 17.8° C, on the August 5, predawn flight. Cooler temperatures were associated with the occurrence of shallow aquifers. Statistical studies indicated, under favorable conditions, that surface temperatures may be used to predict certain features related to the occurrence of shallow aquifers. They were aquifer thickness, thermal diffusivity coefficient, and depth to bedrock.
3. The timing of remote sensing missions -- diurnally and seasonally -- and the optimum meteorological conditions occurring prior to and during the mission, are critical insofar as night thermal missions are concerned. Optimum conditions for daytime missions, though important, are not so stringent.
4. Numerous aircraft missions conducted in connection with this study have demonstrated that repetitive flights made under variable conditions of time of day, seasons, and soil and vegetation, produce

additional evidence to verify the occurrence of shallow aquifers.

5. Imagery from this study, along with ERTS-simulated imagery, indicates the feasibility of applying ERTS A and B data to reconnaissance studies for detection of shallow aquifers.

REFERENCES

- [1] Carson, James E., "Soil Temperature and Weather Conditions," ANL-6470, Argonne National Laboratory, Argonne, Illinois.
- [2] Cartwright, Keros, "Thermal Prospecting for Ground Water" Water Resources Research, Vol. 4, No. 2, April, 1968.
- [3] Chase, M. E., "Airborne Remote Sensing for Groundwater Studies in Prairie Environment," Canadian Journal of Earth Sciences, Vol. 6, 1969.
- [4] Dixon, Wilfrid J., and Massey, Frank J., Jr., Introduction to Statistical Analysis, McGraw-Hill, 1957.
- [5] Hedges, Lynn S., "Geology and Water Resources of Beadle County South Dakota, Part I Geology," Bulletin 18, South Dakota Geological Survey, 1968.
- [6] Howells, Lewis W. and Jerry C. Stephens, "Geology and Water Resources of Beadle County South Dakota, Part II Water Resources," Bulletin 18, South Dakota Geological Survey, 1968.
- [7] Myers, Victor I. and Marvin Heilman, "Thermal Infrared for Soil Temperature Studies," Photogrammetric Engineering, October, 1969.

TABLE I

Simple correlation coefficients used to relate variables X_2 , X_3 , X_4 , X_5 , X_6 , X_7 , and X_8 to optical density, D , of negative thermal film. Data from predawn flight on August 5, 1970.

X_2 , depth to water table	0.074
X_3 , depth to top of aquifer	0.094
X_4 , thickness of aquifer	-0.721**
X_5 , estimated thermal diffusivity coefficient	-0.554**
X_6 , topography	N.S.
X_7 , depth to bedrock	-0.595**
X_8 , type of bedrock material	0.142

**correlation coefficients significant at the one percent level.

N.S. - not significant

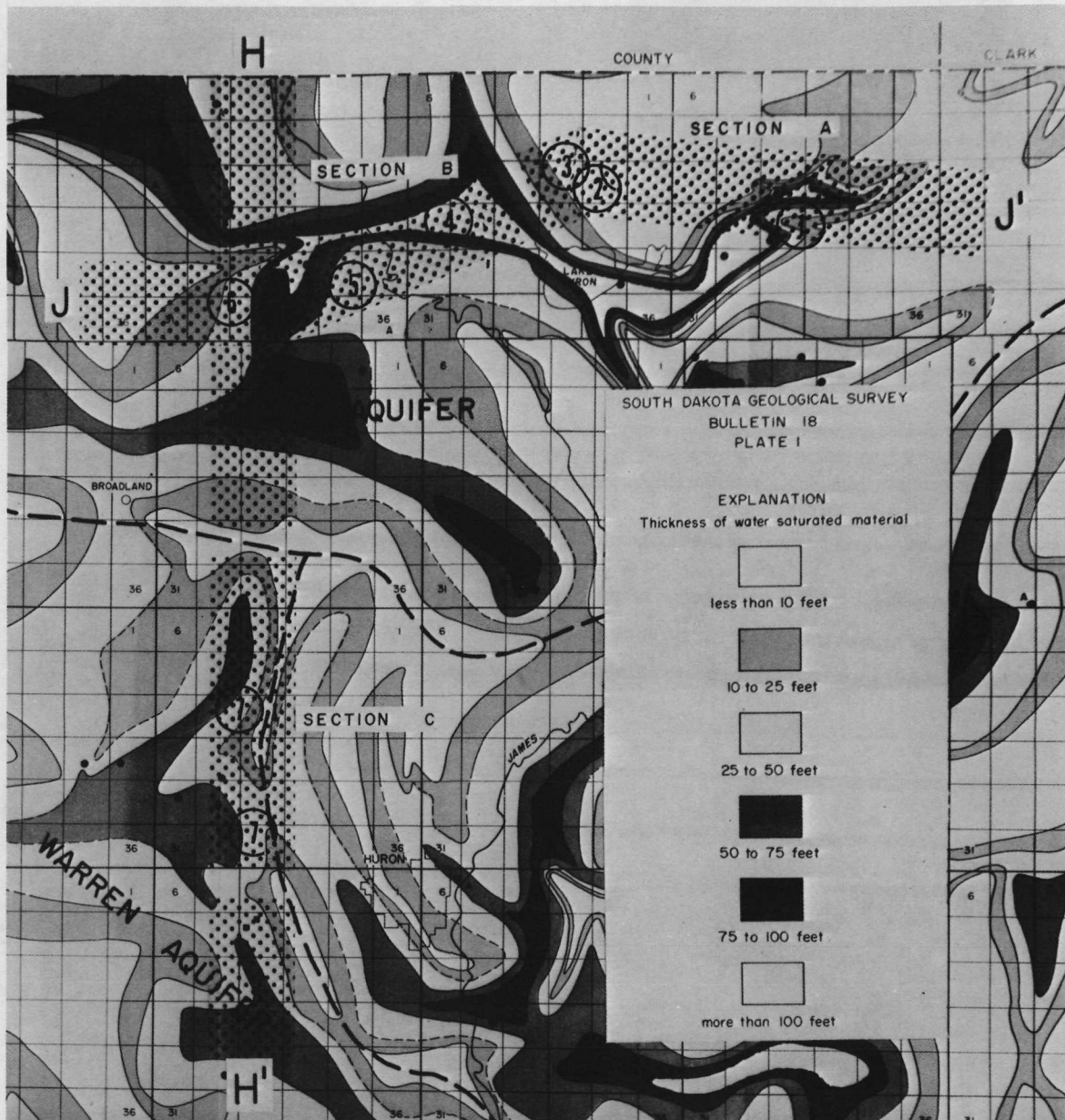
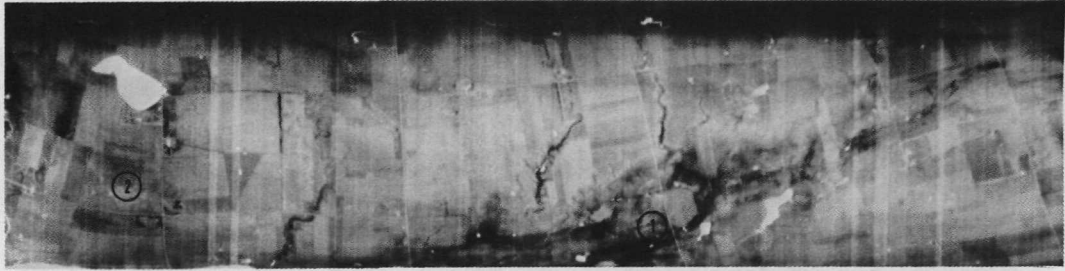
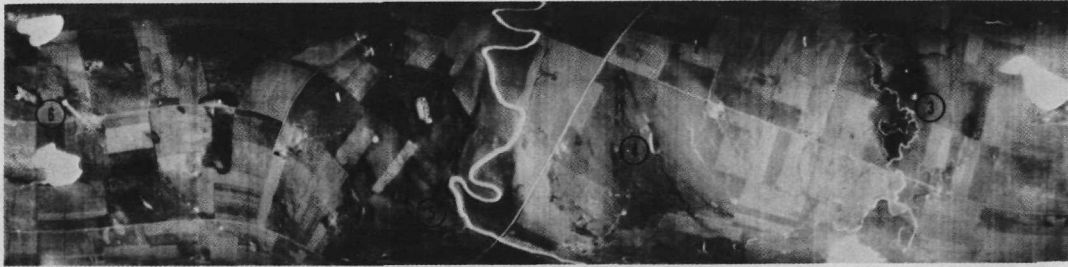


Figure 1. Portion of Beadle County South Dakota showing thickness of water-saturated material in surficial deposits and location of predawn flightlines on August 5, 1970.



SECTION A



SECTION B



SECTION C

Figure 2. Thermograms of sections of flightlines J-J' and H-H', shown in Fig. 1. Dark areas indicate location of possible shallow aquifers (4.5 to 5.5m μ).

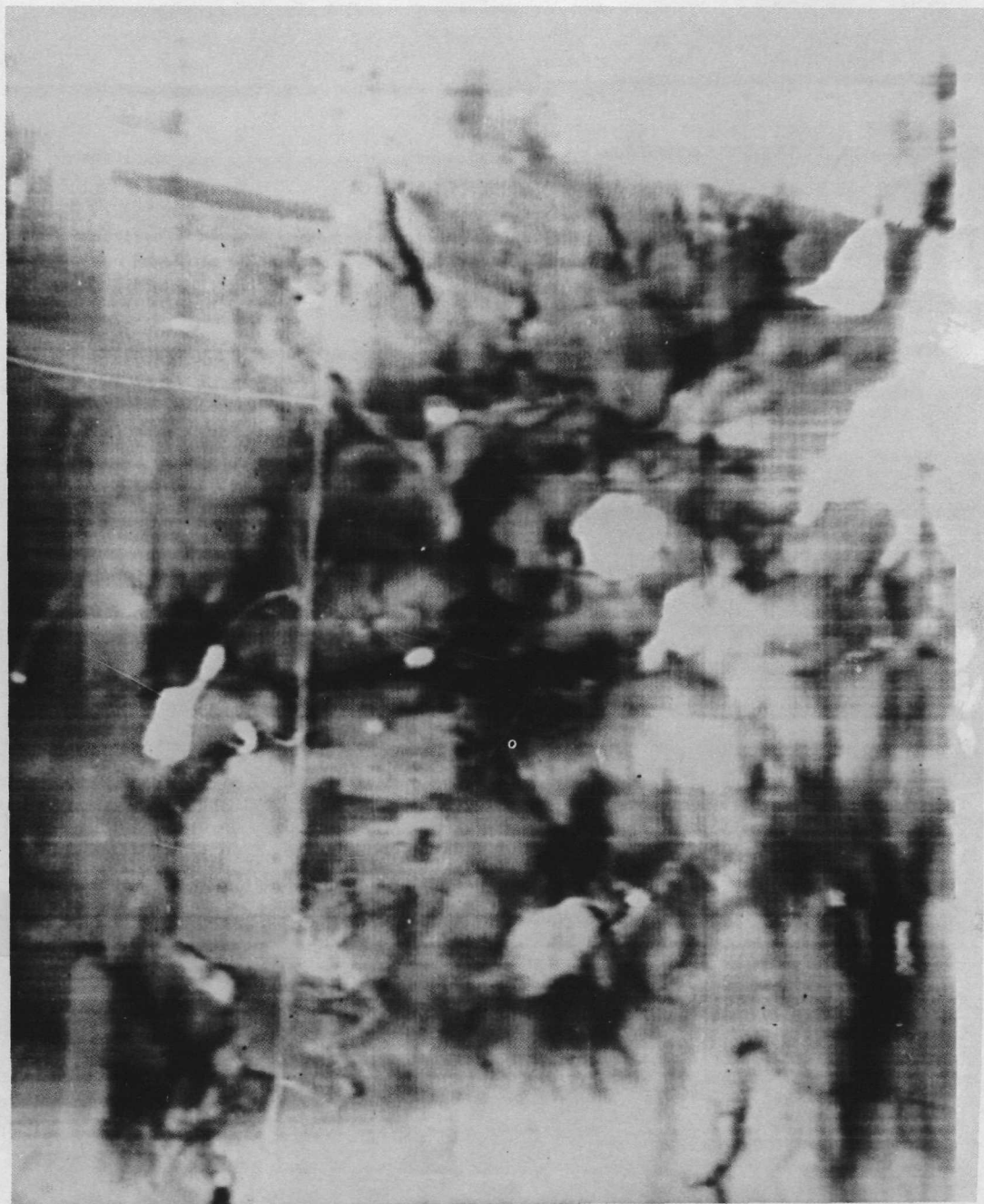


Figure 3. Enlarged thermogram of area shown as ① in Section A of Fig. 2. Obtained on a N-S flightline slightly later than when J-J' was flown.

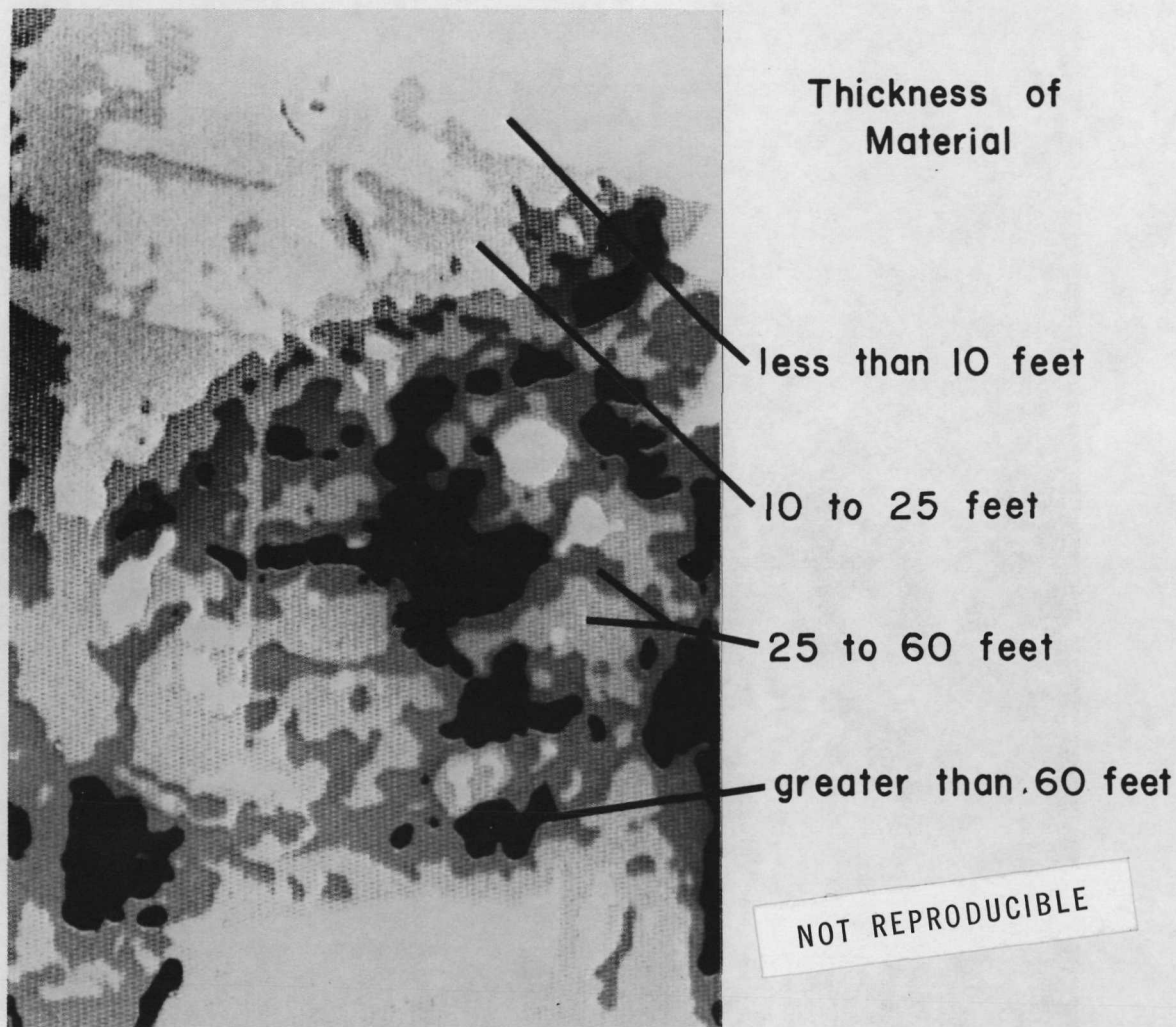


Figure 4. Color encoded map of Fig. 3. Areas with different colors represent various thicknesses of saturated buried aquifer material.

SUMMARY -- REMOTE SENSING SOIL MOISTURE RESEARCH
December 1970

by

Fred A. Schmer, Hydrologist
Hal D. Werner, Research Assistant
Fred A. Waltz, Data Handling

Remote Sensing Institute
South Dakota State University
Brookings, South Dakota 57006

INTRODUCTION

Knowledge of soil moisture conditions is of prime importance to the management of water resource systems. Remote sensing may be able to provide considerable additional information to our water resource managers. Of special concern to agriculture is the ability to evaluate soil moisture conditions in order to enhance our production potential.

During the 1969 and 1970 growing seasons research was conducted to investigate the relationship between remote sensing imagery and soil moisture. The research is being accomplished under two completely different conditions; (1) cultivated cropland in east central South Dakota and, (2) rangeland in western South Dakota. Aerial and ground truth data are being studied and correlated in order to evaluate the moisture supply and water use. Results show that remote sensing is a feasible method for monitoring soil moisture.

RESEARCH UNDER CULTIVATED CROPLAND CONDITIONS

1969 RESEARCH EFFORT

Methodology

The study area for the cultivated cropland condition was located on the South Dakota State University Redfield Irrigation Farm in north central South Dakota. In 1969 soil moisture was studied on various crops on the irrigated part

of the experimental farm. The experiment was designed on the basis of correlating data from sensors on repetitive flights with data taken on the ground. Sensors which were flown include the optical mechanical thermal scanner, the gang of four Hasselblads, and the precision radiation thermometer. Least squares analysis of variance was computed on optical density data as read by a Macbeth densitometer. Days, as a source of variation, was very significant, as were crops and days by crops.

Results and Conclusions

Conclusions drawn were that extraneous variation, namely varying levels of incoming radiation and film processing, affected the optical density to a large extent. Regression analyses on a within day basis yielded large r^2 values of .95 to .97 for each of the days in question.

Simple correlations between Ektachrome infrared optical density and the moisture profile were .7 using a neutral filter, .7 with the red filter, and .02 using the green filter. This leads to the conclusion that in the tri-layered film, the infrared layer was most effective in delineating the moisture profile. However, in the Ektachrome MS film the correlations were .5 to .7 for all four filters. The thermal relationship to depth profile was .021 or extremely low. This occurred in the corn field and leads to the conclusion that the corn canopy effectively destroyed the correlation between the thermal optical density and the depth profile or moisture profile. However, the opposite occurred when the area was fallowed. The correlation between thermal and the moisture profile was .857 in the fallow field. This leads to the conclusion that thermal scanning in the infrared region is highly useful for delineating soil moisture where no crop canopy exists to destroy its affect. However, Ektachrome infrared film is superior where there exists a viable crop canopy and should be used in this manner.

1970 RESEARCH EFFORT

Methodology

In 1970 the study area was reduced in size, different soil moisture conditions were included by the addition of irrigated and non-irrigated plots, and only one crop, grain

sorghum, was used. Besides the irrigated and non-irrigated sorghum, a fallow plot was incorporated into the design as a reference. The field experimental setup is given in Figure 1.

Detailed ground truth data from the field were collected, including soil moisture by soil sample and neutron scattering, soil tension, crop and soil conditions, 35 mm ground photos, incoming and net radiation, and intensive weather data such as rainfall, wind, and temperature. Most of these were directly recorded in digital form.

Aerial data collection was planned in order to correlate closely with data collection from the future EROS projects. The film-filter combinations used correspond to the same general segments of the spectrum as the ERTS satellites. One color and three black and white films were used. Color reversal film was used with three-layer response in the green, red, and near-infrared regions of the spectrum. The black and white films were filtered for corresponding bands. A thermal scanner provided infrared imagery in the region from 4.5 μ m to 5.5 μ m. Incoming and reflected radiation was recorded generally by three solameters filtered in the green, red, and near-infrared portions of the spectrum. In addition, specific weather conditions relating to cloud and haze conditions were recorded at the time of each overflight.

Both aircraft and ground truth missions were scheduled so that the data taken would be most effective in analyzing changes in soil moisture. Missions were planned as soon before and after irrigations as possible and at other critical times of soil moisture and plant maturity. Thirteen aerial missions were flown in 1970 from shortly after plant emergence until just before harvesting of the sorghum. Flight altitudes were at 1000, 2000, and 5000 feet above ground level. Ground truth was collected during each overflight and at other selected times.

Imagery analyses are presently being performed by three methods: (1) visual interpretation, (2) film density measurements, and (3) use of a color encoding film density analysis system specifically designed for imagery interpretation. The timing of this report is such that data analysis has not been completed. However, visual observation of the imagery does allow interpretation of moisture differences during periods of plant stress.

Final analysis will be accomplished by correlation of film densities, and the output from the color encoding density analysis system, with the ground truth data. The overall difference between the total soil moisture supply within the irrigated and non-irrigated sorghum was smaller than expected. Soil moisture differences were substantial in the upper two feet of the profile, but the differences tended to disappear with increasing depth in the profile. The presence of this subsurface moisture could be attributed to the fact that the area with non-irrigated sorghum had been irrigated in preceeding years. Therefore, the non-irrigated sorghum was never severely stressed. Yield results of 7375 pounds per acre for irrigated and 5766 pounds per acre for non-irrigated, or only 21.8 percent difference, supports this theory.

Results

The preliminary results indicate that the soil-crop combination can provide information as to the changing moisture conditions throughout the season. Imagery analyses appear to show that the sorghum will provide an adequate indication of the available soil moisture. While the spectral reflectance of the soil seems to indicate only surface moisture, the crop relates moisture conditions of the soil profile, especially with increased plant maturity.

RESEARCH UNDER RANGELAND CONDITIONS

1970 RESEARCH EFFORT

Water resources is of prime importance to range management. The location and management of water in range areas is many times the ultimate control of stock numbers. Availability of soil moisture is the determining factor in range production. Therefore, during the 1970 growing season a research effort on rangeland conditions in western South Dakota was initiated. In this research effort we are concerned with the delineation of water resources in rangeland.

Methodology

This research effort is being conducted on the South Dakota State University Cottonwood Range Field Station. This

experimental station comprises approximately 2,640 acres located in west central South Dakota approximately 75 miles east of Rapid City. Figure 2 depicts the layout of the experimental station. The six summer pastures are the area of interest in this study.

This research is being accomplished as a cooperative effort with the Animal Science Department at South Dakota State University. The ground truth data to be utilized in the analysis of the remote sensing data are being collected by other active research projects at the station. The collection of ground truth data has been fully coordinated with the collection of remote sensing data.

Biweekly soil moisture data are being collected with a neutron probe to a depth of at least four feet and gravimetric sampling is also being utilized at the shallower depths. Soil temperatures to a depth of 150 cm are obtained daily. Evaporation from a standard weather bureau evaporation pan, maximum and minimum temperatures, continuous recording of humidity and temperature in a standard weather bureau shelter, wind velocity and solar and sky radiation are being recorded. Precipitation is measured with a standard weather bureau recording rain gage. Soils are being described including mechanical analysis, moisture release curves, bulk density, soil organic matter and exchangeable cations by horizons. Above ground biomass is being determined at two week intervals during the period of rapid growth from approximately May 15 to August 15 and at approximately monthly intervals during the remainder of the year except when snow cover prevents sampling. Below ground herbage biomass is being determined at monthly intervals during the period of active growth and at two month intervals the remainder of the year except when frozen soil or snow cover prevents sampling.

Remote sensing data collection missions were made on June 9, 1970, July 7, 1970, August 4, 1970 and September 3, 1970. No data were obtained on the August 4, 1970 mission because of unfavorable cloud conditions. The missions were scheduled during the time period when below herbage biomass was being collected (all other data were also collected at this time) in order to obtain the maximum amount of ground truth data during the approximate time of the overflight. Multispectral imagery compatible with the ERTS A and B film-filter combinations, reflective and incoming radiation data and thermal scanner imagery were scheduled to be collected on each mission.

Imagery Analysis

Analysis of the first year data will be primarily directed toward interpretation of the remote sensing data as it relates to grazing conditions and available soil moisture. Densitometer measurements obtained with a Macbeth Model TD-404 densitometer, and soil moisture data, will be statistically analyzed. A Spatial Data Systems color encoding system will be utilized in interpreting the imagery for grazing conditions and soil moisture. The various remote sensing imagery collected will be evaluated for its effectiveness in determining the resource management factors under study.

Due to the limited amount of available processed ground truth data no detailed analysis of the data has been accomplished as of the writing of this report. However, some visual relationships are evident. As time progresses during the summer season the effect of grazing intensity is evident. Ungrazed areas in pastures 2 and 4 are also easily identified. The black and white imagery with the green filter (number 58) and the color infrared imagery show the grazing practice differences quite well. Pastures 1 and 4 have been heavily grazed, pastures 2 and 5 moderately grazed, and pastures 3 and 6 lightly grazed. Figure 3 is an example of the imagery collected. Figure 3 is a print made from black and white Plus-X film filtered with a 25A Wratten filter. Soil type differences are best identified on the black and white film with the red filter (25A) and these data will be fully interpreted at a later date with the available soils survey of the area.

Results

Preliminary results from the remote sensing data are quite encouraging. Different grazing intensities are quite evident on the imagery. Considerable analysis needs to be accomplished before any conclusions and/or recommendations can be made. The ground truth data and the remote sensing data will be statistically analyzed as soon as the ground truth data is available. The Spatial Data Systems color encoding system will be used for the soil type study and the aerial moisture distribution study.

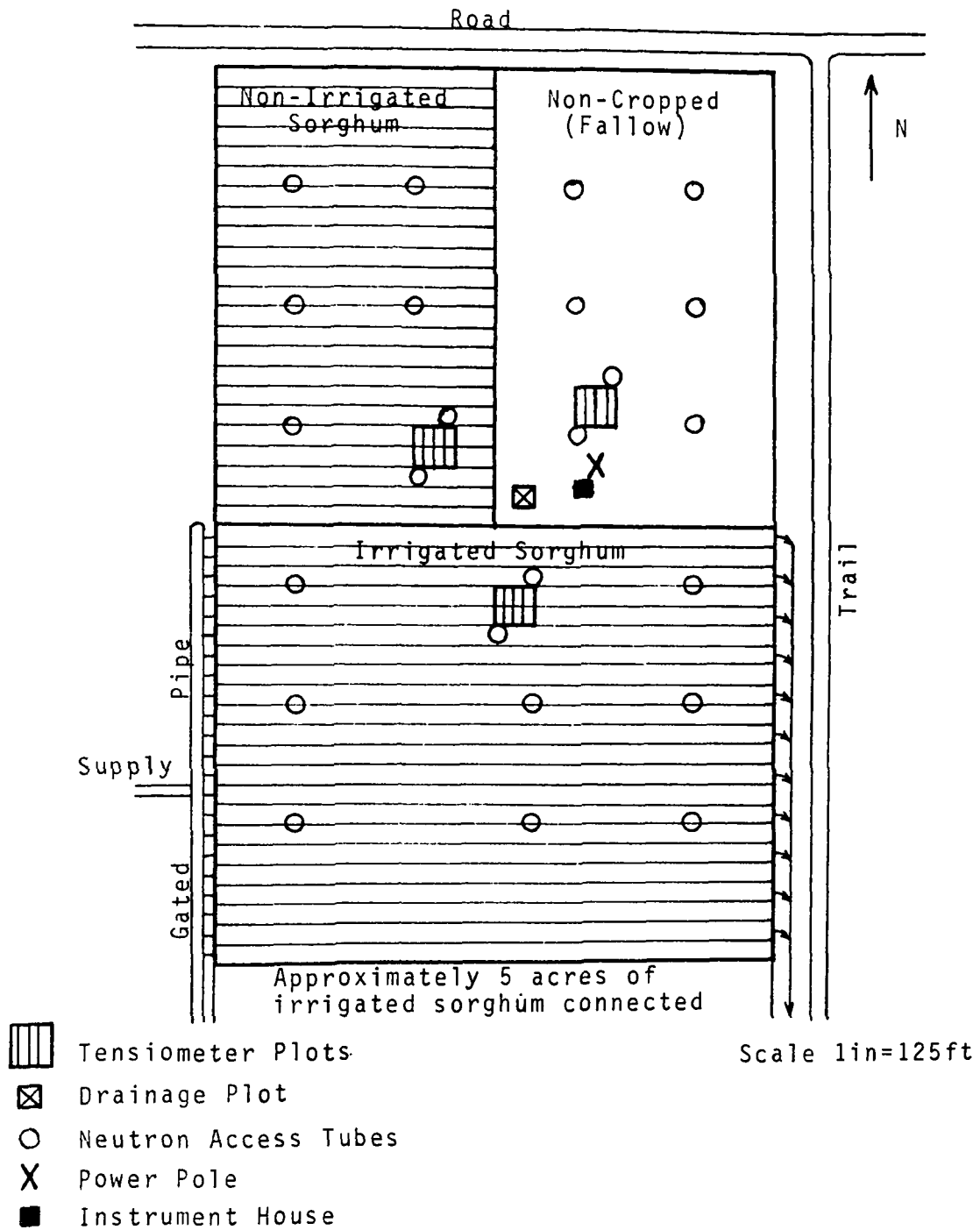


Figure 1. Experimental ground setup for remote sensing soil moisture research under cultivated cropping conditions.

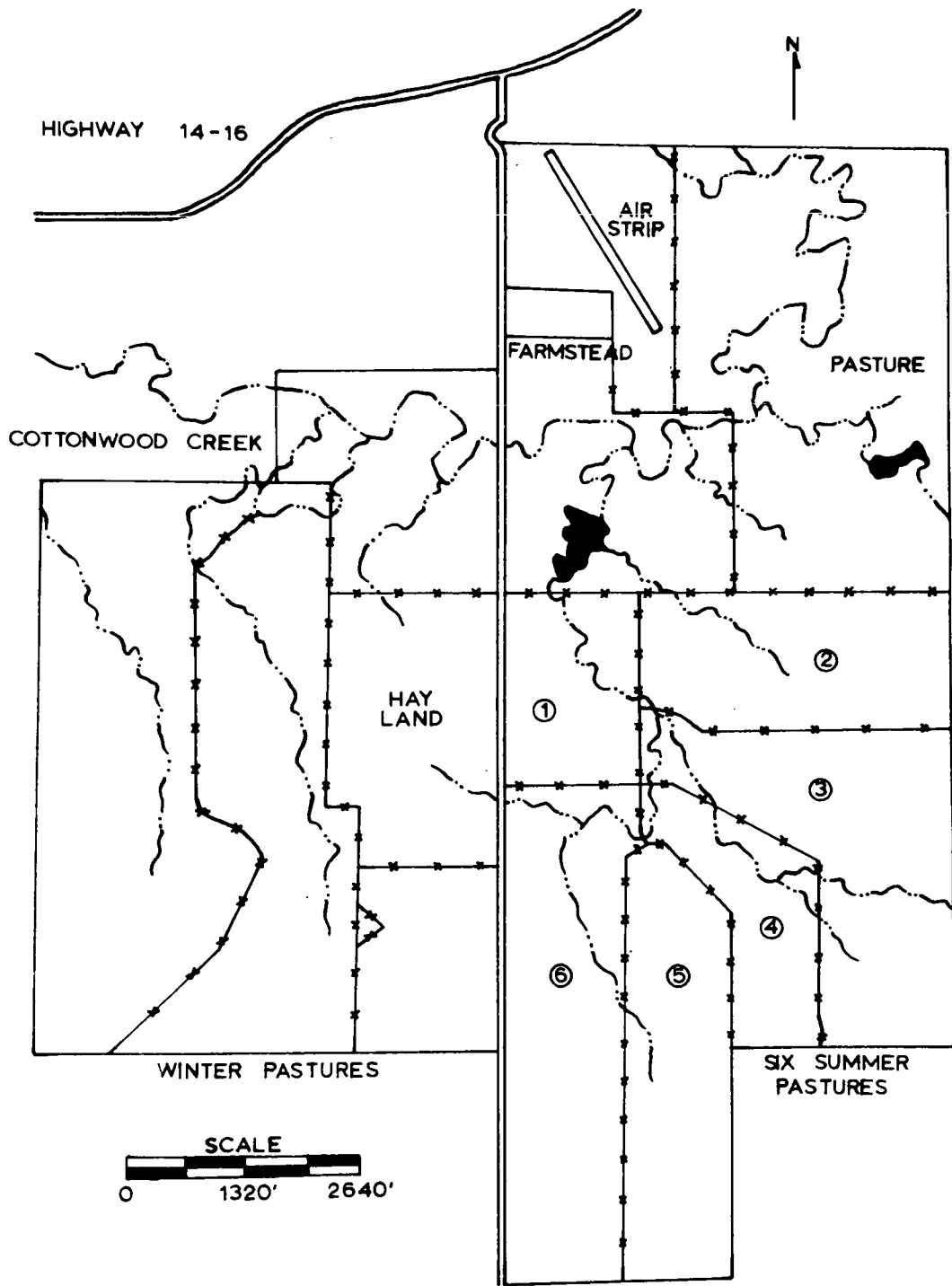


Figure 2. South Dakota State University Cottonwood Range Field Station, Cottonwood, South Dakota.

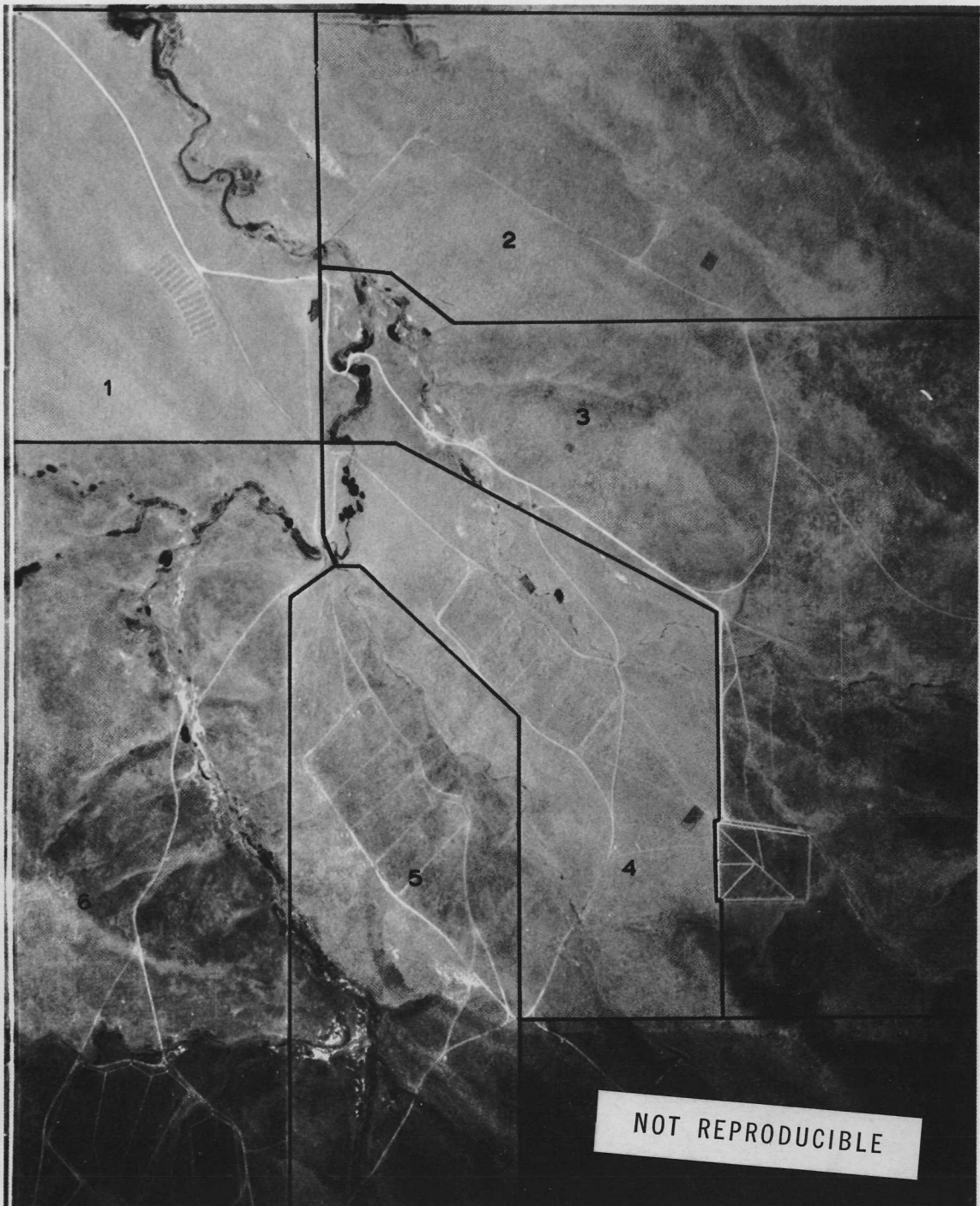


Figure 3. Six summer pastures on South Dakota State University Cottonwood Range Field Station printed from black and white 70 mm Plus-X filtered with a 25A filter.

MEASUREMENT OF PLANT COMMUNITY COVER
FROM AERIAL PHOTOGRAPHS USING
EKTACHROME INFRARED AERO FILM 1/

by

Raymond M. Turner 2/

INTRODUCTION

Color-IR (infrared) aerial photographs of arid-zone vegetation have been used to estimate the amount of green plant material on the ground. The purpose has been to estimate plant cover as it varies with time and space and relate this vegetative measure to hydrologic conditions.

Aerial photographs of the 6,000-acre target area were taken periodically during the past 3 years. The study site is a 15-mile reach of the Gila River valley, San Carlos Indian Reservation, Arizona and is part of the U.S. Geological Survey's Gila River Phreatophyte Project (Culler and others, 1970) under the general direction of R. C. Culler, research hydrologist.

METHODS

Kodak Ektachrome Infrared Aero (EKIR) Film, Type 8443, in 9-inch format was used. Photographs were taken in 1968, 1969, and 1970 from elevations of 8,500, 3,600, and 1,500 feet above ground surface. The photography and film processing was done by the U.S. Geological Survey.

The data collection program was supported by NASA and is supplemental to the NASA aircraft program because the coverage needed could not be scheduled for the Houston-based aircraft. The K17 camera used by the USGS was equipped with a 6-inch Metragon lens. Three Wratten filters, numbers 12, CC20B, and CC30M, were used for all photography.

1/ Publication authorized by the Director, U.S. Geological Survey.

2/ Research Botanist, U.S. Geological Survey, Tucson, Arizona

As with the previous year's work (Culler and Turner, 1970), the film images were analyzed by use of a transmittance densitometer. As a new approach, data in the current year's report are expressed in terms of adjusted transmittances which have been calculated from "analytical densities." The data manipulation attempts to accomplish the following: (1) calibrate and standardize all photography so that photographs taken on different dates may be directly compared; and (2) derive a parameter from the films that is directly proportional to the green plant tissue. It should be emphasized that the photographic process is affected by many variables which have been assumed constant in the analysis. Conversion of integral densities to analytical densities is only semi-quantitative; however we hope in the next year to obtain the necessary photoscience support to correct this deficiency.

Three different sets of ground-truth data are being evaluated. The first is estimates of plant volume determined, as noted in an earlier report (Culler and Turner, 1970), by broadly classifying the vegetation into volume classes based on a combination of field reconnaissance observations and estimates from black-and-white aerial photographs. Because the ground truth is based in part on aerial photographs, it does not provide a wholly independent description of conditions on the ground.

A second set of ground-truth data represents estimates of plant foliar coverage. These values are independent measures of plant ground cover and are arrived at by estimating, in the field, plant coverage with 2 x 5 dm (decimeter) plots. These small plots are located within four plant communities on or adjacent to the Gila River Phreatophyte Project.

The third set of ground-truth data are evapotranspiration values measured at three stations by the energy-budget method.

The densitometric data are expressed as "adjusted red transmittance values." These values, derived from analytical densities on the IR photograph, are defined as the red transmittance (obtained when using the red filter, no. 92), divided by the sum of the transmittances in the red, green, and blue spectral bands, (Wratten filters number 92, 93, and 94, respectively). Each adjusted transmittance is derived from a single area on the photograph.

The rationale behind the use of red transmittances, adjusted as we have done, is based upon the premise that most of the scene reflectance that is expressed as red on the photographs is proportional to IR reflectance from the plants.

RESULTS AND DISCUSSION

Adjusted red transmittances during late March to late December 1968 are shown in figure 1. The curves represent adjusted densitometer readings.

from three separate volume categories of saltcedar. (The data upon which these curves are based were presented in different form at the Second Annual Aircraft Status Review Meeting). Differences with time and differences in space are apparently measurable using the data manipulation outlined above. One important item has not been tested, however; how well do the adjusted densitometer values represent plant foliage cover?

To make a valid comparison between the adjusted transmittances and plant cover, we needed a coverage measure acquired without the use of aerial photographs. To do this, 60 plots 2 x 5 dm in size were established in each of four different plant communities. The plots were spaced 1 meter apart along four 5-meter lines. At the time of each photographic mission foliar coverage was estimated on the 60 plots in each plant community. (Foliar coverage may be conceived as the sum of the shadows that would be cast by green leaves and green branchlets if the sun were at zenith and expressing the value as a percentage of the soil surface covered.) From these values an estimate is obtained of the foliar coverage of the entire community. Because foliar coverage estimates are difficult to make where plants are tall, work has been concentrated in plant communities of low stature that occur within or adjacent to the Gila River Phreatophyte Project.

We made ground-truth measurements on 11 different dates during 1970 but obtained photography on only three of these dates (Fig. 2). The lack of better photo cover is due partly to a change from EKIR Type 8443 film to Type 2443: color-IR film was unavailable to us for several months during this change. We are also in the process of changing camera systems, resulting in further photographic coverage loss. On two dates for which we have acquired ground truth, NASA photographed the target area from about 60,000 feet. We have not yet received these data.

The scanty data are not exactly compelling but we are moderately encouraged by them. Foliar coverage values, expressed as percentage of ground surface covered, appear to be of about the same order as the adjusted transmittance percentages (fig.2). Both values are high (80-90 percent) in the dense alfalfa-barley field and both are lower in the other, more open, plant communities. The correspondence between transmittance and foliar coverage is closest in the two homogeneous cultivated communities. That the differences are greater in the relatively heterogeneous wildland communities (creosotebush and whitethorn) may be the result of sampling error--the 60 plots established there may be too few to adequately sample the communities, at least during certain seasons.

The third set of data show evapotranspiration and corresponding adjusted red transmittances for three different plant communities during September and October 1969 (fig. 3). The evapotranspiration values were obtained by the energy-budget method from three installations on the target area. These values were provided by O. E. Leppanen, research physicist, U.S. Geological Survey. The adjusted red transmittances were

derived from aerial photos of the energy-budget stations taken during three flights at an elevation of 1,500 feet above ground. The densitometry (Culler and Turner, 1970) was accomplished with a 1-millimeter aperture which views, on the photographs, a circular area equivalent to 76 square feet on the ground. Four or five readings were taken in the area surrounding each of the energy-budget towers.

Since evapotranspiration comprises two water-loss components, evaporation from the soil and transpiration from plants, the agreement may not always be close between evapotranspiration and values representing plant volume, especially when the soil surface is wet. Such is the case on the last date in the figure: more than an inch of rain had just fallen and, in spite of the presence of little green plant tissue, evapotranspiration increased over the previous date. The October date represents a period of drouth when leaves and green branchlets were still present. By determining plant volume from the photographs, it may be possible to partition the evapotranspiration values into portions attributable to transpiration and to soil evaporation.

CONCLUSIONS

When in operation, orbiting satellites, such as those planned for the ERTS experiment, will have the capacity for determining short-term changes in the appearance of the earth's surface. Weather conditions permitting, a larger part of the earth will be observed at intervals of only a few weeks. Most of the detectable variability will result from fluctuations in snow cover and changes in the amount of green plant material. Measurements of vegetation change occurring within periods of 2 or 3 weeks can be used to pinpoint likely areas for livestock grazing, to help identify crop types and wildland communities, and to estimate primary productivity and evapotranspiration in plant communities. Although measurements of the earth's variable plant cover are of importance to many resource management fields, the actual measurement of the earth's green covering remains one of the most elusive variables with which biologists and hydrologists must deal. The development of suitable techniques to measure this parameter is a challenge for the photographic scientist and for the hydrologist. The work on the Gila River Test Site support this development.

The future objectives of this study will be to further refine the measurements of plant volume by making the necessary sensitometric and environmental measurements for calculating analytical densities.

Film of 70-millimeter format is now being used instead of the 9-inch film originally employed. This change has been made to improve the feasibility of microdensitometric analysis and yet retain a scale that can be viewed with the macrodensitometer in present use. NASA photography from the current and past highflight series will also be analyzed when data are made available.

REFERENCES

50-5

- Culler, R. C., and others, 1970, Objectives, methods, and environment--Gila River Phreatophyte Project, Graham County, Arizona: U.S. Geol. Survey Prof. Paper 655-A, 25 p.
- Culler, R. C., and Turner, R. M., 1970, Relations of remote sensing to transpiration of flood-plain vegetation: Second Annual Earth Resources Aircraft Program Status Review, Vol. III, p. 37-1 to 37-8.

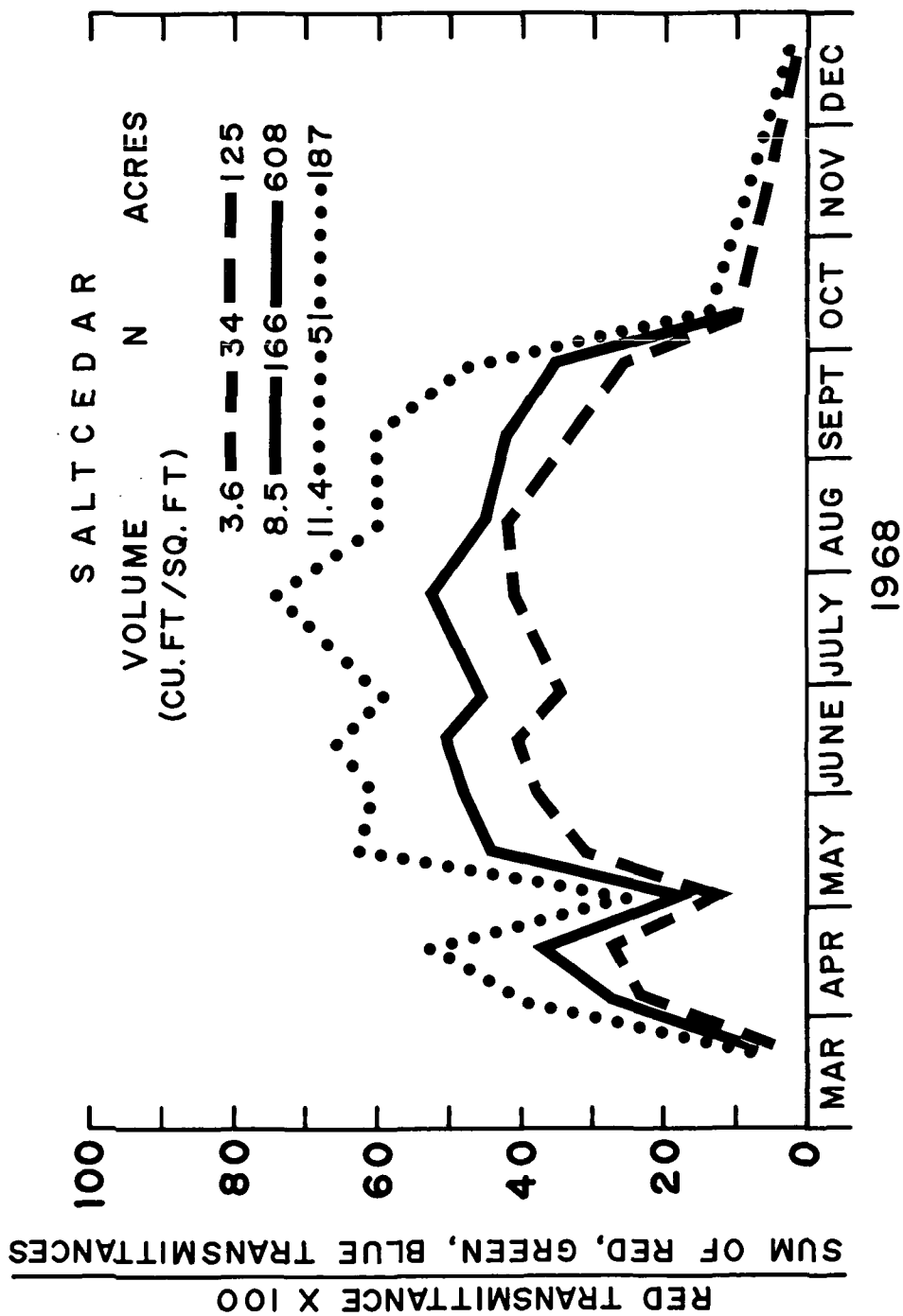


Figure 1.--Seasonal variation of adjusted red transmittances obtained from Ektachrome-IR images of a saltcedar forest, Gila River, Arizona. Data points are mean density values for forest plots representing three different foliage volume classes. N = sample size.

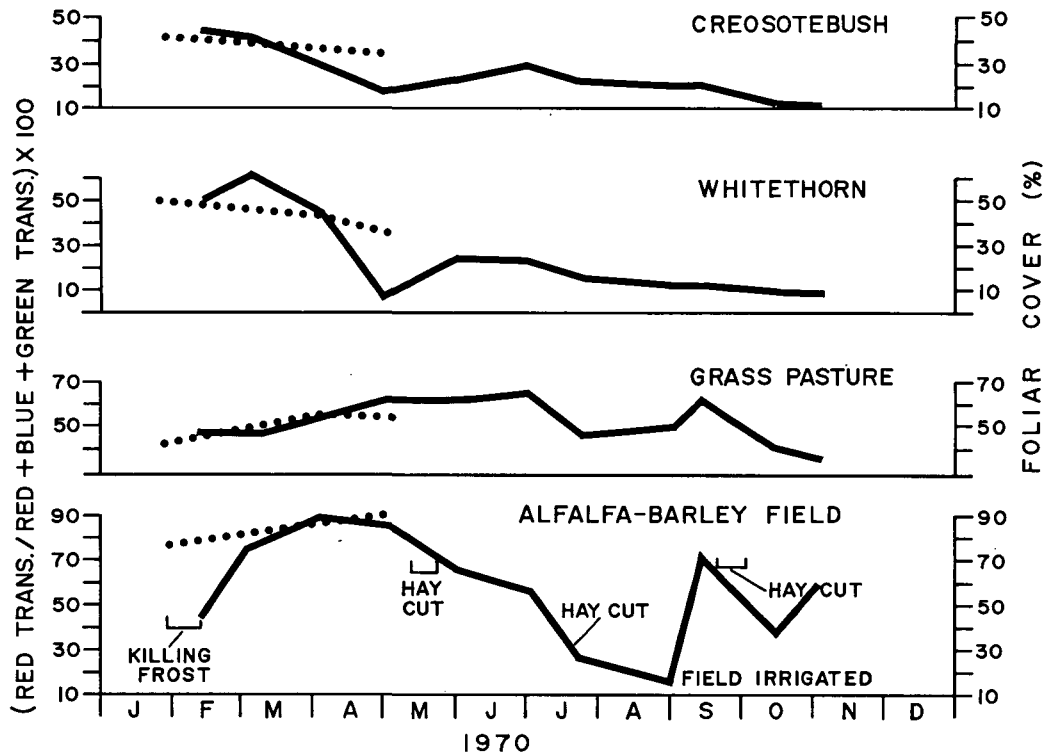


Figure 2.--Comparison of adjusted red transmittances and foliar cover in four plant communities. Transmittance values (dotted lines), were obtained for three dates from 9-inch Ektachrome-IR photographs taken from 8,500 feet above four plant communities. Foliar cover (solid lines), an estimate of the amount of green plant tissue covering the ground, was determined from estimates of 60 small plots in each of the plant communities. The low cover value for February in the alfalfa-barley field resulted from frost damage; cover would have been considerably higher 2 weeks earlier at the time of the first photographic mission.

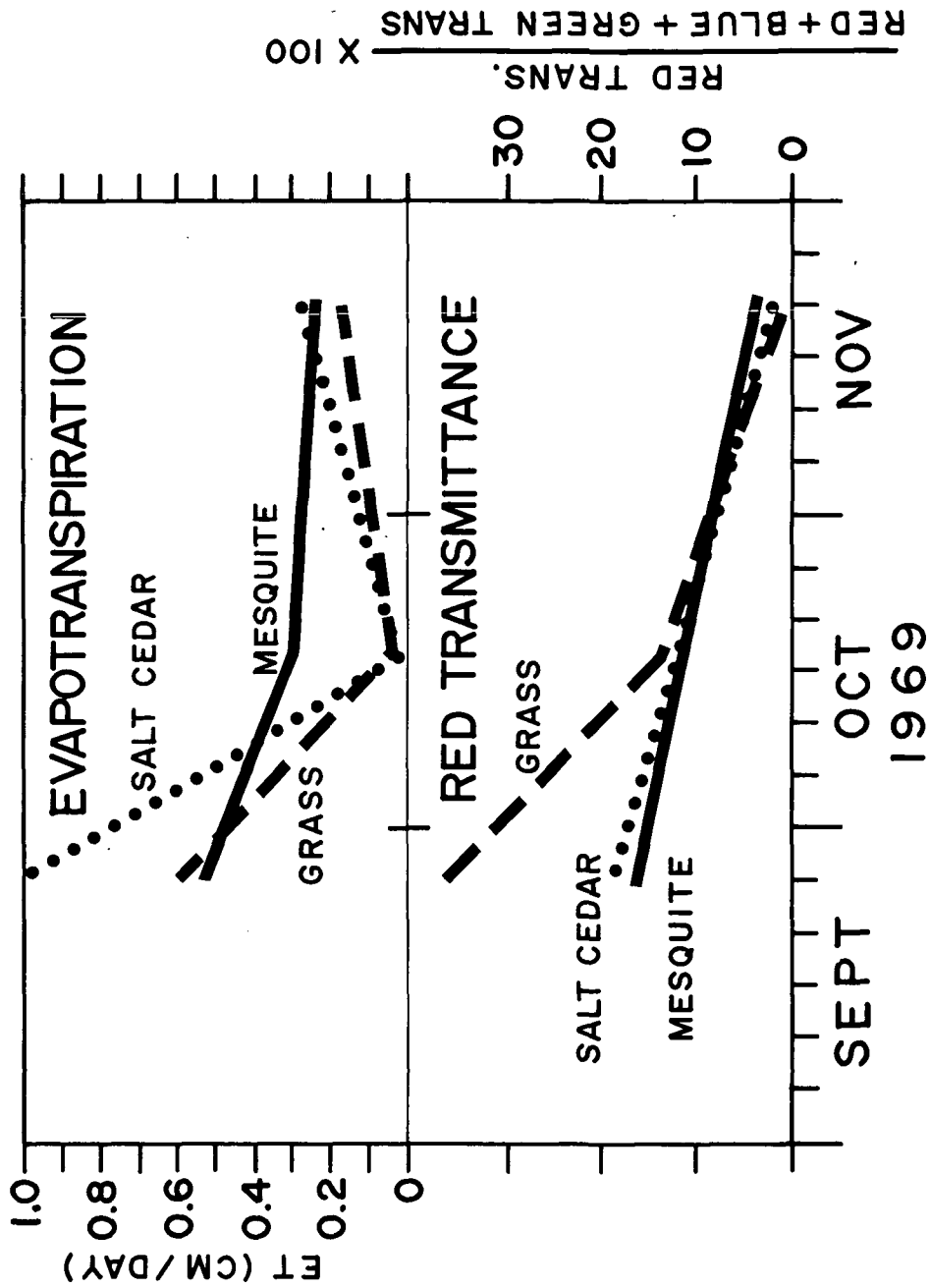


Figure 3.--Comparison of evapotranspiration and adjusted red transmittance in three plant communities on three dates in 1969. Evapotranspiration estimated by energy-budget method. Adjusted red transmittance was obtained from 9-inch Ektachrome-IR photographs taken from 1,500 feet above ground.

EMISSION CHARACTERISTICS OF SNOW AND ICE IN THE MICROWAVE RANGE

by

Mark F. Meier
U. S. Geological Survey
Tacoma, Washington

A. T. Edgerton
Aerojet-General Corporation
El Monte, California

Snow on the ground has very important scientific, practical, and environmental consequences. Not only does it cover about one-third of the land surface of the earth at any one time, it is by far the most variable material lying on the land. Snow can cover 10,000 or even 100,000 km² in a matter of hours, and disappear almost as fast. Its spatial variability, especially in the mountains, is also very great.

Snow reflects solar radiation (it is the material of highest albedo over large areas of the land), causes snowmelt floods, and affects plants, animals, and people in many ways. It is also a resource of great value. For instance, the measurement of the snowpack in the mountain West alone is a program that involves thousands of people and perhaps a million dollars worth of effort each year. The cost of this effort is paid by water users--hydroelectric power developments, irrigation districts, and other groups that need to know the runoff to be expected in the streams when the mountain snowpacks melt.

This resource has important environmental implications. For instance, the amount of Feather River water that can be used to preserve San Francisco Bay vis-a-vis other diversions is directly related to the accuracy with which we can measure the winter snowpack in the Sierra Nevada.

We now know how to measure and monitor this snow at fixed points, using devices that range from the crude snow course to the sophisticated radioactive profiling snow gage. Unfortunately point measurements are not nearly enough to satisfy present day needs. We will never be able to monitor the snowpack with reliability until we can measure the snow not just at a few fixed points but also its broad distribution in time and space. Quite obviously only a synoptic remote sensing program can do this. A big problem here is the fact that the most important changes in the snowpack occur when the atmosphere is cloudy, and therefore a remote sensing system must be devised that can work through clouds. Thus only the microwave frequencies are of any interest. They are of additional advantage over infrared or visual light techniques because the microwave frequencies penetrate below the surface and can

tell us something about the characteristics of the snow throughout its depth, a factor which is of great hydrologic and scientific importance.

This has been known for some time and microwave measurements of snow have been made for a number of years. Unfortunately most of the past work has raised far more questions than it has answered. We now know that snow can be distinguished from many other land surface materials in the microwave region of the spectrum. We also know that microwave brightness temperatures vary as a function of snow wetness, snow depth, snow density, ice layers, and the character of the underlying material. Until the past year most results from microwave snow measurements in the field could only be described as highly confusing.

A 2-year contract between the Geological Survey and Aerojet-General Corporation on the microwave emission from snow has just been concluded. We present here some of the results in terms of new understanding that has been derived, as well as several large enigmas that still remain which may be basic to other microwave observations of layered granular materials. This study included theoretical studies, laboratory measurements of electrical properties of snow and similar materials, numerical modelling of hypothetical and real snowpacks, analysis of microwave data obtained on overflights, and, most important, careful quantitative measurements of natural and artificial snowpacks made in the field.

The critical problem was separating the effects on microwave emission of the various individual snow characteristics. Therefore almost all of the work of the past year was directed to this problem, and the progress has been encouraging.

The results have come slowly because of a number of important difficulties. First of all, liquid water in snow has a complex effect and does not appear to behave as simply as liquid water in soil. Second, natural snowpacks are invariably inhomogeneous so that the ground truth problem is one of sampling the snow exactly where it is being seen by radiometers. Third, snow is a difficult laboratory material to work with, and because of the thermodynamic constraints it is virtually impossible to work with homogeneous wet snow in the laboratory. Fourth, we have not yet been able to find an accurate method of measuring the liquid water content of snow in the field.

Attempts were made to measure the dielectric constant of several dry snow samples using an ellipsometer. Although caution should be exercised in using the results (the snow samples were inhomogeneous and the ellipsometer is strictly valid only for homogeneous samples)

a value near 1.9 was obtained for the real part of the dielectric constant for each sample. The total mass per volume of the snow samples did not vary significantly from 0.5 g cm^{-3} and the temperature during measurement was below freezing. The dielectric constants of air and ice (the limiting values for snow) are well known and our results also agree with other laboratory measurements of artificial snow. The imaginary part of the dielectric constant of dry snow was found to be so low--less than 0.01--that it could not be measured with an ellipsometer. The work of others suggests that this parameter may be a function of frequency and some tentative values have been determined. No measurements were made of dielectric constants of wet snow because this is virtually impossible to do in the laboratory; simple reflectivity measurements were made and considerable information was derived on scattering and surface reflection coefficients.

In the field we carried out experiments this past winter in which almost all snow variables could be held relatively constant except one, resulting in measurements which can be directly compared with analytic models. Figures 1A and 1B show the setup of one of our field experiments conducted at Crater Lake, Oregon. This involved measurement of an artificial snowpack made by laboriously collecting, disaggregating, and spreading snow over a bare soil surface. Field experiments were conducted at microwave wavelengths of 0.8, 2.2, 6 and 21 cm.

Perhaps the most significant experiment that we have yet performed in the field is shown in Figure 2. Microwave brightness temperatures at three different frequencies and two polarizations are plotted as a function of increasing snowpack mass or water equivalent. The smooth and pronounced response of brightness temperature as the snowpack builds up is very gratifying because it does indicate that microwave brightness temperatures can, under certain conditions, be used to directly measure the water equivalent of a snowpack. Water equivalent is the parameter of greatest hydrologic and glaciologic importance. Note that at a wavelength of 0.8 cm the brightness temperatures changed by 50° as this modest little snowpack was built up. Unfortunately the 21-cm radiometer was out of action due to a bad switch and an absolute calibration for the 6-cm radiometer was not available, but we feel that its relative values are correct. The crosses represent the probable errors in the instrumental measurement of brightness temperature and the variation of snowpack thickness and density.

Now we should ask if these changes can be explained qualitatively or quantitatively. Fortunately it is now possible to attempt a quantitative explanation. Stogryn of Aerojet-General has just developed a theory for the microwave emission from layered media, and has adapted this theory to numerical calculation of a snowpack lying over soil,

using the determined electrical properties of snow. Figure 3 shows a typical result in the form of a plot of brightness temperatures versus snow depth (or water equivalent) of dry snow. The curves for other frequencies, snow densities, and soil types are similar (dry soil produces less oscillation and lower frequencies show oscillations of higher amplitude). This graph has two obviously discouraging features: first and foremost, the brightness temperature increases as depth increases and this is not what we see in nature except at the shallowest snow depths. Second, the graph shows numerous oscillations. These are apparently due to multiple reflections from the perfectly sharp, planar boundaries assumed in the numerical model. These oscillations do not occur in our results from snow measurements we then had to face the problem of modifying the theoretical or numerical model to account for more realistic boundaries. First, we tried to incorporate the effects of random inhomogeneities or scattering in the theory but this difficult job could not be accomplished in the time available. At the last minute we tried a substitute approximation. We know that all boundaries in nature are irregular and to some extent gradational so we tried numerical modelling of this field experiment using boundaries which were gradational over a range of a few centimeters. The latter model does eliminate the wild oscillations due to the smoothing effects of a continuous gradation in the dielectric constant near boundaries, but the resulting curve still does not match the field measurements.

Part of the problem is the effect of snow density. As the depth of the snowpack increases in the field, compacting of the lower layers produces an increase in density. Our numerical modelling shows that for a constant depth an increase in density causes the brightness temperature first to increase and then to decrease. A typical result is Figure 4. This effect is too small to account for the strong drop of brightness temperature with depth at high frequencies as measured in the field.

The same problem can be illustrated with an analysis of microwave data obtained from an overflight--in this case a flight over Mount Rainier by the NASA Convair 990 with a 1.55-cm microwave imager. As indicated in Figure 5, there is an enormous scatter in the data and furthermore if there is a trend in the data it does not seem to follow very closely the results predicted by theory. Unfortunately one cannot make definitive experiments out of these overflight data. The snow is different at the location of each resolution element, and we could not possibly measure all the properties of the snow at all of these places. In this case, the airplane flew over an area where no ground truth data existed and we had to extrapolate snow conditions from measurements elsewhere.

Now consider what happens when the snow warms up and liquid water begins to appear. Detection of this condition is very important to hydrologists because no runoff can occur until a water saturated condition is attained. Figure 6 shows the same snowpack as in Figure 2, but after the sun warmed the snowpack and liquid water began to appear at the surface. This produced very large changes in brightness temperatures. The brightness temperature thus indicates rather clearly whether the snow is dry or wet. However, liquid water actually increases the natural brightness temperature of snow, opposite to its behavior in soil. We have obtained virtually the same results by reflectivity measurements in the laboratory and in many other field measurements.

In this case theory and numerical modelling do lend insight into the cause for this interesting phenomena. Figure 7 shows typical numerical results. You note first a sharp rise in brightness temperature followed by a slow decline. This theory indicates that a small amount of free water will not increase the magnitude of the dielectric constant significantly while increasing the loss, so that the emission by soil is not seen. Thus, since the dielectric constant of snow is smaller than that of soil, the effect is to increase the brightness temperature. After the free water has been increased sufficiently, the magnitude of the dielectric constant of the snow begins to increase appreciably and at this stage the brightness temperature begins to decrease.

Figure 8 shows a typical field experiment in which a wet snowpack is built up. This graph is not as interesting as the dry snow results shown earlier. Only the highest frequency shows an appreciable change in brightness temperature (20-25°). However, the other frequencies all show a decrease in the difference between the horizontal and vertical polarized brightness temperatures. The very low frequency radiometer apparently sees the soil even though it is covered by an appreciable fraction of a meter of wet snow.

This program is one of those in which the practical need is very obvious and the backlog of previous work is fairly considerable. However, the problem is so complex that even a sophisticated integrated approach involving theory, laboratory, field, and overflights is yielding quantitative understanding very slowly. This progress, although slow, is gratifying and we are ever more optimistic that a fairly simple combination of microwave polarizations and frequencies can ultimately be used to monitor the water equivalent and free-water content as well as the distribution of snow. It is probable that this understanding will also shed light on the physics of microwave emission from other wet, granular, layered media.



Figure 1A.- Microwave measurements of soil before constructing a snowpack. Crater Lake, Oregon, March 22, 1970.



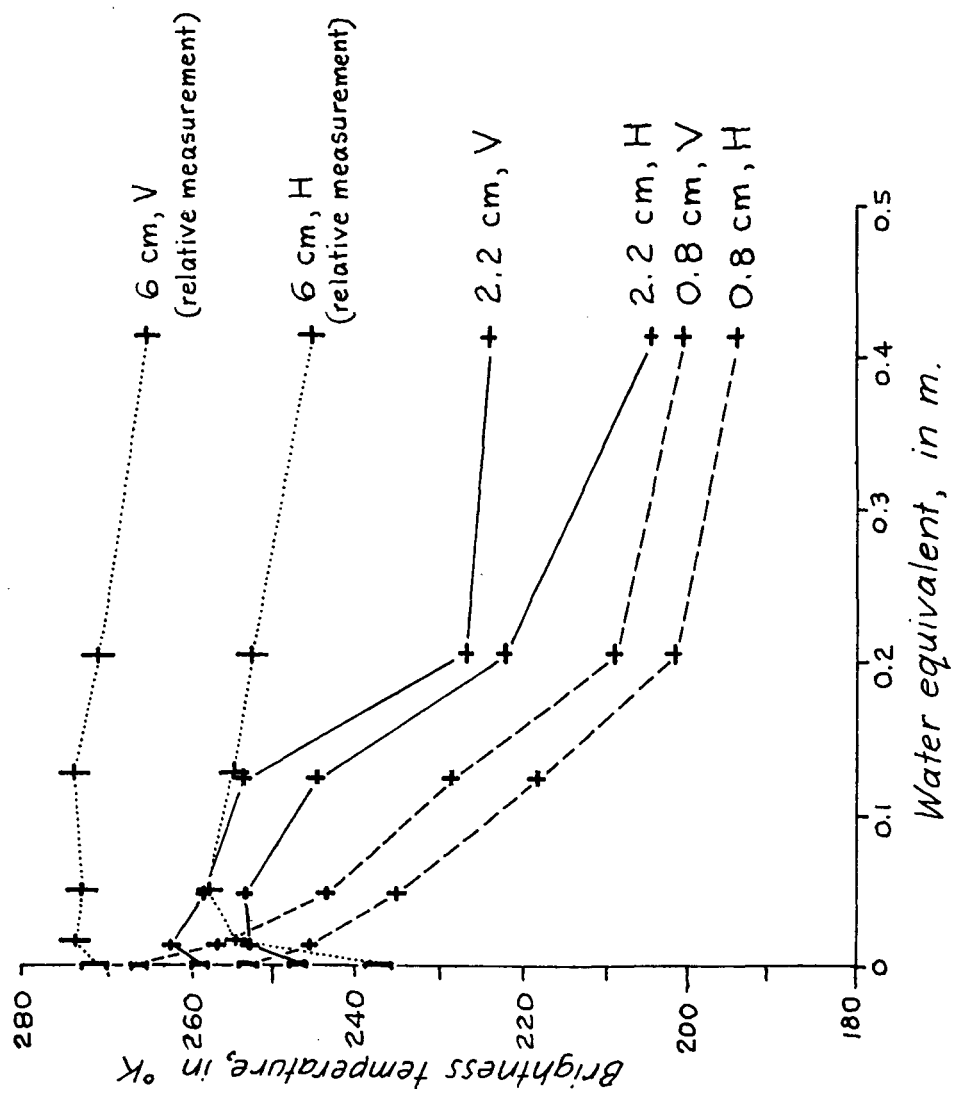


Figure 2.- Measured brightness temperature as a function of snow mass per unit area (water equivalent), for cold, dry snow.

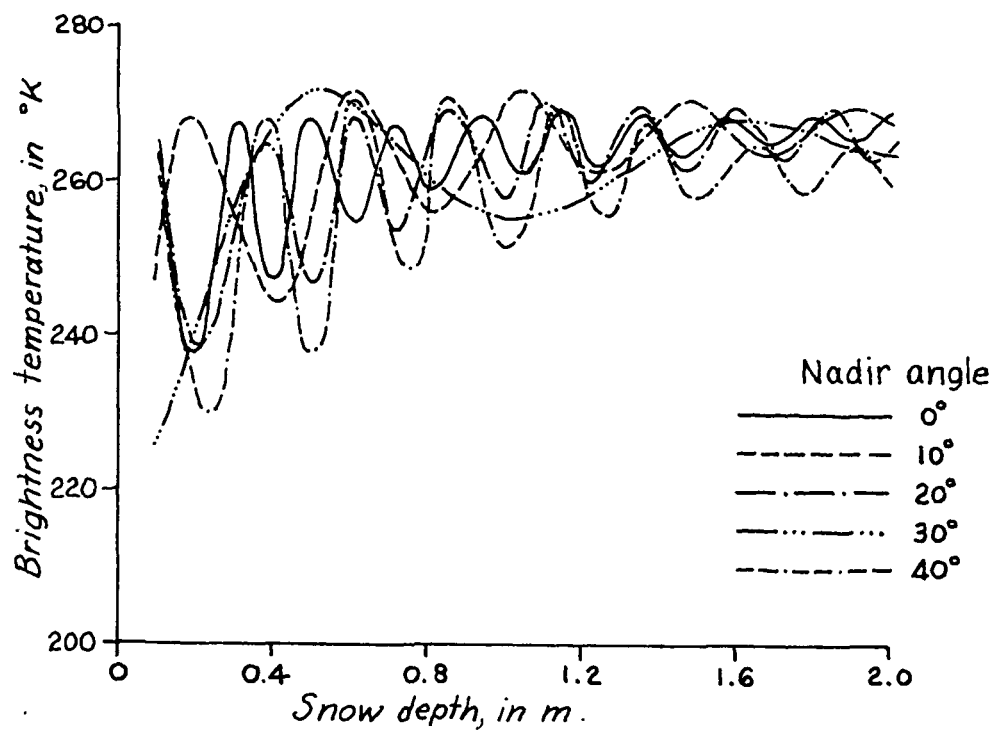


Figure 3.- Numerical simulation of brightness temperature at 0.811-cm wavelength as a function of snow depth. Snow temperature 272° K, snow density 400 kg/m³, soil dielectric constant 6.0 + j 2.0.

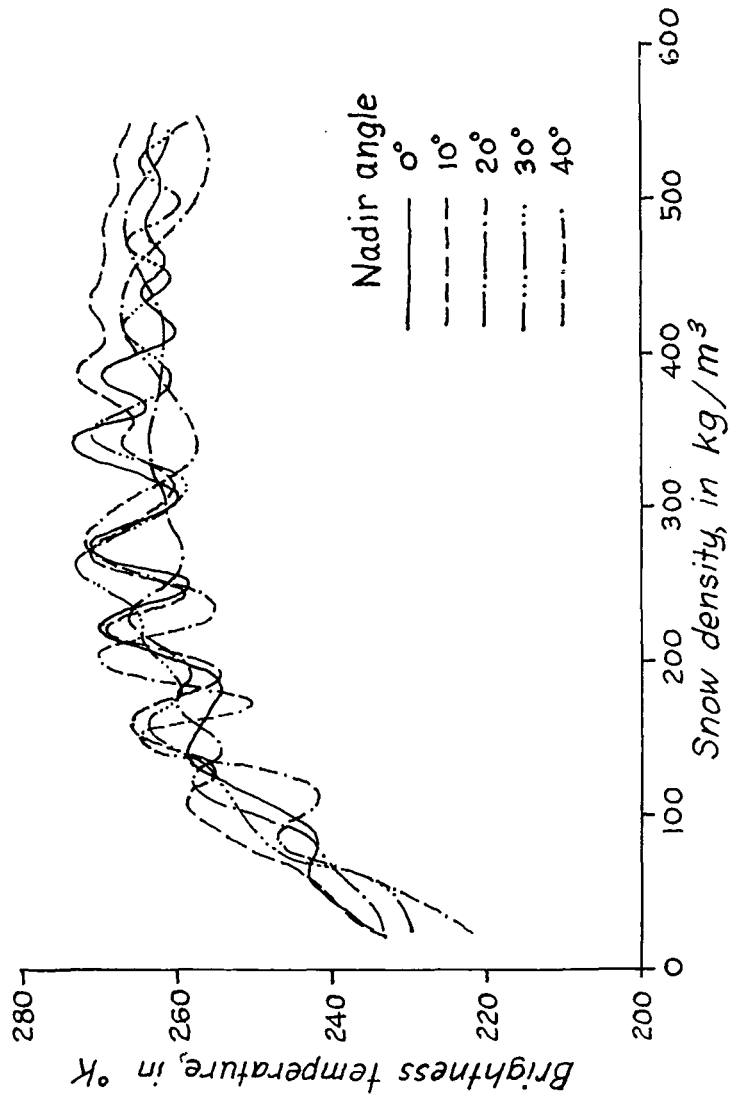


Figure 4.- Numerical simulation of brightness temperature at 0.319 cm wavelength as a function of snow density. Snow temperature 272 °K, snow depth 0.5 m, soil dielectric constant 6.0 + j 2.0, horizontal polarization.

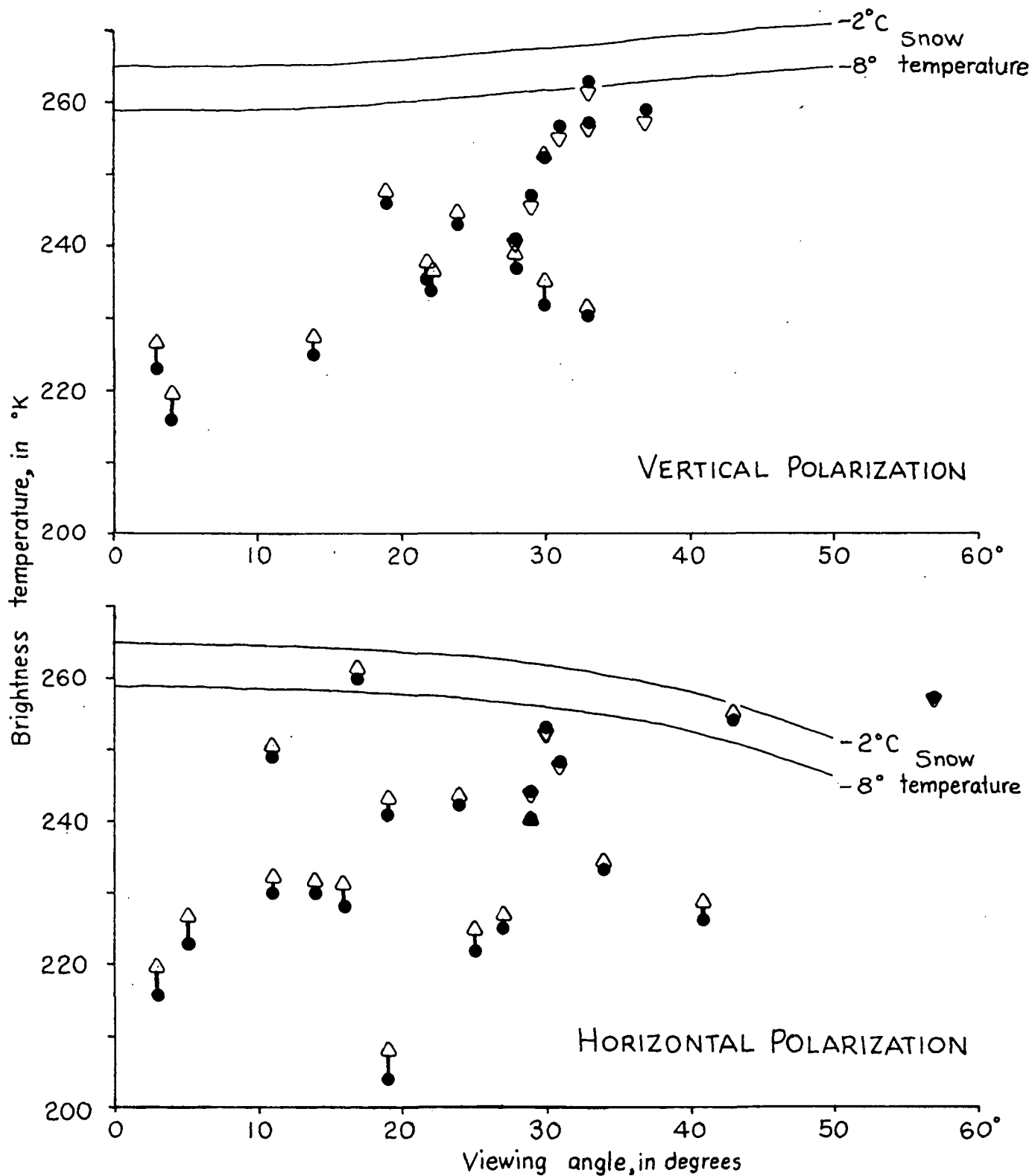


Figure 5.--Brightness temperature as a function of viewing angle, wavelength 1.55 cm, dry snow, Mount Rainier. Solid dots are measured values, triangles are values adjusted to a common snow temperature, lines given by theory (2.2 cm).

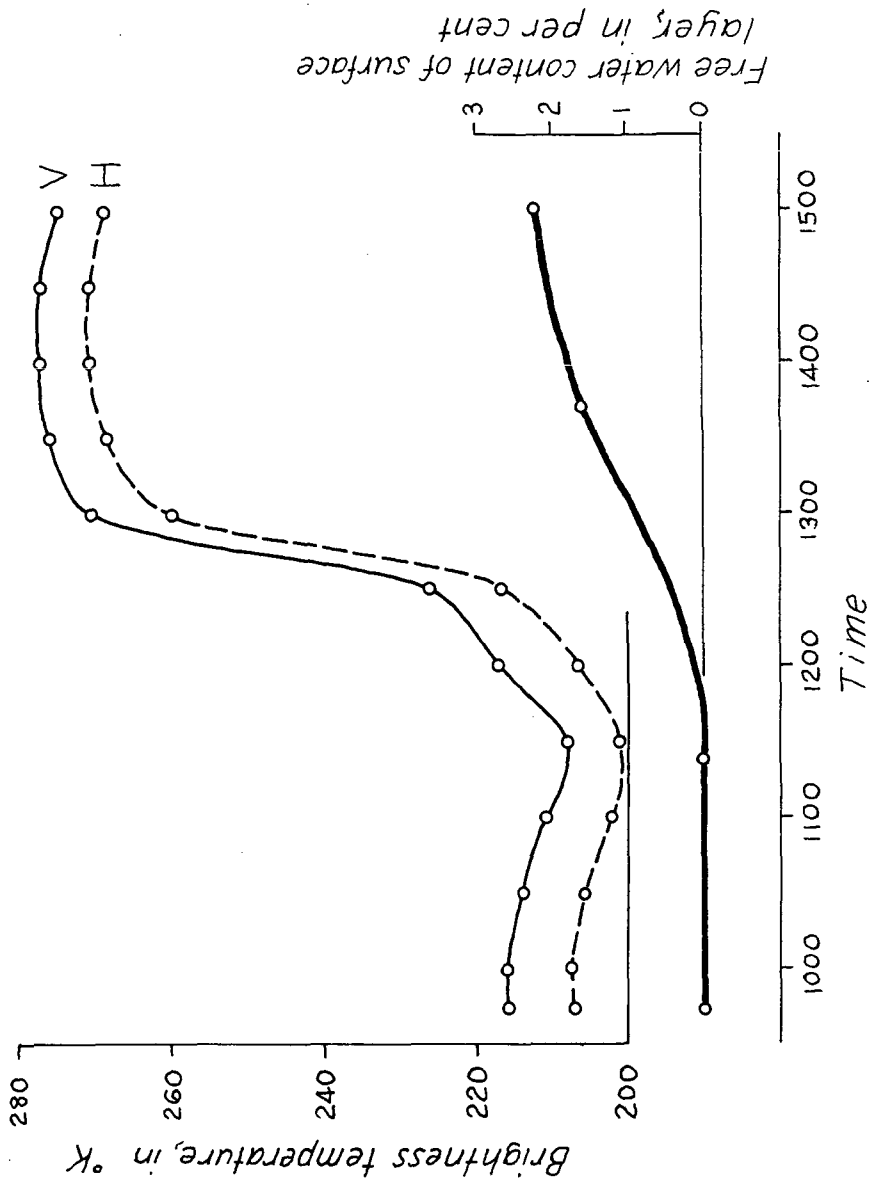


Figure 6.- Brightness temperature and surface free-water changes during the warming of a cold snowpack. Wavelength 0.8 cm, snowpack 0.8 m thick, average density 517 kg/m³.

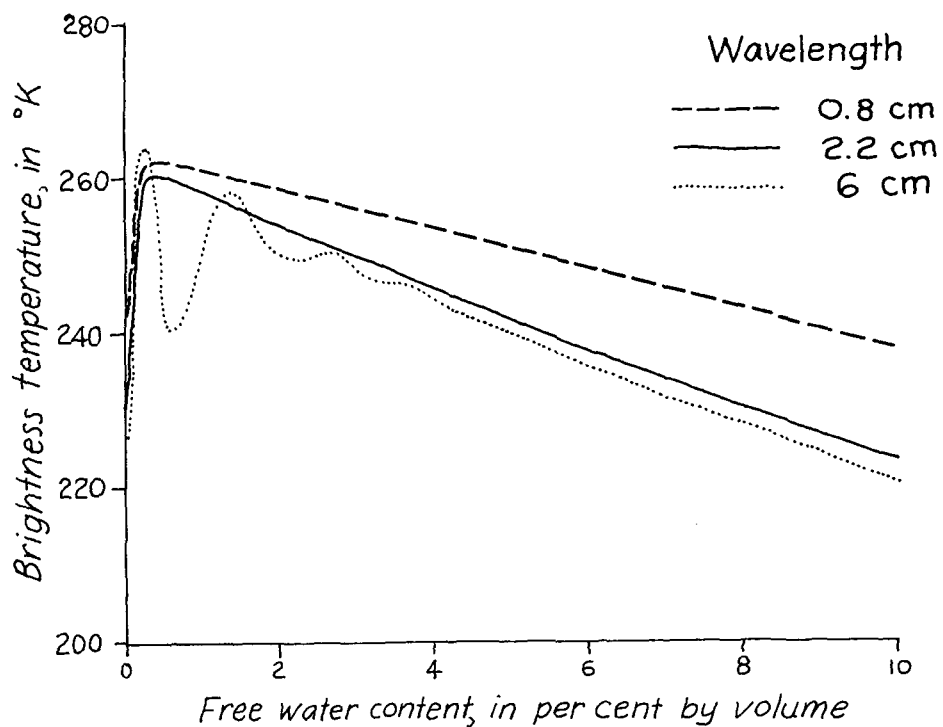


Figure 7.- Numerical simulation of brightness temperature as a function of free-water content in snow. Snowpack 0.5 m thick, density 400 kg/m^3 , zenith sky temperature 20.695° K , soil dielectric constant $6.0 + j 2.0$.

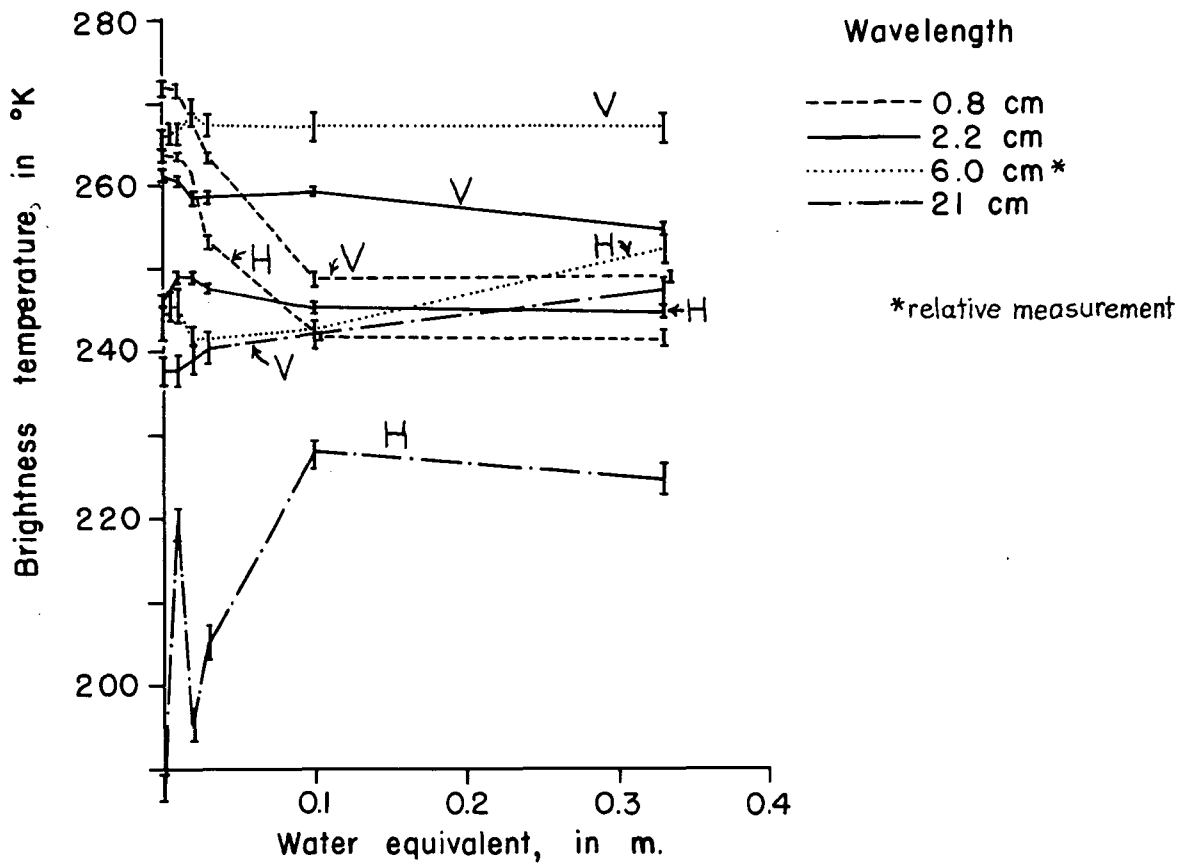


Figure 8.- Measured brightness temperature as a function of snow mass per unit area (water equivalent) for wet snow.

MANAGEMENT APPLICATIONS FOR
THERMAL IR IMAGERY OF LAKE PROCESSES

by

J. M. Whipple
U. S. Geological Survey
Albany, New York

and

R. B. Haynes
U. S. Air Force
Rome Air Development Center

INTRODUCTION

The project centers on the New York State part of the Lake Ontario Basin. The primary study sites are Onondaga Lake, near Syracuse, and the south shore of Lake Ontario, from Oswego eastward. Data from past and current missions of Rome Air Development Center aircraft have been used.

OBJECTIVES

This investigation addressed three general questions:

1. What useful limnologic data can be collected by remote sensing techniques? 2. How must equipment and operations be adapted for optimum data return? and 3. Can local interest in and routine use of such data be developed? In a study of available sensing techniques, thermal infrared scanning was selected because it provided much information previously unavailable to the hydrologist and because it can be adapted from detection to measurement capability, a feature necessary to continuing water management programs. This report considers only questions 1 and 3.

PROJECT APPROACH

The Lake Ontario Basin, in which the study is situated, is well suited to observation by high-altitude sensors because of its large areal extent. The size of the lake alone makes it difficult to obtain simple geometric and time control of data collected at or near the water surface. However, individual small lake phenomena can be studied from low-altitude aircraft platforms preliminary to future studies of broad-scale, basin-wide hydrologic patterns and to efforts for the International Field Year for the Great Lakes.

Figure 1 shows the study area in part of the Lake Ontario Basin in New York State. Actual study sites include the Lake Ontario shoreline near Oswego, some of the Finger Lakes, and Onondaga Lake near Syracuse.

Onondaga Lake evolved as a major study site because it is the most saline lake in the State and because of convenience and economy in operation of the study and the availability of supporting data. The site is less than ideal, however, for it is under the landing approach pattern of the Syracuse airport.

A considerable amount of imagery was made available from Rome Air Development Center because of test-flights of reconnaissance equipment over the area.

Ground-truth measurements were carried out in a limited way and were useful in analyzing logistics problems of the operation for routine surveillance programs.

USEFUL DATA RECOVERED

Illustrations that follow are thermal infrared imagery in which light tones represent hotter water.

Figure 2 is an overview of the 5-mile long Onondaga Lake (19 August 1969). At the northern end of the lake is the outlet (the Seneca River) (O) and in the southern part are a cooling-water discharge (C), industrial process effluent (I), and sewage discharges (S). This image is an inventory of artificial discharges including those not primarily thermal in nature. This thermal sensing capability is useful when visual sensing does not give information, such as when color and turbidity contrast between effluent and receiving water become minimal or when discharges are made at night. By repetitive coverage, consistent detection can be accomplished either by cataloging thermal characteristics or by summarizing random observations. This type of information can be incorporated in the New York State industrial wastewater discharges program.

Figure 3 shows the northern end of Onondaga Lake on two dates when flow through the lake outlet is reversed; that is, when the Seneca River is acting as a tributary. On 31 October, winds were recorded as calm whereas on 8 July the wind was 7 knots from the south and directed toward the outlet.

This phenomenon of cool water entering the warmer lake has been observed on infrared imagery at other times but never had been well documented by traditional means. The event had been suggested by a particular algal specie near the outlet and also by stream-gaging measurements; but the latter were difficult to make in the shallow river and were not considered to be reliable.

Reverse flow is caused by complex regulation of water levels for canals and hydro-power elsewhere in the basin. Knowledge such as this points out that water planners and managers need data on entire watersheds. The remote-sensing information also augments that provided by an intensive gaging-network being established on the lake tributaries for a water-budget study by a county agency. In return, the network provides calibration information for the remote-sensing data.

Figure 4 shows the southern end of Onondaga Lake on 31 October and 6 November 1969. (A change in image scale is referenced by letters "a" and "b"). The point of discharge of industrial cooling-water, reportedly as high as 80 million gallons per day, has changed from location "b" to "a" during the week elapsed. Area "S," the surface expression of a submerged sewage outfall, has been observed on infrared imagery taken at several different times, although only a part of the discharge may ever reach the surface because of varying discharge-velocity and temperature-density relationships. Note also the locations of the sewage treatment plant and the creek entering the lake between the plant and the cooling-water discharge. At times of high runoff, this creek carries both storm and sanitary sewage.

Two aspects of the data are relevant to water management. First, the monitoring of any quality parameters of a variable discharge by fixed-location recorders can be grossly inadequate. Imagery can delineate the general area in which ground equipment can be set up, or real time viewing with air-to-ground communication can direct field parties to specific sites.

The second factor important to management is the knowledge that hot-water and sewage discharges are in close proximity. Because dissolved oxygen (DO) saturation content decreases as water temperature increases and because there is a simultaneous increase in biochemical oxygen demand (BOD) rate, odor formation and organic waste-assimilation capacity of the water are affected. It may be necessary to study the merits of moving the hot-water discharge to a location more remote from that of the sanitary sewage, especially if water circulation is restricted.

The management situation is complex, and county legislators have been considering their contribution to an investment of some \$49 million for a new sewage treatment facility plus about \$2 million annual operating and financing costs. In addition, up to \$150 million has been estimated necessary to correct the combined-sewage discharge through the creek.

Figures 5 and 6 are imagery of the Oswego Harbor in March and summer 1970, respectively. When water does flow out of Onondaga Lake, it eventually discharges here. The circulation patterns of water and ice and water and algae within the harbor are affected by a generating plant thermal effluent and wind, as well as by the Oswego River-canal discharge. Harbor design and maintenance and disposal of additional cooling water are topics of potential concern.

Figure 7 shows the cooling-water discharge from a nuclear generating plant on Lake Ontario. The point of discharge is about 300 feet off shore. Note that the intake lies under the zone of heated water and that nearby is another plant under construction for a different agency. New York State has recently added thermal criteria to its existing water-quality standards. These criteria define thermal discharges and specify permissible temperature differentials for future installations. In addition to providing data relevant to these standards, infrared imagery will portray to the plant managers any interaction between the adjoining systems as well as delineate heat contributions to Lake Ontario.

CONCLUDING REMARKS

Difficulties encountered in the development of an infrared survey program in New York suggest that some of the major obstacles to acceptance of remotely sensed data for routine use are factors of psychology rather than technology. Although there are legitimate objections to the limitations in this type of data, there are also severe handicaps to the traditional point-parameter systems that now operate. Problems of calibration and correlation of ground instruments of varying performance capability, time factors of equipment installation and maintenance at diverse sites, and the basic question of representativeness of a point-sample have been a part of the measuring system for so long that they are often forgotten.

The problem of acceptance of surface thermal data is compounded by the use of the term "temperature" rather than "radiance." The measurement of thermal energy is actually the topic of concern. "Temperature" has been used because we have had available equipment that measured a parameter called that. Because the remote sensor does not measure that identical parameter, the raw numbers of data are not the same and reference to the thermometric "temperature" infers disagreement and unfavorable comparison. Terminology should suit the measurement technique.

In the New York program, a quantitative infrared system will add spatial radiometric data to the chronological thermometric data now collected in the water-quality surveillance network. Therefore, in the interim preceding routine data-collection by high-altitude sensors, some water managers will become accustomed to the evaluation, use, and storage of data collected from above ground.

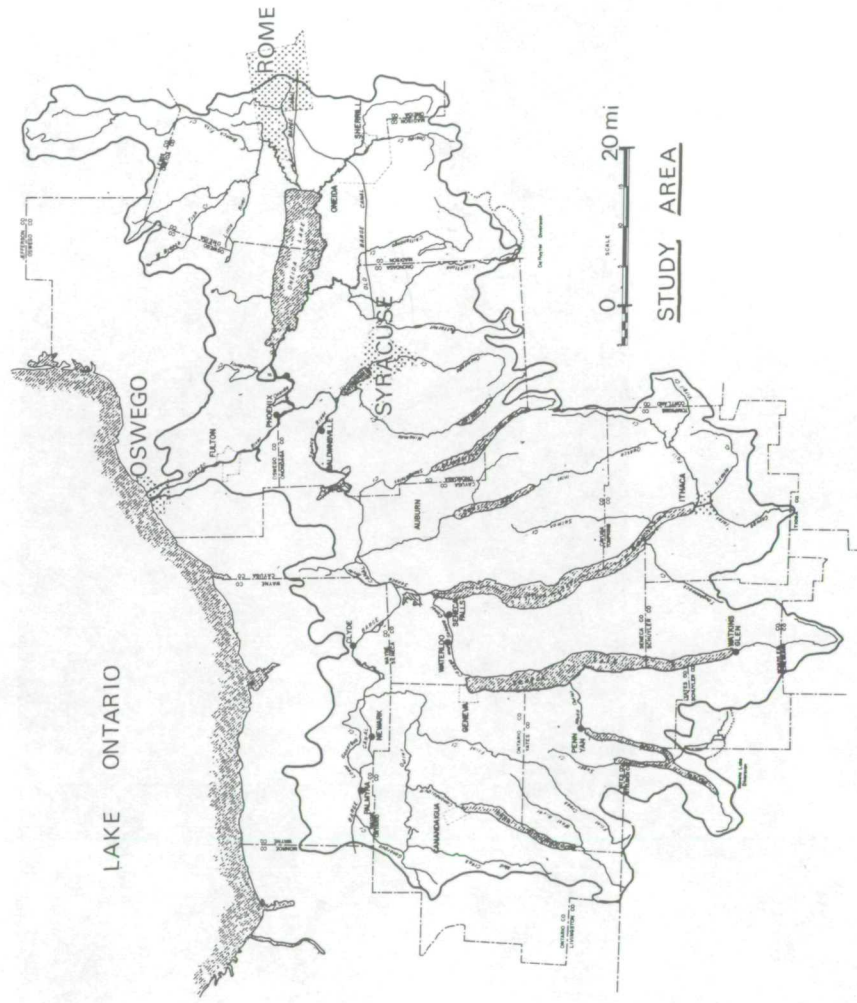


Figure 1. Study area, Lake Ontario Basin.

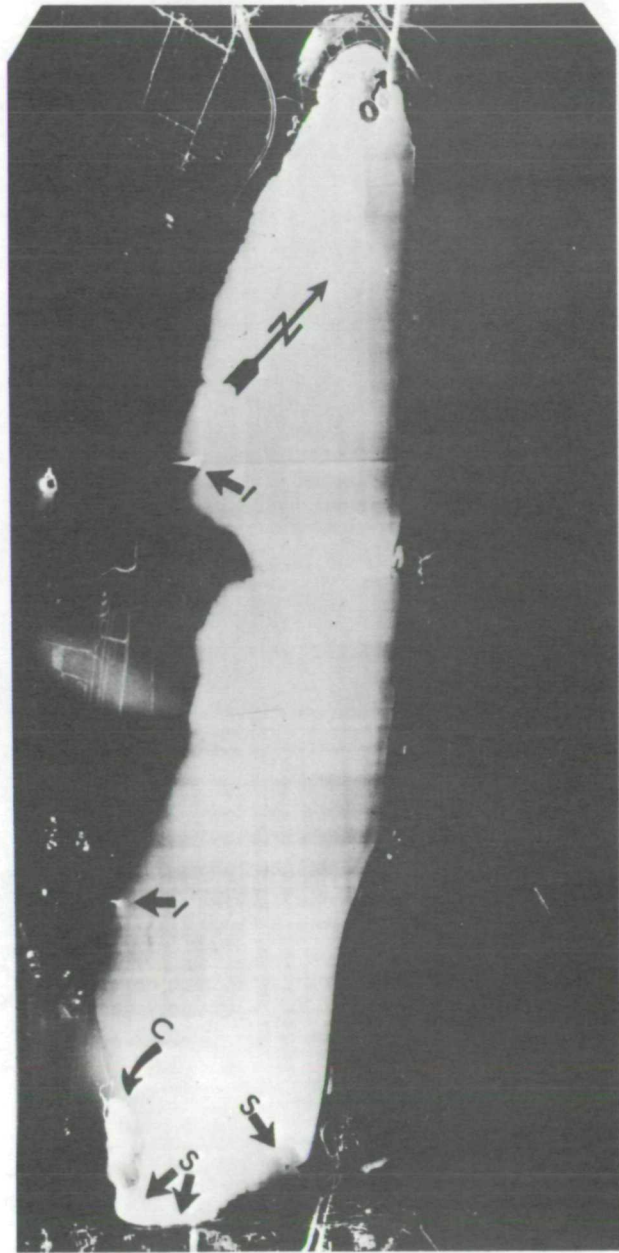
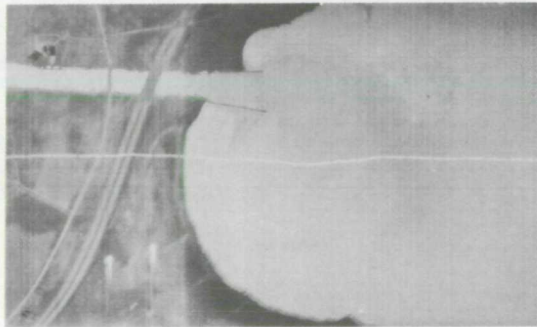


Figure 2. Overview of Onondaga Lake (IR imagery).



8 July 1970



31 October 1969

Figure 3. Northern end of Onondaga Lake (IR imagery).

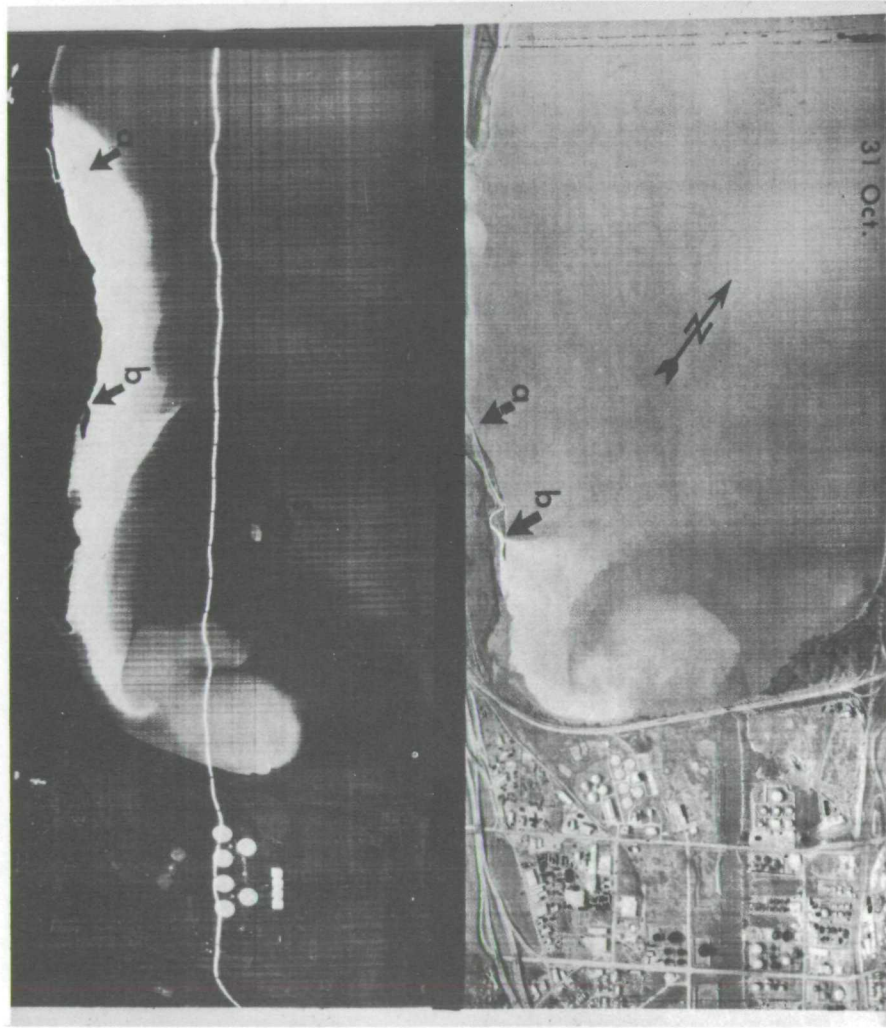


Figure 4. Southern end of Onondaga Lake (IR imagery).

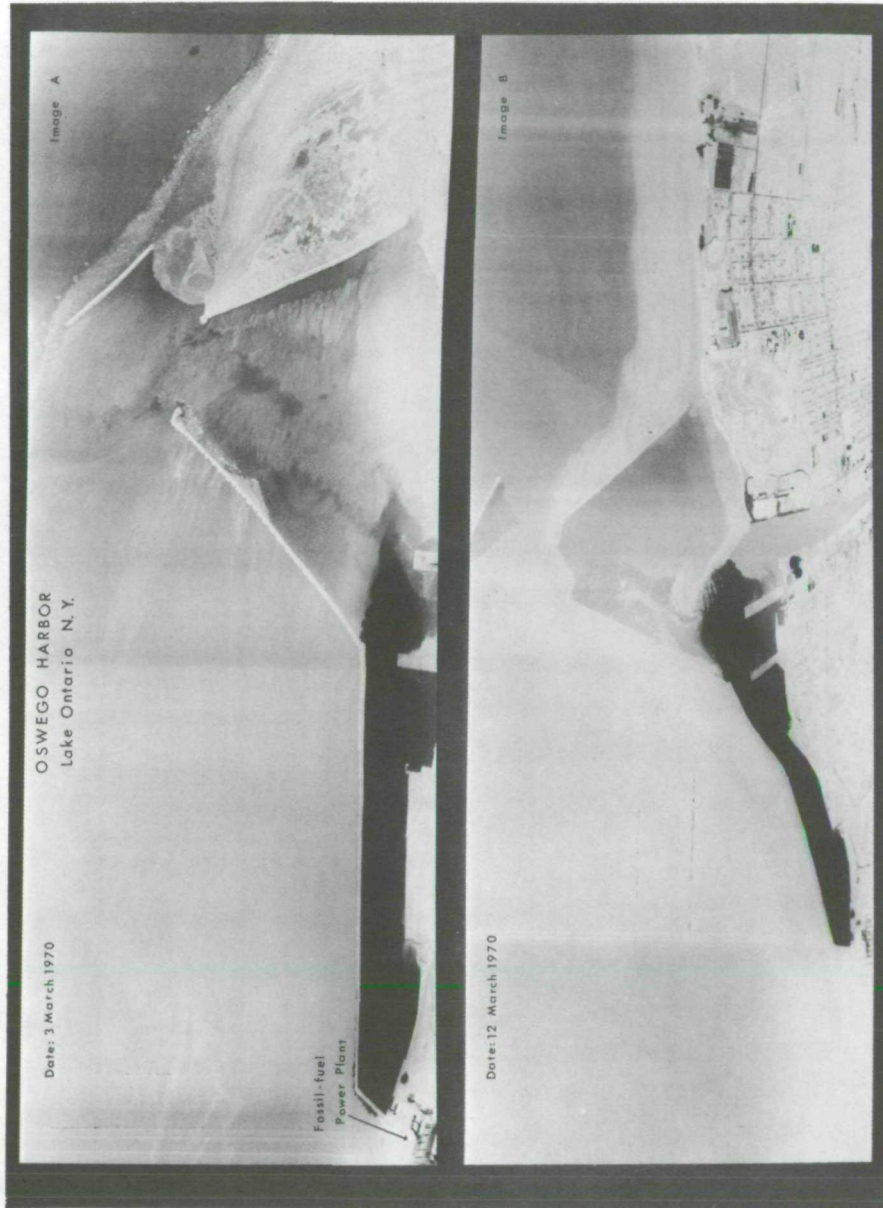


Figure 5. Oswego Harbor, March (IR Imagery).

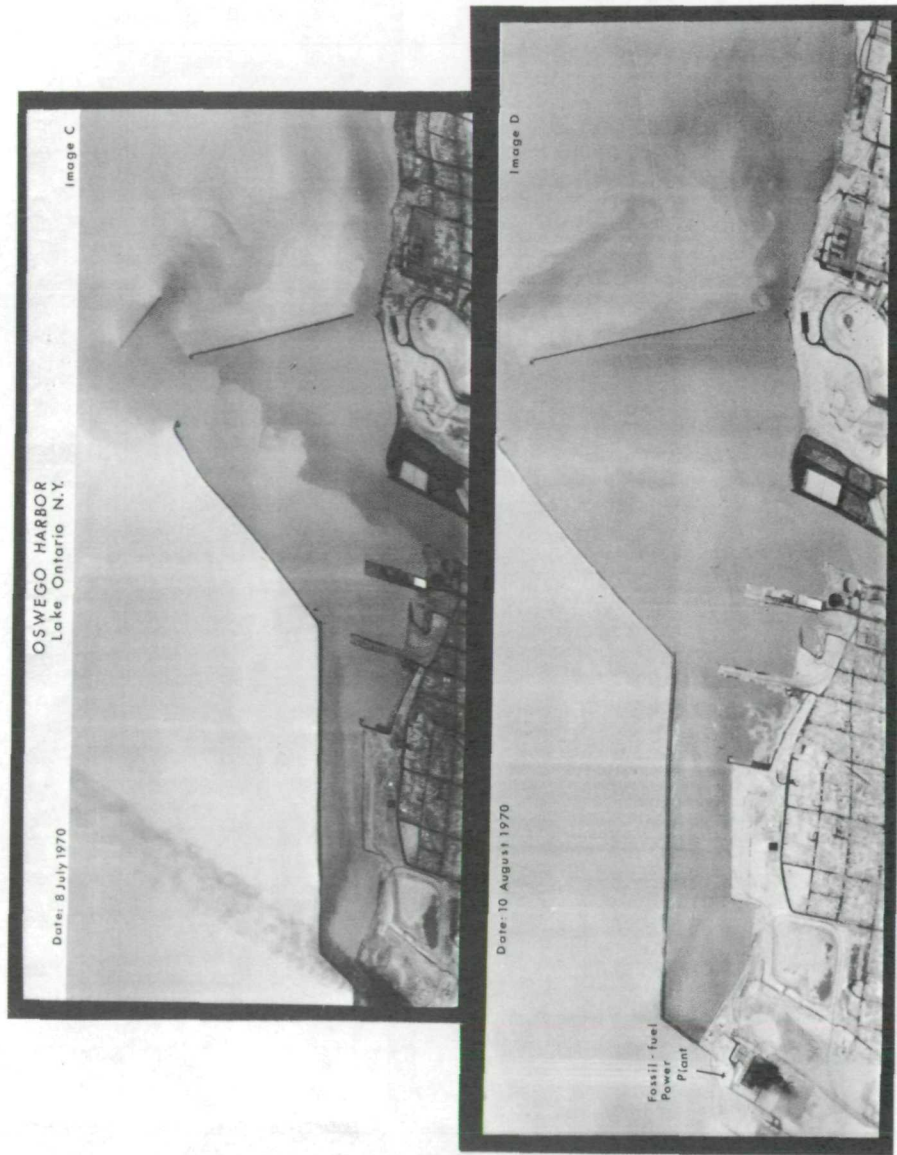


Figure 6. Oswego Harbor, summer (IR imagery).

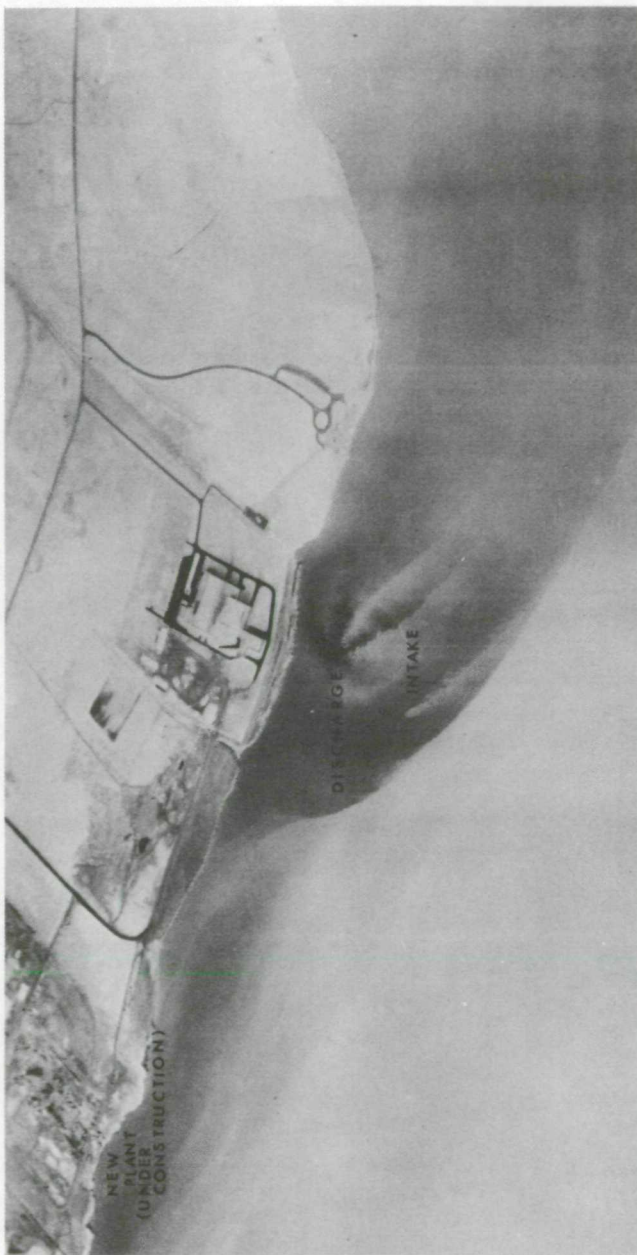


Image A

Date: 10 August 1970

Figure 7. Nuclear power plant, Lake Ontario (IR imagery).

Page Intentionally Left Blank

Spectral Reflectance Characteristics and
Automated Data Reduction Techniques which
Identify Wetland and Water Quality Conditions in the
Chesapeake Bay

By Dr. Richard R. Anderson

Introduction

This report presents progress on research designed to test the usability of multispectral, high altitude, remotely sensed data to analyze ecological and hydrological conditions in estuarine environments. Emphasis will be placed on data acquired by NASA aircraft during fiscal year 1 July 1969 to 1 July 1970 over the Patuxent River Chesapeake Bay Test Site, No. 168. Fig. 1 is a map of the test site.

Mission Nos. 103 (Aircraft RB57F) and 104 (C130 aircraft) were conducted over the Chesapeake Bay during September, 1969. Mission 103 was a high altitude flight (18,460 m) and 104 a low altitude flight (3,070 m). Table 1 shows the types and quality of data received from these missions.

The hypothesis being tested in this phase of the research was that remote sensing techniques found successful in earlier ecological studies of the Patuxent River, Maryland (Missions 74 and 79), would be usable in other, more complex ecosystems (the Chesapeake Bay) and at higher altitudes than previously flown. The principle objectives of Missions 103 and 104 were the following:

1. To determine feasibility of identifying source and extent of water pollution problems in Baltimore Harbor, Chesapeake Bay and major tributaries utilizing high altitude, ERTS analogous remote sensing data.
2. To determine the feasibility of mapping species composition

- and general ecological condition of Chesapeake Bay wetlands, utilizing high altitude, ERTS analogous data.
3. To correlate ground spectral reflectance characteristics of wetland plant species with tonal characteristics on multispectral photography.
 4. To determine usefulness of high altitude thermal imagery in delineating isotherms and current patterns in the Chesapeake Bay.
 5. To investigate automated data interpretive techniques which may be usable on high altitude, ERTS analogous data.

The Chesapeake Bay Test Site

The Chesapeake Bay is the largest estuary on the Atlantic Coast of the United States. With its some 50 major and minor tributaries it constitutes one of the largest estuarine systems in the world. While the surface area of the Bay is large (2,200 square miles) the mean depth is only 28 feet, indicating it is extremely susceptible to physical and biological changes. Increasing urban development along the tributaries of the Bay system will bring inevitable changes in water quality and shoreline aquatic ecosystems. Because of the size of the estuary and the many diverse problems of an ecological nature it presents a unique opportunity for evaluation of ERTS and ERTS analogous imagery in identification and solution of these problems.

Successful management of water resources and attendant biological communities requires coordinated efforts on the part of federal, state, and local authorities. This is particularly necessary in a resource

such as the Chesapeake Bay where four states, the District of Columbia and numerous regional, county and city authorities may at times make independent decisions regarding utilization of the resources of the Bay.

Remote sensing from aircraft and satellite presents a unique method by which the Bay may be observed and studied as whole rather than in piecemeal fashion. Remotely obtained hydrological and ecological data present a focal point around which coordinated physical and biological studies may be feasible and attractive to many diverse groups now doing research in the Chesapeake Bay.

Results and Discussion

A. Water Quality

Results of previous water quality studies, including correlation of ground truth data with spectral signatures on film, have been published and will not be reiterated here except in summary form (1), (2). The following general aspects of water quality conditions in the Patuxent River had been determined in previous studies.

- (1) Estimation of water salinity through color IR interpretation of plant species in wetlands.
- (2) Sources of sediment addition to the estuary.
- (3) Rough quantitative estimate of sediment content in the estuary through tonal quality on color IR film.
- (4) Areas in the estuary where siltation and mudflat development present potential boat navigation problems.
- (5) Sources of ground water inflow into the estuary through thermal IR imagery.

- (6) Sources of nutrient additions to the estuary through color IR photography of algae blooms.

Water quality studies in Chesapeake Bay have been confined to Baltimore Harbor. There are a number of industrial and municipal effluents which empty into the Harbor; therefore, it is an ideal test area for both low and high altitude ERTS analogous multispectral water quality conditions.

As shown in Table 1, both low and high altitude multispectral data were obtained over the test site. The prime reason for requesting the low altitude imagery was to compare spectral signature of water quality conditions with that on high altitude imagery and to determine magnitude of information loss with increase in altitude of the aircraft. Of particular interest was comparison of color and color IR photography since the latter had been found more useful in low altitude studies on the Patuxent River. Unfortunately, much of the color IR data received from these missions were not usable due to underexposure of the film. Therefore, comparison with natural color was not possible.

Ektachrome color photography from both low and high altitude missions was good and it was possible to evaluate loss of information with altitude. Fig. 2 shows a low altitude photograph of Baltimore Harbor. Comparisons with high altitude photographs indicate that more detailed analysis of water quality conditions could be done from low altitude. However, high altitude photography has the advantages of smaller scale and larger areal coverage. General water quality conditions may be ascertained as well as point sources of several effluents

which degrade water quality in Baltimore Harbor.

Algae blooms are excellent, indirect indicators of water quality in bodies of water. Nutrients discharged from municipal sewage effluents, septic tanks and farm runoff all provide conditions for algae blooming during certain times of the year. Problem areas may be quickly identified through these excessive aquatic plant growths. Color IR photography has been shown to be useful from low altitude for delineating algae blooms. Fig. 3 is a high altitude color IR photograph of the Potomac River near Washington, D. C., showing severe algae blooming. Other minor blooms were also evident from the high altitude photography of several tributaries of the Chesapeake Bay. This indicates that areas where eutrophication is a problem may be located from high flying aircraft.

Automated data interpretive techniques for assessing water quality conditions will be discussed later in this paper.

B. Wetlands Studies

Results of previous wetlands studies have been published (2) and will not be repeated here, except in summary form. The following general aspects of wetland ecology have been determined in the Patuxent River, Maryland:

- (1) Infrared spectral reflectances by wetland plants are unique for given species and communities. This results in tonal signatures which are readily discernable and separable on color IR film.
- (2) Changes in plant species composition and vigor from spring to fall in wetlands, results in changes in tonal quality

on color IR film.

- (3) Production of a key for wetland vegetation species utilizing color (shades of pink) alone is apparently not possible due to variations in the quality of color IR film from one roll to the next. However, plant species and communities may be classified according to tone brightness. One will find the same sequence of species tone brightness, from dark to light, regardless of the particular color exhibited on a given roll of color IR film.

Wetlands studies were extended to the Chesapeake Bay due to the presence of plant communities and species not found in the Patuxent River. Also, the larger sized wetlands in the Chesapeake Bay make it feasible to study them from high altitude ERTS analogous aircraft data.

Of particular interest are the 240,000 acres of wetlands along the lower eastern shore of the Chesapeake Bay. They range in type from shallow fresh marsh to salt marsh, with the latter type predominating. The value of these areas to maintenance of good water quality conditions in estuaries, preservation of wildlife habitat, etc., is now widely accepted. High altitude aircraft and satellite data could provide the following information on wetland ecology:

- (1) General species composition of major plant communities;
- (2) Evaluation of different wetland types for importance to certain wildlife populations;
- (3) Rates at which wetlands areas are being lost due to natural and man-made activities.

Missions 103 and 104 were designed to determine loss of information in wetlands (species composition, etc.) with increase in altitude and to determine film and filter combinations which would best delineate wetland plant communities from high altitude (Table 1). Unfortunately, much of the high altitude color IR photography was underexposed. Color IR photography from the Hasselblad cameras (1:240,000 scale, filters 15-G and 25-A) and Zeiss camera (1:60,000 scale, "D" filter) was usable. Fig. 4 is a low (1:20,000) and high altitude (1:60,000) photograph of a wetland area. As can be seen, little information on species composition is lost with this reduction in scale. Interpretation becomes more difficult on the 1:240,000 Hasselblad photography. Plant community zonation lines are blurred and determination of general species composition is considerably more difficult, particularly in fresh water wetlands where there is a large variety of species present.

It appears that photographic interpretation of wetlands on smaller scales will best be done with automated techniques such as density slicing. This will be discussed later in the report.

C. Spectral reflectance characteristics of wetland species

Remotely sensed photographic and imaging data are dependent in most cases upon differences in reflected or emitted electromagnetic radiation from surfaces. It became important in this study to know how plant leaf reflectance differs from species to species, what role season and plant age play in the quantitative and qualitative aspects of this reflectance, and the amount of intraspecies variation that can be expected.

A total of ten marsh plant species have been investigated for spectral reflectance characteristics. Fig. 5 is a comparison of three of the curves derived from the study. All spectral data were collected with an ISCO Model SR Spectroradiometer equipped with an extension probe for field work. Readings were made between 0.4 and 1.35 micrometers using incident sunlight as a reference. Approximately ten individuals of each species were studied to determine intraspecies variation.

The spectral reflectance curves for all plant species are similar in shape, but differ in magnitude (Fig. 5). In the visible range the curves show low reflectivity (1-6%) between 0.4 and 0.5 micrometers, a peak at 0.55 micrometers (6.2-9.1%), a drop to a minimum at 0.675 micrometers (3.3-6.7%). Beyond 0.7 micrometers, the curves rise steeply to a peak at 0.8, 0.85, or 0.9 micrometers in the infrared (30.5-46.6%). Beyond the peaks in the infrared, the reflectance falls gradually with a pronounced dip at 0.95 and 1.24 micrometers. Yellow water lily shows the highest reflectance in the infrared and salt marsh grass, the lowest. In the visible range, wild rice and yellow water lily have the highest reflectance at 0.55 micrometers and salt marsh grass the lowest. Between 0.7 and 0.9 micrometers (the spectral range in which the infrared emulsion layer of Kodak Ektachrome Infrared Aero Film is sensitive) the plants rank in order of decreasing total reflectance: yellow water lily, pickerelweed, sweet flag, wild rice, cattail, reed, rush and salt marsh grass. Fig. 6 shows tonal signatures of some of the above species on color IR film.

Table 2 shows the relationship between spectral reflectance and tonal "signatures" on color IR film. As can be seen by these data,

there is not a complete correlation between tone brightness and percent reflectance in this portion of the IR spectrum. Species such as cattail and salt marsh grass need to be restudied to determine if characteristics such as leaf orientation, leaf stacking, etc. have a significant effect on I R reflectance.

Comparison of spectral reflectance curves indicates that narrow bandwidths around 0.9 and 1.1 micrometers would be best for separation or delineation of all species studied. At 0.9 micrometers, only reed and wild rice cannot be separated. If it is desirable to separate sweet flag, pickerelweed, wild rice and reed, all of which have medium reflectance, 0.75, 0.85 and 1.1 micrometers are good wavelengths at which to work. Low reflectors such as cattail, rush and salt marsh grass separate well at a number of wavelengths -- 0.55, 0.675, 0.75, 0.8, 0.85, 0.9, and 1.3 micrometers. Strong reflectors, yellow water lily and arrow arrum should be easily delimited at 0.75, 0.8, 0.9 and 1.1 micrometers. Film-filter combinations can be chosen to select out narrow bandwidths around these optimum wavelengths or some type of multiband sensor may be used to collect data.

Comparison of spectral reflectance curves for reed (*Phragmites*) made in July and October shows a seasonal change in reflectance (Fig. 7). Color infrared photographs taken of a marsh in late June and late September show a change in color signature from bright pink to dark red or blueish red (Fig. 8). Ground observation in October showed vegetation in area II to consist entirely of mature growth with dry, brittle, grey-spotted leaves. Area I contained a percentage of young growth and the leaves appeared less brittle and discolored. Spectral reflectance in the near IR varies accordingly, being highest for leaves

of reed in July, lower in leaves from area I and lower still in leaves from area II measured in October. There was a large intra-species difference in October which points up one of the difficulties of collecting data near the end of the growing season.

Since season influences the reflectance characteristic of vegetation (aging, disease at the end of the growing season; change in internal structure of the growing leaf at the beginning of the growing season), spectral reflectance curves should be available for spring, summer, and fall.

Measurements of spectral reflectivity have been made primarily on agricultural crops and forest species. Marshlands and estuaries are valuable natural resources which provide nursery grounds for young fish and marine invertebrates as well as feeding areas for wildfowl. For this reason, it will prove desirable to monitor these areas by remote sensing on a regular basis for protection from man-made reductions in productivity. Shifts in vegetative distribution and density exceeding what normally occurs as a result of plant succession may indicate changes in drainage patterns, salinity, siltation and pollution levels. Changes in reflectance as a result of disease, drought, nutrient deficiency, or pollution can be detected quickly by remote sensing and remedial procedures applied.

D. Thermal imaging of estuarine systems

Fig. 1, a map of the Chesapeake Bay, shows the presently operating and planned thermal electrical generating plants in this area. As can be seen there are already areas under thermal stress (Baltimore Harbor) and the potential for stress in the larger system is very real as

greater demands for electricity are made on the industry.

It is extremely important that the baseline studies on thermal characteristics of the Bay be done now. Thermal imaging from aircraft, with concomittant ground truth, presents a rapid means for doing this baseline study. Unfortunately, the thermal imagers aboard the C130 and RB57F aircrafts were not operational during these missions. Data of these types will be requested in future missions.

E. Automated data interpretive techniques

With the advent of ERTS-A and a significant increase in remotely sensed data, it is important to establish automated techniques for data reduction. The sheer bulk of information available from satellites will make eyeball interpretation impractical and obsolete. For this reason data interpretive techniques such as color coded microdensitometry, color additive procedures and density slicing are being investigated for use in wetland and water pollution studies.

One of the more promising techniques being explored at the present time is Datacolor density slicing available through Spatial Data Corporation. Through use of a television camera and up to 32 different colors (actually 8 colors and 4 tones for each color) densities on black and white transparencies are separated and color imaged on a television screen. The machine is capable of separating a maximum of 32 different densities.

Fig. 9 is a print of an image generated by analysis of a black and white Hasselblad photograph (Filter #58), showing distribution of sediment from a stream. The color coded densities representing dispersement of sediment into the Bay are easily separable. Quantitative

values of sediment content could easily be assigned to each density value.

Fig. 10 shows a print of a black and white Hasselblad transparency (scale 1:240,000, Filter No. 58) and a print of the color image generated as a result of density analysis by the Datacolor machine. Sixteen densities were counted in the wetland, indicating that plant species composition may be determined rapidly using small scale black and white photography. It will be necessary to field check the wetland to determine if each density represents a single plant species or community type.

As a part of the wetland study, the author has been cooperating with the Department of Natural Resources, State of Maryland. A new wetland law enacted July 1, 1970, requires the state to delineate state-owned wetlands from those that are privately-owned. The state is claiming ownership to all wetlands that are inundated by each tide. The problem here is to accurately draw a line which separates the two in many wetland areas.

Fig. 11 is a high altitude color IR photograph showing how this delineation is accomplished. Bright tones are interpreted as high marsh (privately-owned) and darker tones as low marsh (state-owned). Fig. 12 shows how this interpretation may be accomplished utilizing an automated technique such as the Datacolor system.

Summary

This paper reports progress in analysis of data received from Missions 103 and 104, September 1969, Site 168, Chesapeake Bay. This was the first flight over the expanded test site and it presented an

opportunity to become familiar with the general topographic and hydrologic features of the Chesapeake Bay as well as to begin ERTS analogous studies of a large, complex estuarine system.

Most of the data received was good; however, a considerable portion of the color IR photography was not usable. This prevented comparison of high altitude natural color with color IR for use in water pollution and wetland investigations. The following general conclusions are a summary of interpretive results.

1. General water pollution conditions in Baltimore Harbor may be inferred from high altitude, small scale, RC-8 color photography. Point source effluents and dispersement of pollutants are imaged on the film.
2. Species composition and general ecological conditions of wetlands may be interpreted from high altitude RC-8 color and Zeiss color IR photography. Little information is lost with increase in altitude.
3. Water quality and wetland studies are more difficult on small scale Hasselblad photography. It appears that automated data reduction techniques may be necessary for adequate interpretation.
4. Spectral reflectance properties of several marsh plant species have been established. Attempts at matching reflectance with tone brightness on color IR photography have yielded mixed results, with little or no correlation observed on two species.

5. Automated data interpretive techniques have been investigated and appear to work well with black and white, small scale photography.

Page Intentionally Left Blank


Literature Cited

1. Anderson, R. R. 1968 Remote Sensing of Marshlands and Estuaries Using Color Infrared Photography. NASA, Earth Resources Aircraft Program Status Review, Vo. III: 26-1 to 26-23.
2. Anderson, R. R. 1969 The Use of Color Infrared Photography and Thermal Imagery in Marshland and Estuarine Studies. NASA, Second Annual Earth Resources Aircraft Program Status Review, Vo. III: 40-1 to 40-29.

Table 1 Types and quality of data received from Missions 103 and 104, Chesapeake Bay Test Site, September 1969.

Mission No.	Data Type	Quality
103, RB 57 F, 18,460 m altitude.	RC-8 Ektachrome Color	Good
	RC-8 Ektachrome Color IR	Poor, Underexposed
	Hasselblad B & W, Filter #58	Good
	Hasselblad B & W, Filter #25A	Good
	Hasselblad Ektachrome Color	Not useable
	Hasselblad Color IR, Filter #15G	Good
	Hasselblad Color IR, Filter #25A	Good
	Zeiss, Color IR, "D" Filter	Good
104, C130 B, 3,070m altitude.	RC-8 Color IR Soll7, Filter #15	Poor, Underexposed
	RC-8 Ektachrome Color	Good
	Hasselblad, B & W, Filter #58	Good
	Hasselblad, B & W, Filter #25A	Partially underexposed

Table 2 Relationship between spectral reflectance and tonal signature on color IR film of selected marsh plant species.

<u>Plant</u>	<u>Tonal "Signature"</u> <u>on Color IR Film</u>	<u>Average %</u> <u>Reflectance</u> <u>0.7-0.9 Micrometers</u>
Cattail	Dark	29.2
Pickerelweed		31.1
Sweet Flag		29.7
Wild Rice		29.4
Salt Marsh Grass		23.9
Yellow Water Lily		Light

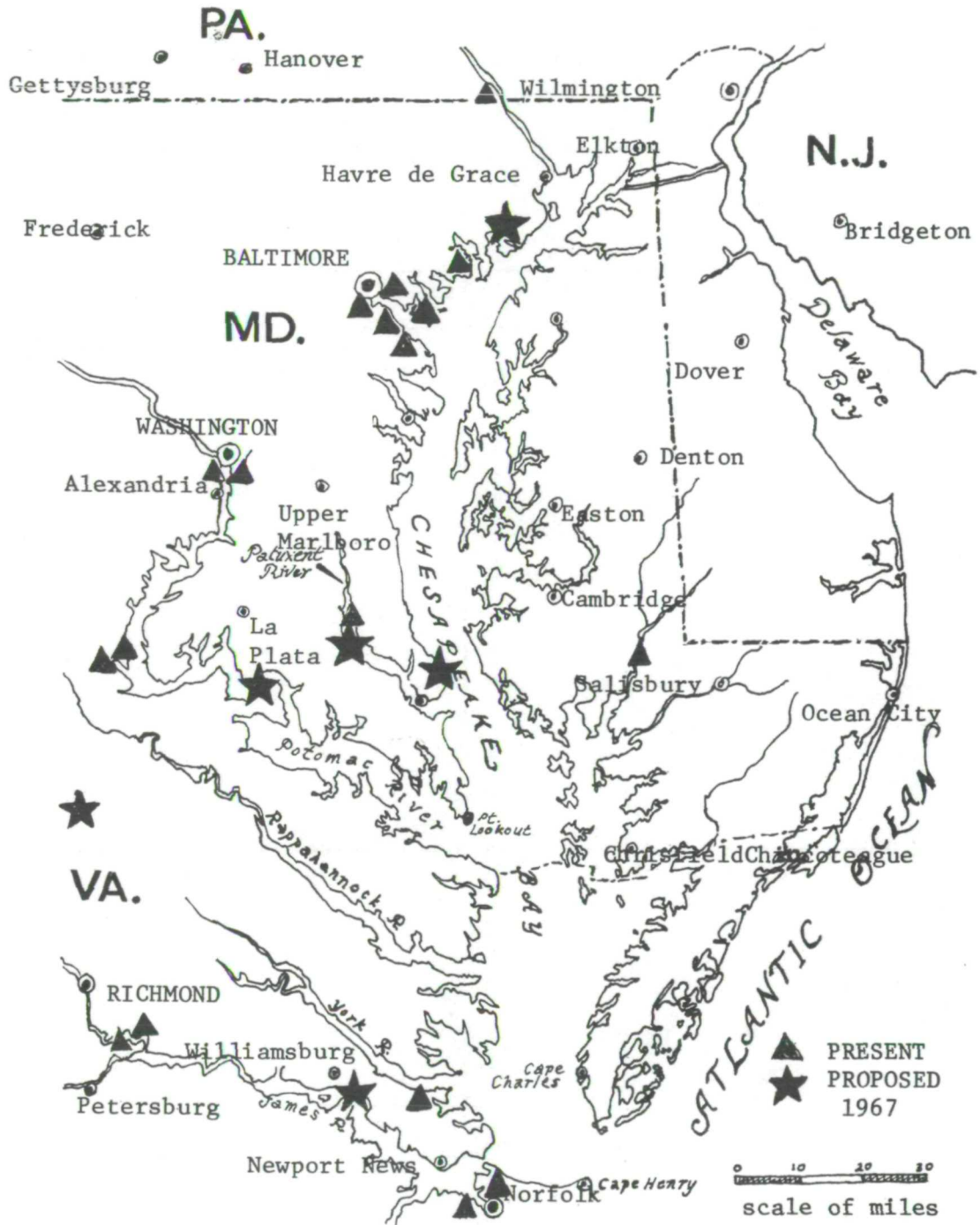


Fig. 1 Map of the Chesapeake Bay showing extent of study area and status of thermal electric power plant development.

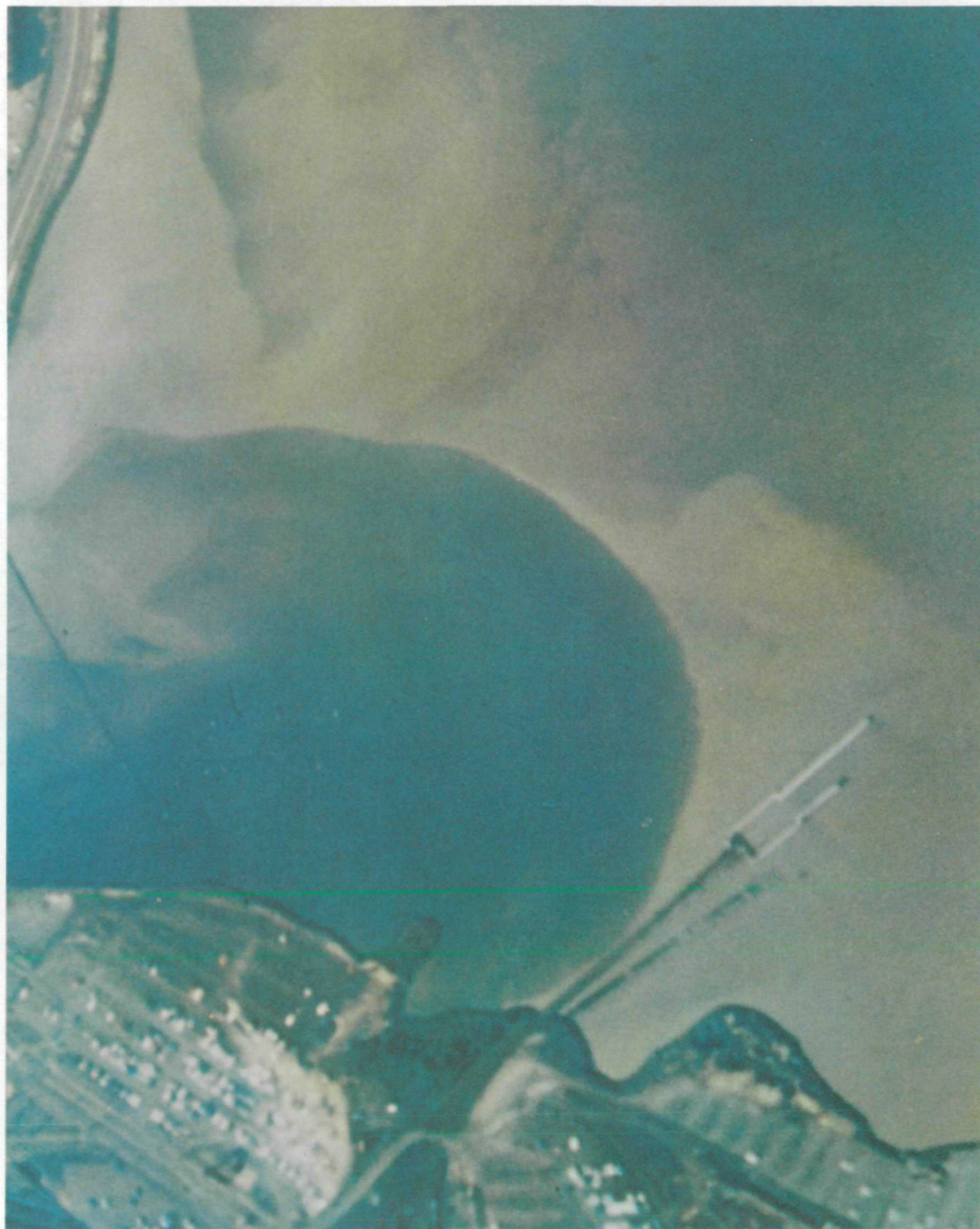


Fig. 2. Low altitude photograph of Baltimore Harbor showing one of several industrial effluents. Ektachrome color. Scale, 1 cm = 55 meters.

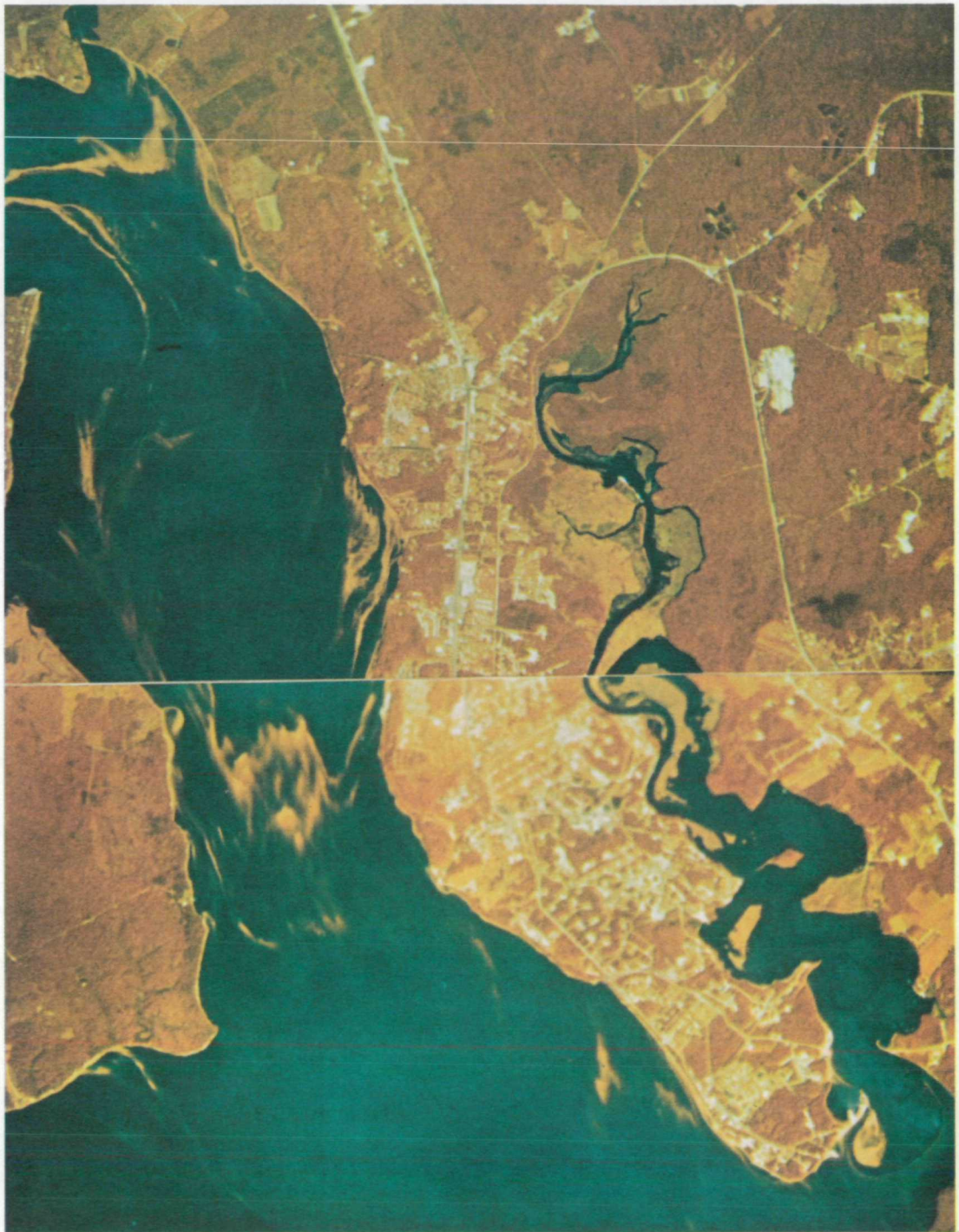


Fig. 3. High altitude photograph of the Potomac River near Washington, D.C., showing severe algae blooms in the water. Ektachrome color IR. Scale, 1 cm - 580 meters.



Fig. 4. Low altitude (top) and high altitude photographs illustrating only slight loss of information in wetland going from low to high altitude analysis. Ektachrome color IR. Scale, 1 cm = 120 meters (low) and 1 cm = 360 meters.

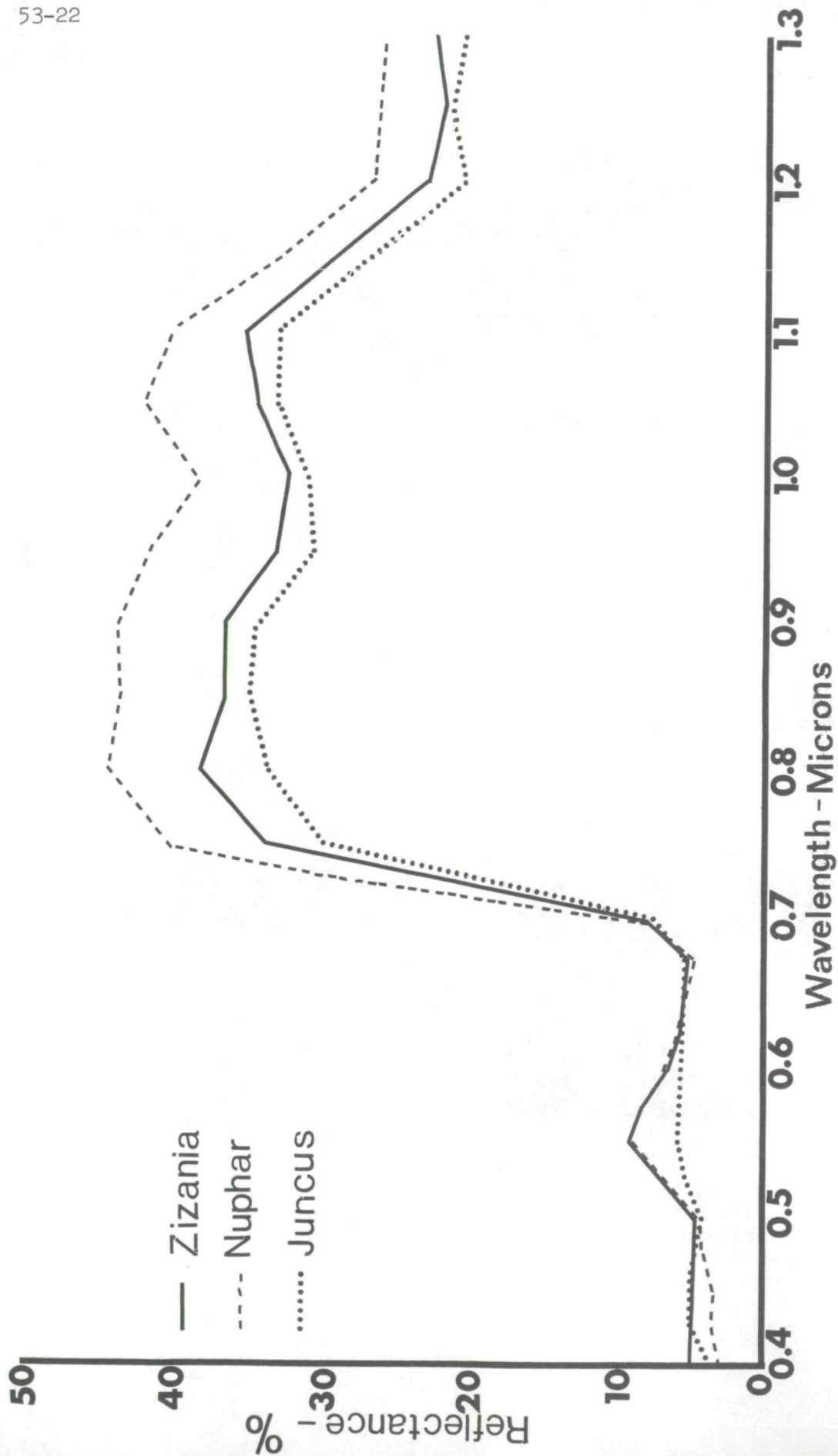


Fig. 5 Compares spectral reflectance characteristics, in the 0.4-1.3 micrometer range, of Zizania aquatica (wild rice), Nuphar advenum (water lily) and Juncus sp. (black rush).



Fig. 6. Color IR photograph showing tonal quality of important wetland species. A - cattail; B - sweetflag; C - wild rice; D - water lily. Scale 1 cm = 120 meters.

Phragmites

— July
 - - - October (I)
 — October (II)

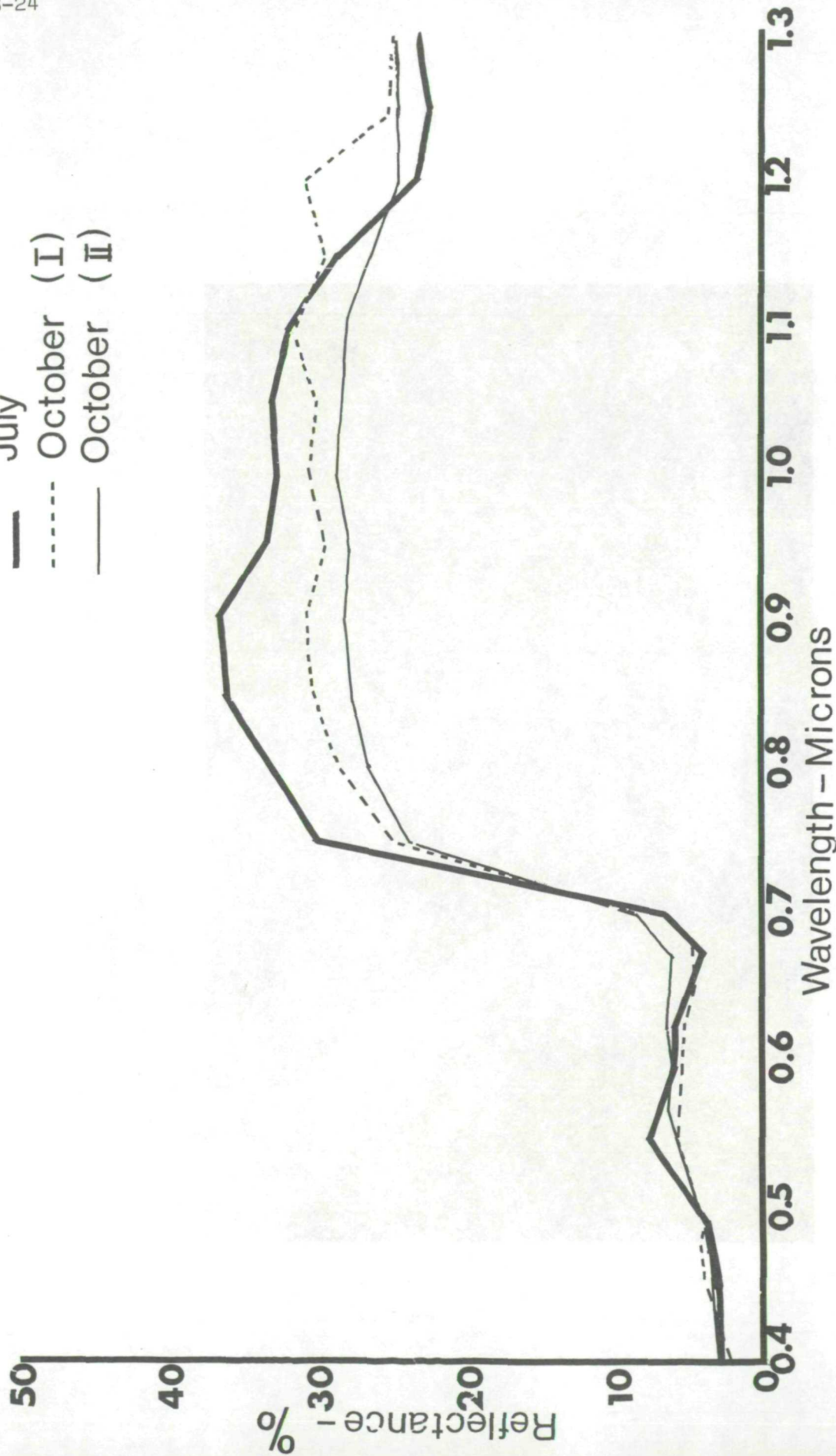


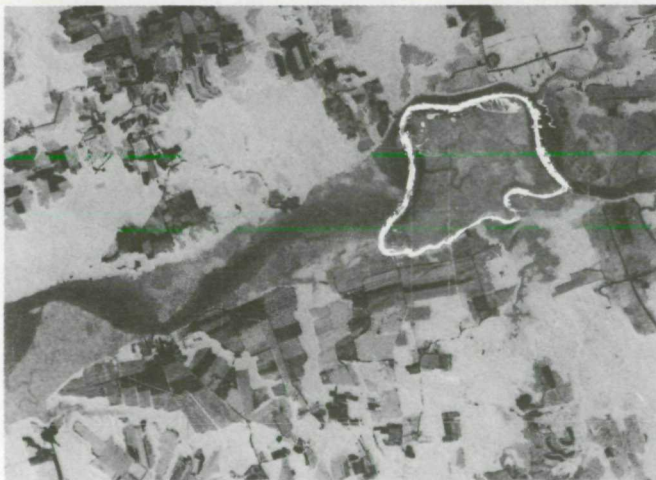
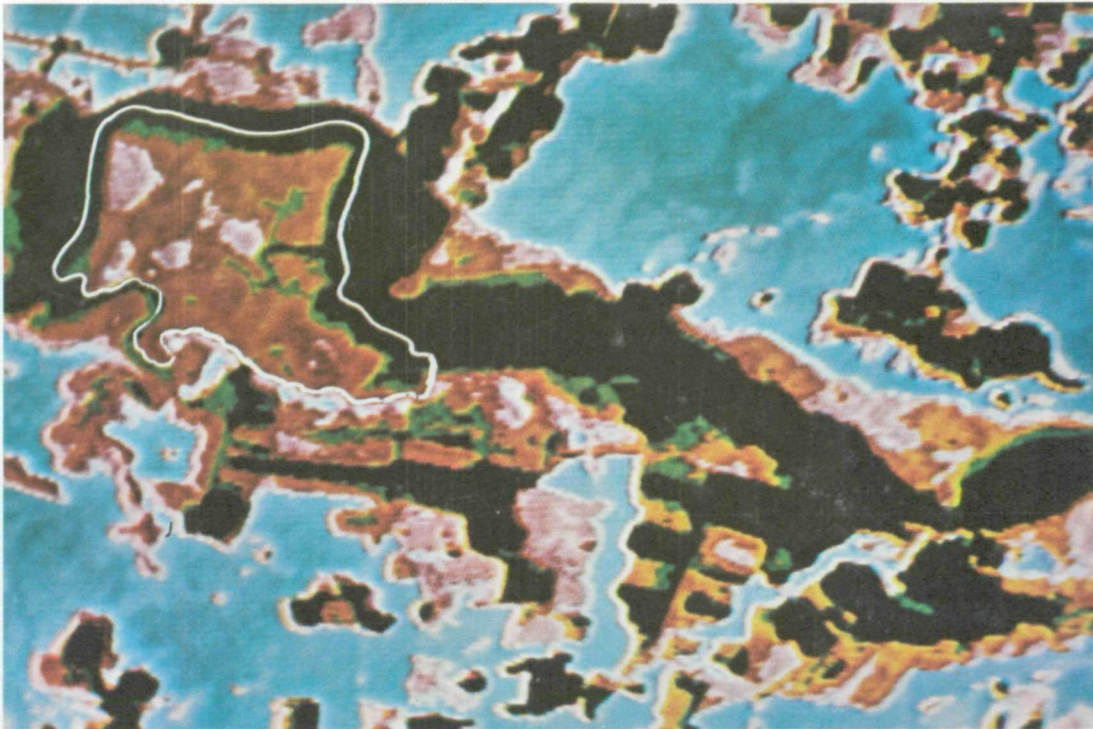
Figure 7. Spectral reflectance curves for *Phragmites communis*. between 0.4 and 1.35 microns. Note the seasonal difference in reflectance between leaves in July and leaves from adjacent areas (I and II) on October 4, as well as the intraspecies difference (I and II) toward the end of the growing season.



Fig. 8. Spring (top) and fall photograph of a wetland area showing seasonal change in reflectance of plant species. Ektachrome color IR. Scale, 1 cm = 120 meters.



Fig. 9. Datasat image showing possible analysis of sediment discharge with this system. "A" is mouth of creek and water with heaviest sediment load. "B", "C" and "D" show decreasing amounts of sediment as it disperses in the estuary. Scale, 1 cm = 100 meters.



NOT REPRODUCIBLE

Fig. 10. Datacolor image (top) and black and white photograph from which image was generated. General delineation of species composition in the wetland (outlined area) can be done from high altitude photography. Scale, 1 cm = 800 meters.



Fig. 11. High altitude photograph of a wetland showing distinctive features of high marsh (brightly colored) and low marsh (dull green color). Ektachrome color IR. Scale, 1 cm = 640 meters.

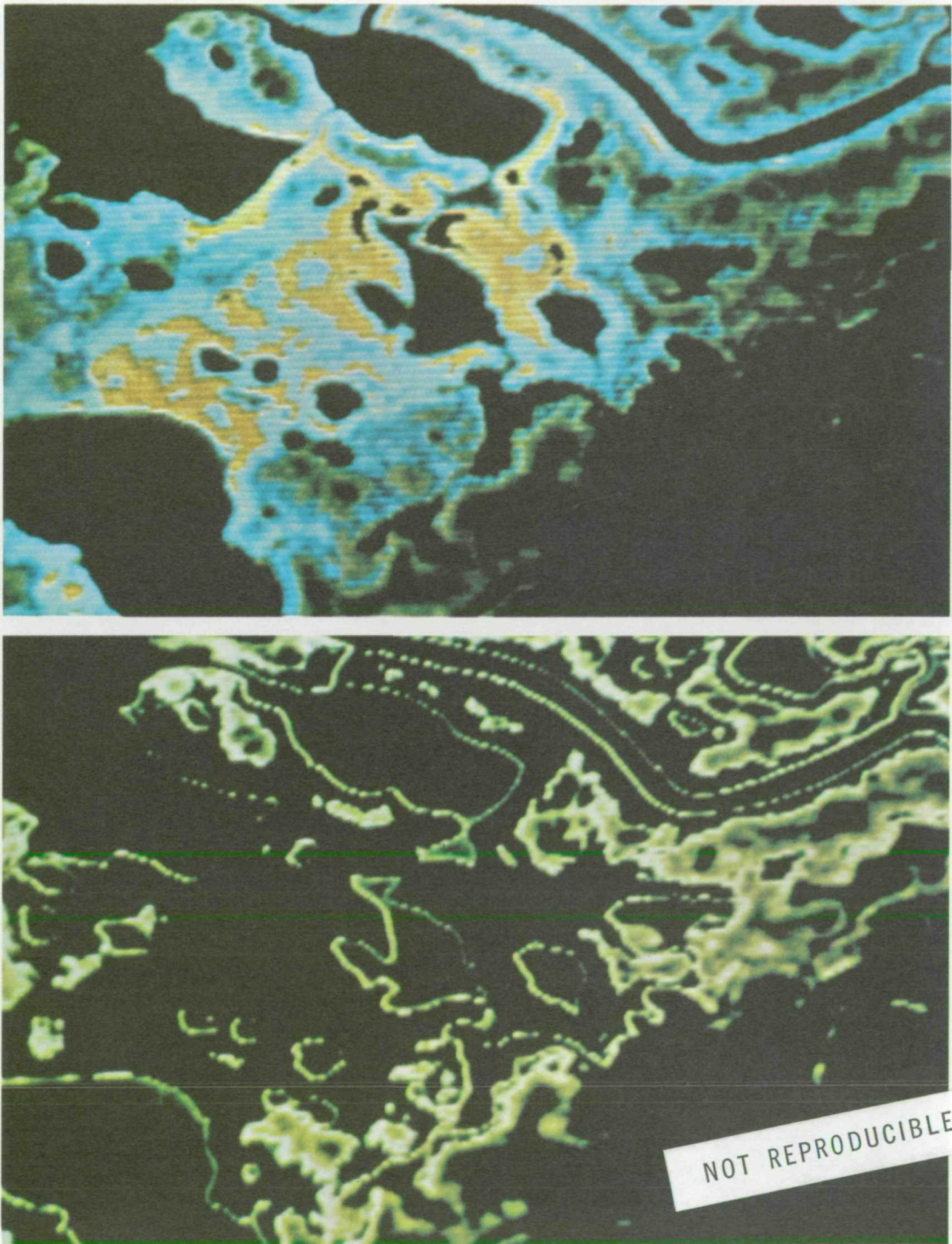


Fig. 12. Datacolor image of wetland showing high marsh (yellow), low marsh (blue) and shallow water (green).

DATA RELAY SYSTEM SPECIFICATIONS FOR
ERTS IMAGE INTERPRETATION 1/

by

James F. Daniel
U.S. Geological Survey
St. Louis, Missouri

INTRODUCTION

Experiments with the Data Collection System (DCS) of the Earth Resources Technology Satellites (ERTS) have been developed to stress ERTS applications in the Earth Resources Observation Systems (EROS) Program. To date (December, 1970), the active pursuit of this policy has resulted in the design of eight specific experiments requiring a total of 98 DCS ground-data platforms. Of these eight experiments, six are intended to make use of DCS data as an aid in image interpretation, while two make use of the capability to relay data from remote locations. Preliminary discussions regarding additional experiments indicate a need for at least 150 DCS platforms within the EROS Program for ERTS experimentation. Results from the experiments will be used to assess the DCS suitability for satellites providing on-line, real-time, data relay capability.

The rationale of the total DCS network of ground platforms and the relationship of each experiment to that rationale will be discussed herein. Technical details of the DCS capability (Daniel, 1970) will not be discussed.

DESIGN GOALS

One of the key elements in determining ERTS performance requirements was, and is, the capability of satellite sensors to monitor change in terrestrial features. Changes occur in important features

1/ Publication authorized by Director, U. S. Geological Survey

of all disciplines which will make use of ERTS data, but the time-frame of change varies from a few minutes or hours for water features to geologic time for some land features. The concept of time-rate-of-change is also important to the DCS. Ground data planned for relay in each of the experiments are applicable to one or more of several goals tentatively grouped into two broad categories of Interpretation Aids and Real Time Uses.

INTERPRETATION AIDS

Ground-sensed parameters which fulfill goals basically categorized as Interpretation Aids, are those which furnish quantitative information regarding:

1. Conditions within an image or image set (solar radiation, air temperature, wind, etc.).
2. Changes in successive images (water levels, precipitation, etc.).
3. Image features (areal extension of point-collected water quality data).
4. Applicability of images to the problem or experiment (water levels are high, low, median, etc.).

Categories 1 and 4 require the collection of background data concurrent with imagery in order to fully satisfy requests for imagery representing specific climatic or hydrologic conditions.

All four of these categories have application to image interpretation whether there is a functioning DCS or not. A report on Apollo 9 photography (Powell and others, 1970) is an example of the use of ground data to help interpret imagery. All hydrologic data within the photographed area for the time of overflight, as well as all historical data for the area, were used to formulate a conceptual working model of the geohydrologic system in that area. This will be a typical and significant use of all ERTS-A data, but it can be done within a leisurely paced time-frame. When interpretation of the imagery must proceed in real time, the DCS is required in order to shorten the data collection process. Additionally, a conceptual or mathematical model of the system being studied must already be in existence. The criteria for experiments with the DCS related to interpretation are: (1) relayed parameters must relate to one or more of the four stated categories; (2) a working model of the image area must be in existence; and (3) interpretation must be

done in near real time (hours or a very few days).

REAL-TIME USES

The other advantages of the DCS, which include ground-sensed parameters useable in real time, are:

1. Ground sensors may be located where they cannot be physically reached in a reasonable time frame (mountainous or estuarine environments).
2. Data may be used by management units for operational decision-making (hydroelectric power development, municipal water supplies, etc.).
3. Data are the basis for standing requests for imagery collection and/or precision processing for specific climatic or hydrologic conditions (ERTS data management).
4. Ground sensors are useful in determining proper exposure or probability of successful exposure of satellite sensors (net or total radiation in ERTS spectral bands; oceanic turbidity near shore for effect on bottom detail).

The last reason specifically relates to satellite sensor management of which little may be done with ERTS-A (excluding tape recorder usage). However, experimentation with these sensors on ERTS-A will allow development of techniques for managing forthcoming operational satellites.

These uses are intrinsically time-related and hence require a real-time data relay system. The sole criterion for experiments with the DCS related to real-time uses is that the DCS be an economic method of data collection at the present time.

In "real world" considerations from a manager's point of view, very few management uses of data can be satisfied with the once-every-12 hour capability of ERTS-A for data collection. Most users will eventually require an on-line capability. Therefore, the performance of the DCS in all the experiments will be used to determine the effectiveness and applicability of an ERTS relay system to the economic alternative of a series of orbiting satellites, geosynchronous satellites, or combination of the two. Each of these alternatives would supply an on-line data relay capability.

PLANNED EXPERIMENTS

There are, to date, eight planned DCS experiments for ERTS, each of which satisfies one or more of the design goals. These experiments represent the major disciplines of hydrology, geology, and geography and will be discussed in the order of listing in Table 1.

DELAWARE RIVER BASIN

This experiment is essentially a microcosm of the entire DCS rationale. The primary purpose is to obtain near real-time data from water-quality monitors and water-level monitors in the basin, to correlate the values with near real-time imagery (as obtained), and to use this information in the management decision processes of the Delaware River Basin Commission. Data from the platforms will also be used in the interim of image overflights as input to management decisions. The experiment will focus primarily on the following questions: Is bulk processed imagery satisfactory for management purposes or is precision-processed imagery required? What logistical problems arise in supplying either type of imagery in real time? How are decisions modified with real-time imagery and real-time data? Therefore, the experiment will add two dimensions to current operations: 1) The dimension of near real-time (12 hours), and 2) the areal extension of point-collected water-quality data.

REGIONAL ECOLOGICAL TEST SITES

Central Arizona, South Dakota, and Lake Ontario (numbers 2-4 in Table 1) are regional test sites for ERTS that will have a few platforms for image interpretation purposes. Because there will be intensive ground truth collection programs at these sites during image orbits, there is a need to be able to assess the ground conditions prior to the overflight. Using data relayed from key sites in the test area, a decision can be made regarding whether conditions warrant a large, manned effort in the area during image overflights. Therefore, the investment of a small amount of money in platforms has a potential benefit of saving several times that amount in unnecessary ground truth collection as well as providing ground truth at key locations.

SAN JUAN MOUNTAINS

The DCS will provide near real-time data in this mountainous Colorado region for use in assessing the efficiency of the atmospheric research being conducted there. Climate extremes will provide a good operational test of the DCS platforms in a hostile environment as well as providing more up-to-date data than are presently available. Image analysis will also be aided in assessing snow moisture conditions on an areal basis.

VOLCANO MONITORING

Experiments 6 and 7 will both be conducted on volcanoes in the Cascade Range in Washington, and in Central America, but in general these experiments will not be using the same platforms. One set of platforms will be located at optimum sites for measuring the number of seismic events and tilt, while the other set will be located at optimum sites for measuring subsurface temperature. These two experiments will utilize the capability of the DCS to relay data from remote locations with the short-term goal of adding to the knowledge of eruptive processes and the long-term goal of eruption prediction at these and other volcanoes.

HOUSTON

The Geographic Applications Program will relay data from eight platforms in the Houston, Texas area for two primary purposes. The first is to provide an intensively instrumented solar radiation test site to determine methods of image processing to reflect atmospheric attenuation conditions. Results from this site will be used to develop methods of extrapolating solar radiation data from a single monitor to larger areas. Successful experimentation would have the impact that recorded solar radiation data from several agencies' ongoing programs (e.g. the National Weather Service's network of ground stations) could be used for image processing control in many other parts of the country. The second purpose is to develop criteria for management of satellite sensors in order to operate those sensors only under acceptable conditions as indicated by real-time solar radiation data.

RELATIONSHIP TO AIRCRAFT PROGRAM

For several of the experiments relating to image interpretation, aircraft imagery in the ERTS spectral bands is required in order to finalize the local DCS networks. As aircraft data are obtained, the local networks of ground sensors (in some cases these number in the hundreds) will be analyzed to determine which types of sensors and how many of each type are desirable for DCS instrumentation. After this preliminary analysis, the final choice of sites will be made. During the actual experiments, aircraft flights are needed at some sites during ERTS image overflights for integrated ground, air and space data collection. Therefore, many of these experiments will be included in the aircraft program.

SUMMARY

The EROS Program plans experiments with the DCS requiring 98 ground platforms but indications are that this number will shortly be increased to 150. Uses of the DCS can be basically categorized as interpretation aids or as near-real time data collection. Although only the Delaware River basin experiment embraces nearly all of the possible reasons for using the DCS, each of the remaining experiments relates in a particular manner to the total rationale.

REFERENCES CITED

- Daniel, J. F., 1970, Satellite (ERTS-A) network of ground data sensors: A user-oriented experiment: National Symposium on Data and Instrumentation for Water Quality Management, Univ. of Wisconsin, July 1970. Preprint No. 29, 12p.
- Powell, W. J., Copeland, C. W., and Drahouzal, J. A., 1970, Delineation of linear features and application to reservoir engineering using Apollo 9 multispectral photography: Alabama Geological Survey Information Series 41, 37p.

Table 1. -- EROS DCS Networks For ERTS Experimentation

Experiment Location	Discipline	Purpose	Parameters	Number of Platforms
1. Delaware River Basin, Pennsylvania, New Jersey	Hydrology	Water Management	Water Quality Stream Stage Reservoir Stage Ground-Water Stage	20 ERTS-A
2. Central Arizona	Hydrology	Arid Hydrology	Precipitation Solar Radiation Air Temperature	2 ERTS-A 4 ERTS-B 6 Total
3. South Dakota	Hydrology	Snow and Ice, Shallow Aquifers	Ground-Water Stage Air Temperature Solar Radiation	2 ERTS-A 4 ERTS-B 6 Total
4. Lake Ontario, New York, Canada	Hydrology	Prototype Ocean, Circulation	Water Quality Current Velocity and Direction Solar Radiation	2 ERTS-A 4 ERTS-B 6 Total
5. San Juan Mountains, Colorado	Hydrology	Atmospherics Modification	Precipitation Snow (water equivalent) Wind Stream Stage Rime Ice	12 ERTS-A
6. Cascade Range, Washington, Central America	Geology	Volcano Monitoring	Seismic Events Tilt	10 ERTS-A 20 ERTS-B 30 Total
7. Cascade Range Washington, Central America	Geology	Volcano Monitoring	Temperature	5 ERTS-A 5 ERTS-B 10 Total
8. Houston, Texas	Geography	Image Evaluation	Solar Radiation	8 ERTS-A
				98 Total

THE ROLE OF REMOTELY SENSED AND RELAYED DATA
IN THE DELAWARE RIVER BASIN

by

Richard W. Paulson
U.S. Geological Survey
Harrisburg, Pennsylvania

INTRODUCTION

For several years the U.S. Geological Survey has operated a system of water-quality monitoring stations in the Delaware River Basin that provides riverine and estuarine water-quality data to water-resources agencies in the basin. This report is a discussion of the planned integration of the existing monitoring and data processing systems with a data-relay experiment proposed for the Earth Resources Technology Satellite (ERTS)-A, which will be launched in 1972. The experiment is designed to use ERTS-A as a data relay link for a maximum of 20 hydrologic stations in the basin, including streamgaging, reservoir level, ground water level, and water-quality monitoring stations. This experiment has the potential for reducing the timelag between data collection and dissemination to less than 12 hours. At present there is a significant timelag between the time when the data are recorded at a monitoring site and the water-resources agencies receive the data. The timelag exists because most of these instruments operate in remote locations without telemetry, and the data records are removed manually, generally at a weekly frequency. For most water-quality monitoring, the data do not reach water-resources agencies for a period of 2 weeks to 2 months.

WATER-RESOURCES MANAGEMENT IN THE DELAWARE RIVER BASIN

Several governmental agencies are concerned with the daily status of the quality and quantity of surface and ground waters in the Delaware River Basin. The lead water resources agency in the basin is the Delaware River Basin Commission (DRBC), which was authorized by the Delaware River Basin Compact, Public Law 87-328. This Compact, whose signatory parties are the United States Government and the states of Delaware, New Jersey, and New York and the Commonwealth of Pennsylvania, became public law in 1961. It requires the DRBC to develop, adopt, and maintain a Comprehensive Plan for the orderly development of the basin's water resources. The Basin Commissioners, who are the governors of the four states and a Presidential appointee (currently the Secretary of the Interior), have a permanent staff that is charged with the management of the water resources of the basin. Projects and areas of research for the Plan include water supply, flood protection, stream quality, recreation, fish and wildlife, pollution abatement, and regionalization of waste treatment.

The largest single task undertaken by the DRBC has been the abatement of pollution in the Delaware River estuary. This abatement program is designed to improve the estuary's quality to meet the water-quality standards adopted by the Commission in 1968. The pollution-abatement plan includes "... the adoption of basin-wide regulations for implementing and enforcing the Standards, the assignment of wasteload allocations to each estuary discharger, and the establishment of a broad surveillance program to keep fulltime check on discharge effluents and stream quality" (DRBC 1968).

Engineering and computer studies of the estuary's capacity to assimilate oxygen-consuming waste provide the DRBC with a basis for assigning wasteload allocations to dischargers once water quality standards were adopted. Soon after the wasteload allocations were issued, estuary dischargers were required to submit, for DRBC approval, schedules of compliance showing how long it would take the particular discharger to complete waste-treatment facilities required to reduce wasteload to meet the allocation. Schedules of compliance by most estuary dischargers should be complete by 1970, and a measurable improvement in the water quality in the estuary is expected to be attained in "... the-early-to-mid-1970's" (DRBC 1969).

As a Federal-State Compact, the DRBC is a uniquely authorized regulatory agency that has adopted a plan for managing the water resources of the Delaware River basin, including pollution abatement in the Delaware River estuary. The pollution-abatement plan is expected to produce a measurable improvement in water quality in the next several years at a cost of several hundred million dollars. The water-quality monitoring program of the Survey is one of several sources of data for the Commission.

For many years the City of Philadelphia has been interested in the water resources of the Delaware River Basin and the water quality of the Delaware River estuary. Since 1946, the City's Water Department, which uses the estuary as a major water-supply sources, has spent "... nearly \$300 million to expand and modernize its wastewater system. About \$100 million of this has gone into facilities that directly protect the rivers" (City of Philadelphia, 1970). In participating in the DRBC's pollution-abatement plan, Philadelphia "... will expand its water pollution control plants and replace many of the older tributary sewers" at a cost that "... may exceed \$200 million in the next decade" (City of Philadelphia, 1970). The Water Department has supported the operation of the water-quality monitoring system to "...warn of industrial spills, temperature rises, salt water influx, sewage problems, other forms of pollution (and to provide) data for long-range prediction of river conditions." (City of Philadelphia, 1970).

A third agency concerned with the daily status of water resources in the basin is the U.S. Geological Survey's Office of the Delaware River Master. The River Master is charged with implementing a Decree of the United States Supreme Court, which resolved a conflict of water-supply need. Water is exported from New York City reservoirs in the upper reaches of the basin to the New York City water supply system. Because the water is exported from the basin it is not available (for other uses) downstream from the reservoirs. During periods of drought the conflicting needs for the exported water by New York City and downstream users have become acutely apparent. When this conflict was brought to the Supreme Court, originally in the early 1930's and again in 1954, the Court decreed limits of withdrawal of water by New York City and a minimum level of streamflow downstream from the reservoirs. Thus, on a daily basis, and in accordance with the decree, the River Master prescribes releases of water from New York City reservoirs to maintain the required level of streamflow and monitors withdrawals from the reservoirs for New York City's water supply.

State health and natural resource agencies, municipalities, and Federal agencies, including the Army Corps of Engineers and the Federal Water Quality Administration also have need for water resources information in the basin.

DELAWARE RIVER BASIN WATER-QUALITY MONITORING AND DATA-PROCESSING SYSTEMS

The Geological Survey's water-quality monitoring system is composed of continuously operating instruments that record dissolved oxygen concentration, temperature, specific conductance at 25° C, and pH at 11 sites in the basin. (See fig. 1) The system, which is cooperatively supported by the Survey, the City of Philadelphia Water Department, the Delaware River Basin Commission, the Delaware Geological Survey, and other local, state and Federal agencies, provides water resources agencies with data on stream quality in the major rivers of the basin in addition to the Delaware River estuary and Delaware Bay.

Many of the monitors operate in remote locations where seasonal ranges in temperature and humidity are large, where sediment, algae, and other debris in the water adversely affect sensors and water-sample transfer systems, where ice and wave motion can damage sensors in the stream, and where vandalism contributes to equipment failure. For example, two of the stations frequently operate for long periods of time between servicing visits because they are on islands in the Delaware River estuary and Bay and are very difficult to service, especially during the winter months when high winds and ice make conditions very hazardous. A continuing effort is made to protect the instruments from environmental hazards, and field calibration checks are run on the instruments at every opportunity. Nevertheless, although monitors work well most of the time, they do fail occasionally. As will be discussed subsequently, data must be continuously screened for equipment failures, some of which cannot be detected in the field.

Data collected by monitors are recorded either on an analog strip chart or a 16-channel paper tape. These data records are retrieved from the monitors weekly by a technician who performs calibration tests on the instruments. The data records are returned to the Survey's Current Records Center (CRC) in Philadelphia where they are computer processed. At the end of each calendar month, data are processed to produce two computer printouts, examples of which are shown in figures 2 and 3. The printout in figure 2 contains a listing of all the hourly values of one water-quality parameter at one station. Figure 3 is a listing of daily statistics including the daily maximum, mean, minimum, range, and standard deviation, the number of missing hourly values for each day of the month, and a comparison of each day's data with recently adopted DRBC stream quality objectives (standards). Frequently, data for a particular calendar month are not completely processed until 2 weeks to 2 months after that month. The timelag varies within this range as a function of the performance of the monitors.

Although the monitors work very well most of the time, the initial steps in the data-processing system presuppose that malfunction may have taken place during the period between calibration checks. Briefly, the data at the beginning and end points of the data record are compared to independent field analyses of the four monitored parameters, and the data record is computer graphed for human screening. Human intervention in the system serves two purposes. The first purpose is to detect and eliminate spurious data from the data record, and the second is to provide a feedback loop of equipment performance back into the monitoring system. The feedback loop is necessary because some monitor malfunctions can only be detected in the data record. For example, an electronic component that behaves erratically at infrequent intervals may not be detected during a routine calibration check but may produce spurious data that can be detected by human or computer screening. Initial screening of data is made a few days after a data record is retrieved, and the feedback loop can then be closed quickly to prevent continued malfunction of the monitor.

Therefore, the data-processing system provides rapid initial screening and release of data, on a monthly basis, to water resources agencies.

The value of the large mass of water quality data presently being collected is diminished because of the timelag between data collection and dissemination. In recognition of this, efforts are made to disseminate some of these data more rapidly. The monitoring station at the Benjamin Franklin Bridge (Pier 11 North) is in one of the most heavily polluted reaches of the estuary and is near the Survey's CRC office. This station is serviced daily, and preliminary water-quality data are released via teletype (figure 4) to several agencies. A summary of water-resources conditions is also placed in a telephone recorder each day and agencies can dial the recorder directly for information. These releases provide the DRBC with data from a key estuary station. A second key station is at Reedy Island Jetty, Delaware, where the quality of the water tends to improve after passing through the more upstream Philadelphia-Chester reach of the estuary, where water quality tends to be low. This station also is a key station because it is in the salt water intrusion zone of the estuary and because a large nuclear electric generating station, potentially capable of altering the thermal regime of the estuary, is being constructed near the station. In response to the key role of the station, the DRBC has requested that the Survey install landline telemetry from the Reedy Island monitor to the CRC during fiscal year 1971. Upon installation of telemetry, the daily release in Figure 4 will be expanded to include these data.

In addition to the daily teletype summaries, preliminary weekly and monthly summaries also are released for data not yet completely through the CRC processing system.

AN APPROACH TO PROCESSING SATELLITE-RELAYED HYDROLOGIC DATA

It is expected that a maximum of 20 hydrologic sites in the basin will be instrumented with radio telemetry at the time of launch of ERTS-A. The 20 sites will include most, or all, of the water-quality monitors in Figure 1, plus key stream-gaging stations and reservoir and ground-water level stations. Data from these sites will provide water resources management agencies with indices of water-quality, streamflow, reservoir levels, and ground-water levels. In at least one instance the radio telemetry will provide a redundant communications link with a station, because by March 1972 the Reedy Island monitor will have landline telemetry. The landline telemetry will help to provide a sound basis for measuring the utility and accuracy of three modes of operation; (1) no telemetry, (2) conventional landline telemetry, and (3) satellite relayed telemetry.

Radio-telemetry instrumentation, which is still under development, will be designed to broadcast a brief data message from each station once every 90 or 120 seconds. Although the data will be telemetered continually, data will be relayed only when the satellite passes over the stations and is simultaneously in view of both the radio transmitter at the station and a receiving station, called an acquisition site. The acquisition site for data relayed from the Delaware River Basin is at the National Aeronautics and Space Administration's (NASA) Goddard Space Flight Center in Greenbelt, Maryland. Figure 5 gives the four or more periods of time, during the daily passes of the satellite over the basin, when a hydrologic station and the acquisition site are both in view of ERTS. A data message is broadcasted every 90 or 120 seconds; so, there will be 5 to 7 data messages sent during a 10-minute period of mutual visibility every 12 hours. Seventeen days are represented in figure 5 because the orbital pattern is repeated at a 17-day frequency.

The NASA Goddard Acquisition Site will have a very high probability of receiving satellite-relayed data from each of the Delaware Basin stations at least once every 12 hours. These data will be processed and relayed by NASA to the CRC on the Bell system teletype network, which is the system the CRC uses for data dissemination. After the CRC receives data from a water resources station the data will be screened before dissemination.

The screening process for data from a particular station, while highly speculative at present, will probably include a comparison of the data with data recently received from the station. This comparison will be done at estuary stations at least because the day to day changes of water-quality conditions usually are small. On the other hand, daily changes in stage can be large at stream-gaging stations, especially during periods of heavy rainfall.

It also will be useful to compare the data with summaries of recent historical data at a station. Summaries for Delaware estuary stations are becoming available as a result of a recent CRC effort to provide water resources agencies with comparisons of recent water-quality conditions to the new DRBC stream-quality objectives. Figures 6, 7, and 8a and b are examples of computer-generated summaries for dissolved oxygen concentrations, temperature, and specific conductance.

The dissolved oxygen concentration summary (Merk, 1970) presented in figure 6 has time as the ordinate, or vertical coordinate. The water year (October 1-September 30) is broken down into 122 periods of 3 days each. The abscissa or horizontal coordinate is dissolved oxygen concentration, in milligrams per liter (mg/l), from 0 to 15 mg/l. The period October 1, 1964 - September 30, 1969, or water years 1965-69, is summarized on the graph. The summary indicates the maximum and minimum concentration recorded for each 3-day period during the 5-year period, plus statistical information on the distribution of the 15 daily means. The DRBC stream quality objectives are also plotted to provide a comparison of these data to the objective of the DRBC pollution abatement program. Thus, dissolved oxygen data received from this station can be referenced to this graph to determine whether or not the data are in the range of variation recently experienced. Of course, the graph will have to be updated as water quality conditions improve in the estuary.

The summary for temperature in figure 7 follows the same general format as the dissolved oxygen graph, except statistical information on the distribution of 15 daily-maximum values (rather than daily means) is plotted with the extremes. As the DRBC stream-quality objective for temperature is stated as the permissible daily maximum rather than the daily average, as is the case for dissolved oxygen, statistical information on the daily mean is given for dissolved oxygen.

Because specific conductance (an indication of total dissolved solids in the water) is not as seasonally dependent as are the two previous parameters, the computer summaries for this parameter were not ordered by season. The largest contribution of dissolved solids to the estuary comes from ocean salts that disperse upstream. The upstream limit of these salts can differ significantly from the vicinity of the station at the Benjamin Franklin Bridge to the station at Reedy Island, a distance of about 50 miles. The strength of salinity intrusion into the estuary is strongly correlated to fresh-water inflow to the estuary. Figures 8a and 8b show two computer summaries of specific-conductance data (Paulson, 1970). The graph in figure 8a contains cumulative frequency distributions of the daily maximum, mean, and minimum specific conductances that were measured at the Reedy Island station for all days in the period October 1, 1964 to September 30, 1969, when the daily mean flow of the Delaware River at Trenton, N. J. was within 250 cfs (cubic feet per second) of the flow level of 2,000 cfs. Figure 8b is the same graph for that station for the flow level of 11,500 cfs. Notice that the vertical 50 percentile line crosses the daily maximum curve at about 18,800 micromhos (about 33% the salinity of ocean water) in figure 8a, but the 50 percentile line intersects the daily maximum curve at about 9,300 micromhos (about 15% of the salinity of ocean water) in figure 8b. The Delaware River estuary is a large body of water and does not respond instantly to changes in fresh water inflow. In fact, its response is more adequately described as sluggish. The graphs in figures 8a and 8b are crude summaries, and the basis for a more refined summary -- based on antecedent conditions -- must be determined by further research. Yet, the graphs do provide an expected range for 20 flow intervals that have been summarized for each estuary station.

When the CRC receives satellite-relayed data they will be screened against the hydrologic range and variability of historical station data before being released. Criteria may have to be established to flag data when the hydrologic condition is an extreme condition or outside the range of a permissible level, as established by water resource management officials. Flagging of the data may be provided as a service to management officials.

CONCLUSION

Frequently, water resources management agencies have difficulty taking action against unfavorable water-resources conditions because of lack of data or knowledge of the condition and of the lack of means to affect a change. The result may be a persistent undesirable condition, such as pollution, or -- as in early 1960's during the Northeast drought -- an imperiled water supply in part of the Delaware River Basin. Difficulty may also be met in coping with short-term natural disasters such as the severe flooding, and concomitant loss of life and property, that occurred in August 1955 when two hurricanes swept across the Delaware River Basin.

In meeting its obligation under the Delaware River Basin Compact, the DRBC has a Comprehensive Plan to develop the water resources of the basin. The Plan will provide the DRBC with the means of safeguarding the basin's water resources. In order to implement the Comprehensive Plan, the DRBC has encouraged and directly supported the system of hydrologic stations maintained by the Survey in the basin and has supported the installation of telemetry at key locations. Thus, progress is being made to overcome some of the conditions that constrain water resources officials from managing the basin's water resources.

The satellite data relay experiment discussed herein will determine whether satellite relay data will be adequate to meet the data needs for responsible river basin management. It should provide the basis for determining whether or not data collected once every 12 hours from a tidal estuary is sufficient to meet these needs when the large ranges of particular parameters are weighed against time of collection within a tidal cycle. For some parameters, such a measure may not be adequate, while for others it may.

The experiment will also provide impetus to develop an operational system of real-time data processing and dissemination to handle the large quantity of data that will be obtained from the stations in the basin. A library of the characteristics of hydrologic conditions at each site will be developed as reference material for screening the data as it enters the CRC. Where possible, digital computer techniques for data summarization and screening will be developed. Human intervention in the system will probably be necessary to maintain quality control on the data.

Finally, as water resources agencies develop the means for managing river basins, the results of this experiment will demonstrate the relative merits of satellite relay of data versus conventional means of data telemetry and will provide a basis for the development of operational satellite relay of hydrologic data.

REFERENCES

Delaware River Basin Commission, 1968, Annual Report; Trenton, N. J.
21 p.

_____ 1969, Annual Report, Trenton, N. J. 21 p.

City of Philadelphia Water Department, 1970, Clean Streams for
Philadelphia, the City's \$500 Million River Cleanup, Philadelphia,
Pa. 36 p.

Merk, Charles, F., 1970, A graphical summary of dissolved oxygen data
for the Delaware River estuary for water years 1965-69; U.S. Geol.
Survey open file report, 15 p.

Paulson, Richard W., 1970, A graphical summary of specific conductance
data for the Delaware River estuary, as correlated with Delaware
River flow at Trenton, N. J.; U.S. Geol. Survey open file report,
120 p.

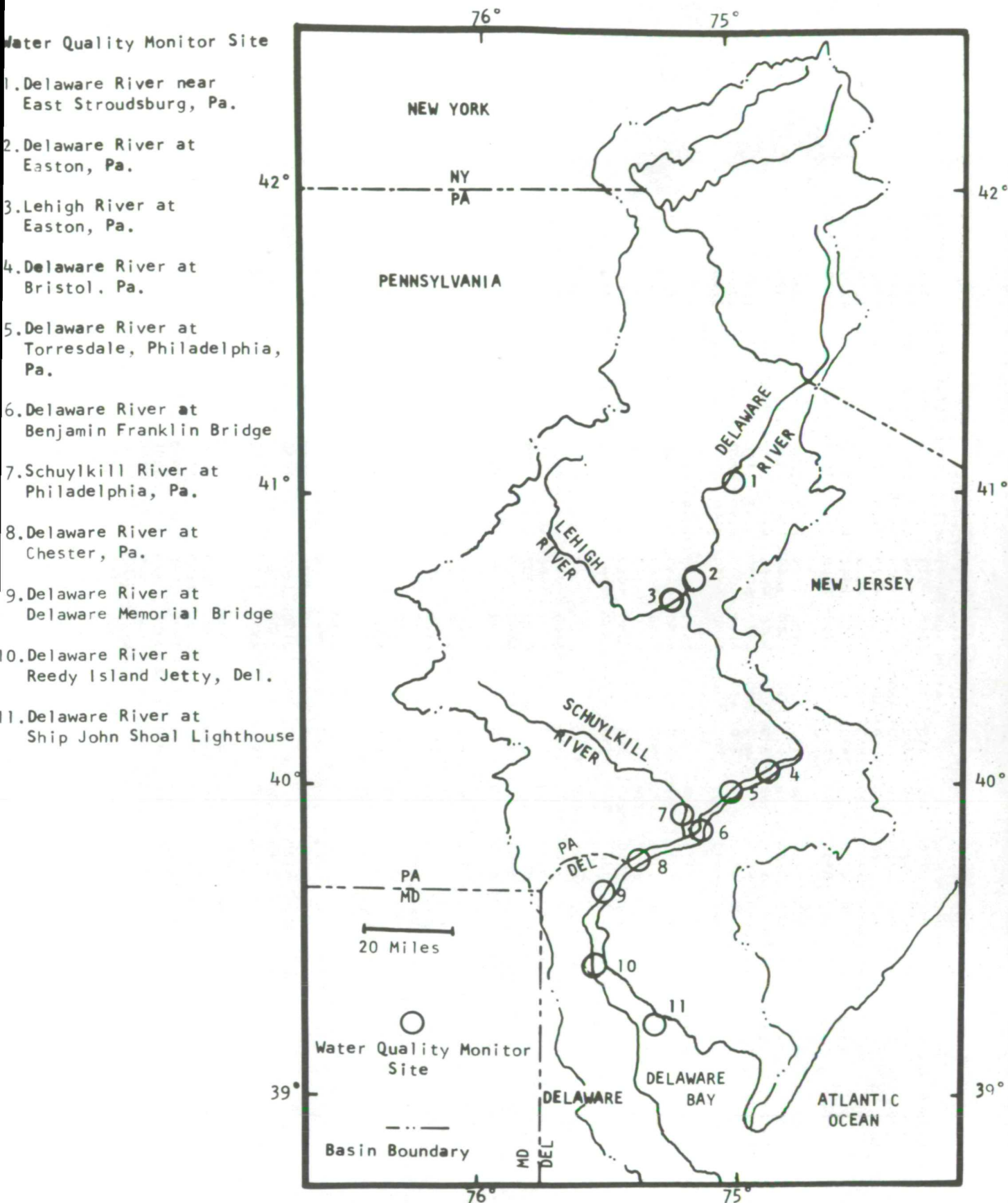


Figure 1.- Map showing location of U.S. Geological Survey water-quality monitors in the Delaware River Basin.

HOURLY VALUES OF SPECIFIC CONDUCTANCE IN MICROMHOS

DELAWARE WEEK AT DEL MEM BRIDGE	STATION NUMBER 01-4821.00 MILE POINT												NOVEMBER			
	305	306	307	308	309	310	311	312	313	314	315	316	317	318	319	1969
HOUR/DAY NO.	305	306	307	308	309	310	311	312	313	314	315	316	317	318	319	
100	3840	3500	4440	4560	4800	4600	4600	5640	5540	6660	6760	5980	4360	3360	2280	
200	4180	3840	3960	3880	3980	4000	4600	5040	5100	5560	6300	4940	4940	4180	3580	
300	4920	4180	3480	3400	3400	3460	3800	4460	4720	5120	5940	4580	5340	5260	4160	
400	5780	5180	4600	3940	3220	2860	3220	3760	4020	4700	4840	4720	4100	5140	4480	
500	6480	6000	5120	4580	3520	2480	3060	3340	4020	4360	4220	3780	3780	4220	4540	
600	6080	6600	5320	5380	4800	2920	3080	2780	2760	3400	3540	3560	3220	3800	3720	
700	5800	6340	6320	5880	5100	3900	4220	3400	2700	2900	2780	2740	2820	3360	3600	
800	5420	5760	6500	5860	6200	4560	4900	4560	3640	3060	2320	2120	2140	2820	3340	
900	5080	5620	5640	5900	6540	5300	5960	5680	4500	4220	2720	1920	1480	2120	2560	
1000	4380	5440	6040	6560	6060	5460	6700	6420	5000	5060	3760	2560	1500	1640	1920	
1100	3880	4720	5500	5420	6420	6420	7160	6000	6140	5200	5200	3820	2580	1700	1340	
1200	3520	4160	4820	4680	5380	4700	5680	7100	6580	7240	6000	3620	2580	1700	1160	
1300	3820	4060	4080	3900	4620	4480	5120	5420	6640	7540	7560	5960	4520	3480	2260	
1400	4980	4420	3740	3340	3940	4080	4880	5400	5980	6540	7400	7820	5400	4640	2980	
1500	5480	5260	3960	3060	3320	3500	4320	5180	5460	7060	6060	6720	6460	6240	4160	
1600	6380	6200	4460	3340	2880	2960	3700	4380	4940	6260	5360	5460	6400	6260	4500	
1700	7040	7640	5760	4560	3240	2580	2960	3560	4080	5220	5360	5060	4860	6200	5380	
1800	7100	8820	6520	5280	3960	2780	2820	2780	3500	4560	4360	4660	4520	5160	4860	
1900	6420	7800	7320	6140	4580	3860	3360	2720	2840	3660	3360	3880	4120	4880	4140	
2000	6080	6760	7440	6800	5400	3980	4640	3360	3040	2980	2460	2900	3180	4540	4060	
2100	5780	6800	6240	6700	5800	5120	5540	4560	3900	3400	2140	1980	2500	3620	3340	
2200	4940	6360	6340	5640	5860	5600	6100	5500	4700	4560	2780	1740	1700	2980	2440	
2300	4420	5440	5780	5660	5180	5860	6500	6500	5960	5000	3780	2240	1540	2220	1860	
2400	3880	4960	5140	5140	5160	4840	6040	6560	6600	6240	5040	3780	1540	2200	1880	
2500	320	321	322	323	324	325	326	327	328	329	330	331	332	333	334	
100	1080	940	1780	2500	3300	2340	2120	2880	2540	2220	2200	1860	1600	1420	880	
200	1260	880	1240	1900	2420	2120	2180	2220	1920	2280	2280	2140	1860	1820	1480	
300	2300	1300	1080	1420	1800	1580	1600	2180	1900	1720	1960	2040	2040	2080	1500	
400	2760	1660	1640	1320	1280	1140	1200	1520	1560	1600	1760	1540	1860	2220	1860	
500	3580	2680	2440	1760	1000	780	840	1040	1060	1280	1400	1400	1500	1760	1920	
600	3640	3220	2960	2720	1100	900	700	740	700	900	1020	1140	1440	1640	1420	
700	3400	3780	3640	3360	1700	1460	960	580	520	600	640	840	980	1460	1520	
800	2920	3600	4140	4200	2580	1720	1680	840	520	520	540	580	700	1060	1200	
900	2760	3080	3360	4660	3580	2640	2160	1560	920	700	580	580	520	740	860	
1000	2200	2700	3400	5100	3700	3060	2780	2100	1380	1440	1240	840	640	600	620	
1100	1660	2420	2900	3980	3900	3540	3480	2600	2020	1600	1400	1400	960	700	580	
1200	1120	1800	2440	3500	2960	3140	3700	2980	2440	2320	1820	1620	1320	1440	1020	
1300	880	1420	1760	3280	2900	2620	2780	2880	2720	3260	2260	2320	1860	1700	1340	
1400	1280	1180	1540	2440	2600	2480	2460	2300	2520	2720	2460	2980	2300	2320	1760	
1500	2320	1460	1260	2040	1900	1880	2420	2180	2160	2320	1880	2580	2940	2900	2300	
1600	2600	2280	1440	1820	1380	1400	1740	1800	1980	2120	1980	2000	2260	2960	2680	
1700	3260	2980	2500	1980	940	960	1260	1200	1420	1700	1580	1860	2060	2560	2740	
1800	3740	3820	2960	3260	880	760	860	860	980	1140	1160	1620	1980	2140	1900	
1900	3820	4620	3740	3780	1440	920	720	600	640	840	800	1100	1480	2060	2180	
2000	3000	4320	4600	4520	2200	1560	840	620	540	600	520	780	980	1480	1860	
2100	2780	3600	4460	5620	2640	1820	1560	860	620	620	420	580	740	1000	1260	
2200	2400	3420	3580	5160	3100	2700	2220	1460	1100	940	540	580	580	700	1000	
2300	1800	3000	3380	4400	3140	2960	2660	1880	1340	1440	1120	780	660	600	680	
2400	1400	2400	3000	4120	2360	2940	2840	2280	2020	1920	1280	1300	880	560	580	

Figure 2.-A computer listing of hourly-value data for 1 month.

DISSOLVED OXYGEN DAILY STATISTICS IN MILLIGRAMS PER LITER
 DELAWARE RIVER AT BRISTOL STATION NUMBER 01-4646.00 MILE POINT 119.21 JUNE 1967

DAY NUMBER	MAXIMUM	MEAN	MINIMUM	RANGE	STD. DEV.	NO. OF VALUES MISSING FOR THE DAY	DEV FROM STRM QUAL OBJ
152	6.9	6.3	5.8	1.1	0.3	0	-0.2
153	6.2	5.6	5.3	0.9	0.2	0	-0.9
154	5.3	5.0	4.8	0.5	0.2	0	-1.5
155	5.0	4.4	4.2	0.8	0.2	0	-2.1
156	4.5	4.0	3.8	0.7	0.2	0	-2.5
157	3.9	3.5	3.2	0.7	0.2	0	-3.0
158	3.4	3.0	2.8	0.6	0.2	0	-3.5
159	3.2	2.8	2.5	0.7	0.2	0	-3.7
160	3.6	2.9	2.5	1.1	0.3	0	-3.6
161	3.7	3.0	2.6	1.1	0.3	0	-3.5
162	3.7	3.1	2.6	1.1	0.3	0	-3.4
163	3.4	3.0	2.7	0.7	0.2	0	-3.5
164	3.6	3.1	2.8	0.8	0.2	0	-3.4
165	3.8	3.1	2.7	1.1	0.3	0	-3.4
166	3.5	3.0	2.6	0.9	0.3	0	-3.5
167	3.8	3.0	2.6	1.2	0.4	0	-2.0
168	5.8	4.5	3.1	2.7	0.8	0	-0.5
169	6.4	5.8	4.8	1.6	0.5	0	0.8
170	6.6	6.3	5.9	0.7	0.2	0	1.3
171	6.6	6.3	6.0	0.6	0.2	0	1.3
172	6.4	6.2	6.1	0.3	0.1	0	1.2
173	6.3	6.1	5.9	0.4	0.1	0	1.1
174	6.3	6.0	5.6	0.7	0.2	0	1.0
175	6.7	6.0	5.6	1.1	0.3	0	1.0
176	6.2	5.9	5.5	0.7	0.2	0	0.9
177	6.0	5.6	5.0	1.0	0.2	0	0.6
178	5.7	5.4	5.1	0.6	0.1	0	0.4
179	5.5	5.3	5.1	0.4	0.1	0	0.3
180	6.1	5.5	5.0	1.1	0.3	0	0.5
181	6.2	5.5	5.1	1.1	0.3	0	0.5

MONTHLY STATISTICS

SUBCLASS (LOWER BOUND)	2.5	3.0	3.5	4.0	4.5	5.0	5.5	6.0	6.5
HOURS IN SUBCLASS	120	118	41	28	33	87	122	155	16
	6.9	4.6	2.5	4.4	1.4	0			

NO OF OBSERVATIONS = 720 TOTAL OF VALUES = 0.334360E 04 TOTAL OF SQUARED VALUES = 0.168473E 05

Figure 3.-A computer listing of daily-statistics data and deviations from Delaware River Basin Commission stream-quality objectives for 1 month.

GEO SURVEY-PH
710-670-3438

WE WISH CONF WITH:

510-650-0815
510-650-0814
510-681-7455
510-681-7478
510-685-9564
END

FM: US GEO SURVEY PH

TO: GEO SURVEY TNT, GEO SURVEY HBG, WB-TNT, WB-HBG, DRBC

SUBJ: DAILY WATER QUALITY OF DELAWARE ESTUARY AT
BEN FRANKLIN BRIDGE (PIER 11 NORTH) PHILA PA

DATE	D.O. (MG/L)	TEMP. (F)	SPEC. COND. (MICROMHOS)	PH
10/1	0.5 - 0.0	76 - 75	399 - 352	6.7 - 6.6
10/2*	0.4 - 0.0	75 - 75	398 - 362	6.7 - 6.7

* PROVISIONAL MAX AND MIN VALUES (MIDNIGHT - 8AM)
END/CRC

GEO SURVEY-PH

Figure 4.-A daily teletype release of Delaware River estuary water-quality data.

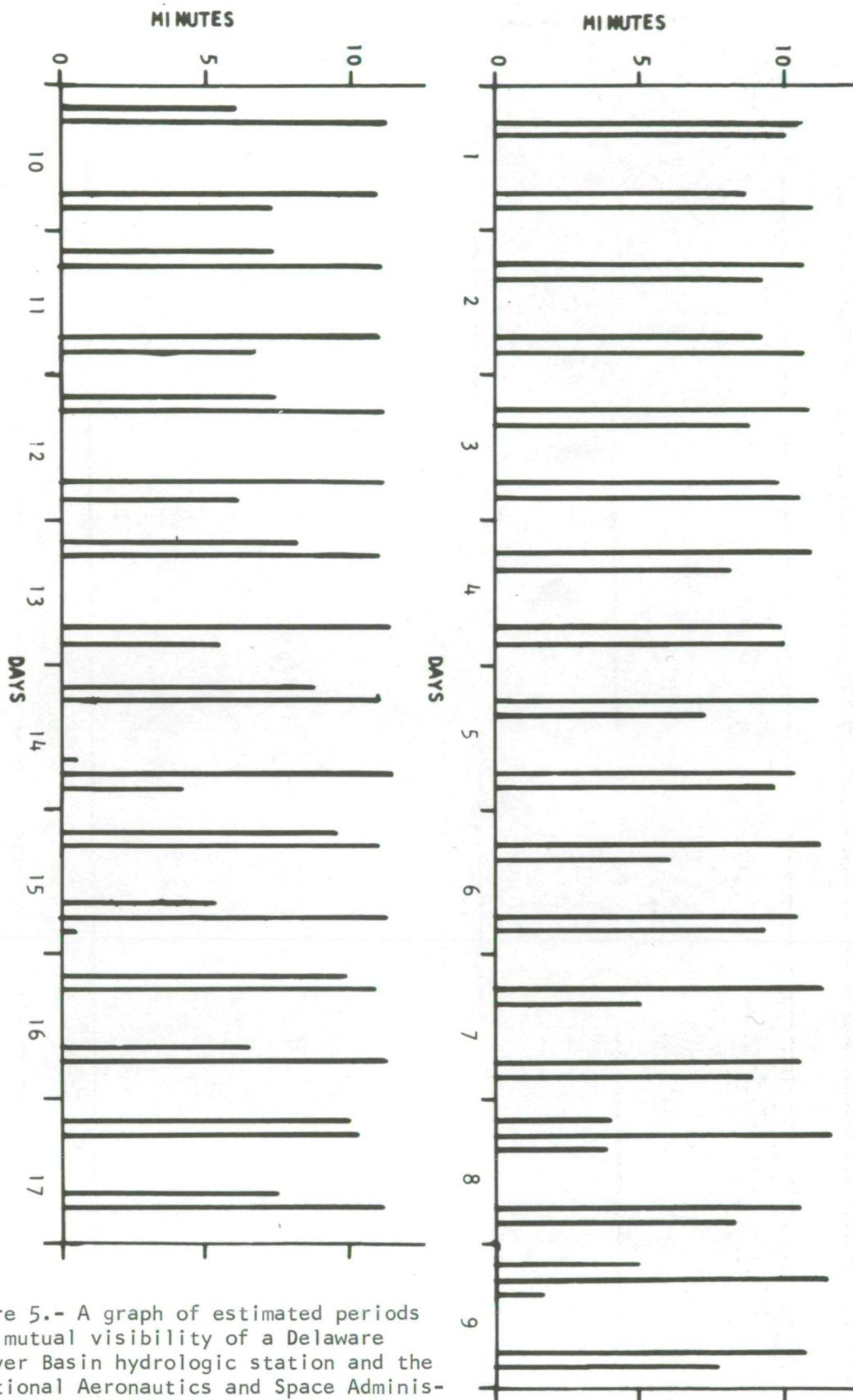


Figure 5.- A graph of estimated periods of mutual visibility of a Delaware River Basin hydrologic station and the National Aeronautics and Space Administration's Goddard Space Flight Center from a typical orbital pattern of the Earth Resources Technology Satellite.

SUMMARY OF DISSOLVED-OXYGEN CONCENTRATION OF THE DELAWARE RIVER AT PIER 11 NORTH FOR WATER YEARS 1965-69, WHERE (+) IS THE MAXIMUM VALUE FOR EACH THREE DAY PERIOD DURING THE FIVE YEARS, (-) IS THE MINIMUM VALUE, (*) IS THE MEAN VALUE OF THE FIFTEEN MEANS AND (.) IS THE VALUE ONE STANDARD DEVIATION FROM THE MEAN. THE DELAWARE RIVER BASIN COMMISSION STREAM-QUALITY OBJECTIVE IS DENOTED BY (S).

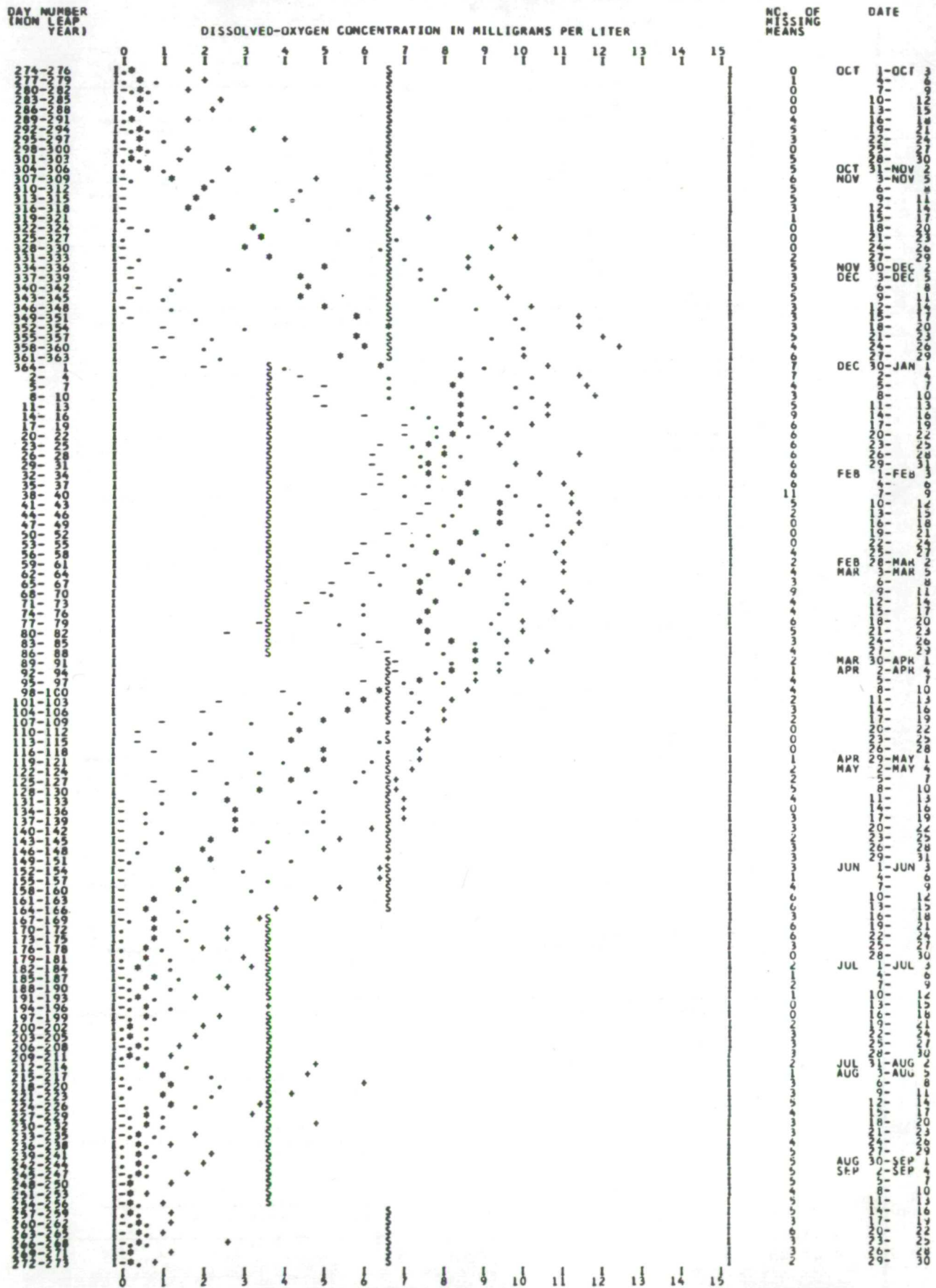


Figure 6.-A computer summary of dissolved oxygen concentration data.

SUMMARY OF TEMPERATURE DAILY STATISTICS OF THE DELAWARE RIVER AT PIER 11 NORTH FOR WATER YEARS 1965-69, WHERE (+) IS THE MAXIMUM VALUE FOR EACH THREE-DAY PERIOD, (-) IS THE MINIMUM VALUE, AND (O) IS THE AVERAGE OF THE FIFTEEN MAXIMUM VALUES. (D) DENOTES THE DELAWARE RIVER BASIN COMMISSION STREAM-QUALITY OBJECTIVE.

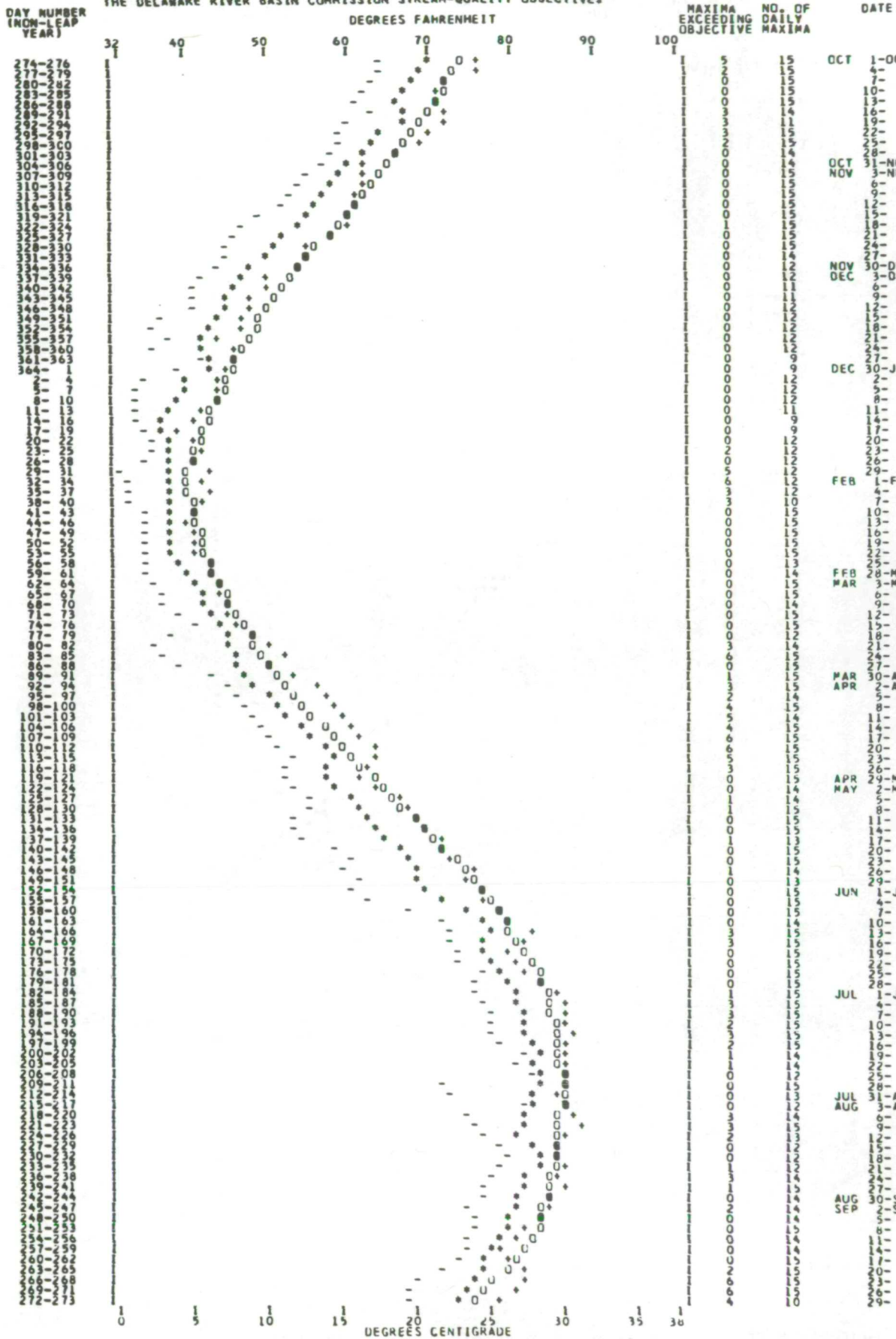


Figure 7.-A computer summary of temperature data.

THIS IS A PLOT OF THE CUMULATIVE FREQUENCY DISTRIBUTION OF DAILY MAXIMUM, MEAN, AND MINIMUM SPECIFIC CONDUCTANCE AT THIS STATION FOR ALL THE DAYS DURING WATER YEARS 1965-69 WHEN THE DAILY MEAN FLOW OF THE DELAWARE RIVER AT TRENTON WAS WITHIN 250 CFS OF 2000.CFS

STATION REEDY ISL

UPPER LIMIT OF CONDUCTANCE INTERVAL

CUMULATIVE FREQUENCY DISTRIBUTION OF MAX(+), MEAN(*), AND MIN(-) IN PERCENT (STRICTLY LESS THAN)

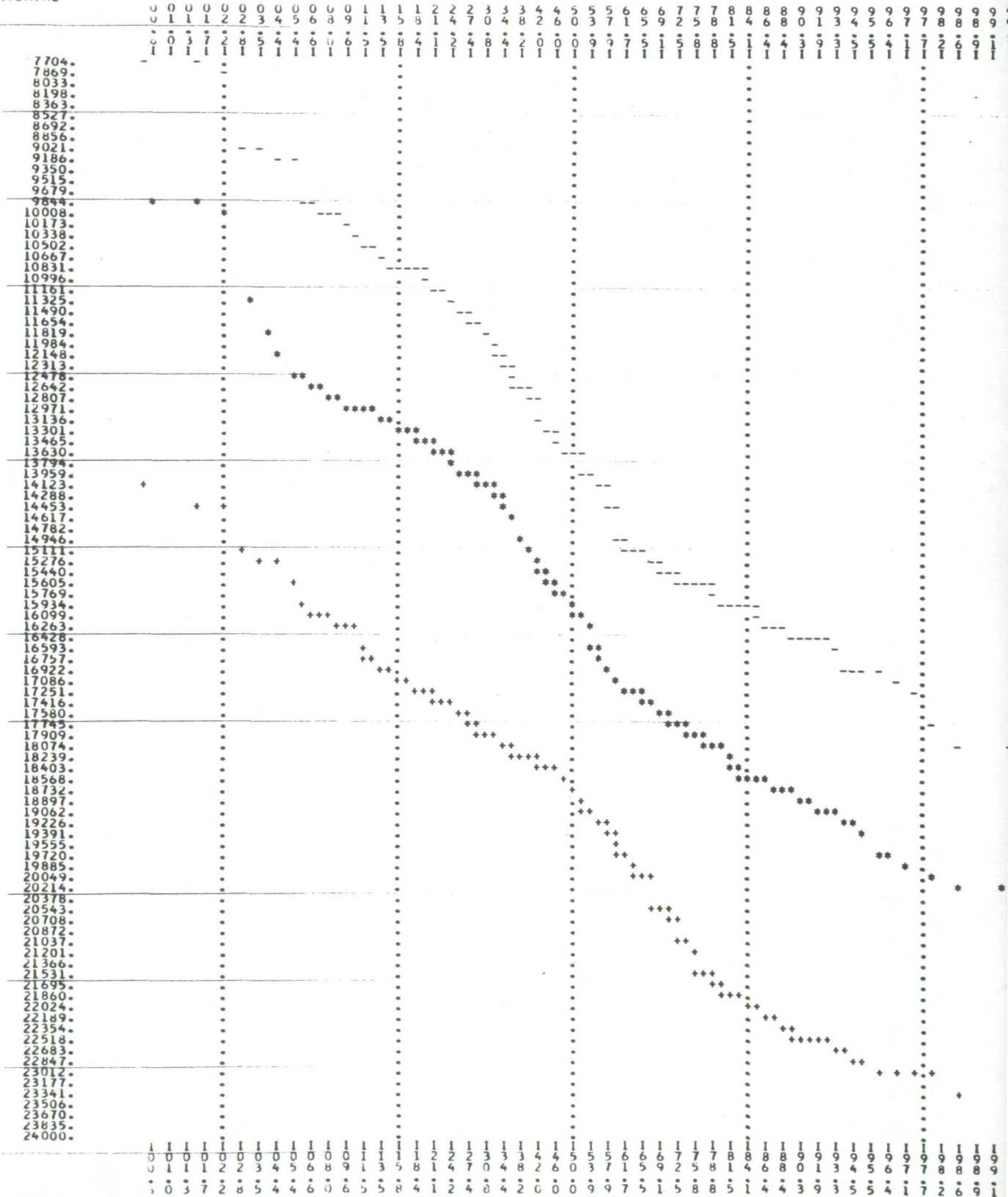


Figure 8a.-Computer summaries of specific conductance data.

NOAA's OCEANOGRAPHY STUDIES UNDER THE
EARTH RESOURCES SURVEY PROGRAM

by

E. Paul McClain
National Oceanic and Atmospheric Administration
U. S. Department of Commerce
Washington, D. C.

INTRODUCTION

The long-range objective of NOAA's program of oceanography studies is to develop, in-house and through contracts, techniques for comprehensive, repeated, and timely satellite mapping of the following oceanic variables on a local, regional, or global basis: (1) sea surface temperature; (2) sea surface roughness and near-surface winds; and (3) ice concentration and condition. An integral part of this objective is to assist in the development of applications of these remotely-acquired data to operational and research problems in oceanography and closely related efforts in meteorology. Most of this research is being carried out or technically monitored by personnel of the Environmental Sciences Group (ESG) of NOAA's National Environmental Satellite Service (NESS). A portion is being performed by researchers in NOAA's Atlantic Oceanographic and Meteorological Laboratories (AOML).

Among the short-range objectives of these studies supported under NASA's Earth Resources Survey Program are:

(1) Continue studies to define and develop methods of suppressing system noise and cloud contamination in satellite measurements of infrared window radiation emitted from Earth's surface. Refine techniques for sea surface temperature mapping over cloudfree and partly cloudy areas and use to generate multi-day composite thermal charts for large areas, including global.

(2) Relate sea surface temperature patterns in the vicinity of the Gulf Stream and in the Gulf of Mexico to associated thermal front structure at greater depth, or to the presence of associated phenomena such as currents or upwelling, with the aid of infrared data from Nimbus or the Improved TIROS Operational Satellite (ITOS).

(3) Test the feasibility of mapping sea surface roughness and low-level wind speed over the tropical oceans by means of sequential imagery from the Application's Technology Satellites (ATS) in the sun glitter zones.

(4) Continue limited study of microwave radiometer measurements from aircraft and theory for determination of optimum wavelength(s), polarization, etc. for future applications to oceanography, with particular emphasis on their usefulness and limitations for all-weather mapping of surface roughness, sea ice conditions, and possibly surface temperature.

(5) Evaluate the newly-available scanning radiometer (SR) data (visible and infrared channels) from ITOS for purposes of mapping snow and ice conditions.

A few recent results from some of the aforementioned studies are discussed briefly in the following sections.

SEA SURFACE TEMPERATURE STUDIES

Nimbus II and Nimbus III (nighttime) HRIR data have been examined by NESS over selected areas to study the problem of noise in the data and to develop a technique to derive sea surface temperatures over various size grid intervals (Smith et al, 1970). The method infers surface temperatures from histograms of generally cloud contaminated brightness temperatures within areas 100 km or more on a side. The brightness temperature associated with the clear atmosphere model, peak radiance is the statistically most probable surface temperature within the area. Comparison of temperatures inferred from Nimbus II HRIR data over the North Atlantic and Pacific, and from Nimbus III data over the BOMEX area, with ship observations showed good agreement. This technique is now being used to generate, by computer, global sea surface temperature maps using ITOS-1 SR measurements (see Fig. 1). Relative and absolute differences (RMS) of approximately 1°C and 2°C, respectively, have been attained with respect to ship observations in spite of noise (attributed to the ITOS on-board tape recorder) in the data.

A technique which reduced the effect of noise and cloud interference in the NIMBUS HRIR data, and which yields sea-surface temperatures with a spatial resolution of about 37 km was developed under contract with the Research Triangle Institute (Vukovich, 1970).

Ground truth data were gathered by the Cape Fear Technical Institute's Research Vessel (R/V) ADVANCE II in the Phase III BOMEX grid, and by the Duke University Marine Laboratory's R/V EASTWARD, off the North Carolina coast. The comparison between the processed HRIR data and the ground truth data revealed a high degree of correlation. The best agreement was attained in the Gulf Stream studies off the North Carolina coast.

Recent infrared imagery (Fig. 2) and quantitative temperature mapping (Fig. 3) derived from direct readout of data from ITOS-1 appears to be virtually noise-free and demonstrate that full-resolution (i.e. 8 km scan spot) sea surface temperature mapping is possible during cloud-free conditions. The image in Fig. 2 was displayed to bring out the thermal contrast between the warm Gulf Stream (darkest tone) and the cooler water farther inshore. Note what appears to be a secondary thermal front west and north of the primary Gulf Stream front. In Fig. 3 the Gulf Stream front is defined by the gradient from 22°C to 26°C on the northwest side of the 26°C water. Lower temperatures in the southeast and northeast corners are associated with cold clouds. The thermal gradient from ocean to the cooler land grossly defines the major features of the coastline.

Since infrared sensors on aircraft and satellites are capable only of detecting the surface thermal gradient associated with such phenomena as the Gulf Stream front, AOML researchers used bathythermograph data from 100 crossings of the Gulf Stream to investigate the relationship between the surface temperature front and the deeper thermal front identified with the core of the stream (Hansen & Maul, 1970). It was found that the mean separation between the surface front and the maximum horizontal temperature gradient at 200 meters depth was 14.5 km. An AOML study of ART and other data acquired by NASA Houston and Navy ASWEPs aircraft in conjunction with Nimbus II overflights of the C&GS vessel EXPLORER was completed. A strong linear correlation was found between sea surface temperature as measured by ART and the water vapor content of the atmosphere beneath the aircraft. There was good agreement among the ship, aircraft, and satellite observations with respect to the position of the surface thermal front and the magnitude of the thermal gradient.

SEA SURFACE ROUGHNESS STUDIES

Earlier ESG research relating sun glitter patterns in ESSA satellite pictures to ocean roughness and near-surface wind speeds, (Strong & Ruff, 1970), has been extended to include digitized brightness distributions from sequences of ATS imagery taken over a period of a few hours on given days. Glint is detectable over a

broad area that sweeps westward across the tropics with Earth's rotation. Local time variations of the brightness are a function of distance from the specular point track (known) and the roughness of the sea surface (inferred). Preliminary results based on a limited data sample indicate the feasibility of mapping the distribution of wind speeds, at least at the lower end of the speed range, from geosynchronous altitude. Further experimentation in this area was precluded by lack of computer time to process additional samples of ATS data.

An ESG study of the microwave data (1.6 cm) from the Salton Sea 1967 flights by NASA confirmed Stogryn's prediction of a cosine function fall-off of brightness temperature with increasing nadir angle out to about 30° (Stogryn, 1967), and a general increase of brightness temperature with increasing roughness of the sea surface. The slight dip in temperature at and very near zero nadir predicted by theory is inconclusive due to extreme scatter in the data at these angles. The uniform brightness temperatures across the Salton Sea prove the success of the radiometer in measuring small-scale roughness effects (small ripples and/or capillaries)--no upwind shore fetch-limited effects are seen.

SEA ICE STUDIES

Computer produced 5-day Composite Minimum Brightness (CMB) charts (McClain & Baker, 1969) have been used by ESG to study large-scale changes in snow and ice conditions in the Arctic. The CMB technique has proven effective in removing or suppressing the effects of cloudiness on the brightness of the scene. A method of using these data quantitatively to delimit sea ice conditions was developed (McClain, 1970). In this method the brightness data taken over the central Greenland ice cap and cloudfree ocean areas are used as a means of external calibration in order to adjust to observations to yield an internally consistent data set (Fig. 4). The adjusted relative brightness have been used to study sea ice conditions in the North American Arctic during the late Spring and Summer of 1969. Characteristic brightness levels have been found corresponding to the various ice concentrations and conditions summarized in Table 1.

Under a contract with Allied Research Associates, High Resolution Infrared Radiometer (HRIR) data from the Nimbus II and III satellites were used to develop improved techniques for ice mapping (Barnes et al., 1970). Sea-ice distributions in the autumn of 1969 mapped from Nimbus III HRIR film strips are compared with distributions previously mapped

from Nimbus II for the similar period of 1966. Ice is also mapped for two winter months, a season for which data had not previously been available. In order to obtain a more objective interpretation of the gray-scale variations in the HRIR film strips, densitometric measurements were also carried out.

The results of the film-strip analyses indicate that principal sea-ice boundaries in the Arctic can be reliably mapped using the techniques developed in an earlier study. Of particular interest is that ice mapping from infrared data appears most reliable during winter, the season of maximum polar darkness during which other data sources are severely limited. Despite the success in identifying ice boundaries through relative temperature differences, the densitometric analyses show that it is impossible to obtain quantitative interpretation of the film strips, even when the gray-scale wedges are used as reference. Through an improved scheme, however, the data can be presented in a format from which accurate quantitative information can be visually derived and in which features of importance to sea-ice mapping are more clearly defined.

Microwave radiometer data (19.3 GHz or 1.6 cm) taken from a 1967 NASA aircraft mission over the Arctic Ocean near Point Barrow, Alaska, were examined (Strong and Fleming, 1970). The microwave brightness temperatures corresponding to varying ice pack conditions were correlated with simultaneous photography and infrared radiation data. Microwave measurements of the surface taken both through and from beneath a stratus cloudcover were investigated for atmospheric attenuation and emission effects. It was found that the influence of clouds was greatest when the radiometer was viewing surfaces such as water, which appears cold at microwave frequencies because of its low emissivity. In general, cloudiness diminished the capability of the 19.3-GHz radiometer to discriminate between ice and water. Polynya and other openings displayed a characteristic brightness temperature nearly 100K° below that for pack ice when viewed through a cloud-free atmosphere, whereas this differential decreased by as much as $20\text{-}40^\circ\text{K}$ when clouds intervened between the surface and the radiometer.

CONCLUDING REMARKS

Knowledge of winds and waves is important to safer and more expeditious commercial ship routing, to naval operations, and to rescue and recovery at sea. Knowledge of the sea surface temperature distribution is important in the understanding of certain oceanic and atmospheric processes, and in the detection and monitoring of

ocean currents, upwelling zones, and other thermal or motion systems. Knowledge of sea ice distribution and condition is vital to commercial and military ship movements in the Arctic and Antarctic. Ice cover is also important in the heat balance of polar regions, and this in turn influences the general circulation. Thus an economic and scientific requirement exists for large-scale mapping of oceanic conditions. Comprehensive and repetitive survey by means of surface-based observation systems or by means of sensors carried in aircraft or similar vehicles would be hazardous, time-consuming, and very costly because of the vast areas to be covered. A polar-orbiting Earth satellite, however, could provide a practical means of obtaining oceanographic information for research and operational purposes.

The work briefly described above contributes to the Earth Resources Survey Program because the experience and knowledge gained in validation, interpretation, handling, and applications of available satellite and/or aircraft data can be brought to bear directly on refining requirements and specifications for analogous data acquisition and usage from the future Earth resources survey satellites. This research relates to stated NOAA requirements for data from ERTS A and B in the area of oceanography and meteorology, although part is more applicable to later satellites or manned spacecraft (e.g. SKYLAB) carrying microwave sensors.

REFERENCES

1. Smith, W.L., P. K. Rao, R. Koffler, & W. R. Curtis: "The Determination of Sea Surface Temperature from Satellite High Resolution Infrared Window Radiation Measurements," Monthly Weather Review, Vol. 98, No. 8, pp. 604-611, August 1970.
2. Vukovich, Fred M., "Physical Oceanography Feasibility Study Utilizing Satellite Data: Part II, "Final Report, Contr. No. E-236-69(N), Research Triangle Institute, Research Triangle Park, North Carolina, 72 pp, October 1970.
3. Hanson, D. V. & G. A. Maul: "A Note on the Use of Sea Surface Temperature for Observing Ocean Currents," Remote Sensing of Environment, Vol. 1, pp. 161-164, Summer 1970.

4. Strong, A. E. & I. S. Ruff: "Utilizing Satellite-Observed Solar Reflections from the Sea Surface as an Indicator of Surface Wind Speeds," Remote Sensing of Environment, Vol. 1, pp. 181-185, 1970.
5. Stogryn, A.: "Apparent Temperatures of the Sea at Microwave Frequencies," IEEE Transactions on Antennas and Propagation, Vol. AP-15, No. 2, pp. 278-286, March 1967.
6. McClain, E. P. & D. R. Baker: "Experimental Large-Scale Snow and Ice Mapping with Satellite Composite Minimum Brightness Charts," ESSA Technical Memorandum NESCTM 12, Dept. of Commerce, Washington, D. C., 16 pp., 1969.
7. McClain, E. P.: "Quantitative Use of Satellite Vidicon Data for Delimiting Sea Ice Conditions," Paper presented at 21st Alaska Science Conference, College, Alaska, August 1970.
8. Barnes, J. C., D. T. Chang, & J. H. Willand: "Improved Techniques for Mapping Sea Ice from Satellite Infrared Data," Final Report, Contr. No. E-67-70(N), Allied Research Associates, Concord, Mass., Nov. 1970.

CATE- GORY	ADJUSTED CMB AVERAGE	ICE CONCENTRATION	ICE CONDITION
1	9-10	COMPACT OR VERY CLOSE PACK (10/10-9/10)	SNOW COVERED ($>7/10$)
2	7-8	COMPACT OR VERY CLOSE PACK (10/10-9/10)	SNOW FREE ($< 3/10$); LITTLE OR NO PUDDLING ($< 1/10$)
3	5-6	VERY CLOSE OR CLOSE PACK (9/10-7/10)	SOME PUDDLES AND THAW HOLES (1/10-3/10)
4	2-4	OPEN PACK (6/10-4/10)	MUCH PUDDLING ($>3/10$) AND ROTTEN ICE
5	0-1	VERY OPEN PACK (3/10-1/10) OR ICE FREE WATERS	—

TABLE I.- COMPOSITE MINIMUM BRIGHTNESS (CMB) VALUES FOR
VARIOUS ICE CONCENTRATIONS AND CONDITIONS

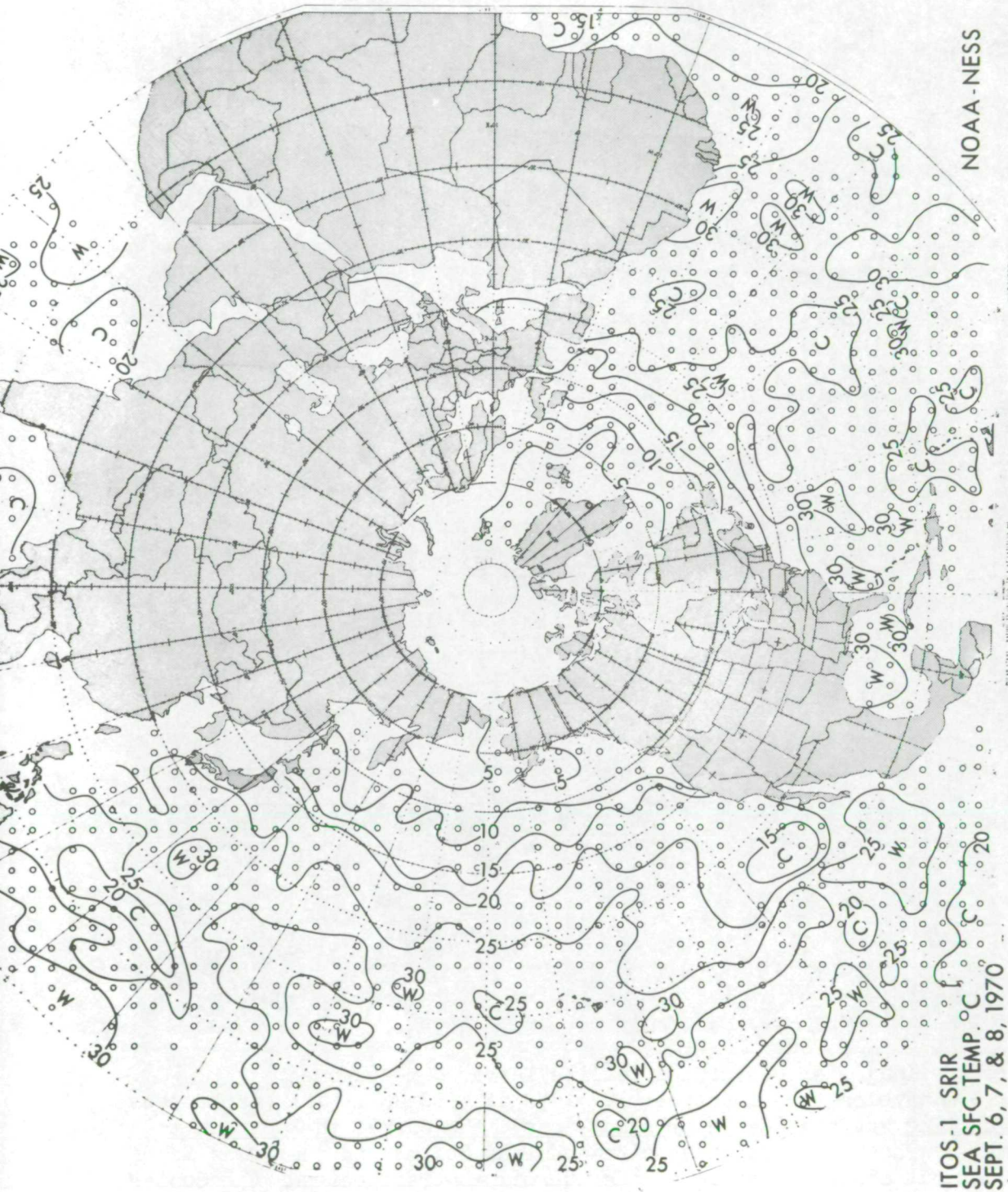
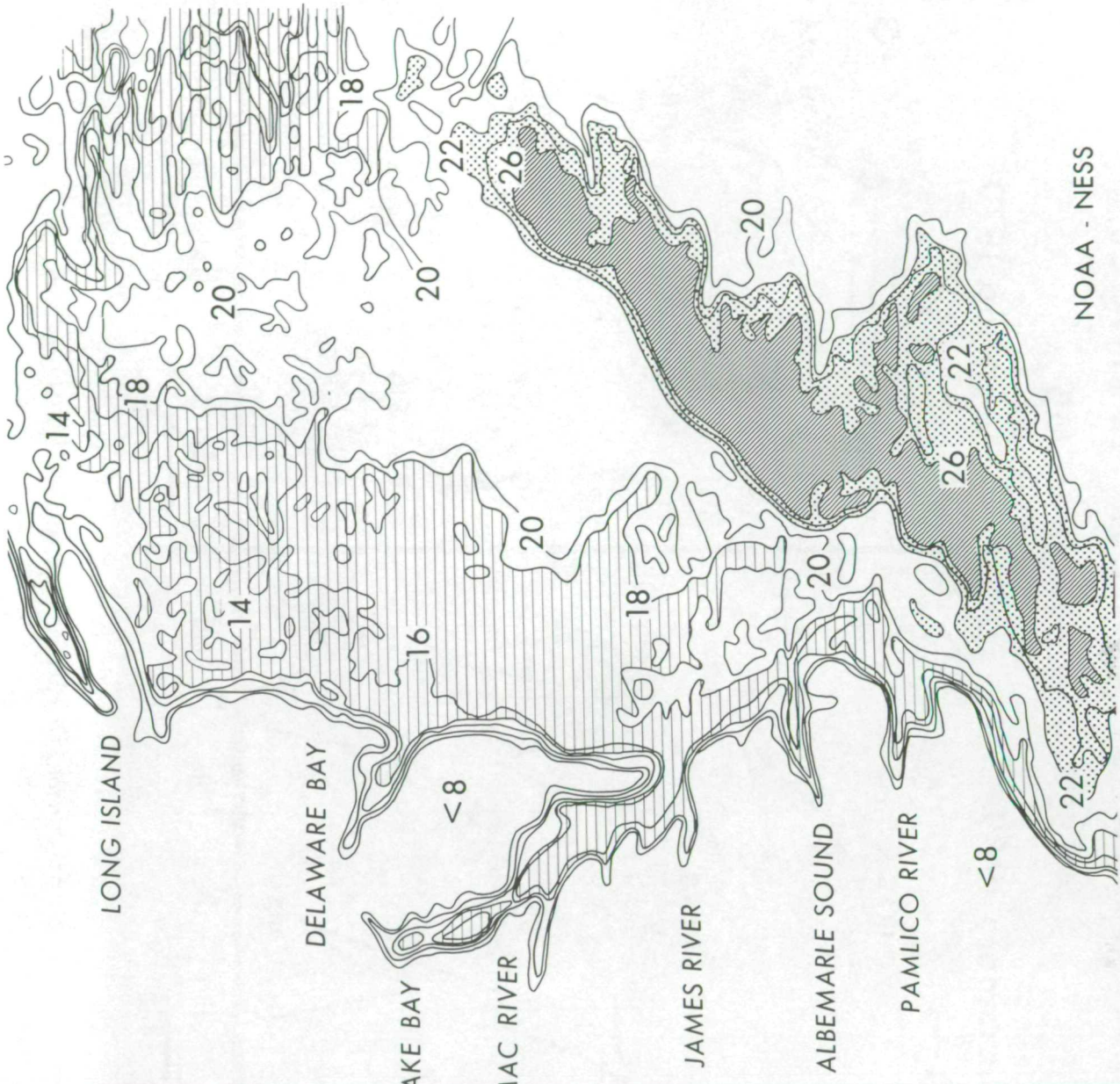


Figure 1.- Three-day composite chart of sea surface temperature derived statistically from all satellite infrared measurements falling within 280 km grid areas. An open circle is shown at the center of each grid where a temperature could be derived. Persistent cloudiness or noisy data prevented temperature derivation in the remaining grid areas.



Figure 2.- Image derived from satellite infrared measurements (10.5-12.5 m wavelength) on October 19, 1970 at 0900 GMT. The warmer the radiating surface (Earth or cloud tops), the darker the tone in the image. Thus the east coast of the United States and the Great Lakes stand out clearly because of the thermal contrast between the cooler land and the warmer water. The coldest (lightest) areas are clouds.



**ITOS 1 SRIR DIRECT
19 OCTOBER 1970
0900 GMT**

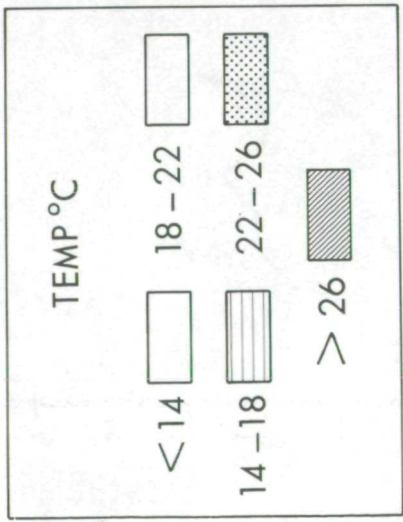
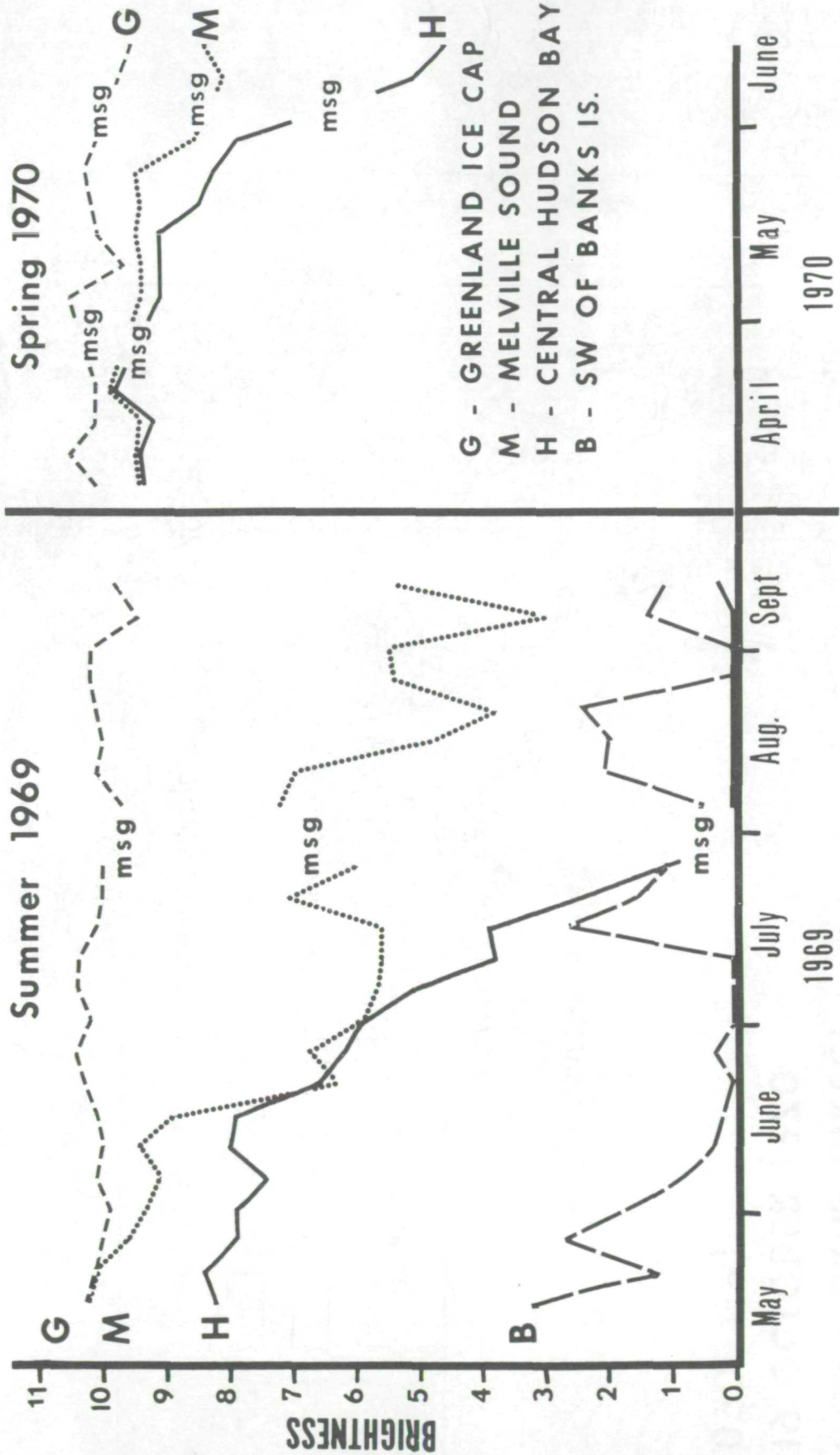


Figure 3.- Sea surface isotherms analyzed from scan-spot listings of satellite infrared measurements for the same time and for a portion of the same area as in Figure 2.

Adjusted Brightness Averages

ESSA 9 5 - day CMB



NOAA-NESS

Figure 4.- Seasonal variation of Composite Minimum Brightness (CMB) values for several sea ice areas in the North American Arctic. CMB values are routinely derived for 5-day periods from digitized and mapped vidicon data obtained by ESSA operational satellites. The notation "msg" means

NOAA's Hydrology Studies Under the
Earth Resources Survey Program

by

E. Paul McClain
National Oceanic and Atmospheric Administration
U. S. Department of Commerce
Washington, D. C.

INTRODUCTION

The long-range objective of NOAA's program of hydrology studies is to develop, in-house and through contracts, techniques for comprehensive, repeated, and timely satellite and aircraft information on the areal distribution of hydrologic factors on a local and regional basis, and to assist in the development of applications of this data to operational and research problems in hydrology and meteorology. Most of this research is being performed or technically monitored by researchers in the Environmental Sciences Group (ESG) of NOAA's National Environmental Satellite Service (NESS).

Among the short-range objective of these studies carried out with the support of NASA's Earth Resources Survey Program are:

(1) Obtain more data with a multifrequency (5) microwave system so that the range of soil moisture amounts and types can be extended. Secondly, if data permit, to establish instrument and data specifications for microwave sensing of soil moisture from satellite and aircraft.

(2) Refine the procedures for mapping snow cover that have been developed using satellite and aircraft remote sensor data in the visible spectrum. To begin the evaluation of satellite and aircraft infrared observations for determining their information content with respect to snow cover, ice cover, and water temperature over large lakes (e.g., Lake Ontario).

A few recent results from some of these studies are discussed briefly in the following sections.

SOIL MOISTURE STUDIES

From 10-24 July 1970 measurements of the microwave emission of soil as a function of moisture content were performed under contract with Aerojet General Corporation at the United States Water Conservation Laboratory near Phoenix, Arizona. Measurements of the microwave emission, soil moisture content and soil temperature were acquired along with micrometeorological data as a soil plot was allowed to dry from a flooded condition to as low a moisture content as feasible.

The purpose of these efforts was to perform a systematic study of microwave emission at 21, 6, 2.2 and 0.81 cm wavelengths of soil over a range of moisture conditions. Toward this end, microwave measurements were performed as a function of observational wavelength, antenna viewing angle, and polarization.

All radiometric data have been initially reduced and appear satisfactory in answering some basic hydrologic questions. The warmest radiometric temperatures at all wavelengths occurred for the first and driest test plot. Similarly, the coldest radiometric temperatures occurred for the wettest soil moisture conditions. Temperatures steadily decreased by about 5 deg. K for each percentage point increase in water content of the soil by weight (see Fig. 1).

SNOW COVER STUDIES

Under an earlier contract for developing methods of mapping snow boundaries in mountainous terrain scientists at Allied Research Associates concluded that mountain snow can be reliably identified in satellite photography and that mapping accuracy is as good as, or better, than in flat terrain (Barnes & Bowley, 1969). In an extension of this work, ESSA 3, 5, 7, 9 AVCS pictures, Nimbus III daytime HRIR and IDCS imagery, and Apollo 9 color photographs (hand held camera) over the western mountain states were used to map mountain snow distribution onto working base maps for comparison with aerial snow cover surveys. Climatological and ground survey data summaries were used in evaluating mapping accuracy.

The results of these investigations (Barnes & Bowley, 1970) indicate that of the three regions tested, satellite imagery provided the most reliable measurements of snow extent in the southern Sierras. For typical river basins in this region, snow extent in terms of percentage of basin covered can be determined from satellite photographs to within $\pm 5\%$ of the aerial-survey measurement (see Fig. 2). In the Kings River Basin, the satellite snow-line elevation was within 500 feet of the aerial-survey snow-line elevation, with the satellite value being higher in 10 of 11 cases analyzed.

In the Upper Columbia Basin satellite snow mapping was less reliable because the region consists of more densely forested mountain ranges, each with a relatively small horizontal snow-cover extent. Furthermore, springtime cloudiness is more prevalent in this region. In the Arizona mountains considerably lesser snow depths than in the other two regions can be mapped because of the sparse vegetation.

In-house, development of the five-day composite minimum brightness (CMB) chart (McClain & Baker, 1969) for delineating major snow boundaries has been extended by examining quantitative CMB values. The CMB technique has proven effective in removing or suppressing the effects of cloudiness on the brightness of the scene. Using brightness data taken over the Greenland ice cap and over cloudfree ocean areas as calibration references at the bright and dark ends of the range, respectively, the CMB values were adjusted to obtain an internally consistent data set. Adjusted brightness averages over areas about 40 km on a side were obtained for all available five-day periods in two Spring/Summer periods of 1969 and 1970 in several areas of Canada. Preliminary results of this study are shown in Fig. 3. The brightest areas, as expected, correspond to snow-covered frozen lakes and tundra. Snow-covered, dense coniferous forests are substantially less bright. Brightness drops to minimum values as the snow and ice cover melts and evaporates.

LAKE TEMPERATURE STUDIES

On several occasions during 1970, ITOS-1 satellite infrared (10.5 - 12.5 μ m) data were obtained of the Great Lakes. These have been corrected for atmospheric "limb darkening" and nominally mapped for comparison with aircraft infrared spot measurements along selected tracks. Furthermore, comparison has been made with ship and buoy in

situ surface-water temperature measurements. The satellite's Direct Readout InfraRed (DRIR) mode provides a signal that, during cloud-free conditions, enables a synoptic view of all the Great Lakes. Aircraft coverage of the same area would require several hours or even days.

Using this ground-air-space sensor system, confirmation was made of all the large-scale (10-20 n. miles) thermal features. In some instances features were present in the satellite imagery that were missed by the aircraft. Satellite imagery was obtained that closely correlated with monthly aircraft monitoring flights made by the Canadian's Department of Transport. One such comparison is shown in Figure 4. In November 1970, an unusual cooling was noted in the deeper, more central portion of Lake Ontario. The more typical cooling pattern is closely depth dependent and progresses from shallow near-shore waters toward the middle of the lake.

CONCLUDING REMARKS

The world's natural water supply is perhaps our single most essential earth resource, and man's ever increasing use of this vital commodity demands optimal management of it. Improved measurement or estimates of hydrologic factors on an areal basis are needed to improve forecasts of stream flow and water storage, for these in turn strongly affect power generation, irrigation, water quality (pollution), flood control and forecasting, shipping, manufacturing, and recreation. Thus, there exists an economic and scientific requirement for comprehensive and timely mapping of hydrologic parameters, especially over watersheds where hydrologic data are inadequate for proper conservation, management, and forecasting of the water resources of the region. Collecting this amount of hydrologic information by means of surface-based observation systems would be time-consuming and costly at best, hazardous at worst, because of the large areas involved and, frequently, because of their inaccessibility. Spot observations at ground-level can be supplemented by aircraft surveys, but these also are costly if large areas and/or repeated surveys are required. A polar-orbiting satellite, however, could provide a practical means for getting hydrologic observations for operational and research purposes, although a synergistic approach wherein ground-based and aircraft observations were employed in conjunction with satellites would be the most powerful.

The work described briefly above contributed to the Earth Resources Survey Program because the experience and knowledge gained

in validation, interpretation, handling, and applications of available satellite and/or aircraft data can be brought to bear directly on refining requirements and specifications for analogous data acquisition and usage from the future Earth resources satellites. This research relates to stated NOAA requirements for data from ERTS A and B, as well as to later satellites or manned spacecraft (e.g. SKYLAB) that are likely to carry microwave sensors, in the area of hydrology.

REFERENCES

1. Barnes, J. C. & C. J. Bowley: "Satellite Surveillance of Mountain Snow in the Western United States," Final Report, Contr. No. E-196-68, Allied Research Associates, Concord, Mass., 78 pp., June 1969.
2. Barnes, J. C. & C. J. Bowley: "The Use of Environmental Satellite Data for Mapping Annual Snow-Extent Decrease in the Western United States," Final Report, Contr. No. E-252-69(N), Allied Research Associates, Concord, Mass., 105 pp., June 1970.
3. McClain, E. P. & D. R. Baker: "Experimental Large-Scale Snow and Ice Mapping with Satellite Composite Minimum Brightness Charts," ESSA Technical Memorandum NESCTM 12, Dept. of Commerce, Washington, D. C., 16 pp., 1969.

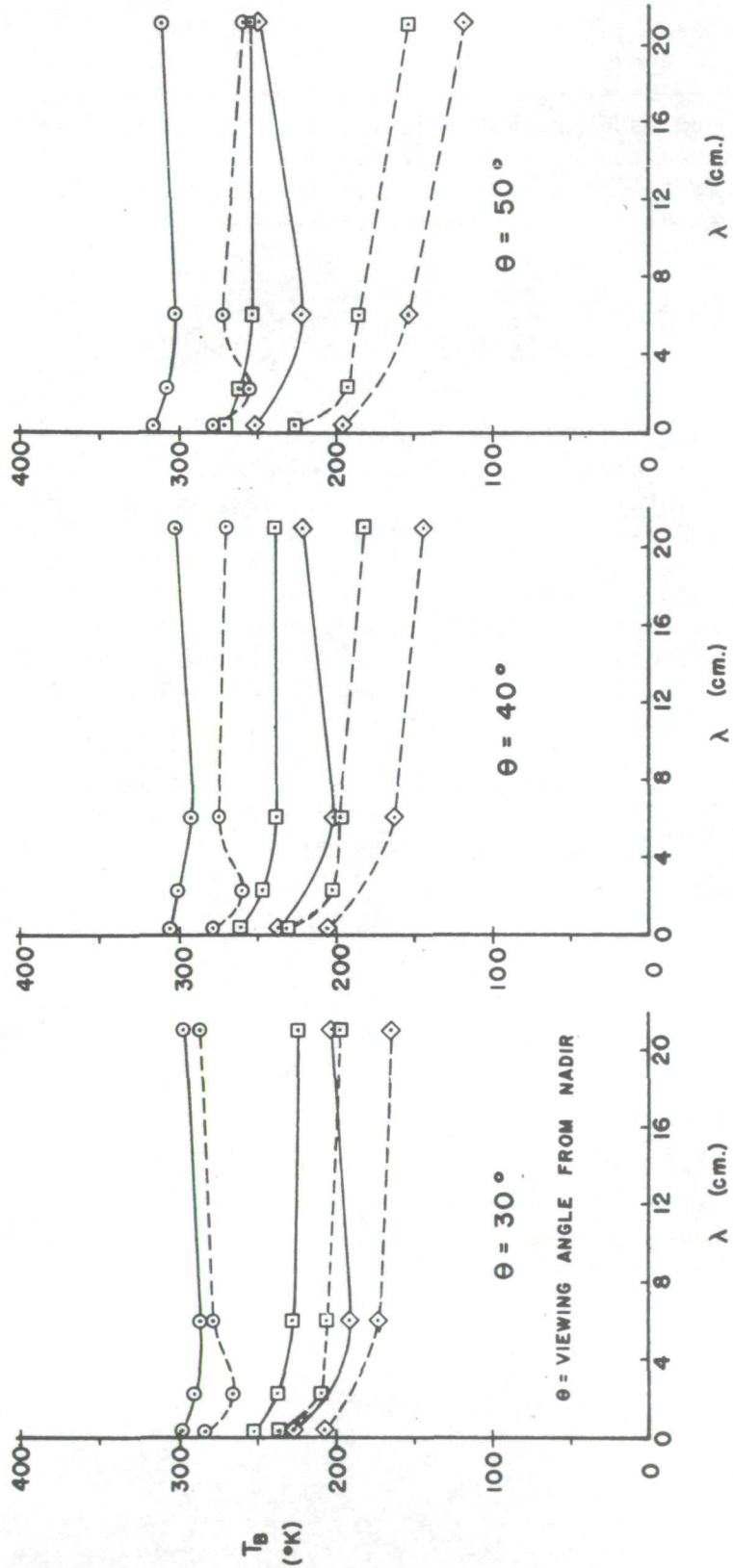
POLARIZATION

- Vertical
- - - Horizontal

FIELD MEASUREMENTS PERFORMED AT THE
 U.S. WATER CONSERVATION LABORATORY,
 TEMPE, ARIZONA 10-24 JULY 1970.
 WAVELENGTHS 0.81, 2.2, 6, AND 21 cm.

AVERAGE SOIL MOISTURE

- 5 %
- 15 %
- ◇ 25 %



RADIOMETRIC TEMPERATURE VS. MICROWAVE WAVELENGTHS

DATA OBTAINED FROM AEROJET-GENERAL CORP. — MONTHLY REPORT NO. 1684M-1
 16 AUGUST 1970

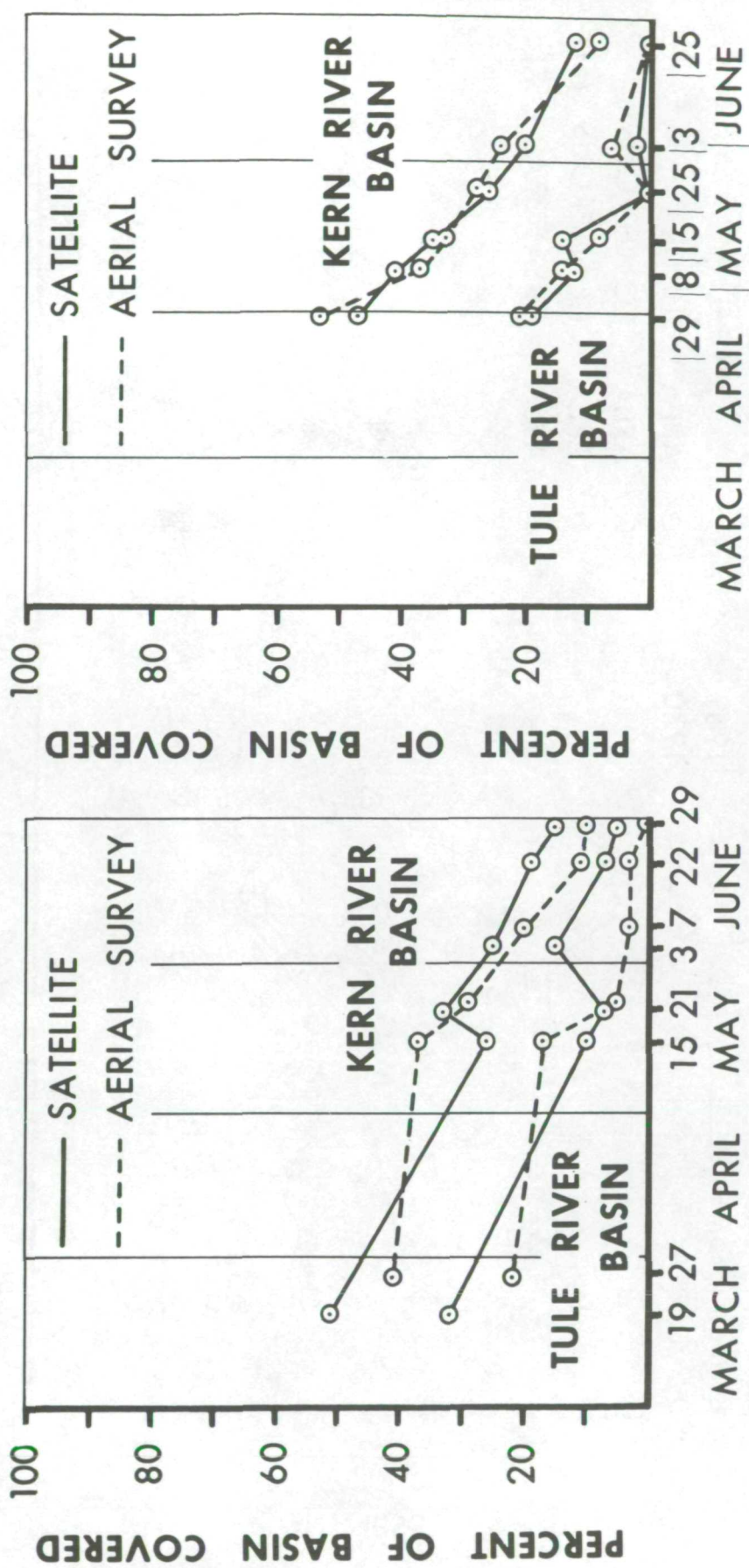
NOAA/NESS/ESG

Figure 1.- Results of field measurements of microwave brightness temperature at three levels of soil moisture. Measurements are shown for three viewing angles, four wavelengths, and at vertical and horizontal polarization.

SNOW EXTENT DECREASE

SOUTHERN SIERRAS REGION

DATA FROM ALLIED RESEARCH ASSOCIATES CONTRACT NO. E-252-69(N), Pp. 54-56



AREAL EXTENT 1969

KERN - 2074 Sq Mi

TULE - 391

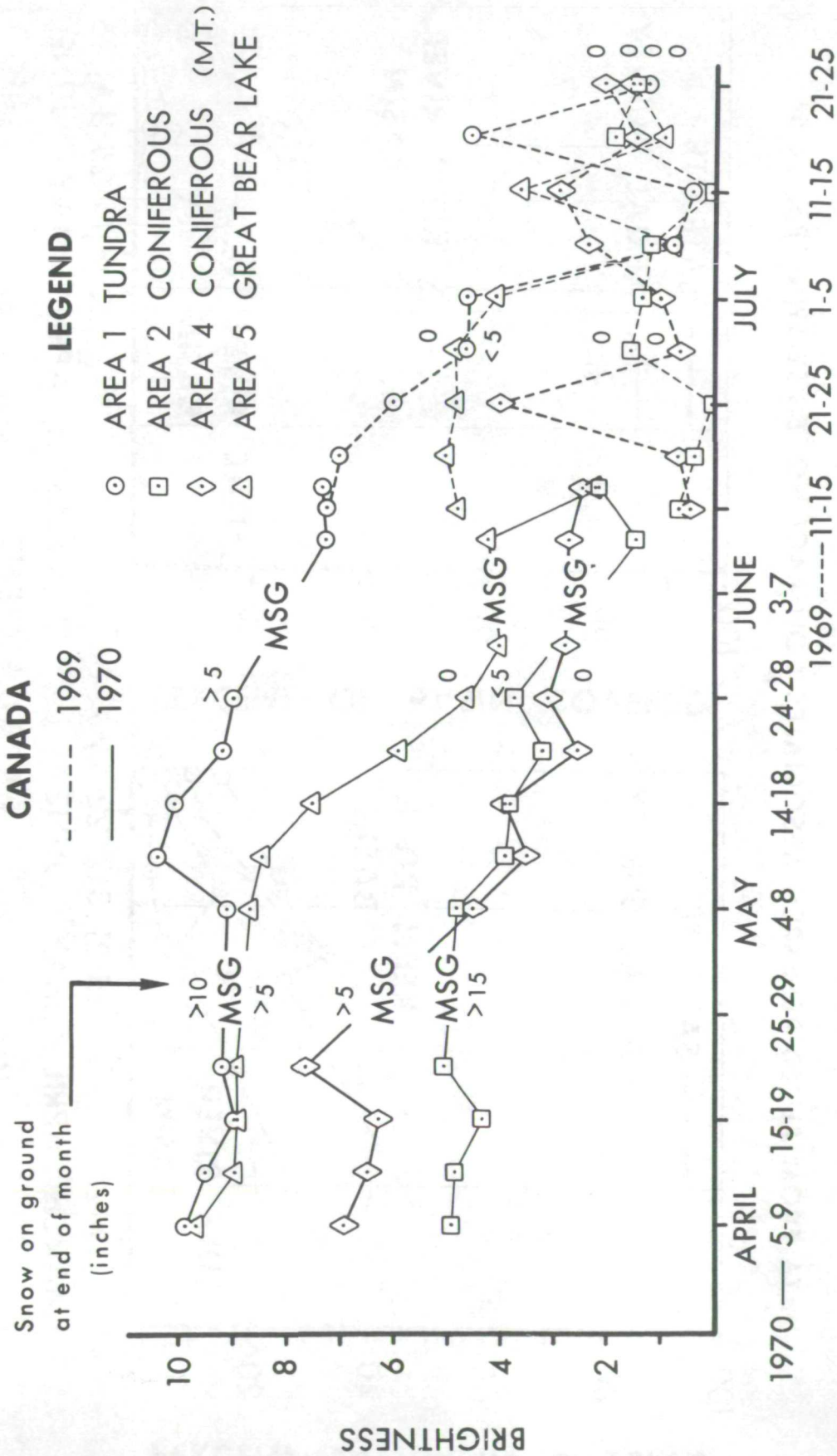
1967

NOAA-NESS

Figure 2.- Comparison of satellite and aerial survey measurements of Spring decrease in snow extent (percent of basin covered).

ADJUSTED BRIGHTNESS AVERAGES

ESSA 9 5-DAY COMPOSITE MINIMUM BRIGHTNESS



NOAA-NESS

Figure 3.- Seasonal variation of Composite Minimum Brightness (CMB) values for snowy areas in northern Canada having different vegetative cover or topography. CMB values are routinely derived for 5-day periods from digitized and mapped vidicon data obtained by ESSA operational satellites. The notation "MSG" means "missing data."

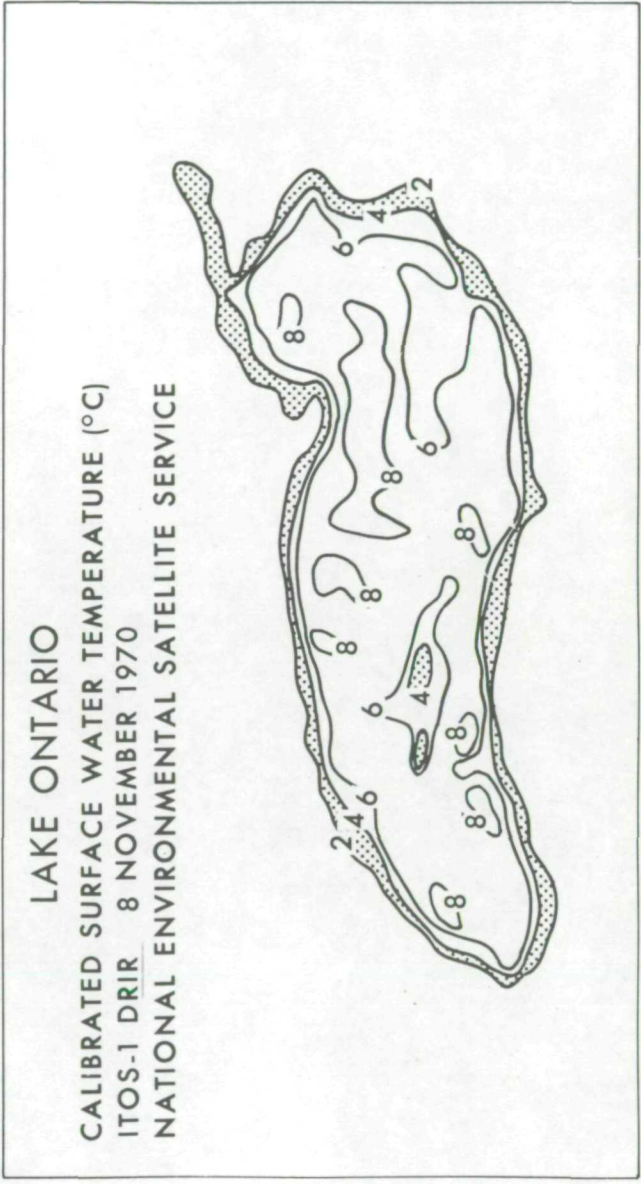
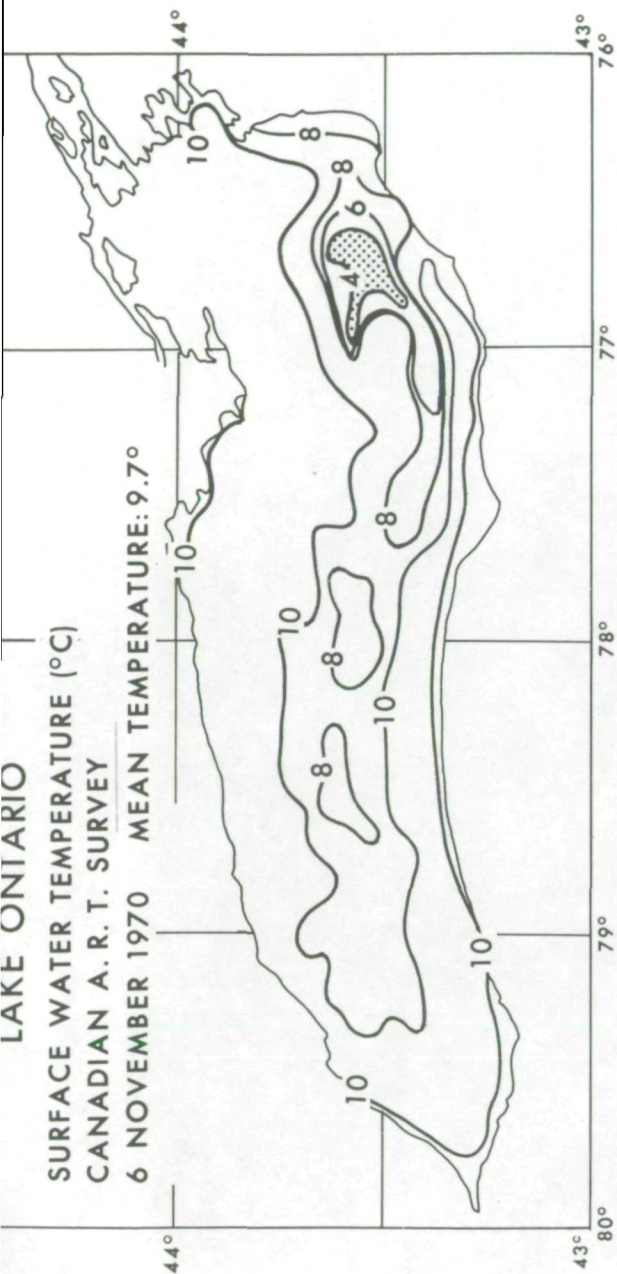


Figure 4.- Comparison of aircraft (ART) and satellite (DRIR) surveys of surface water temperature. The satellite analysis is based on unrectified scan-spot listings. The lake boundary is grossly defined by the thermal gradient between the warmer lake and the cooler land.

REMOTE SENSING AND THE PELAGIC FISHERIES

ENVIRONMENT OFF OREGON

by

William G. Pearcy
Department of Oceanography
Oregon State University
Corvallis, Oregon

INTRODUCTION

Remote-sensing oceanography at Oregon State University is part of a multidisciplinary research program (1) to learn more about nearshore oceanographic processes and how they affect the production of marine life and the availability of albacore tuna and (2) to provide fishermen with information in near real-time that will be useful in scouting for albacore concentrations.

Participants in this broad project are listed below:

I. Remote Sensing Aircraft

NASA - Convair 240A, Lockheed P-3, RB-57
U.S. Coast Guard - HU-16
U.S. Air Force - HU-16
University of Michigan - C-47

II. Oceanographic Vessels

Oregon State University - YAQUINA, CAYUSE
Fish Commission of Oregon - SUNRISE
Bureau of Commercial Fisheries - DAVID STARR JORDAN, JOHN N. COBB
Albacore boats with bathythermographs

III. Commercial Albacore Boats

IV. Albacore Advisory Service - "Albacore Central"

OSU Sea Grant's Marine Advisory Program
Fishery - Oceanography Center, La Jolla, California
Pacific Northwest Bell Telephone Company

METHODS

Sea surface temperature was measured on all flights at an altitude of 500 or 1000 feet with a Barnes PRT-5 radiation thermometer filtered to 8.0-13.5 microns and equipped with a 2° field-of-view. The PRT-5 output was continuously recorded on a strip chart with resolution of 0.1°C.

The PRT-5 was calibrated against a thin aluminum plate, covered on one side with Parson's Black Paint, and encased within styrofoam to reduce transient thermal gradients. Plate temperature was measured directly behind the spot viewed with the PRT-5 using a thermistor bonded on the plate with silicone grease. PRT-5 and thermistor measurements between 5°C and 18°C agreed within 0.1°C.

PRT-5 data were corrected for atmospheric absorption and for infrared radiation reflected from the sea surface using the method described by Saunders (1967). The apparent temperatures of the sea surface viewed normal to the surface and at an angle of 60° from the normal were recorded and the difference between these two readings was applied as a correction. This correction assumes that: (1) doubling the path length doubles the effect of atmospheric absorption; (2) infrared radiation reflected from the surface at 60° is approximately double that reflected normally; and (3) the sea surface temperature does not change significantly over the distance (approximately 500 yards) perpendicular to flight track, or along the flight track between measurements. We attempted to make these calibrations in areas where no thermal gradient existed. When the before and after readings normal to sea surface differed, the calibration was not used.

The validity of these assumptions was checked by taking simultaneous measurements with PRT-5 radiometers from an aircraft at 1,000 feet altitude and from a ship. In the two successful "ground-truth" experiments the PRT-5 reading from the ship (corrected to a black plate) agreed within 0.1°C of the PRT-5 reading from the aircraft (calibrated with a black plate and corrected with 60° calibration values).

Based on these experiments, and the results reported by Saunders (1967), we feel that infrared radiometers can measure the sea surface temperature to 0.1°C in the immediate vicinity of a 60° calibration and to 0.2°C over a relatively extensive flight pattern, provided sufficient 60° calibrations are made to ensure that changes in conditions are taken into account.

Standard bucket temperatures during the two successful ground-truth experiments were within 0.5°C of the infrared measurements of sea surface temperature. The IR measurements are of the microsurface temperature; hence, the two methods do not necessarily measure the same phenomenon.

The scanner used on the C-47 in 1969 included a wide angle, uncalibrated scanner: $.40-.44\mu$, $.46-.48\mu$, $.52-.62\mu$, $.62-.66\mu$, $.66-.72\mu$, $.80-1.0\mu$, and $8.0-12.5\mu$, and narrow field of view calibrated scanner: $8.0-13.5\mu$ (high gain and low gain) and $4.5-5.5\mu$. An altitude of 500 or 1000 feet was maintained, except where high altitude scanner coverage was obtained on several flights. A TRW Ocean Color Spectrometer and an L-band microwave radiometer were used on NASA's P-3 in 1970.

High altitude (60,000 ft) multispectral photography was obtained from NASA's RB-57 on May 21, 1969 and July 16, 1969. The July flight consisted of six flight tracks parallel to the coast each 10 miles apart. The following camera/film-filters were used: four Hasselblad cameras with Kodak 3400 film and either Nos. 58,25-A, 2E + 38 or 65A filters; Zeiss camera with Kodak infrared SO-117 film and a 15G filter, and an RC-8 camera with Ektachrome 2448 film. Measurements of optical densities in the blue ($.41-.47\mu$) and green ($.54-.58\mu$) regions of the spectrum were made of water color using the Ektachrome transparencies.

Besides obtaining ground-truth for remote sensing flights, surface ships were engaged in studies on physical, chemical and biological processes and properties related to pelagic fisheries. Several commercial albacore boats were outfitted with expendable or mechanical bathythermographs (BT's) so that data on thermal structure could be obtained along the fish catch. The U.S. Navy Fleet Numerical Weather Facility, Monterey, California provided expendable bathythermograph (XBT) probes and Sippican Corporation loaned us two XBT launchers for this project.

Data from aircraft and vessels were communicated to "Albacore Central" on the OSU campus, combined with information from the Fishery-Oceanography Center (BCF) La Jolla and the Weather Bureau, and broadcasted twice daily by the Astoria Marine Operator (Pacific Northwest Bell) to the albacore fleet. Most of the information on sea surface temperature for these radio broadcasts were obtained from the aircraft overflights. Another Albacore Central product for the fishermen was the weekly bulletin which included a sea surface temperature chart. These were distributed to canneries and fishing ports along the coast of Oregon (Panshin, 1970).

The fishermen were important participants in the project. Besides being "consumers" of data on ocean conditions, they had a vital role in providing data on albacore catches. Over 400 albacore logbooks were distributed to fishermen from San Diego, California to Seattle, Washington. They were asked to record detailed information on catches several times a day so that catches could later be correlated with small-scale oceanographic features.

The results to date are all preliminary. The catch data from the multispectral scanner, the spectrometer, and microwave are on tape and are also being analyzed.

RESULTS

Two oceanographic phenomena dominate Oregon waters during the summer: coastal upwelling and the Columbia River plume. Both are detectable by gradients of surface temperature and by water color, hence are amenable to remote sensing. Both of these large-scale processes are extremely dynamic and produce rapid changes. Repeated synoptic surveys by remote sensing therefore are an ideal way to study temporal changes associated with these events.

During the summer cold water upwells along the coast as a result of northerly wind stress and the rotation of the earth. This cold water is rich in nutrients and results in high biological productivity. A common pattern of upwelling is reflected by the sea surface temperatures shown in Fig. 1. Cool water is found along the coast, and warm water is found offshore. Isotherms are almost parallel to the coast off northern Oregon but diverge farther offshore along the southern coast where the strongest winds and coldest temperatures often occur. Thermal fronts, large changes of temperature over small distances, were often associated with areas of active upwelling.

Changes in water color were also found in upwelling areas, and abrupt color changes sometimes coincide with thermal fronts. In general, inshore waters were green because of the large standing stocks of phytoplankton. Offshore waters were blue or blue-green in color. These trends were revealed by plotting blue:green ratios from either the scanner data or from densitometric measurements of the high altitude color photography. Within small areas, however, this trend for an increasing blue:green ratio with distance offshore may be reversed. Sometimes blue-green water was found near shore, presumably in newly upwelled water. Farther offshore water color changed to green and then brown, perhaps followed by a rapid change (front) to blue-green again. These changes are probably related to the production and stratification of phytoplankton as pulses of upwelled water move offshore.

The Columbia River, the second largest river in the United States, injects huge quantities of fresh water into the ocean off Oregon. Unlike coastal streams, peak runoff occurs in the spring and early summer. These waters also respond to local wind stress and usually flow to the southwest as a plume of low-salinity water during the summer. Because plume waters are fresher and lighter, they form a thin layer over the denser ocean waters. Hence the radiant heat they absorb is constrained near the surface where heating takes place more rapidly than outside the plume where mixed-layer depths are greater. As a result, plume waters can be distinguished by their temperatures, especially during the early summer (Fig. 2). At this time high surface temperatures correlate well with low salinities.

The plume also affects water color and has been detected by pronounced reflectance of longer wave lengths in both multispectral photograph and scanner imagery (Pearcy and Mueller, 1970). We have also observed interesting "wave-like" patterns near the mouth of the Columbia River in our high altitude photography. The separation between individual wave "crests", which appeared essentially motionless over a 10-minute period, was 70-100 m. Bands of green and brown water were observed during a low-altitude flight in this same region on another date. We suspect that these patterns were caused by convergence-divergence cells that may be accentuated in the region of sharp density discontinuities around the plume.

ALBACORE TUNA

Albacore, Thunnus alalunga, are fast swimming oceanic tuna that migrate into nearshore waters off the west coast of North America during the summer. The distribution of albacore in the northeastern Pacific is known to be influenced by sea temperatures. Clemens (1961) and Flittner (1961) reported that albacore abundance was greatest where sea surface temperatures were between 15° and 20°C in California waters. In the Pacific Northwest, where yearly fluctuations in landing are extreme, highest catch rates occurred between 14° and 17°C (Alverson, 1961; Johnson, 1962). Although sea surface temperatures are an important determinant in the migration and zoogeography of albacore, fishing within the "preferred" range does not insure good catches, or even the presence of albacore. Hence the best correlation is a negative one: low catches are found outside the preferred thermal range.

Panshin (1970; 1971) plotted the catches of troll-caught albacore against sea surface temperature for the months of the 1969 season off Oregon. He found that the average temperature decreased from 16.9°C in July to 16.5°C in August and 15.7°C in September. Thus the average temperature was not constant but decreased by about one degree Celsius from early season to late season. We interpret this change as follows. In July when albacore migrate into Oregon waters, they are associated with the warmest waters available, i.e., waters of the Columbia River plume where heating takes place rapidly (Fig. 3). Later in the summer maximum temperatures in the region are higher and the area of warm water (14-17°C) expands. However, large catches of albacore are frequently made farther inshore, in waters adjacent to areas of upwelling. Consequently the disparity between average temperature of catches and the maximum water temperature available tends to be greater in August than July.

In 1970, the troll albacore fishing off Oregon was excellent late in July but then rapidly declined to low catches in August, traditionally the

month of maximum catches. Figures 4 and 5 show sea surface temperatures for July 29 and 30 as measured by infrared radiometry. Albacore catches were large, averaging about 400 fish/boat/day during calm sea conditions on July 28. The sea temperatures recorded on our IR flight on July 29 (Fig. 4) also reflected the absence of northerly winds: water temperatures were warm, even the inshore zone where cold water usually occurs. Warmest water (18.0°C) was found nearshore in a pool of plume water. The albacore fleet was localized in $15.5\text{-}16.0^{\circ}\text{C}$ blue-green water off the Columbia River.

Figure 5 shows that by the next day, July 30, winds had increased to velocities over 10 knots from the north, inducing upwelling and resulting in the immediate return of cold water near the coast. Moreover, the warmest water offshore was 16.5°C compared to 18.0°C on the previous day. Thus, within a day, rapid changes in both absolute temperatures and the temperature pattern were associated with a change of winds. On July 30, the albacore fleet was still localized off the mouth of the Columbia River, but now closer to shore.

After July 29 albacore catches declined and never recovered during the 1970 troll season off Oregon. The decline occurred despite the presence of favorable surface water temperatures for albacore. Temperatures of 14 to 17°C were common throughout August as in other "good" albacore years. Therefore factors other than sea surface temperature have an important influence on albacore availability.

CONCLUSIONS

- 1) Albacore fishermen presently use sea surface temperature, water color, and fronts to assist them in locating albacore. These features can be detected by remote sensing. Remote sensing is especially useful because large areas can be surveyed in short periods of time and near-synoptic maps can be constructed. Moreover some of these data can be made available to fishermen in near real-time. This is an important consideration for fisheries in coastal and upwelling regions where oceanographic conditions change rapidly, particularly for highly motile fishes like tuna.
- 2) Factors other than sea surface temperature are obviously important within the "preferred" temperature range of albacore. Sea surface temperature may be correlative with other more basic oceanographic features, but these more salient factors are yet to be identified.
- 3) Lastly we need a better understanding of the biology and behavior of albacore and other commercially important species. This was clearly emphasized by the demise of the 1970 troll season off Oregon which was unpredictable and has yet to be explained.

ACKNOWLEDGMENTS

This research was supported by the U.S. Navy, Spacecraft Oceanography (Contract No. N622306-70-C-0414) and the Bureau of Commercial Fisheries (Contract No. 14-17-0002-333).

REFERENCES

1. Saunders, P. M. 1967. Areal measurement of sea surface temperature in the infrared. *J. Geophys. Res.* 72:4109-4117.
2. Panshin, D. A. 1970. Oregon's albacore research project. *Trans. 35th No. Amer. Wildl. and Natural Res. Conf.* 222-227.
3. Pearcy, W. G. and J. L. Mueller. 1970. Upwelling, Columbia River plume and albacore tuna. *Sixth Intern. Symp. Remote Sensing Environment.* p. 1101-1113.
4. Clemens, H. B. 1961. The migration, age and growth of Pacific albacore (*Thunnus germo*), 1951-1958. *California Dept. Fish and Game, Fish. Bull. No. 1159* 118 p.
5. Flittner, G. A. 1961. Cooperative trolling program, 1961. *Calif. Fishery Market News Monthly Summary*, Dec. 1961.
6. Alverson, D. L. 1961. Ocean temperatures and their relation to albacore tuna (*Thunnus germo*) distribution in waters off the coast of Oregon, Washington and British Columbia. *J. Fish. Res. Bd. Canada* 18:1145-1152.
7. Johnson, J. H. 1962. Sea temperatures and the availability of albacore tuna off the coasts of Oregon and Washington. *Trans. Amer. Fish. Soc.* 91:269-274.
8. Panshin, D. A. 1971. Albacore tuna catches in the northeast Pacific during the summer of 1969 as related to selected ocean conditions. Ph.D. Thesis, Oregon State University.

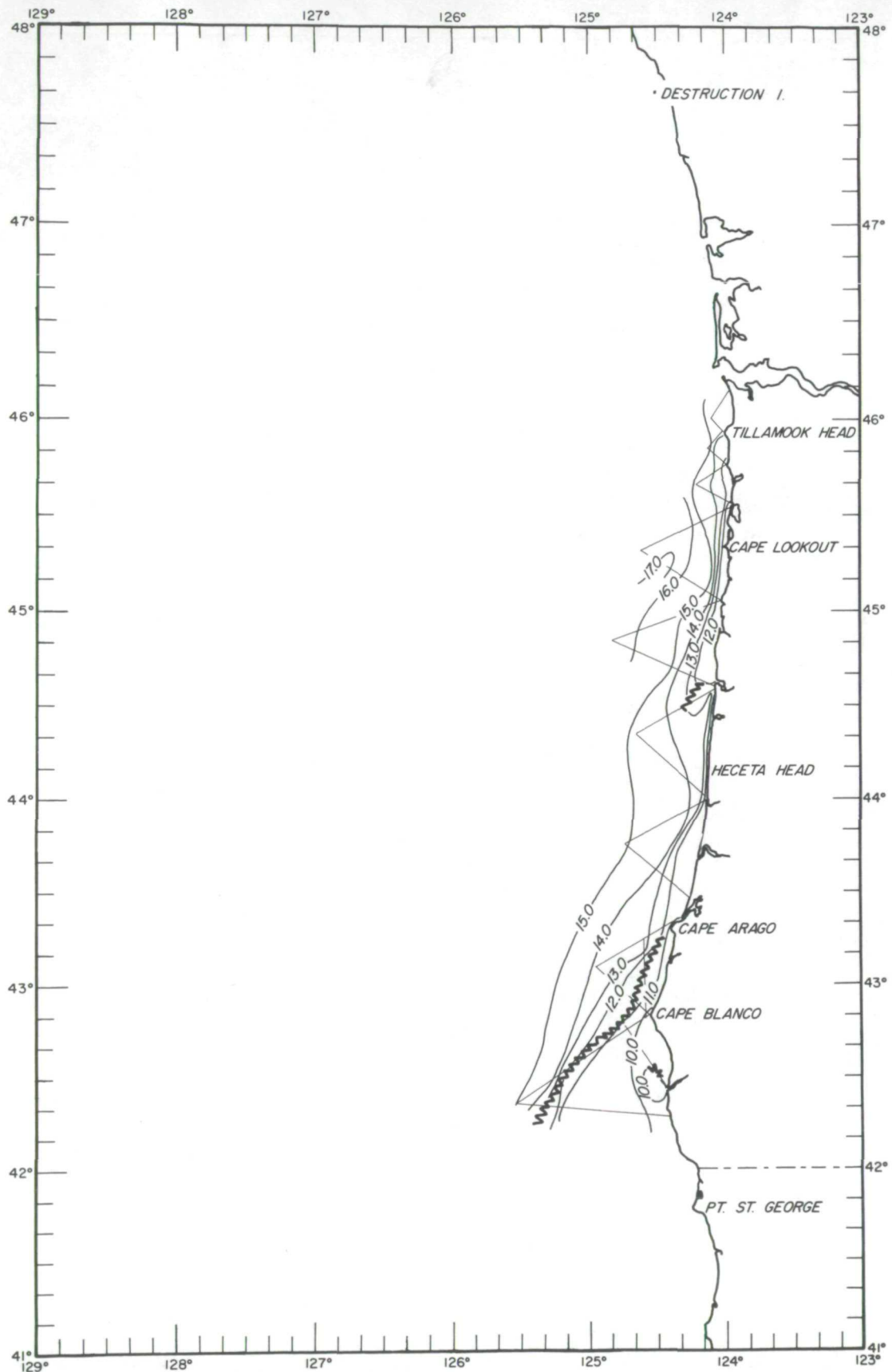



Figure 1. Sea Surface Temperature from Airborne PRT-5 radiometer survey. NASA Manned Spacecraft Center CONVAIR 240A on 12 August 1969.  - thermal front.

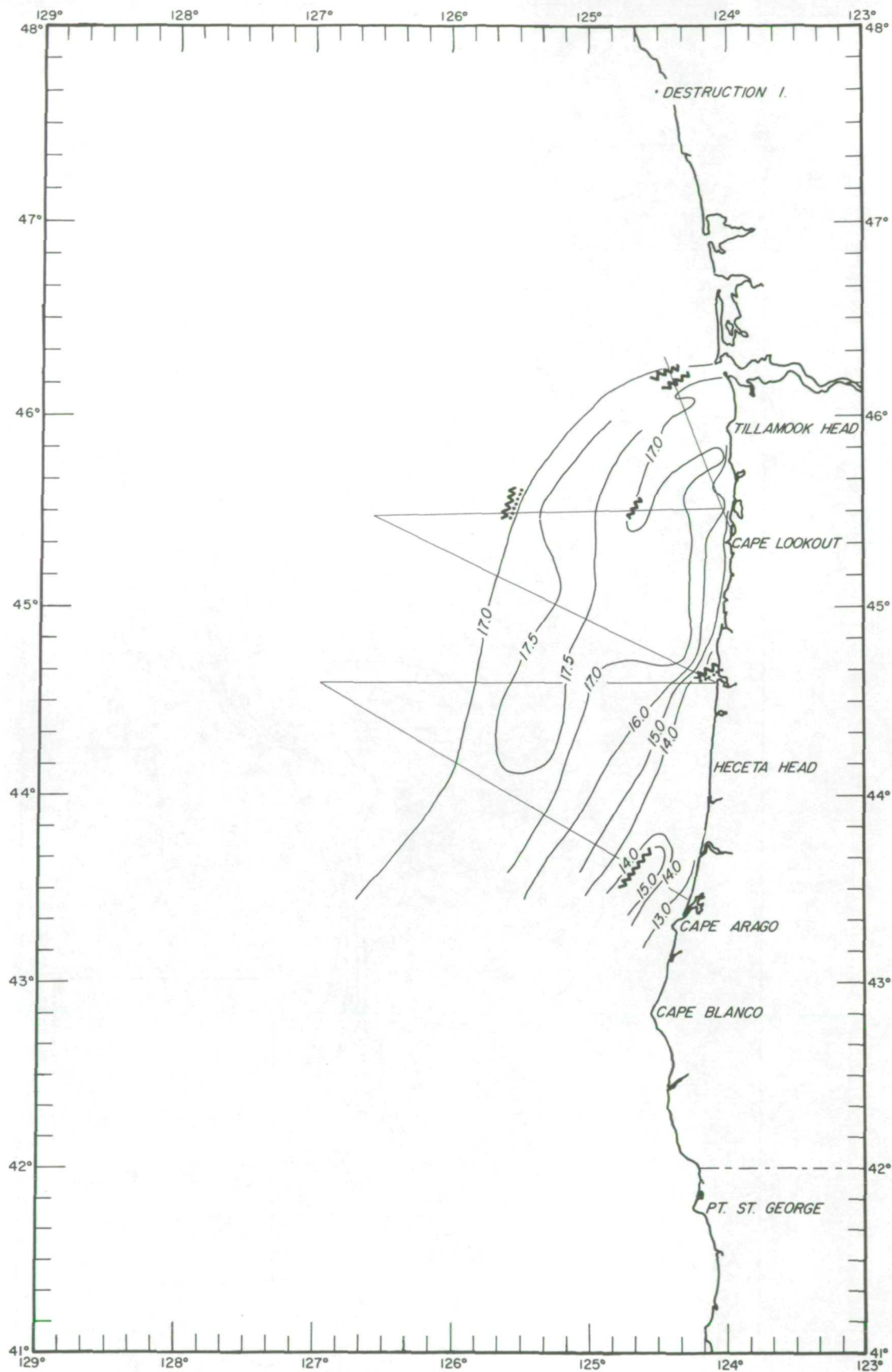




Figure 2. Sea Surface Temperature from Airborne PRT-5 radiometer survey. University of Michigan C-47 on 13 July 1969.  - thermal front,  - color front.

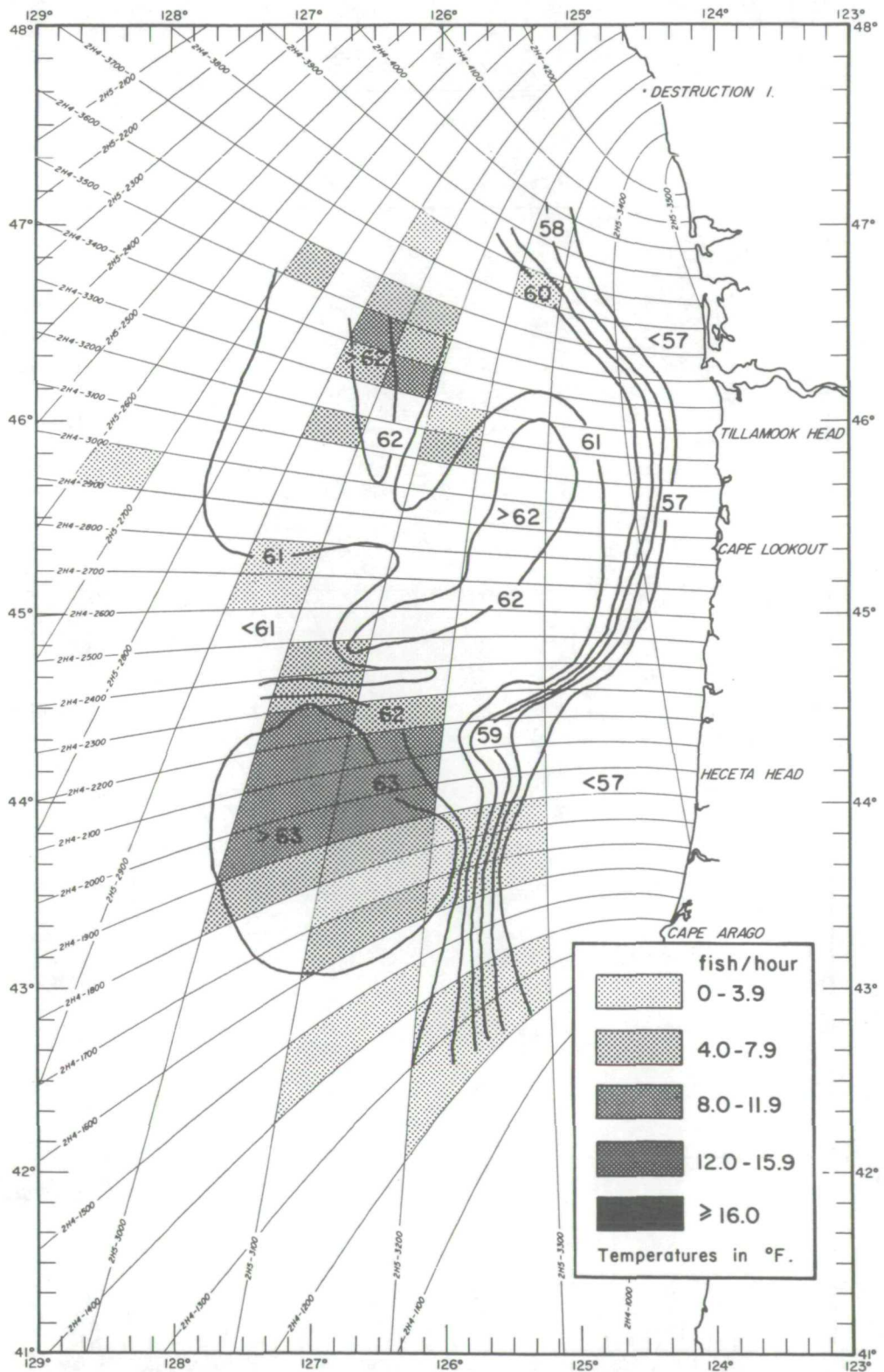


Figure 3. Catches of albacore tuna by Loran blocks and sea surface temperature, 17-23 July 1969. Note that the highest catches are associated with the warmest water.

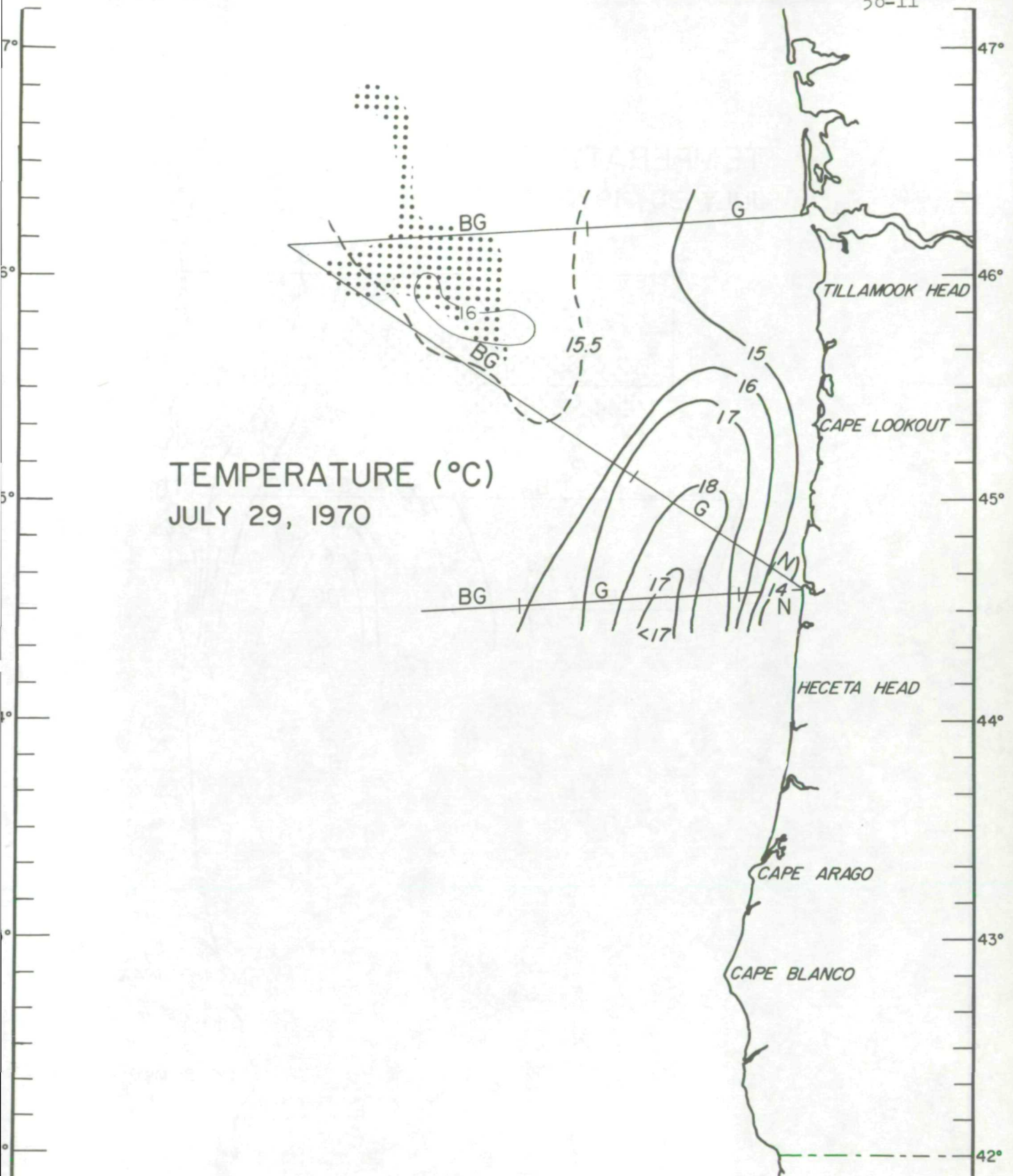


Figure 4. Sea Surface Temperature from Airborne PRT-5 radiometer survey. U.S. Air Force (304th ARRS) HU-16 on 29 July 1970. Visual observations of water color: N = brown, G = green, BG = blue-green. Dotted area designates location of albacore boats.

TEMPERATURE (°C)
JULY 30, 1970

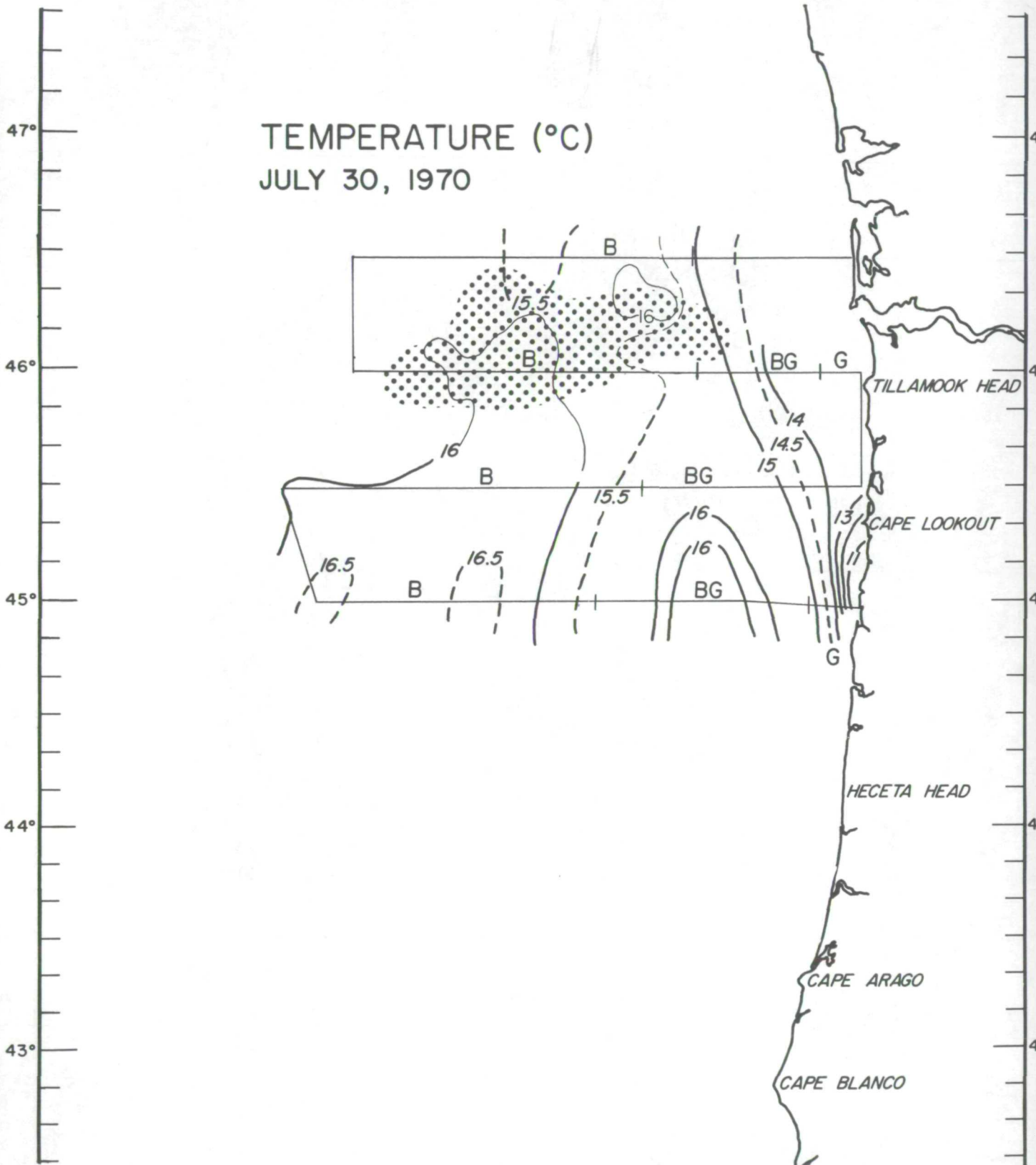


Figure 5. Sea Surface Temperature from Airborne PRT-5 radiometer survey. U.S. Coast Guard, Port Angeles HU-16 on 30 July 1970. Visual observations of water color: G = green, BG = blue-green, B = blue. Dotted area designates location of albacore boats.

Remote Sensing of Ocean Color From Aircraft

by

G. L. Clarke and G. C. Ewing*

Over 3,000 ocean spectra of sunlight backscattered from the upper layers of the sea have been obtained at flight altitudes to 10,000 feet together with detailed ground truth. These spectra are from stations which include a wide range of water masses differing as to biological and physical condition. This data bank and the analysis already performed demonstrates the probable feasibility of using ocean color as a parameter to locate areas of special significance to physical oceanographers and marine biologists from aircraft and satellites.

The relationship between light extinction and biological productivity has been studied by Dr. Carl J. Lorenzen. "The penetration of light into the ocean is of fundamental importance since photosynthesis can only occur if light intensity is above a minimum level. The quantity and quality of light at any given depth is controlled by absorption and scattering within the water column by water itself and by dissolved and suspended substances of biological and non-biological origin.

"Light attenuation in the euphotic layer is affected by 1) water itself, 2) plankton algae, and 3) a mixture of other suspended and dissolved substances. In regions characterized by high standing crops of phytoplankton, the euphotic layer is thin and most of the light attenuation can be attributed to plants.

*Paper presented by G. C. Ewing.

At the other extreme, where the euphotic zone is thicker, water itself absorbs and scatters most of the light. Between these extremes light attenuation is due largely to materials other than plants and water molecules." (Ref. 1).

The chief problems are:

1. to assay the effect of varying illumination,
2. to estimate and eliminate interference from air haze,
3. to identify the various biochromes, terrigenous materials and pollutants characterized by their spectral signatures.

The spectrum of the backscattered light from the sea has been measured in absolute units using the TRW spectrometer flown in aircraft at altitudes ranging from 500 ft. to 10,000 ft. The reduced equivalent thickness of the atmosphere above 5 km is only 54 percent of that at the surface and is relatively less variable at higher altitudes. It is therefore probable that interference from "air light" (radiation scattered by the atmosphere and materials in the atmosphere) becomes less with increasing altitude, and therefore it is expected that this type of measurement can be made at indefinitely higher altitudes. The backscattered light in each part of the visible spectrum has been calculated as a percentage of the incident downwelling irradiance at the sea surface. The spectrum thus obtained reveals the action of the water itself and of materials (living and non-living) suspended and dissolved in the water. Certain important materials such as chlorophyll have recognizable

spectral signatures. Thus the shape of the spectrum can be used to measure the kinds and amounts of substances present in the surface waters of the ocean. This may well be the only feasible method for remote assay of the material content of oceanic waters.

Our investigations have demonstrated the feasibility and utility of this remote sensing technique to detect chlorophyll over the range of concentrations characteristic of the open ocean (Ref. 2). Spectra have been obtained from water masses with concentrations up to 3 mg chlor/m³ and higher values could easily be recorded (Fig. 1). Blackburn has shown that variations of 0.1 mg/m³ at concentrations as low as 0.1 mg/m³ are of particular significance in biological and fisheries investigations (Ref. 3, 4). It is expected that further analyses of curves of this type will enable us to recognize changes in the spectra due to other important materials in the water, including pollutants.

To investigate the capability to discriminate such small variations at low concentration, a special study was carried out in 1969 over the transition between the coastal water south of Georges Bank and the Sargasso Sea. Here over a distance of a mile or so the chlorophyll concentration changed from 0.3 to 0.1 mg/m³ and the temperature from 18°C to 23°C. Spectra were taken on the two sides of the transition at altitudes ranging from 500 ft. to 10,000 ft. (Figs. 2, 3, 4, 5, 6). Although the shape of the spectra changed character-

istically with altitudes, the differences between members of each pair and their contrast ratio remained nearly the same and clearly showed the location of the transition (Figs. 7 and 8).

References

1. Lorenzen, C. J., 1970. "Extinction of light in the ocean by phytoplankton." Contribution No. 2558 from the Woods Hole Oceanographic Institution. In press.
2. Clarke, G. L., G. C. Ewing and C. J. Lorenzen, 1970. "Spectra of Backscattered Light from the Sea Obtained from Aircraft as a Measure of Chlorophyll Concentration," Science, 20 Feb. 1970, pp. 1119-1121.
3. Blackburn, Maurice, 1969. In "Useful Applications of Earth-Oriented Satellites: Oceanography 5," NAS, p. 12.
4. Blackburn, Maurice, 1969. "Applications to fishery oceanography" in The Color of the Ocean, Rept. of Conference held at W.H.O.I. August 5-6, 1969, sponsored by Earth Survey Office, Electronics Research Center, Cambridge, Mass., pp. 3-1 to 3-11.

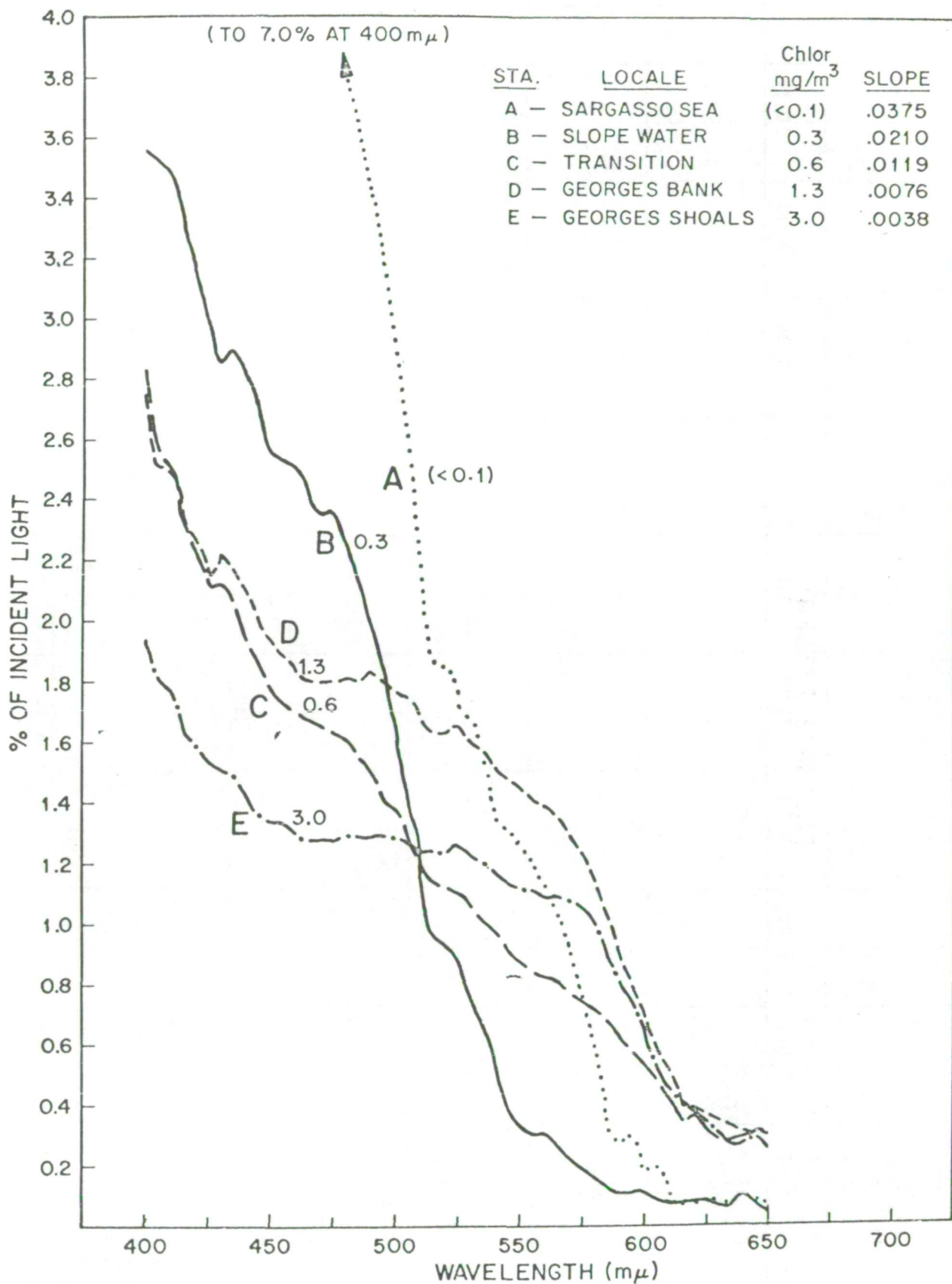
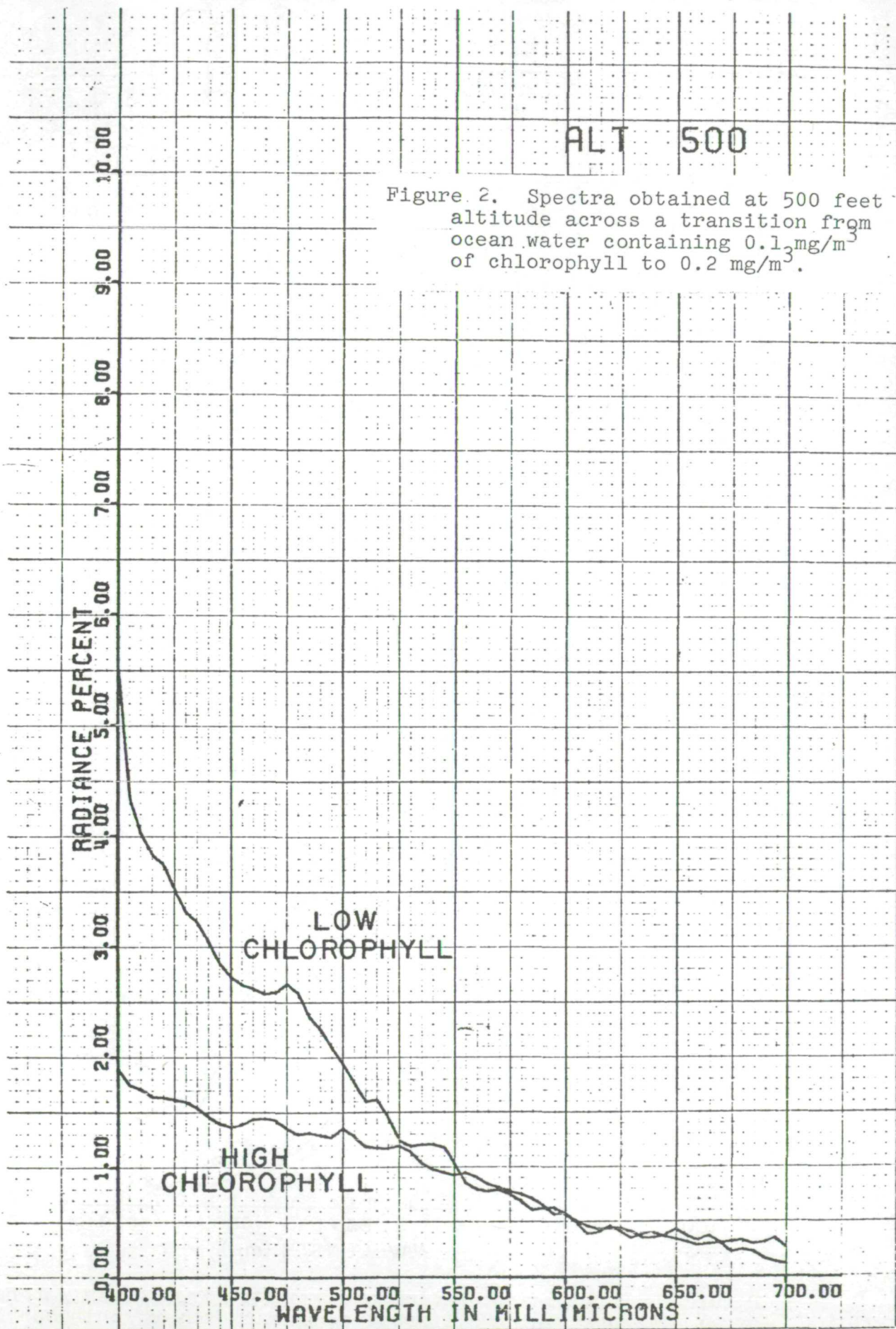
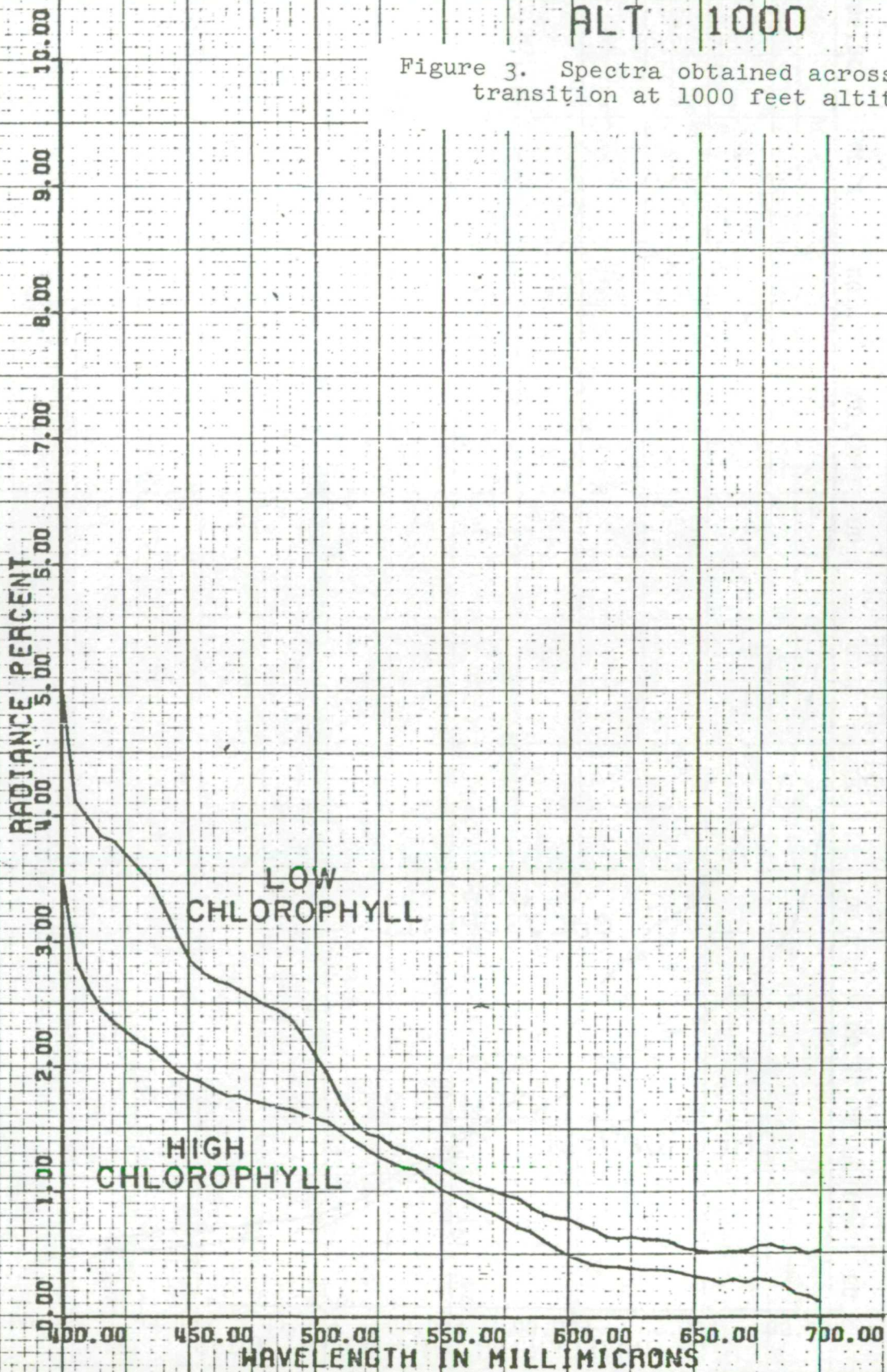


Figure 1. Examples of reflectance spectra from ocean waters containing different concentrations of chlorophyll.



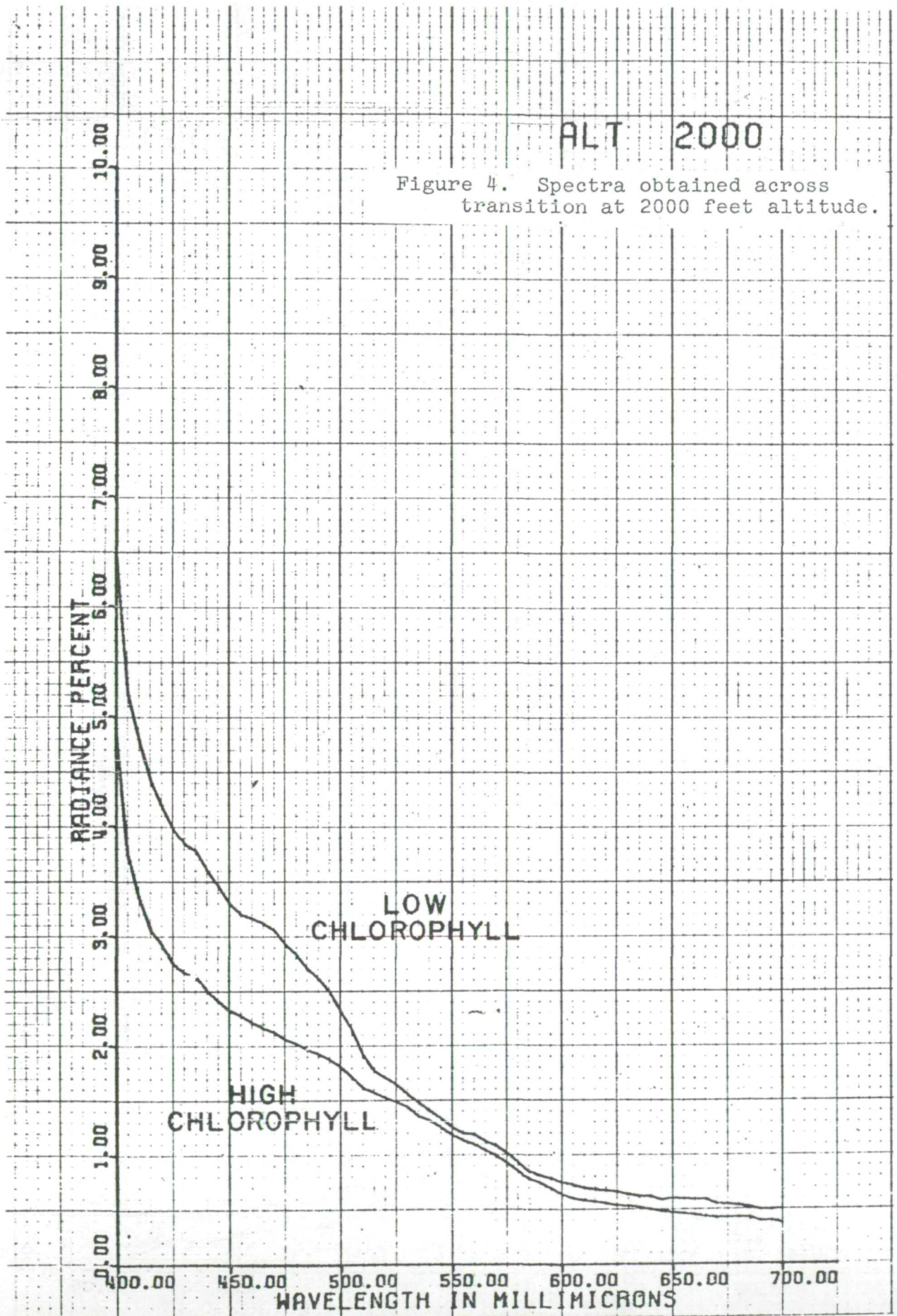
ALT 1000

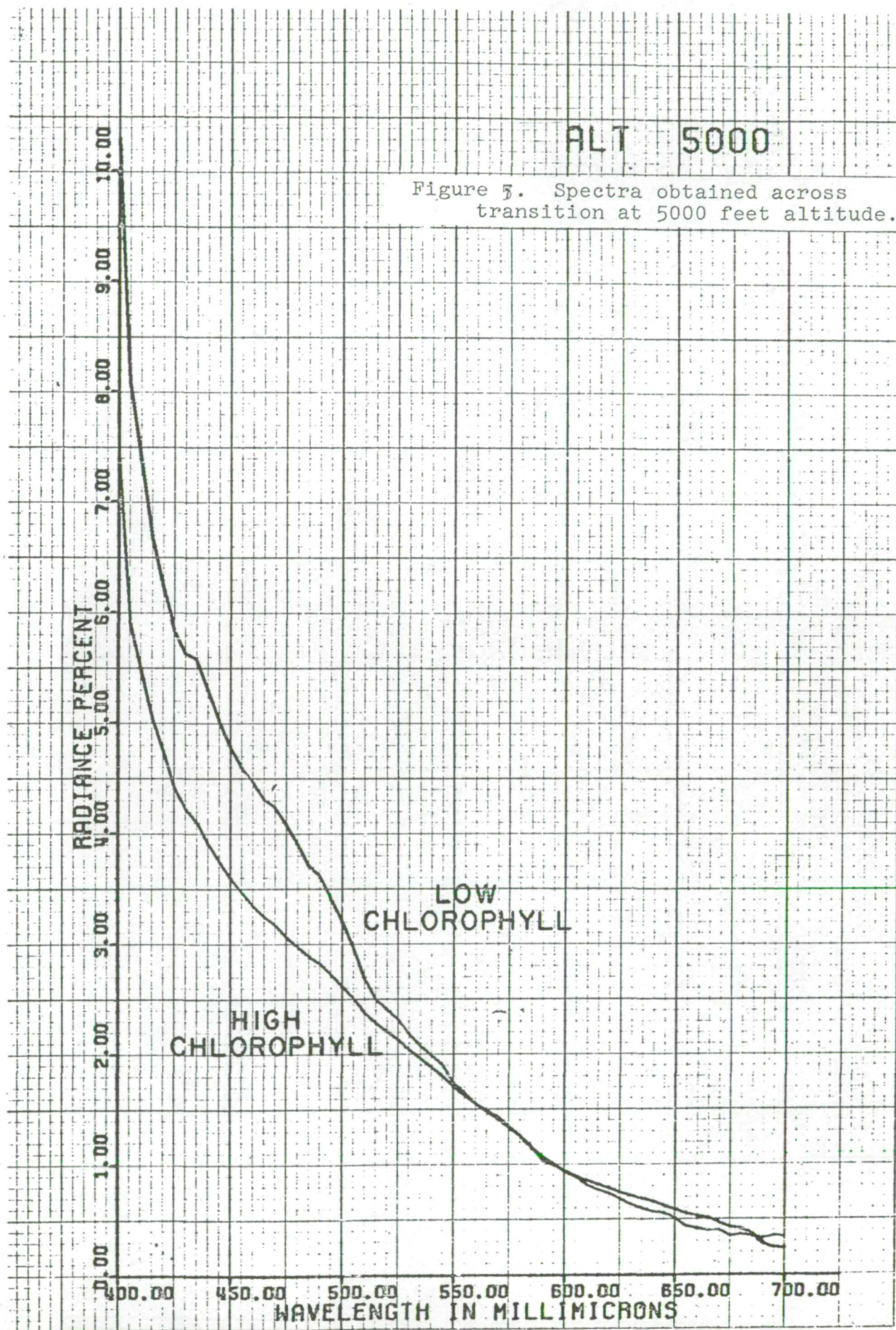
Figure 3. Spectra obtained across transition at 1000 feet altitude.

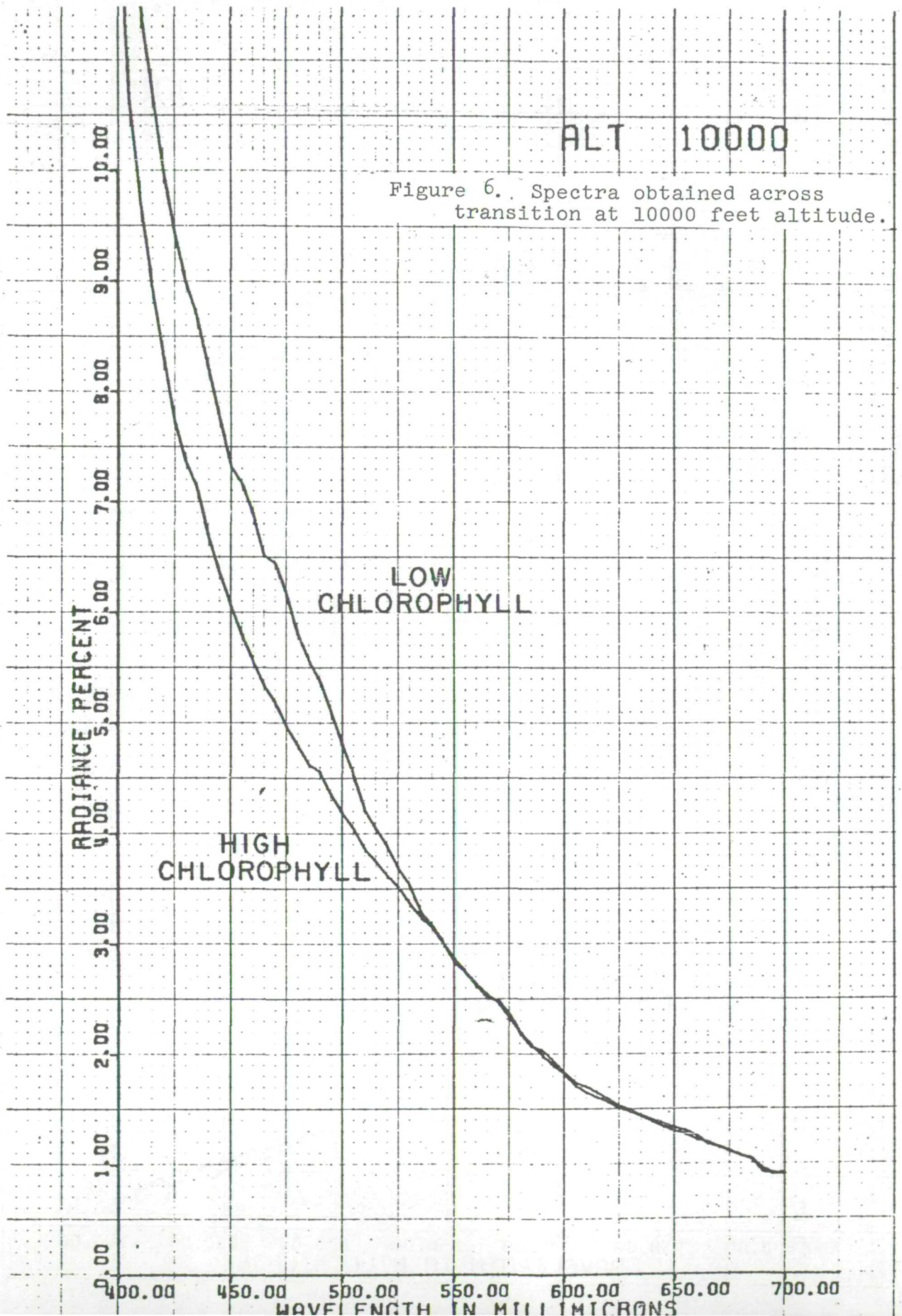


ALT 2000

Figure 4. Spectra obtained across transition at 2000 feet altitude.







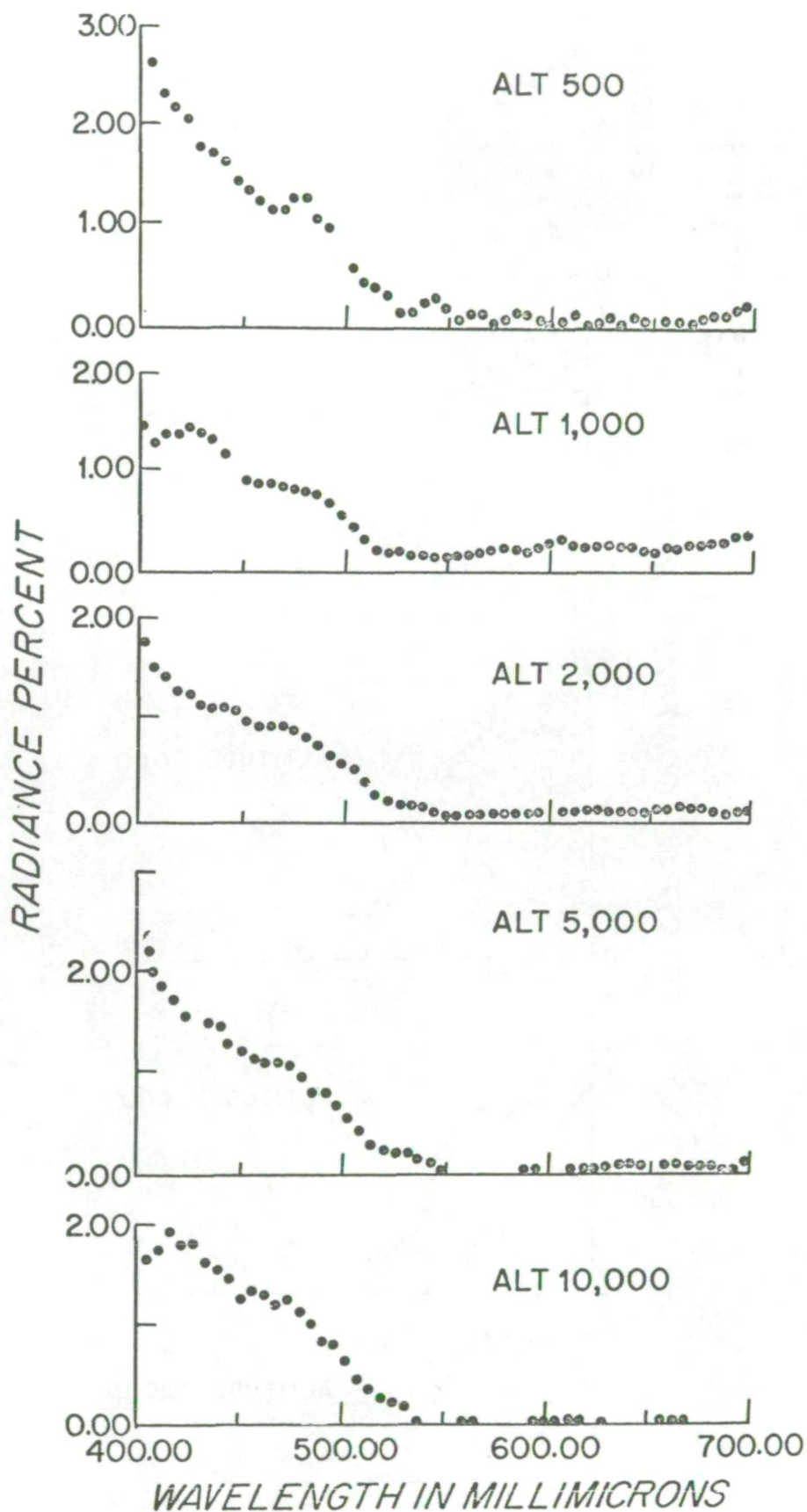


Figure 7. Difference of spectra across a transition in ocean color at flight altitudes (ft.) shown.

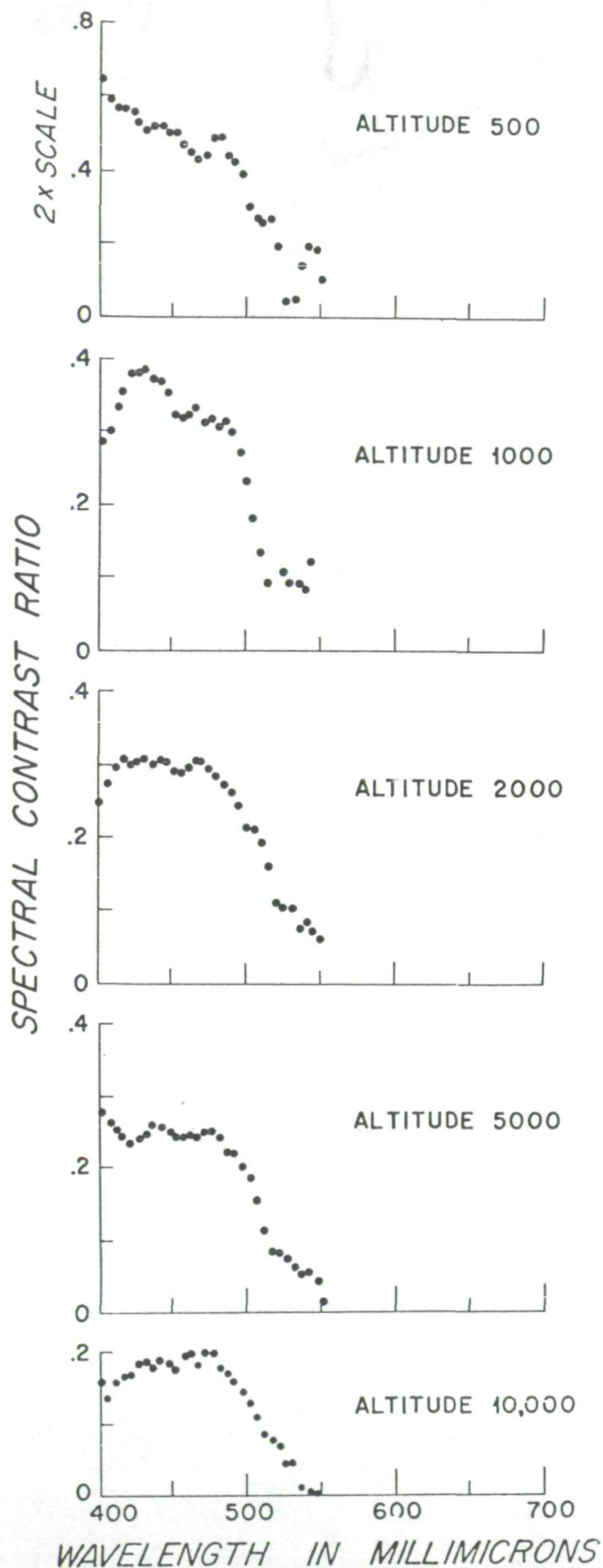


Figure 8. Contrast ratio, of light differences to total light, across transition

THE REMOTE SENSING NEEDS OF ARCTIC GEOPHYSICS

By

William J. Campbell

Introduction

The dynamic world of snow and ice embraces a great part of the earth, and it is one part of the earth's environment that can only be properly studied by remote sensing from aircraft or satellite. At any given time snow covers approximately 13% of the world ocean area. In terms of influence on the earth's heat budget, snow and ice are prime movers because of their very high albedo. In both of these substances very large space scale variations can occur at very small time scales--for example, almost the entire midwest of the United States can make the transition from being snow-free, with an albedo of 0.3 - 0.4, to being covered with a light layer of snow, with an albedo of 0.8 - 0.9, in just a few days.

Perhaps in the whole field of geophysical investigations the most difficult area in which science is attempting to determine the cause and effect of nature is in the Arctic. Both polar areas are very difficult to study because of the great logistical problems, but I think it is fair to say that Antarctic work has proceeded very well, partly because the continent of Antarctica is a fairly stable platform. It is a high ice cap with ice 2-3000 meters thick which flows with typical slow glacier speeds (a piece of ice generated at the south pole takes tens of thousands of years to flow off the polar plateau and calve into the Antarctic Ocean). Also, in terms of understanding its energy balance, it is less complex than the Arctic because essentially no melting of the surface snow occurs over the plateau, therefore there are no great albedo changes, and no fractures exposing liquid water occur except in the sea ice surrounding the continent.

In comparison, the Arctic is extremely dynamic. The sea ice covering the Arctic Ocean is a mere veneer compared with the great Greenland and Antarctic ice caps. Its mean thickness is about 3 meters. Its motion is extremely rapid--individual ice floes within the multi-year ice canopy have been observed to move as fast as 50 km/day. In Figure 1 is shown the drift track of ice island T-3

for the last 18 years, during which it moved tens of thousands of kilometers. In the Arctic summer the entire surface of the ice canopy melts and great albedo changes occur very quickly over vast areas. Not only do great motion and albedo changes occur within the ice canopy, but the boundaries undergo large fluctuations so that annually the mean areal extent of the Arctic sea ice fluctuates about 10%. All in all, the sea ice cover is one of the most variable physical features of the earth's surface.

A key problem in Arctic research is to understand its heat and water budget at meso- and macro-scales in space and time. The sea ice has a profound influence on the heat exchange within the Arctic Ocean and between the ocean and the atmosphere. Knowledge of the fluctuations of the snow and sea ice media and of their influence on the earth-atmosphere interface is important in studies of atmospheric circulation and the world water balance. Much of the needed data, in the form of macro-scale synoptic images at short time intervals, can potentially be achieved with the use of remote sensing satellites.

Permafrost, Snowpacks, Glaciers, and Ice Caps

Essentially nothing is known of the temporal and spatial variations of snow cover north of the Arctic Circle. Snow depths are measured at a few points in that vast area, but these data are entirely insufficient to meet present research needs, let alone help in the future development of predictive computer models for the region.

On the land masses in Arctic regions the snow cover is a very irregular and variable feature. A varying layer of snow lies on the permafrost, glaciers, and icecaps most of each year. An understanding of the mass and energy balance of any of these ice features is dependent upon the understanding of the energy balance of the snow cover. It would be most useful to know the dates of the onset of snow melting and disappearance. Recent work by Meier and Edgerton (1971) indicates that snow can be distinguished from many other land surface materials using passive microwave radiometers, and that microwave brightness temperatures vary with snow wetness, snow density, ice layers, snow temperature, and base material. Although the exact quantitative relationships between the microwave brightness temperatures and each of these parameters is not presently known, it is clear that an understanding of the physics of microwave emissions by snowpacks is emerging and that an all-season, all-weather means of monitoring snow packs is a real possibility.

Over 25% of the Earth's surface is covered by permafrost (perennially frozen ground), and much more is subject to seasonal freezing and thawing, yet it can safely be said that even less is known about its temporal and spatial variations than about snow cover. Although study of permafrost by remote sensing promises to be more difficult than in the case of snow and ice, it appears that both active and passive microwave sensing may prove useful.

Considerable remote sensing work has been done on South Cascade Glacier (in Washington state) by National Aeronautics and Space Administration aircraft. Meier, Alexander, and Campbell (1966) have shown that a variety of important snow and ice parameters related to the glacier's mass balance can be studied by available remote sensing techniques. Little work of this kind has been done on Arctic glaciers. The current behavior of Arctic glaciers may hold important clues to an understanding of worldwide climate variations and trends. Perhaps the greatest problem remaining to be solved in the field of glacier dynamics is the mechanism controlling the glacier-bed rock friction. Of specific present interest is the phenomenon of glacier surges, or sudden very rapid movements of glaciers in which jumps in velocity of more than an order of magnitude occur. The greatest known surge occurred on Nordaustlandet (North East Land), Svalbard (Glen, 1941) and was remotely sensed by photography by a Norwegian pilot. A few glaciers in the act of surging and numerous ones that have surged have been photographed by Austin Post of the U.S. Geological Survey, and his work (Meier and Post, 1968) has shown that remote sensing is perhaps the prime tool in studying the numerous glaciers of the Arctic.

The Greenland ice cap is second in size only to the Antarctic ice cap. It is comparable to the Antarctic, and Benson (1967) after making many comparisons, both general and specific, feels that the potential of using Greenland as a laboratory for polar ice sheet research is good. The interaction of the ice sheet with the surrounding ocean is an important area of research, especially as it bears on determining the mass balance. Certain aspects of the Greenland ice cap mass balance, such as snow cover, which is more spatially homogeneous than elsewhere in the Arctic, might be amenable to study using satellite imagery with its relative poor resolution, but synoptic view.

The Arctic Ocean

The circulation of sea ice in the Arctic basin is an exceedingly complex phenomenon. The seemingly chaotic drift trajectories (Figure 1), which at present are understood theoretically for only large period average drifts, are the result of an interplay between forces whose exact physical basis is poorly understood. The long-period circulation of sea ice in the Arctic Ocean can be said to have two main features--the trans-polar drift stream and the Beaufort gyral. During the last 80 years the drift tracks of ships embedded in the ice, ice islands of glacial origin embedded in the ice, and select pieces of manned ice floes have given sufficient data to delineate the trans-polar drift stream, which runs from the Siberian coast, over the north pole, and out the Greenland-Iceland trench, and the Pacific or Beaufort gyral, an anti-cyclone which is centered in the Beaufort Sea and around which ice island T-3 has been rotating for some time (Figure 1). The heterogeneous character of the ice flow within the icepack results in strong compressive shearing and tensile forces so that the icepack is composed of ice floes ranging in size from pieces with an area as large as tens of square km to pieces the size of ice cubes. Small cracks between individual ice floes are called leads (Figure 2), and the large cracks are called polynyas, the Russian word for pond (Figure 3). When these openings close, usually a ridge is formed (Figure 4). When thin ice forms in polynyas and is rafted over itself in successive bands, finger ice forms (Figure 5). Until very recently it was believed that the total area of the Arctic Ocean which was open at any given time was very small--less than 1%. However, recent data (Wittmann and Schule, 1966) show that throughout the year roughly 10% of the ice cover may be open water. This figure is in keeping with the relatively large quantity of young ice which has been observed, but contradicts much of the supposedly well-established knowledge of the heat budget. Experiments by Badgley (1966) indicate that the heat flow per unit area through a lead or polynya from the ocean to the atmosphere is at least two orders of magnitude greater than through the old sea ice. These studies suggest that the heat budget of the entire ocean and the flux of water from the ocean into the atmosphere are essentially determined not by the ice but by the fractures in the ice.

Essentially nothing is known about the creation, movement, and closing of polynyas. We have observed families of polynyas in certain parts of the Arctic Ocean that had individual polynyas with dimensions as large as 10 x 70 km. Families of polynyas of

this size have been observed in the center of the Beaufort Sea and north of Greenland, and in both cases overflights two days later revealed that the polynyas were gone. Most observers who have lived on the sea ice for any period of time have on occasion observed great shearing motions in their immediate area. The fragmentary and piecemeal evidence we have on polynyas indicates that they move with great speed and can occur in all parts of the Arctic Ocean. Present scanty data indicate that the formation of the polynyas is associated with cyclone passage.

The great part of the surface research in the Arctic Ocean has been carried out by a series of Russian and American ice floe stations. This kind of activity of single stations drifting at separate times at great distances apart in the ocean has failed to give any idea of the cause and effect of the polynya movement in relation to atmospheric, oceanic, and internal ice forces. Before any real understanding of the basic physics of the polynyas and the ice dynamics which produce them can occur, two things are necessary. 1) A means must be developed to acquire sequential, synoptic imagery of the Arctic Ocean during all weather and seasons. 2) Direct measurements of the strains in the sea ice canopy and the heterogeneous character of the air and water stresses acting on that canopy should be made for a group of drifting stations.

Satellite imagery has been shown to be useful in delineating large polynyas in sea ice. Nelson et. al. (1970) have demonstrated this using visible-spectrum images, and Barnes et. al. (1970) have done so using infrared images. A comprehensive study of airborne camera, infrared, and side-looking radar images and laser profile records of Arctic sea ice (Raytheon, 1970) shows that a great variety of extremely detailed information on sea ice morphology can be obtained from aircraft. In 1970 the National Aeronautics and Space Administration flew its two chief remote sensing aircraft, the NP-3 from NASA Houston and the Convair 990 from NASA-Ames Research Center, over the Beaufort Sea, and sensed the Arctic surface with a variety of instruments. Figure 6 shows a side-looking radar image of sea ice approximately 320 km north of Point Barrow, Alaska, obtained in the spring of 1970. Five fairly large polynyas having a preferred orientation can be distinctly seen. This image was obtained through a cloud cover several thousand feet thick.

Some of the most exciting sea ice data obtained recently are the passive microwave images of sea ice from the June 1970 Convair 990

flight (Nordberg, et.al., 1971). One very interesting aspect of microwave sensing of sea ice is that at frequencies in the order of 30 gigahertz the apparent brightness temperature difference between sea ice and open water is as much as 150°K, thus we have a tool which will discern polynyas from floe ice or very thin finger ice through a cloud cover. Figure 7 shows a passive microwave image of multi-year sea ice with two large polynyas. The images also show that large-scale variations in the ice surface texture are detectable as contrasts in microwave emissivities. Brightness temperatures over ice covered with dry snow are 5% lower (radiometrically cooler) than over melted and recrystallized snow or bare ice surfaces.

Not only is the Arctic dark for half of the year, but most of the important changes on both the sea ice and land areas occur when they are covered by clouds. Therefore, the remote sensing tools of side-looking radar (SLAR) and passive microwave appear to be the ones that will prove to be most useful in Arctic geophysics.

A project to measure ice strains and air and water stresses on the ice already exists. The Arctic Ice Dynamics Joint Experiment (AIDJEX) was formed in 1970 by a group of interested American and Canadian scientists as an interdisciplinary investigation designed to obtain data about the ice canopy which will hopefully enable the creation of predictive computer models for its dynamics and heat budget. Investigators from Russia, Norway, and Japan have expressed a willingness to join in this international study. AIDJEX will mount a series of simultaneous manned drifting stations in the Beaufort Sea region starting in 1973. Before these field experiments occur, a series of pilot experiments will have been performed. The first AIDJEX pilot experiment took place approximately 320 km north of the MacKenzie Delta in March 1970. A similar small-scale experiment took place in the same area in March 1971. Both of these pilot expeditions experimented with means to measure ice strains, the water and air stresses on the ice, and the structure of the ocean currents. In March 1971 the NASA Convair 990 flew a series of five missions over the AIDJEX expedition. Both low-level and high-level data were collected with emphasis on SLAR and microwave sensors. The U.S. Navy and Coast Guard also flew a series of missions over the AIDJEX site. The comprehensive and detailed remote sensing and ground truth experiment resulted in the best data of its kind ever collected. These data will be invaluable in establishing design criteria for the full-scale 1973 AIDJEX experiment.

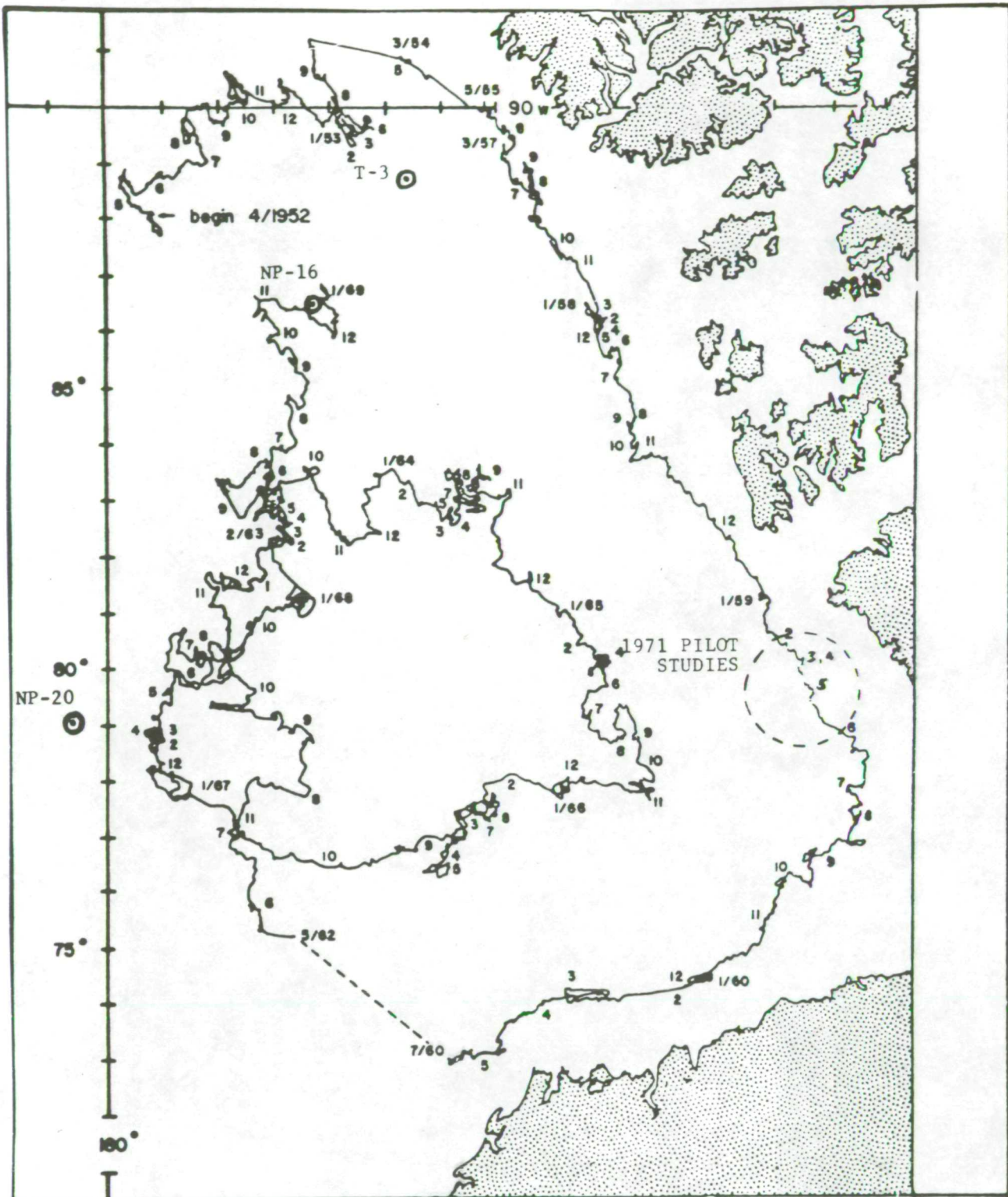
Conclusions

The Arctic is an area in which nature's cause and effect can be understood only with the help of the sequential, synoptic imagery obtainable with remote sensing tools. A real need exists for detailed data obtainable from aircraft and large-scale data obtainable from satellites. Of apparent greatest potential are images, both passive and active, in the microwave region.

A detailed, long-term, international experiment called AIDJEX is already underway, but its great efforts can only be brought to fruition with the aid of remote sensing data.

REFERENCES

- Badgley, F.I., Heat budget at the surface of the Arctic Ocean, Proceedings of the Symposium on the Arctic Heat Budget and Atmospheric Circulation, Edited by J.O. Fletcher, pp. 267-277, The Rand Corporation (RM-5233-NSF), 1966.
- Barnes, James C., David T. Chang and James H. Willand, Improved Techniques for mapping sea ice from satellite infrared data, Final Report under contract no. E-67-70(N), 1970.
- Benson, Carl S., Polar regions snow cover, Proceedings of the International Conference on Physics of Snow and Ice, Hokkaido University, Sapporo, Japan, 1967.
- Glen, A. R., The latest map of North East Land, Geographical Journal, 98, 206, 1941.
- Meier, M.F., R.H. Alexander and W.J. Campbell, Multispectral sensing tests at South Cascade Glacier, Washington, Proceedings of the Fourth Symposium on Remote Sensing of Environment, Ann Arbor, Michigan, pp 145-159, 1966.
- Meier, M.F. and Austin Post, What are glacier surges?, Canadian Journal of Earth Sciences, 6, 807, 1969.
- Meier, M.F. and A. T. Edgerton, Microwave emission from snow--a progress report, Abstract submitted to the Remote Sensing Symposium, University of Michigan, May, 1971.
- Nelson, Helen P., Susan Needham and Thomas D. Roberts, Sea ice reconnaissance by satellite imagery, Final Report to the National Aeronautics and Space Administration, 1970.
- Nordberg, W., A. Edgerton, and others, Aircraft Measurements of Microwave Emission from Arctic Sea Ice, 1971.
- Raytheon Company, Data reduction of Airborne sensor records, Final Report to U.S. Department of Transportation, 1970.
- Wittman, W., and J. Schule, Comments on the mass budget of arctic pack ice, in Proceedings of the Symposium on the Arctic Heat Budget and Atmospheric Circulation, edited by J. O. Fletcher, pp. 215-246, The Rand Corporation (RM-5233-NSF), 1966.



POSITIONS OF DRIFTING STATIONS ON SEPT. 9, 1970
 AND T-3 DRIFT TRACK. WHERE WILL THEY BE
 IN MARCH 1972 and MARCH 1973?

T-3	84.5N	103.1W
NP-16	85.1N	135.8W
NP-18	80.7N	144.9E
NP-19	78.3N	147.6E
NP-20	78.9N	177.3E

FIGURE 1

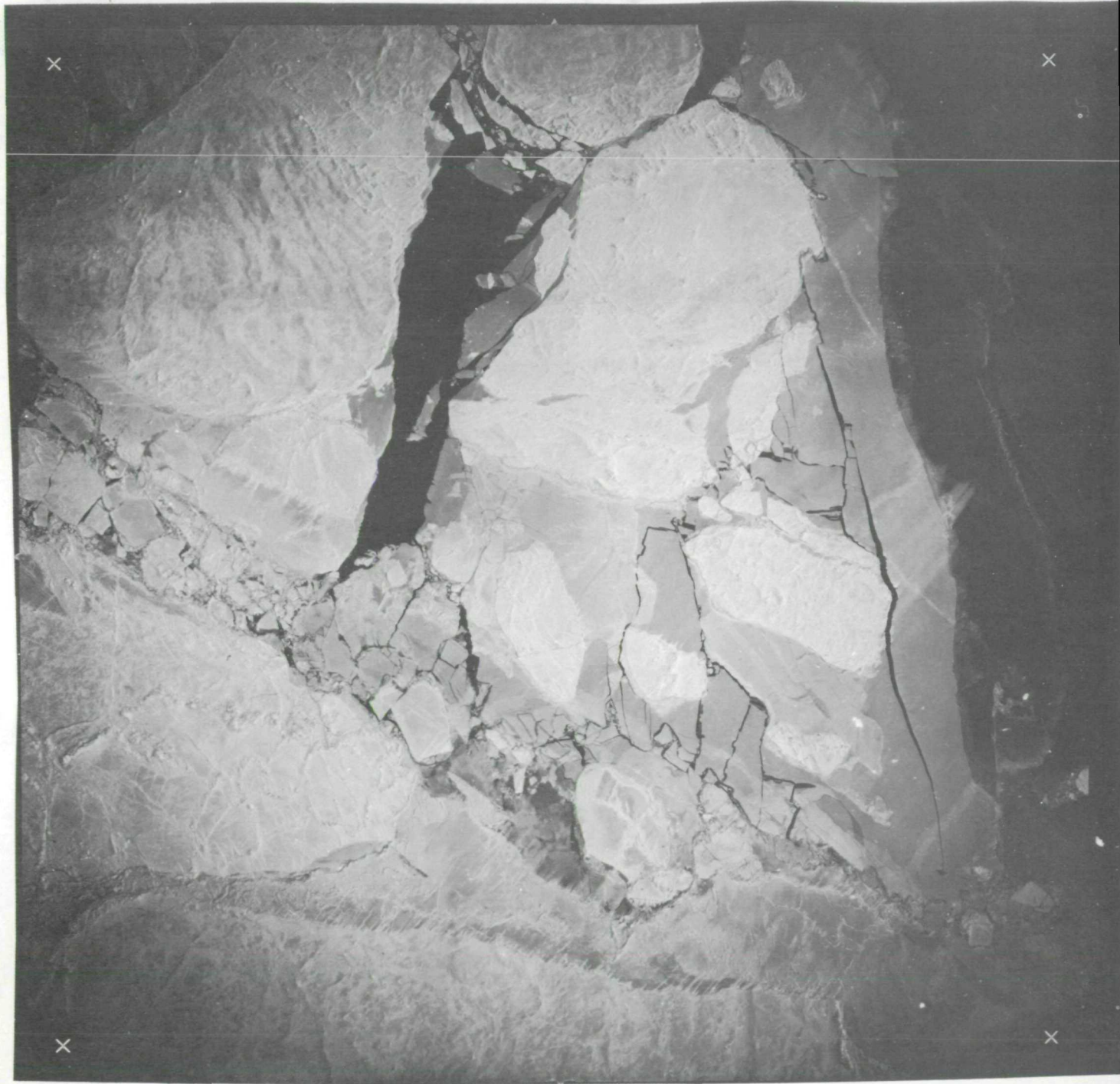


FIGURE 2



FIGURE 3

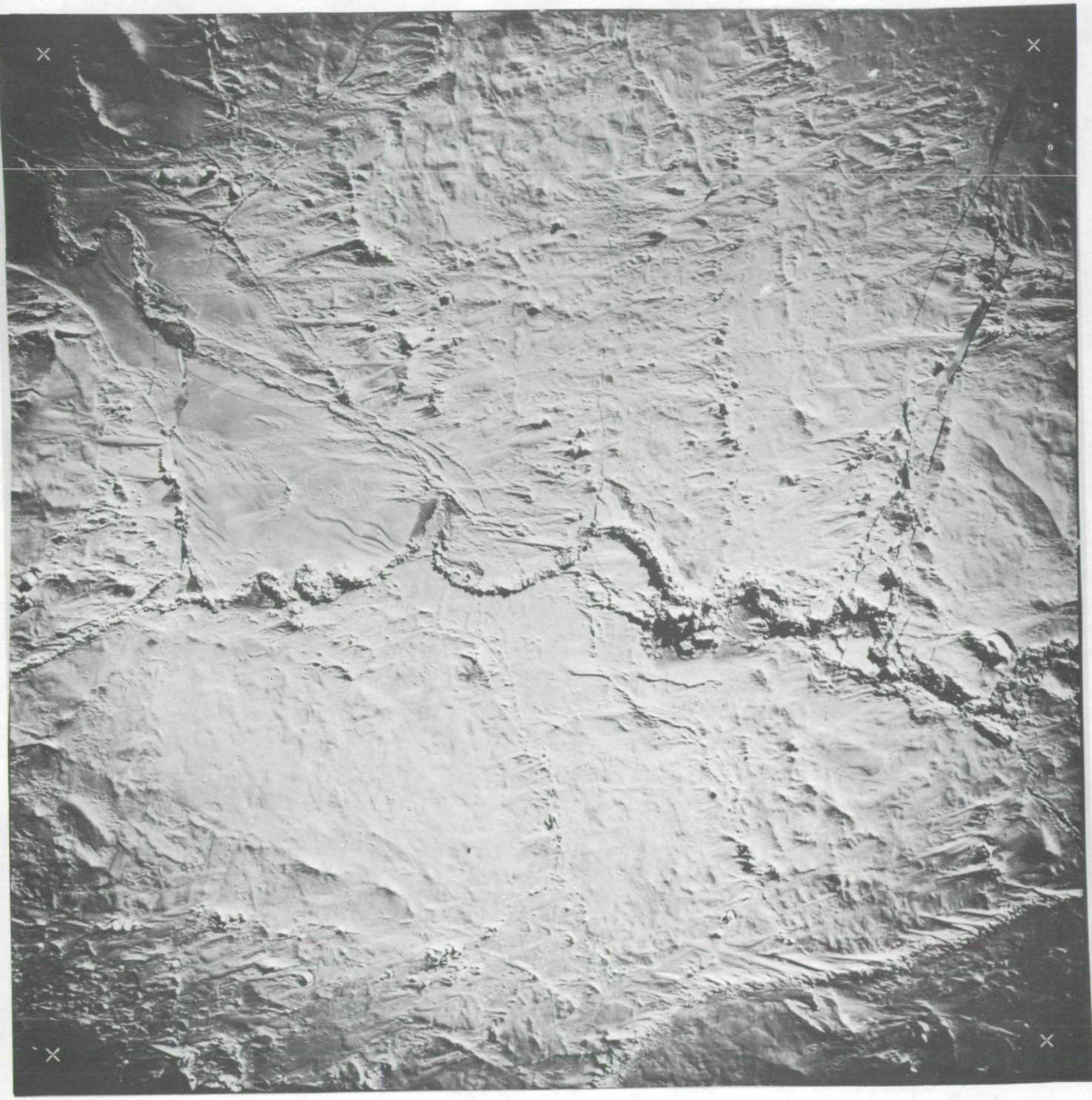


FIGURE 4

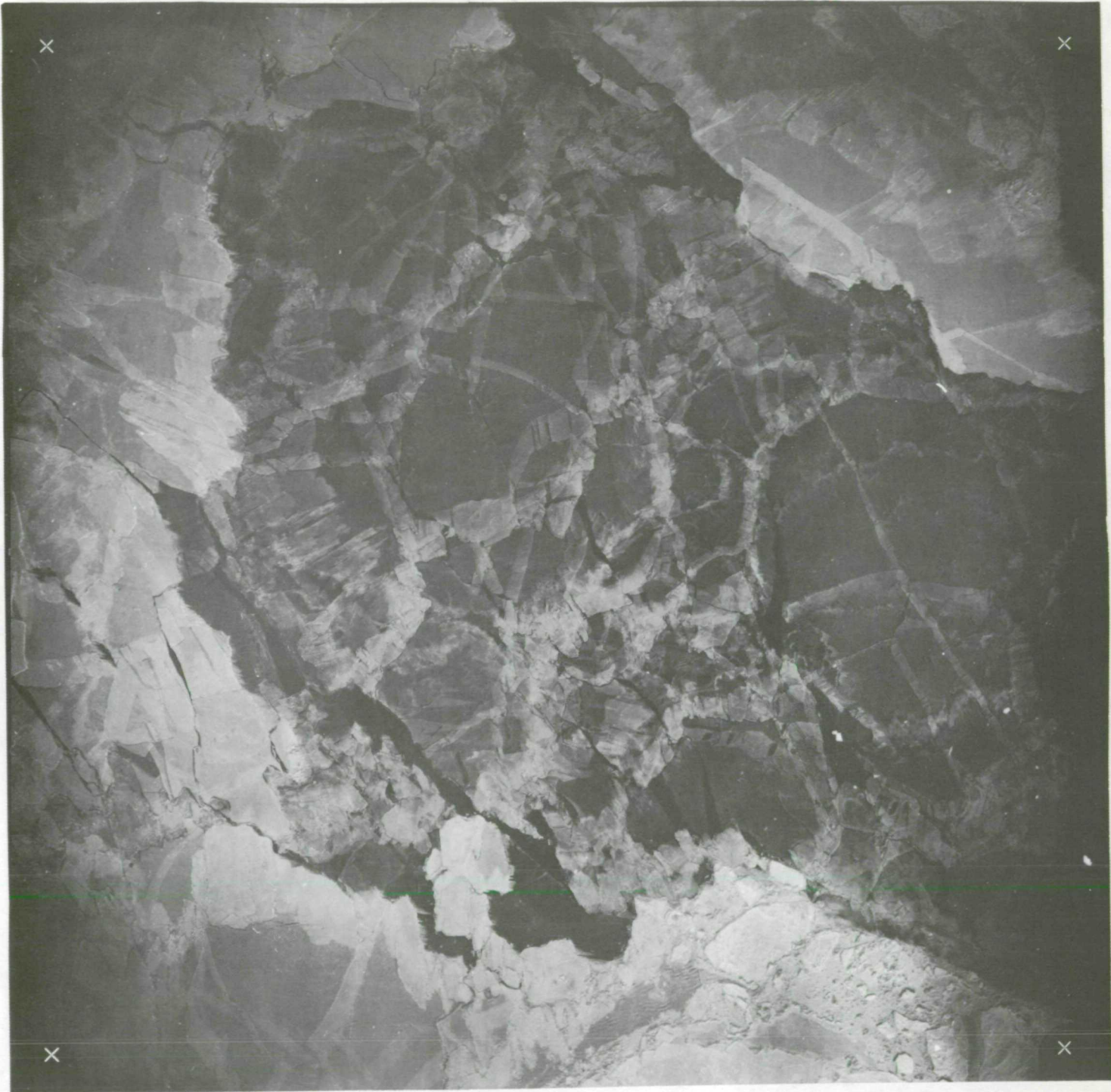


FIGURE 5

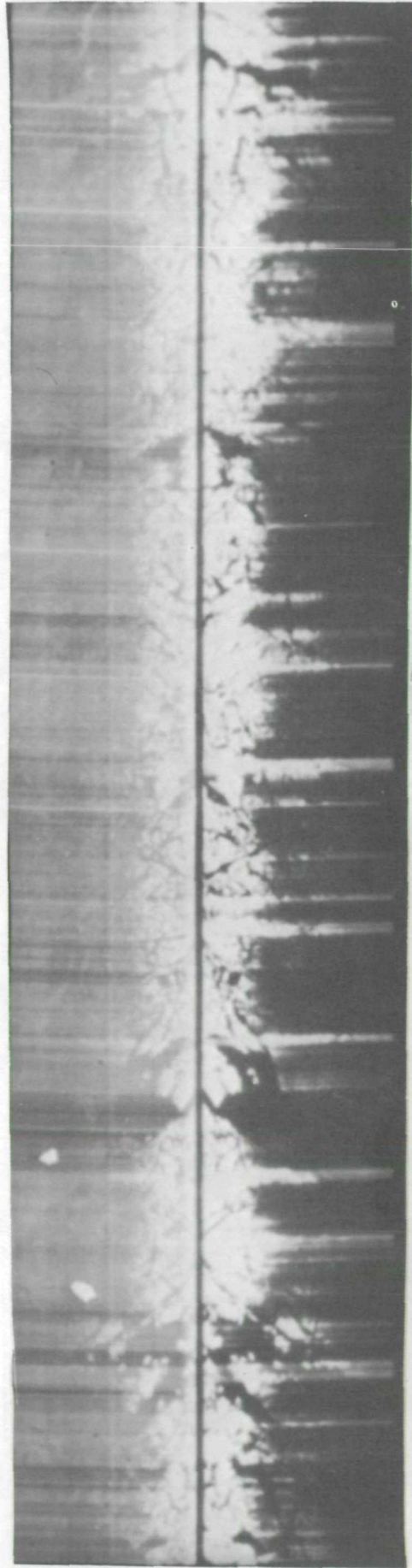
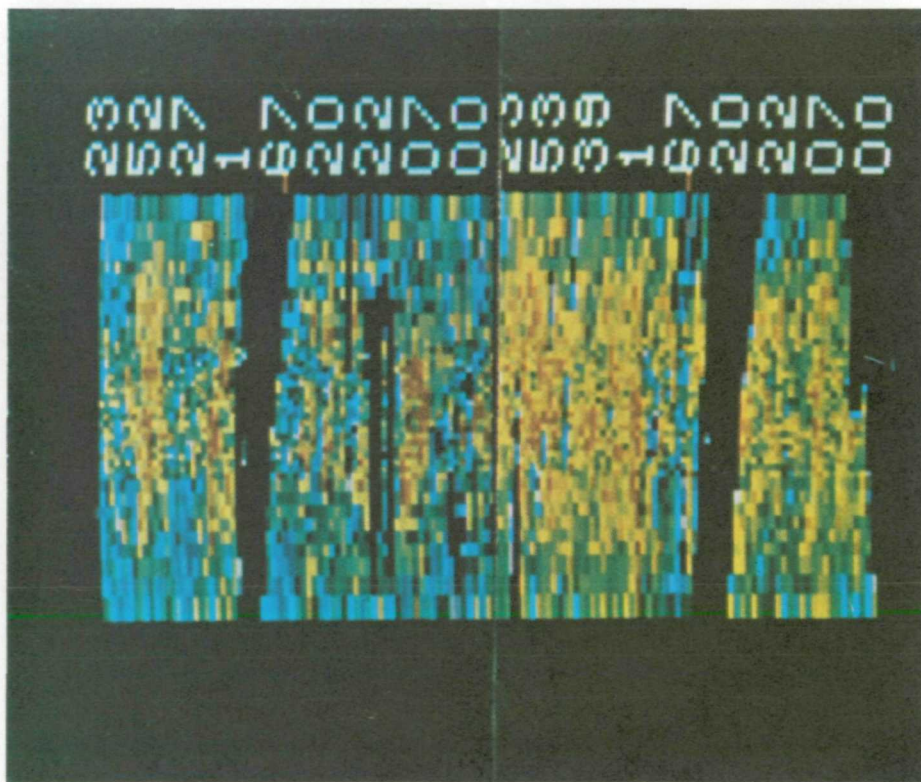


FIGURE 6

PASSIVE MICROWAVE IMAGE OF MULTI-YEAR SEA ICE
WITH POLYNYAS (LARGE LEADS)



AIRCRAFT ALTITUDE	150 M	SENSOR WAVELENGTH	1.55 CM
AIRCRAFT SPEED	450 KM/HR	ANTENNA BEAMWIDTH	2.80
APPROX. DIMENSIONS	0.3KM x 30 KM	SCAN WIDTH	+500

60-15

FIGURE 7

THIRD ANNUAL REVIEW
NASA EARTH RESOURCES PROGRAM
HOUSTON, TEXAS

MEASUREMENT OF WATER DEPTH BY MULTISPECTRAL RATIO TECHNIQUES

by F. C. Polcyn

This work supported by NASA has been a continuation of the program started under contract to NAVOCEANO and technically monitored by Mr. John Sherman, III, Program Manager for SPOC. In previous review sessions, we discussed the results of our work in which three observables were identified that could be used by remote sensors for the measurement of water depth. The first of these was wave refraction techniques using aerial photographs and the subsequent use of the Fourier transform technique to measure the wavelength changes undergone by waves as they approach shore or shoal areas. The second was the multispectral ratio technique using data from a multispectral scanner and taking advantages of the absorption properties of different wavelengths of light and thirdly, was the use of time difference measurements from a laser ranging device which measures the time difference between the surface reflection and the bottom reflection received at the sensor.

Last year we discussed the progress made using the wave refraction technique. This year we wish to report on the work done with data from a multispectral scanner. Next year we plan to report on the use of the scanner techniques coupled with a laser depth ranging device.

In review, we note in Figure 1 (which depicts a scene taken in the Florida Keys) how the light penetrates the water in different bands. In the blue region the light scattering from particles in the water reduces the

contrast of objects seen beneath. As one moves toward the blue-green wavelengths, where maximum light penetration takes place, a more detailed underwater scene can be observed at deeper depths. In the red region where water absorption is greater, only the shallow features can be observed. Finally, in the near-infrared region we find that only water and land boundaries can be distinguished. There is very little penetration of the light into the water.

Making use of this property of the selected transmission at different wavelengths an equation was developed relating the outputs of at least two channels of the multispectral scanner, to an estimate of water depth. Figure 2 shows this equation expressed by a number of variables. The α_1 and α_2 represent the extinction coefficients of water at two different wavelengths. The ρ_1 and ρ_2 represents the bottom reflection in two different bands. The K represent constants of the instrument which are known, where the H represent the incoming solar radiation which is measured by sun sensor aboard the aircraft and the voltages, V_1 and V_2 are the analog signals observed in the multispectral scanning of the shallow features.

One can see that having a priori knowledge of the alphas and the rho's one can compute an estimate of water depth since the other parameters are known by measurement. In looking at the function of absorption coefficient vs. wavelength for different kinds of water, we have found the curves to be similar but displaced so that the difference term for $(\alpha_1 - \alpha_2)$ at two different wavelengths tends to be less variable than having to rely on knowing absolute values, for the different kinds of water. Also the fact that the ratio of the reflectances of the bottom material appears in the equation and that one can choose the wavelengths in this calculation, for smoothly reflecting functions,

such as the reflectance of sand, this ratio tends towards one for spectral channels that are near each other. Furthermore laboratory measurements can be made and this function can be determined for commonly occurring bottom sediments. We have used this equation in a test case with data taken along the Lake Michigan shoreline. A number of calculations were made using different pairs of channels from the 12 channel spectrometer employed in The University of Michigan multispectral system. Figure 3a and b show the plot of these calculations against the known water depths. One can see how different channel pairs produced an estimate to the known depths. One can also see that the accuracy in the shallower water depths is much better than for the deeper depths. This was investigated and found to be related to the choice of values for the extinction coefficient. In order to calculate the true values for α and ρ we used the equation in reverse. Knowing the water depth at several locations we calculated the values for alpha for the fresh water situation. We also computed a reflectance for the sand from the data. Having done this for test locations for a known depth, we proceeded to apply the equation at other depths which gave more accurate estimates over the entire flight line. A digital map was then produced in which each symbol represented a depth range. This depth chart is shown in Figure 4.

In some cases, because of low signal/noise ratio a smoothing function can be used and for the case of the Lake Michigan shoreline, where one has a gradual slopping beach, averages over several resolution elements can be made and a more accurate depth map can be produced. An estimate of this averaging process is shown in Figure 5. We have also applied this to the Ceasar Creek area in the Florida Keys where instead of a slopping sandy beach, a situation of coral reefs occurs so that a more random set of depths are encountered and different bottom reflectances are present. The depths calculated for this

case were produced as a digital printout (Figure 6) to show the various depths and in checking against the available charts for this area, reasonable correlations were found.

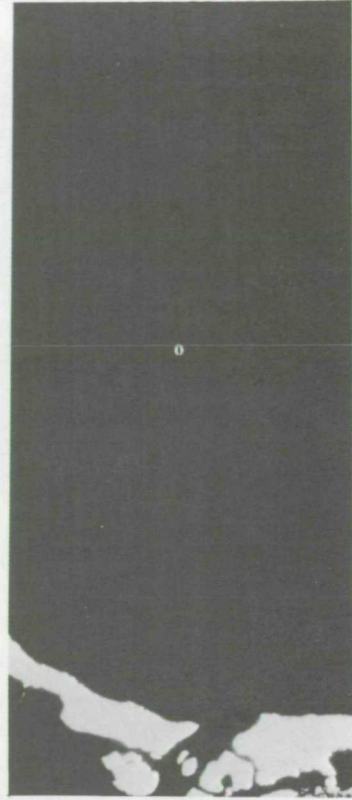
Our plans for the future are to implement this technique in conjunction with a laser ranging device which would then supply a number of sample points of known water depth along the flight line. These known depths would be used to calculate the appropriate values for α and ρ and does reduce the dependency on estimates of these two particular functions. A combination of the multispectral scanner and the laser system should prove to be a unique system which would have the ability to measure rapidly the water depths and underwater topography along the coastlines. It should prove useful in updating shoreline maps, reducing hazards to navigation, and verifying the existence of shoals and changes in beaches especially after major storms each year. We look forward to the next year's research project, in which we hope to demonstrate the potential of the combination of these two systems.



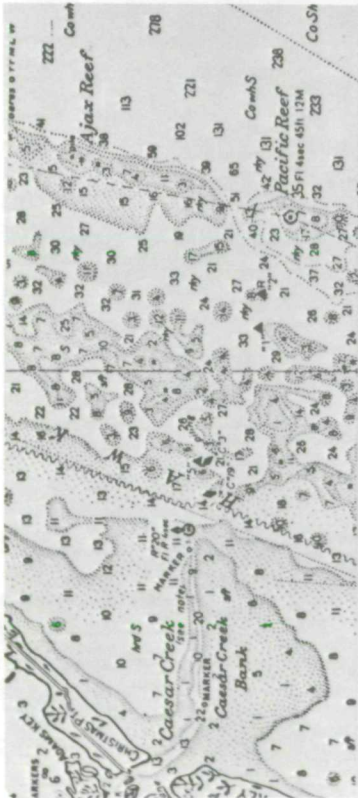
.55 to .58 μ



.62 to .68 μ



.80 to 1.00 μ



.40 to .44 μ



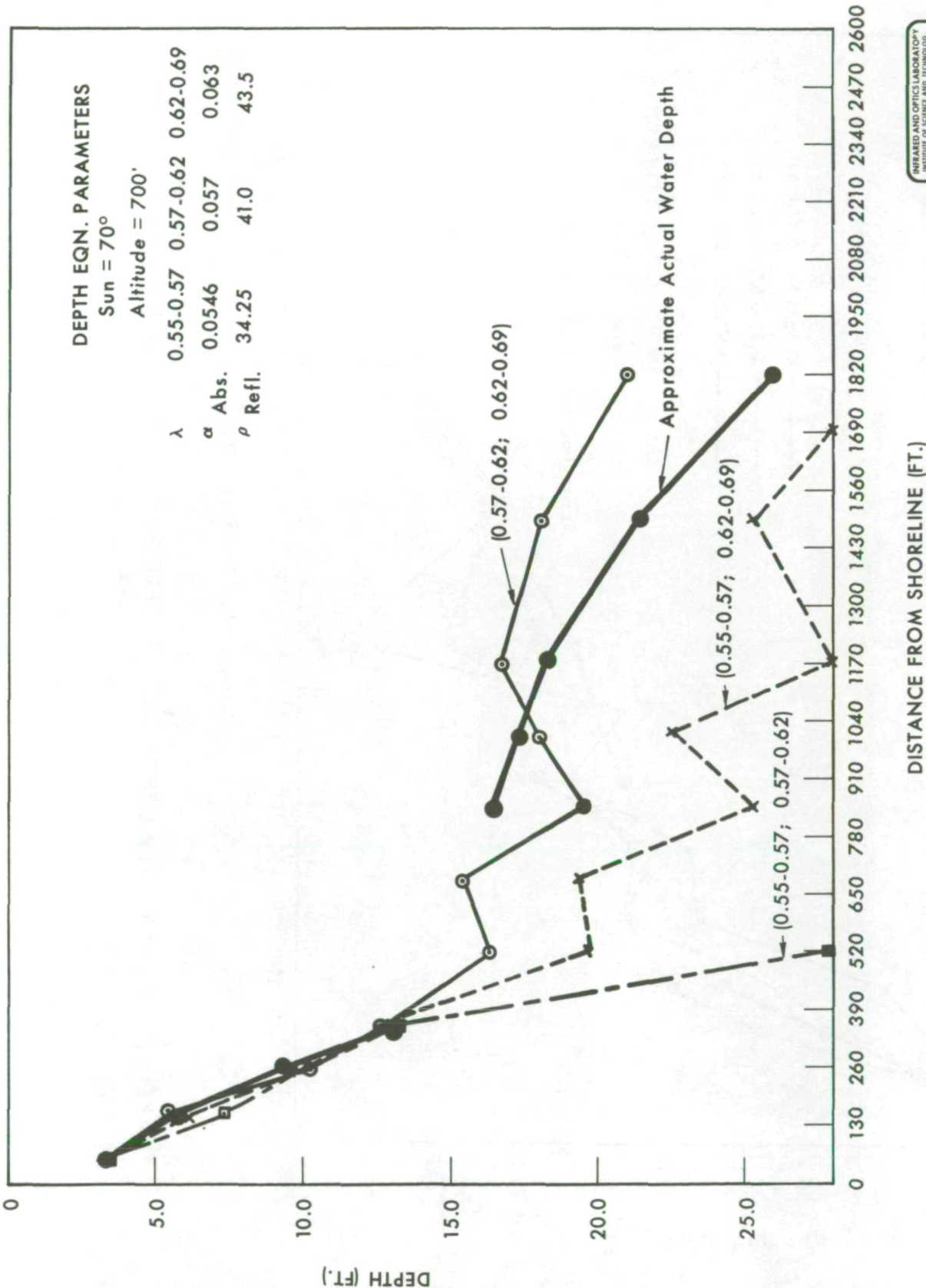
.50 to .52 μ

Figure 1

$$V_{\lambda} = K_{\lambda} \rho_{\lambda} H_{\lambda} e^{-\alpha_{\lambda} Z (\cos^{-1} \theta + \cos^{-1} \phi)}$$

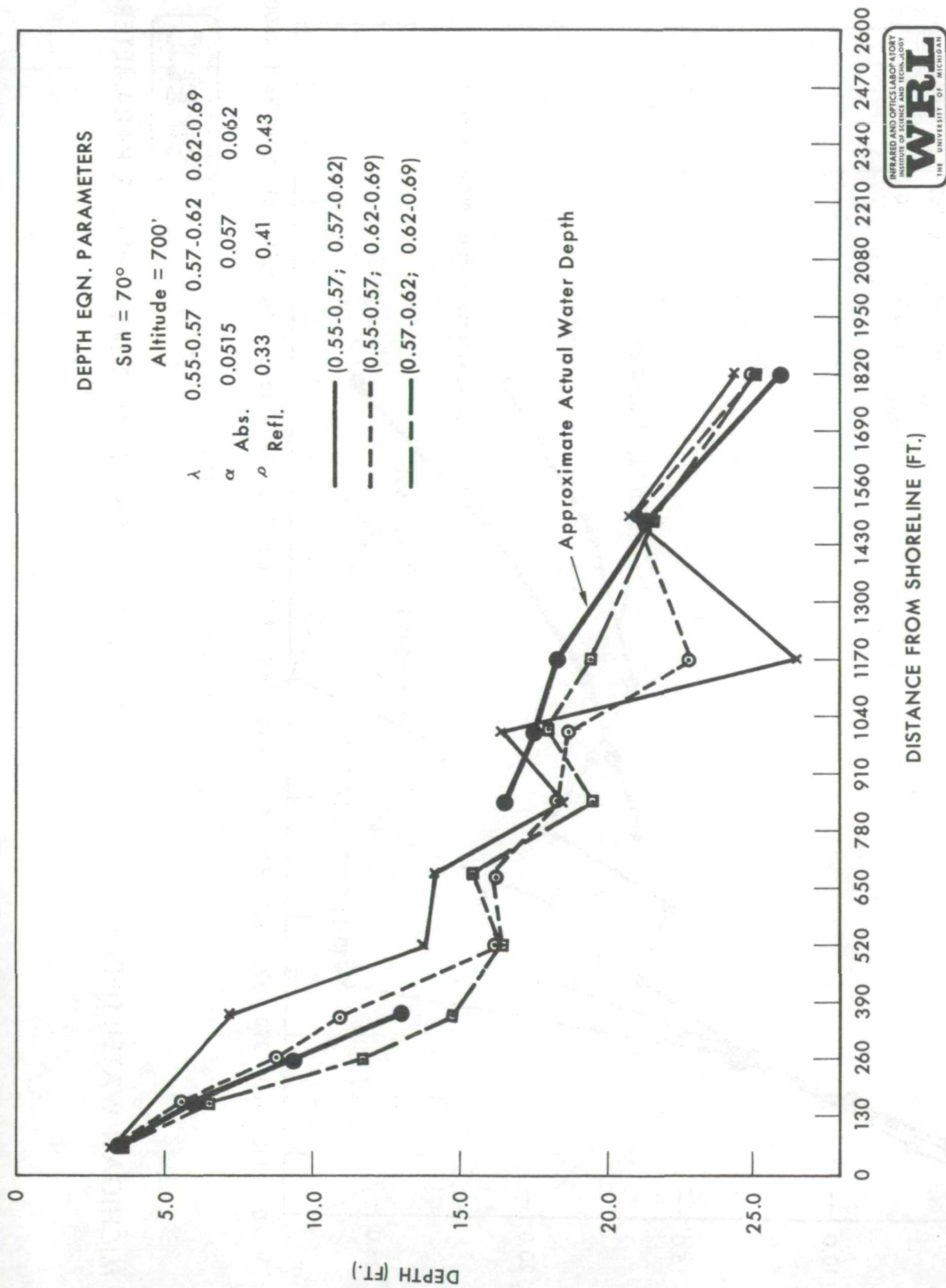
$$Z = \frac{1}{(\alpha_{\lambda_2} - \alpha_{\lambda_1}) f(\theta, \phi)} \ln \frac{V_{\lambda_1} K_{\lambda_2} \rho_{\lambda_2} H_{\lambda_2}}{V_{\lambda_2} K_{\lambda_1} \rho_{\lambda_1} H_{\lambda_1}}$$

Figure 2.



LAKE MICHIGAN WATER DEPTH CURVES GENERATED FROM SHALLOW, TURBID WATER PARAMETERS

Figure 3a



LAKE MICHIGAN WATER DEPTH CURVES GENERATED FROM DEEP WATER PARAMETERS

Figure 3b

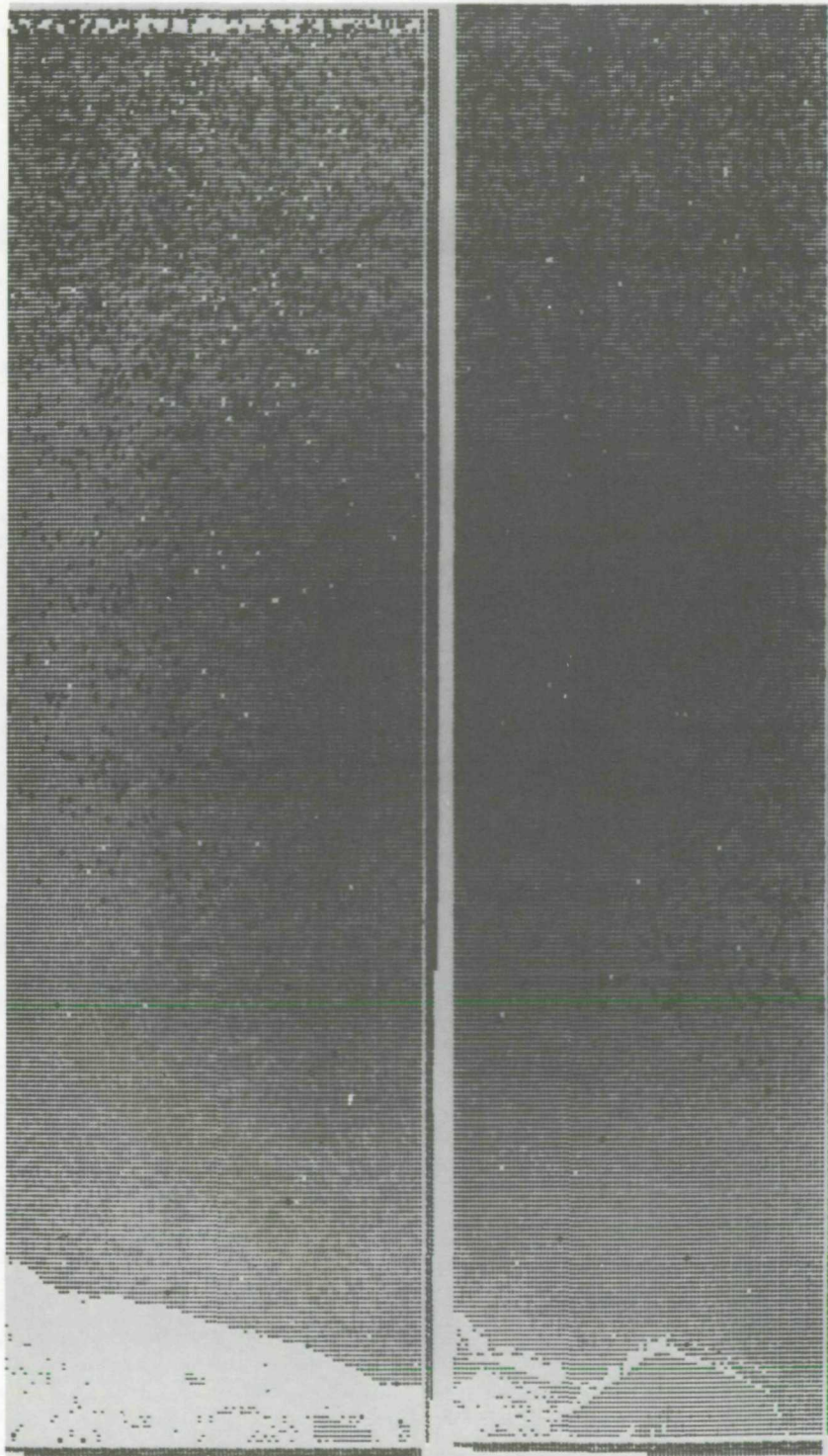


Figure 4.



Symbol	Depth
—	0 - 4'
=	4 - 8'
*	8 - 12'
θ	12 - 16'
⊖	16 - 20'
⊗	20'

NOT REPRODUCIBLE

DIGITAL PRINTOUT OF WATER DEPTH OVER LAKE MICHIGAN



Figure 5

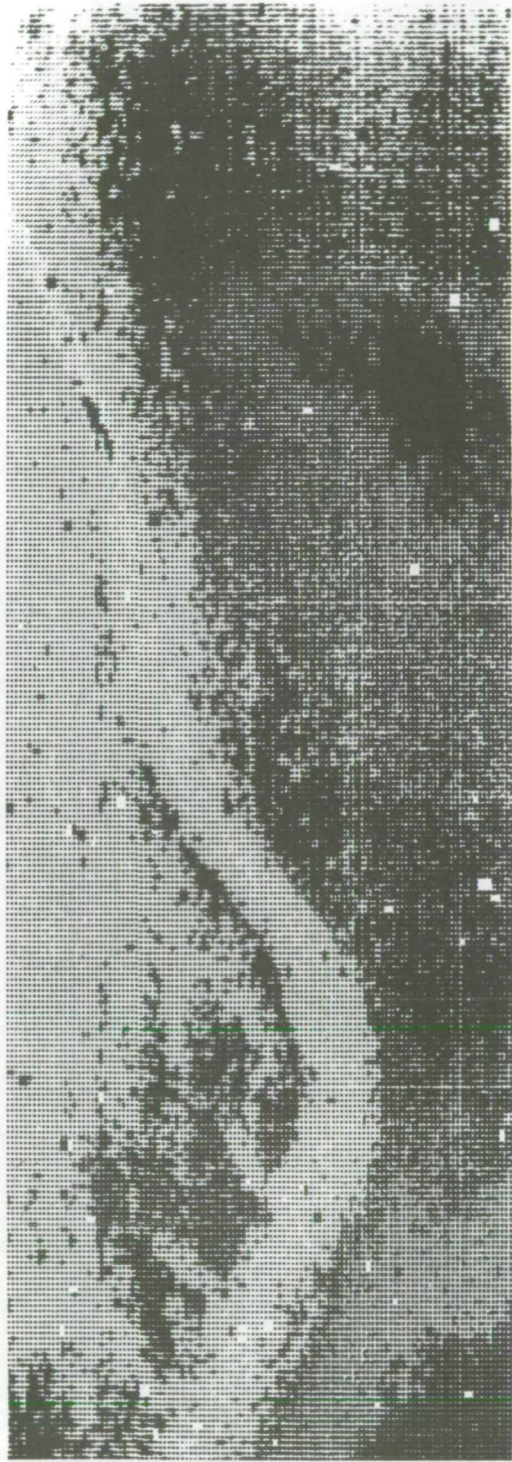


Figure 6.- (Repeated) depth chart - Caesar Creek - obtained by digital processing of multispectral scanning.

NOT REPRODUCIBLE

Page Intentionally Left Blank

RADAR MONITORING OF OIL POLLUTION

By N. W. Guinard
Naval Research Laboratory
Washington, D.C. 20390

ABSTRACT

Radar is currently used by the Naval Research Laboratory for detecting and monitoring oil slicks on the sea surface. The four-frequency radar system is used to acquire synthetic aperture imagery of the sea surface on which the oil slicks appear as a nonreflecting area on the surface surrounded by the usual sea return. The value of this technique was demonstrated at Chedabucto Bay, Nova Scotia, in February 1970, when the four-frequency radar system was used to image the oil spill of the tanker Arrow which had wrecked on Cerberus Rock in the bay. Imagery was acquired on both linear polarization (horizontal, vertical) for frequencies of 428, 1228, and 8910 megahertz. Vertical returns strongly indicated the presence of oil while horizontal returns failed to detect the slicks. Such a result is characteristic of the return from the sea and cannot presently be interpreted as characteristic of oil spills. Because an airborne imaging radar is capable of providing a wide-swath coverage under almost all weather conditions, it offers promise in the development of a pollution-monitoring system that can provide a coastal watch for oil slicks.

VISIBLE REGION REMOTE SPECTROSCOPY OF
POLLUTED WATER

By

Peter G. White
TRW Systems Group**ORIGINAL CONTAINS
COLOR ILLUSTRATIONS**INTRODUCTION

The data described in this report was taken in order to see if correlations could be obtained between airborne and surface measurements of subsurface pollutants. Figure 1 illustrates some of the problems associated in making this type of measurement. In the right hand column the electro-magnetic spectrum from ultra-violet through infrared is displayed. In the adjacent column, the areas in which the atmosphere interferes with observations are shown. At the shorter wavelengths, atmospheric particles scatter radiation to the extent that the back-scattered light effectively obscures the signal from the target. At the longer wavelengths, the atmosphere effectively absorbs all the useful measureable signal. The middle column shows a similar effect due to the water itself. At the short wavelengths, water molecules scatter radiation received from above much as the atmosphere did in the previous case. At wavelengths greater than .7 microns, the absorption coefficient of water is so high that effectively, any signal from beneath the surface never reaches the surface. Therefore, the only region of the spectrum which is useful in making measurements of pollutants beneath the surface of the water is within the approximate range of .38 to .7 microns. Pollutants at, or near, the surface of the water can be detected and measured over a considerably larger portion of the spectrum as is shown in the left-hand column of Figure 1.

TEST PROCEDURES

Our tests involved the flight of an airborne spectrometer flown in a Cessna 180 aircraft at 1,000 ft. altitude over a flight path slightly more than 2 nmi. long located in Los Angeles Harbor. Surface truth measurements were taken from a small boat in the harbor, along the same path.

Figure 2 shows the northern portion of the flight path during the tests. The lines indicated on the photograph are the path traced out during individual spectral scans by the spectrometer in the aircraft. The circles are areas in which water samples and surface measurements

were made from the boat. Notice that at the top of the photograph, a large sewage outfall is seen on the right. This outfall is used by the City of Los Angeles to discharge sewage after primary treatment. On the left a smaller outfall can be seen which is associated with a fish cannery in the area, and another cannery outfall is located somewhat below this, but just out of the left-hand edge of the picture, and is not visible.

While taking measurements, experimenters on the boat noticed that in the immediate vicinity of the sewage outfall, the water was substantially warmer. This prompted us, on a subsequent date, to fly an 8 to 13 micron infrared linescanner to obtain a thermal image of the scene. This is shown in Figure 3. Notice that the two outfalls seen in the preceding Figure 2 are both visible and that their flow patterns show up in a very similar manner.

Some typical spectral reflectance signatures, obtained by the spectrometer, are shown in Figure 4. Notice the large differences between the three signatures shown, even though their locations are not too distant from one another.

The upper curve is typical of water near the sewage outfall. The lower curve is typical of water some distance away, and water that prevailed all the way out to the Los Angeles breakwall and even beyond.

Figure 5 is a photograph taken from 8,000 feet altitude showing the complete flight path of the aircraft. Every tic mark along the line represents a point at which a spectral signature was obtained. Water measurements on the surface were made along the same line.

The sewage outfalls mentioned previously are visible near the upper part of the picture, and in the lower portion, indications of a plankton known as gonyaulax sometimes referred to as "Red Tide" may be seen. Some recent research has indicated that plankton concentrations are frequently higher in regions adjacent to sewage outfalls.

Figure 6 is a map of the same area showing more accurately the areas measured by the spectrometer as small rectangles and the points at which all water samples and ground measurements were made, shown as dots.

DATA ANALYSIS

Certain characteristics of the spectral signatures obtained were noted. Referring back to Figure 4, we see that the area in the immediate vicinity of the outfall shows a very distinct increase in reflectivity between 4000 and 5000Å. In all cases in which sewage was present in the water, this rise in reflectivity was noted in this region and in

addition, it was noted that the slope of the reflectance curve here appeared to change as a function of the sewage content in the water. On the other hand, in the areas of the harbor which contain plankton, this same portion of the reflectance curve had a slope in the other direction, as shown by the lower curve. In this case, regardless of the plankton content of the water, the slope remained fairly constant. In order to see if these observations were indeed real, the parameter K_1 , shown in Figure 7 was devised. K_1 is the difference in reflectivity between 5250 and 4000Å with the total quantity normalized by dividing by the reflectance at 5700Å. K_1 is plotted against Secchi depth, which is a measure of the clarity of the water. The higher the Secchi depth, the clearer the water.

The sewage points on the curve show a very definite relationship between K_1 and the Secchi depth. This is consistent with our observation of the change in slope of the reflectance curve with sewage content of the water.

On the other hand, no trend is noticed when K_1 for algae is plotted against Secchi depth. Once again, this is in agreement with our observation of no change in the slope of the reflectance curve from 4000 to 5250Å.

The plankton or algae under observation was a type known as gonyaulax which contains a pigment called pycobilin. Pycobilin absorbs radiation in the region of 5250Å. This absorption shows up in the lower curve in Figure 4 and was very characteristic of all spectral curves obtained over waters containing this algae. Therefore, Figure 8 is a plot of a parameter K_2 . K_2 is an attempt to determine the concentration of pycobilin pigment and hence algae, in the water. K_2 is defined as the difference in reflectance between 5700 and 5250Å, once again normalized by dividing by 5700Å. In other words, K_2 is a measure of the depth of the pycobilin absorption. In this case, as shown in Figure 8, we have indeed developed a relationship between K_2 and the Secchi depth for the algae. As the depth of the pycobilin absorption increases, K_2 becomes larger and the Secchi depth or the clarity of the water decreases. Perhaps surprisingly, another relationship between K_2 and Secchi depth seems to be apparent for water containing sewage, although this is not as strongly marked as was K_1 .

Another feature of water containing algae is an absorption due to chlorophyll- α at 6700Å. This too, can be seen in Figure 4, and in the case of Figure 9, we have plotted parameter K_3 which attempts to measure the absorption at 6700Å. Once again, we have developed a relationship that seems to hold for concentration of algae and again, a different relationship for concentration of sewage, when plotted against Secchi depth.

In the case of Figures 7, 8, and 9, the clear water values of K are indicated from data obtained previously and this, of course, is the value that K would have at a Secchi depth of the order of perhaps 50 feet. It serves as an indication of the direction in which the curve shown will tend. Figure 10 shows reflectance curves from two areas containing algae; in the one case, a fairly high concentration, shown as the dashed curve, in which the Secchi depth was only 8.3 feet, and in the other case a lesser concentration in which the Secchi depth was 15.5 feet. The algae counts shown on the curve represent the number of cells of algae counted in a given area on a microscope slide and show correlation with the Secchi depths as might be expected.

One of the most striking features of Figure 10 is the sharp drop in reflectance at wavelengths higher than 5700Å. In order to see if there was meaning to this observed phenomena, Figure 11 shows a parameter K_4 which is a measure of that drop. It is the difference in reflectance between 5700 and 6100Å divided by the reflectance at 5700Å. In this case also, a relationship develops between K_4 and the Secchi depth. The point of inflection in the curve near the right hand side is due to the fact that the value of K_4 for clear water is somewhat less than .30.

CONCLUSIONS

The significance of the preceding results is that they show that some form of quantitative measurement may be made from an airplane of phenomena associated with subsurface pollutants. There is definite evidence that some measure of the concentration of sewage may be obtained remotely and a measure of associated algae growths. Both measurements may be made independently of one another.

The scatter shown in the curves is probably primarily due to the non-homogeneity of the water and, in addition, to an uncertainty of the location of the boat during the time the measurements were made. The location of the boat was known to probably 150 feet on the surface, whereas the spectral reflectance curves made by the spectrometer from the air were known to within 50 feet.

It is reasonable to expect that with more careful and accurate ground truth measurements, particularly particle size distributions to a depth of 10 or 20 feet, and with more accurate navigation data, that the scatter shown in these curves will be substantially reduced and that, in addition, new relationships not at present apparent will be seen.

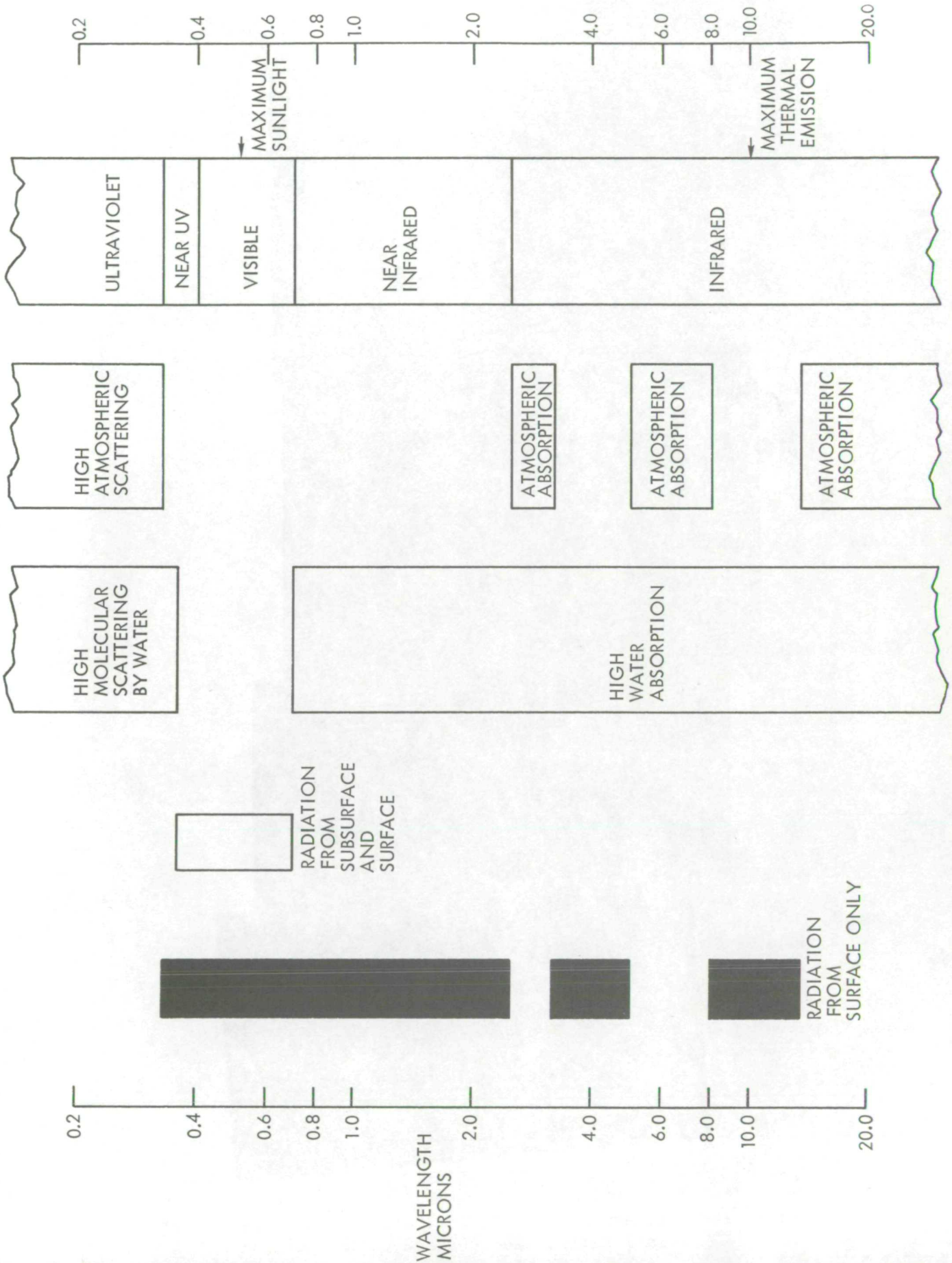


Figure 1 - Spectral regions suitable for remote polluted measurements.

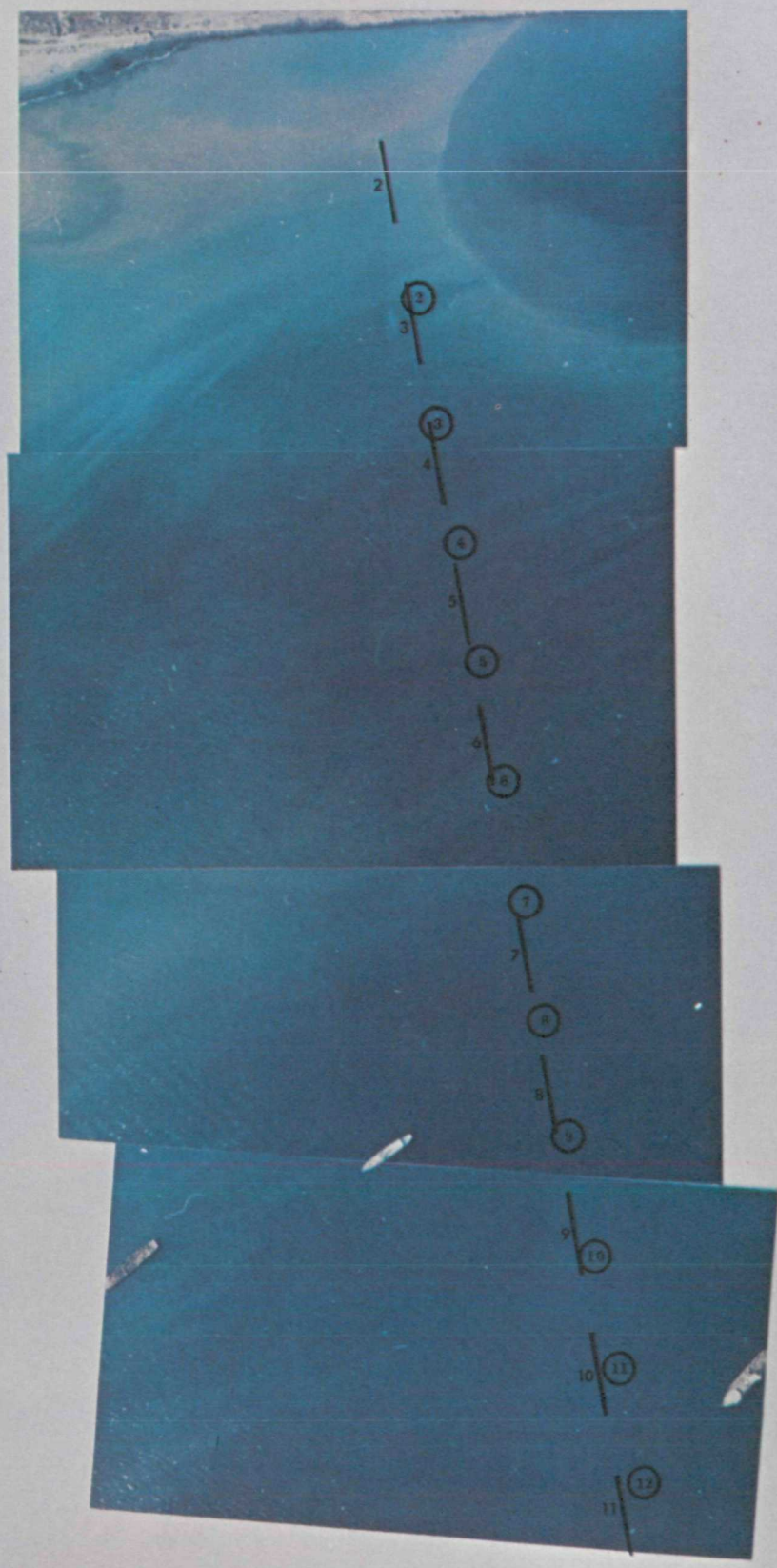


Figure 2 - Northern Portion of test area showing spectrometer scan locations and surface truth points.

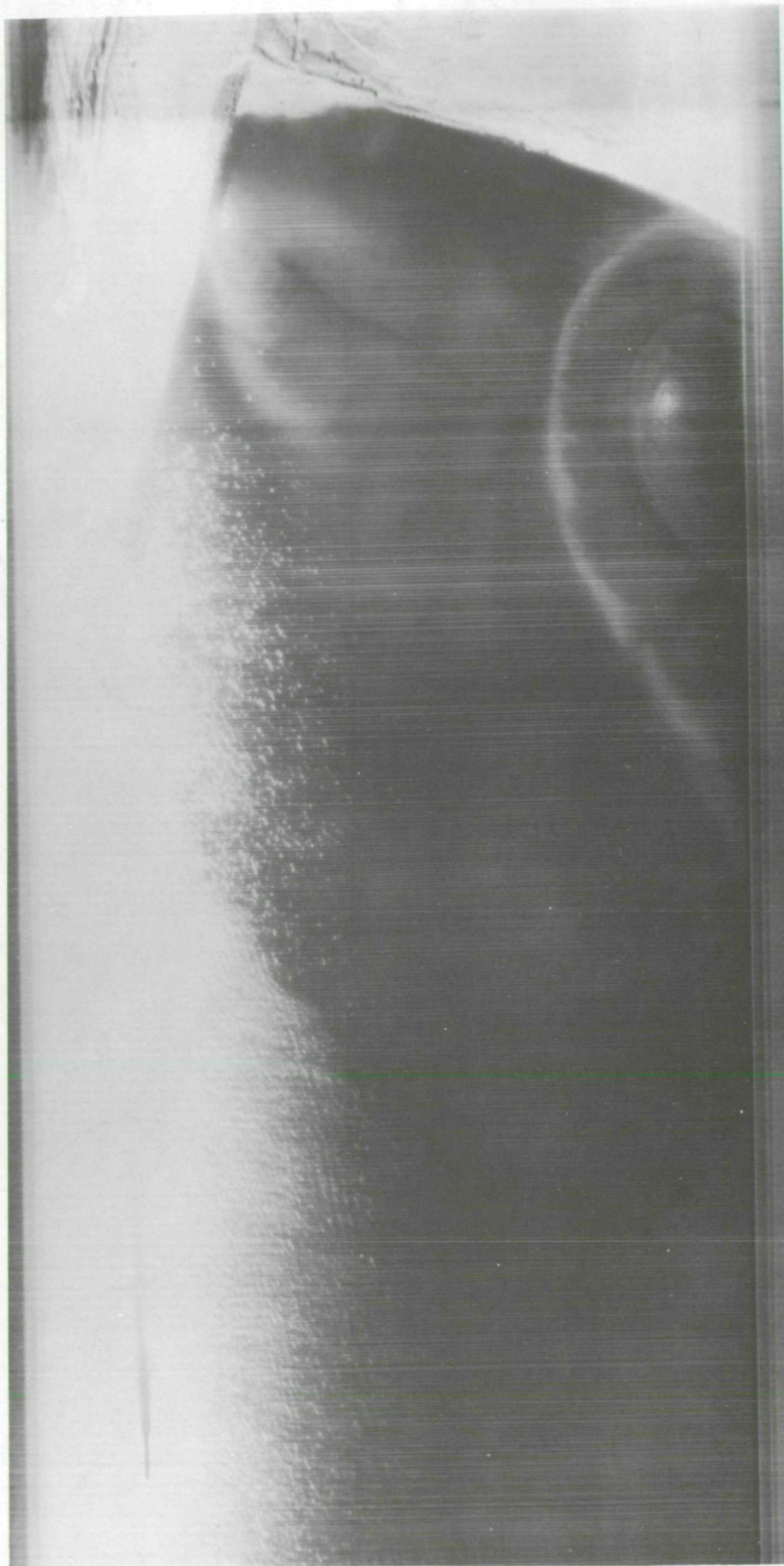


Figure 3 - Thermal image of northern portion of test area.

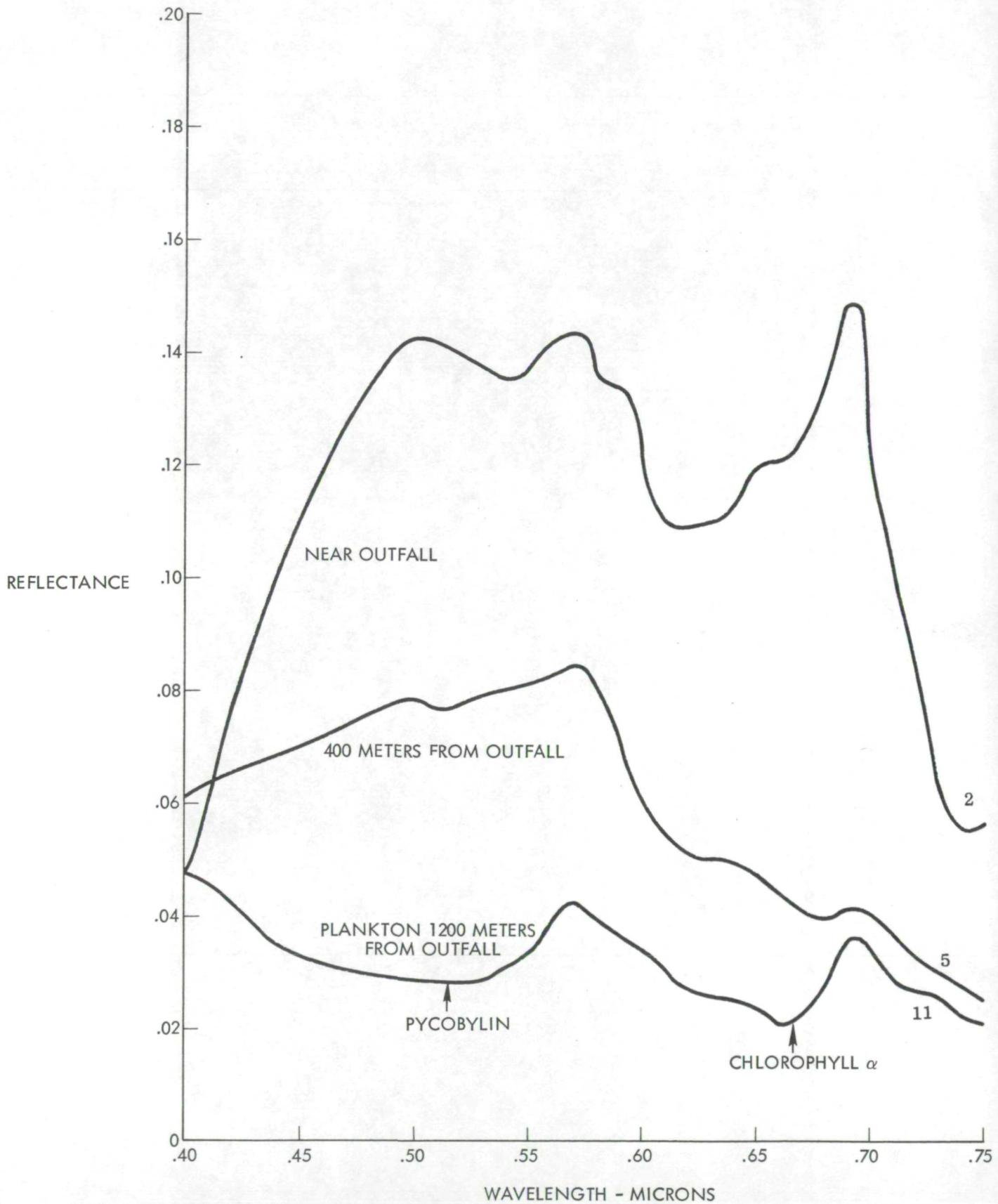


Figure 4 - Typical spectral reflectance signatures.

LOCATION OF SPECTROMETER SCANS IN LOS ANGELES HARBOR 10/18/70

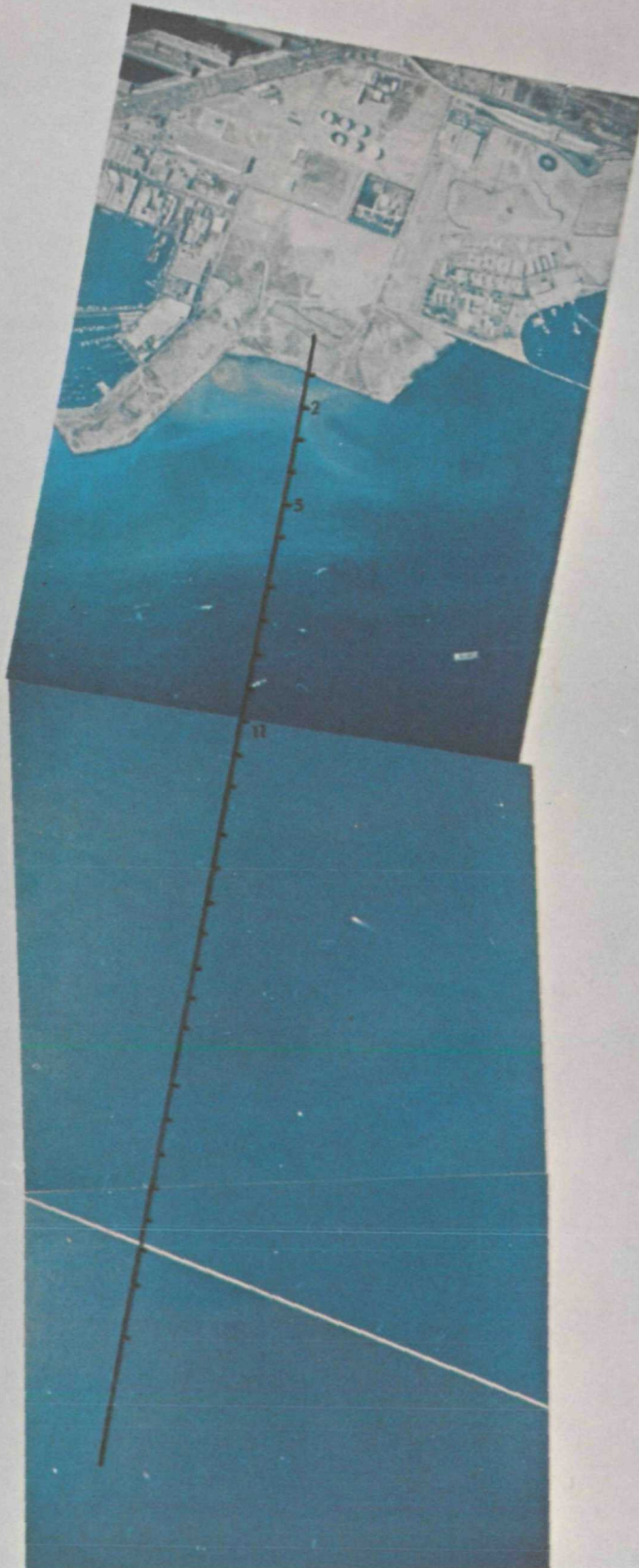


Figure 5 - Complete test area.

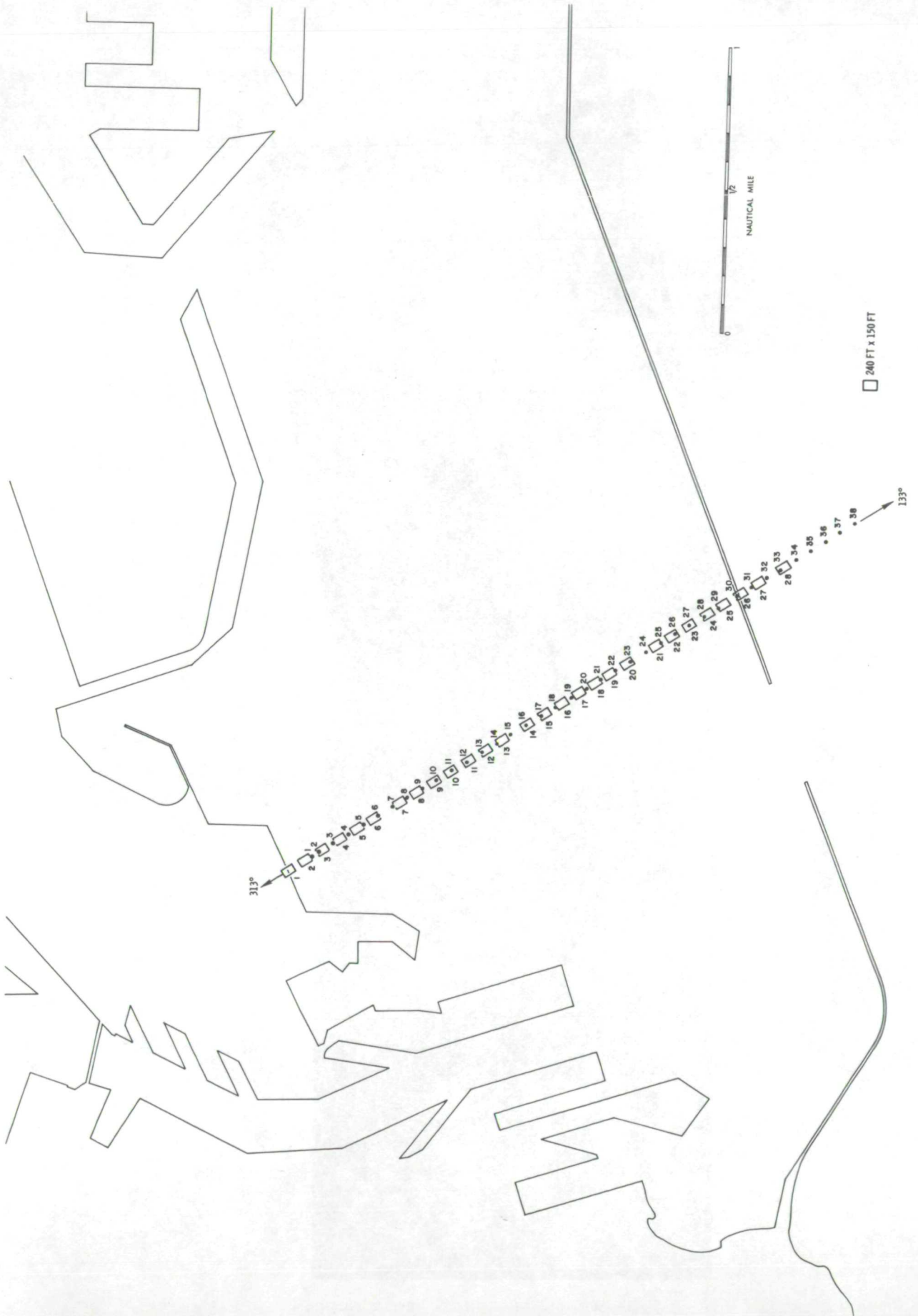


Figure 6 - Map of test area showing measurement locations

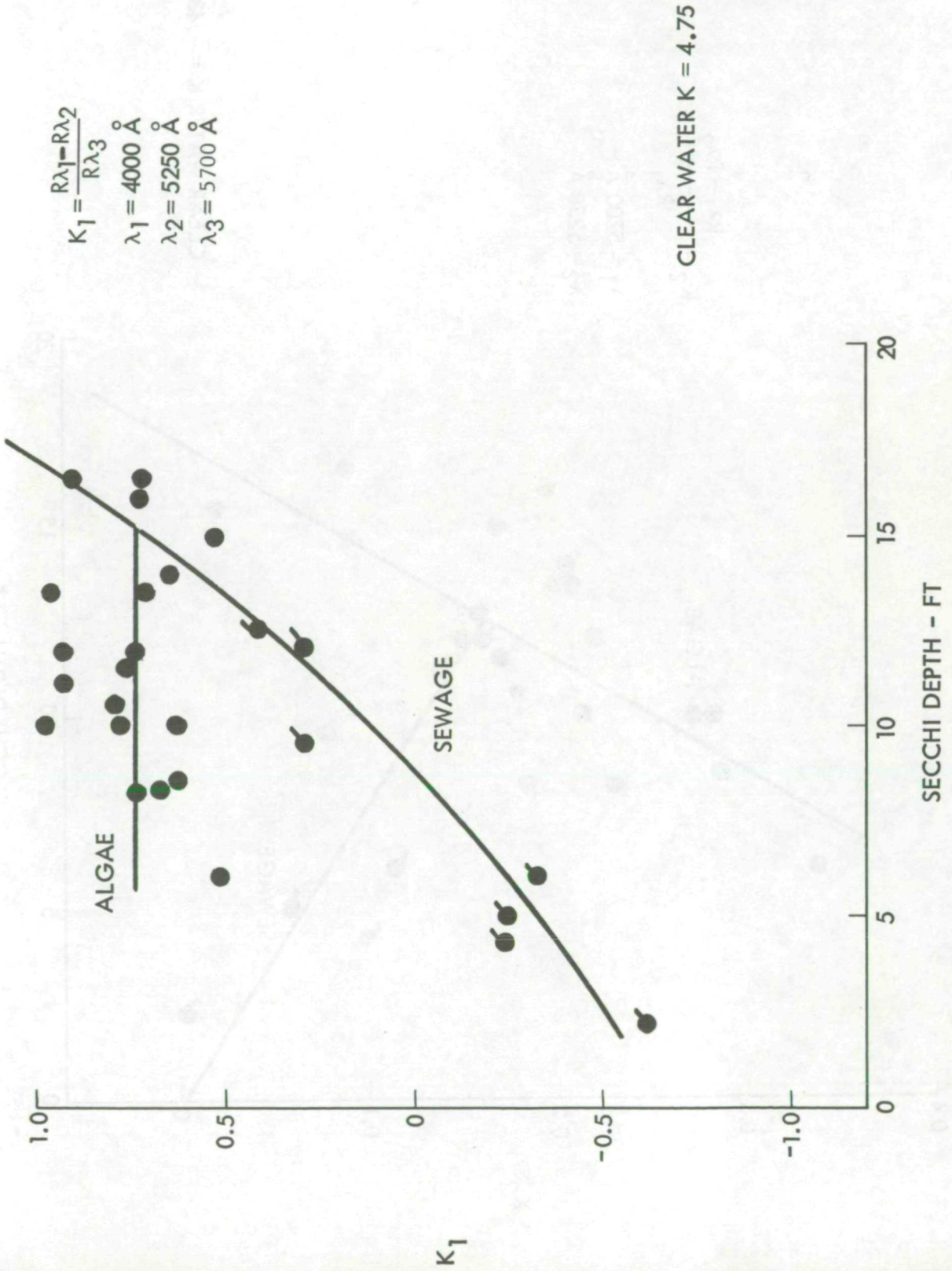


Figure 7 - Parameter K_1 vs. Secchi depth.

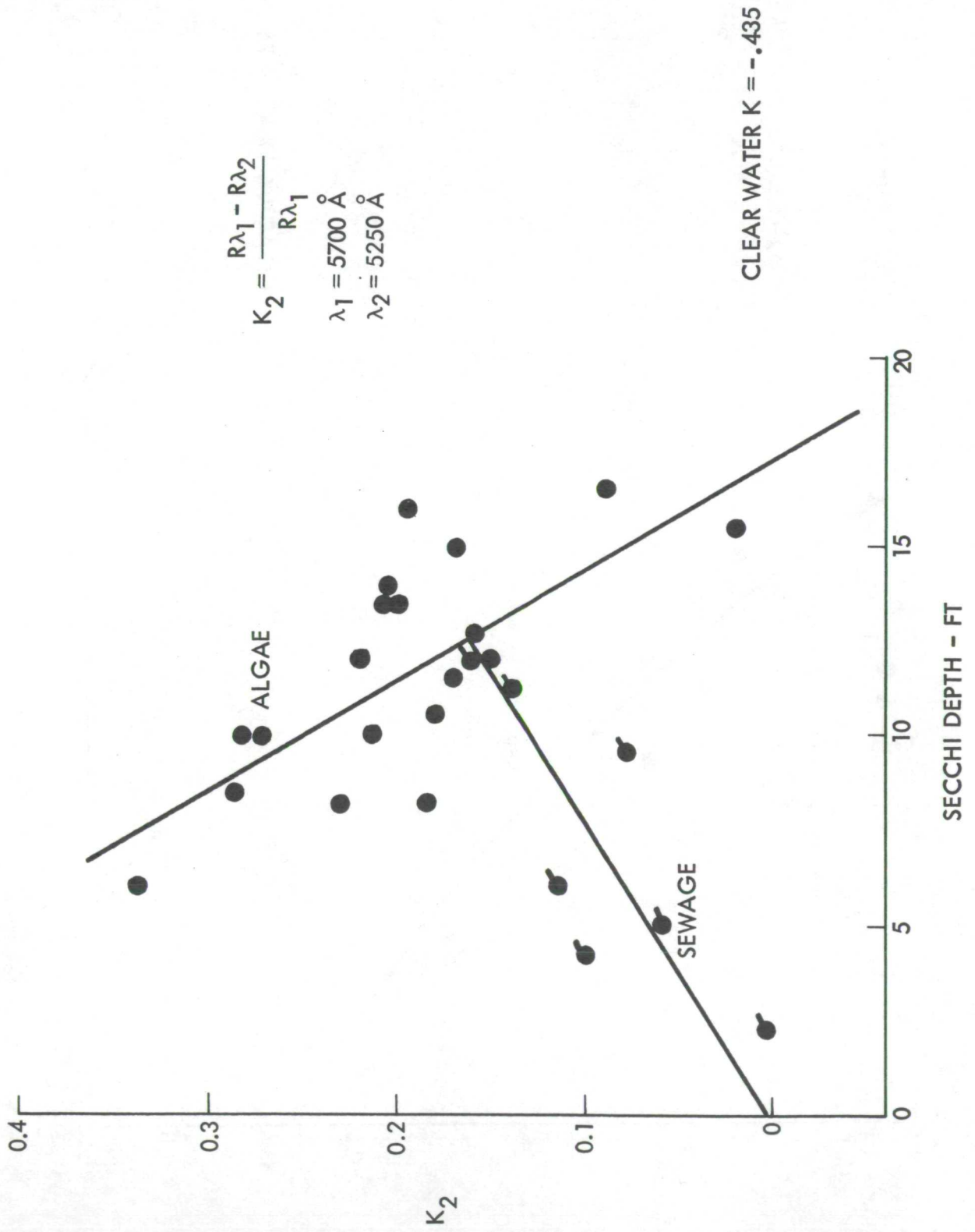


Figure 8 - Parameter K_2 vs. Secchi depth.

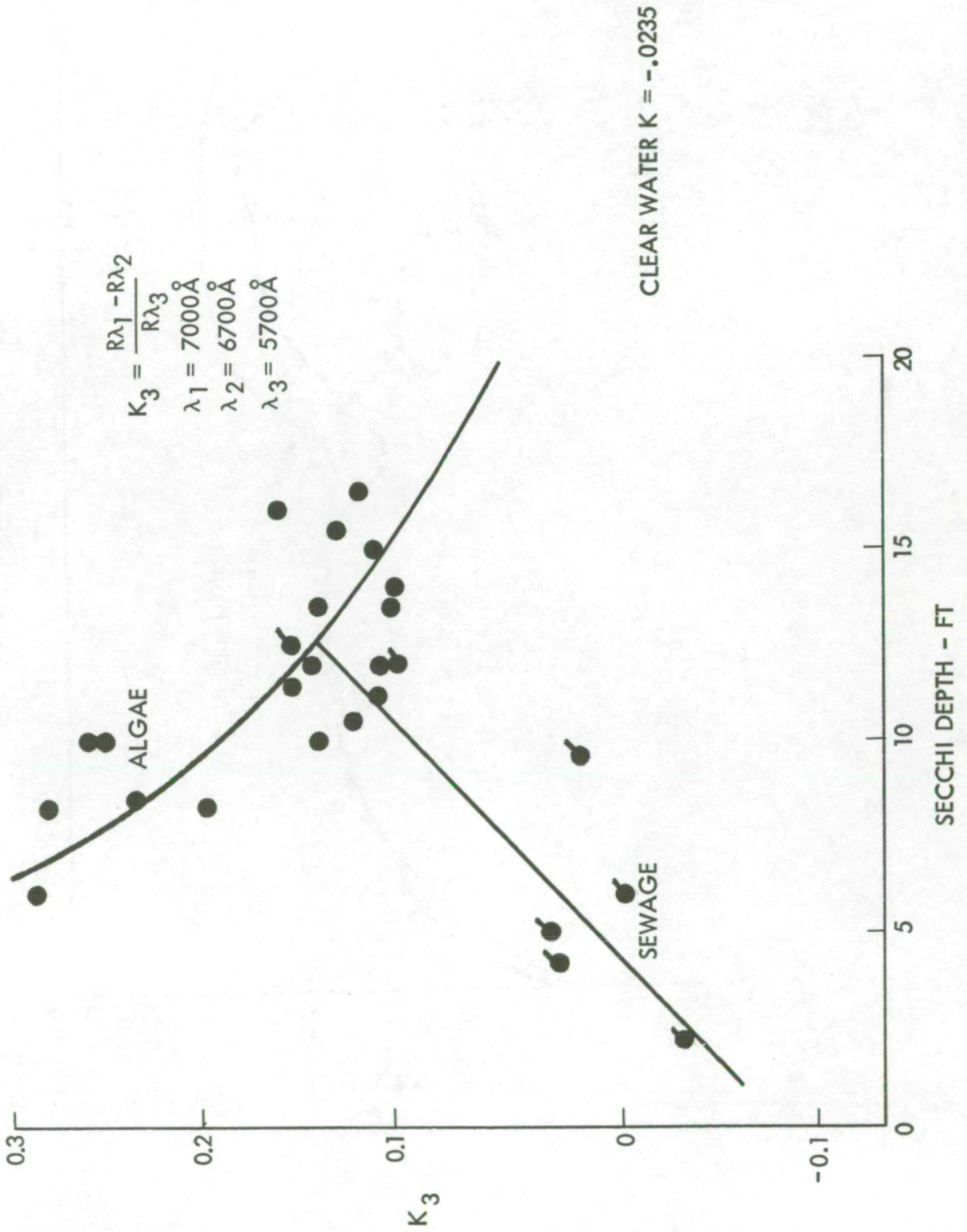


Figure 9 - Parameter K_3 vs. Secchi depth.

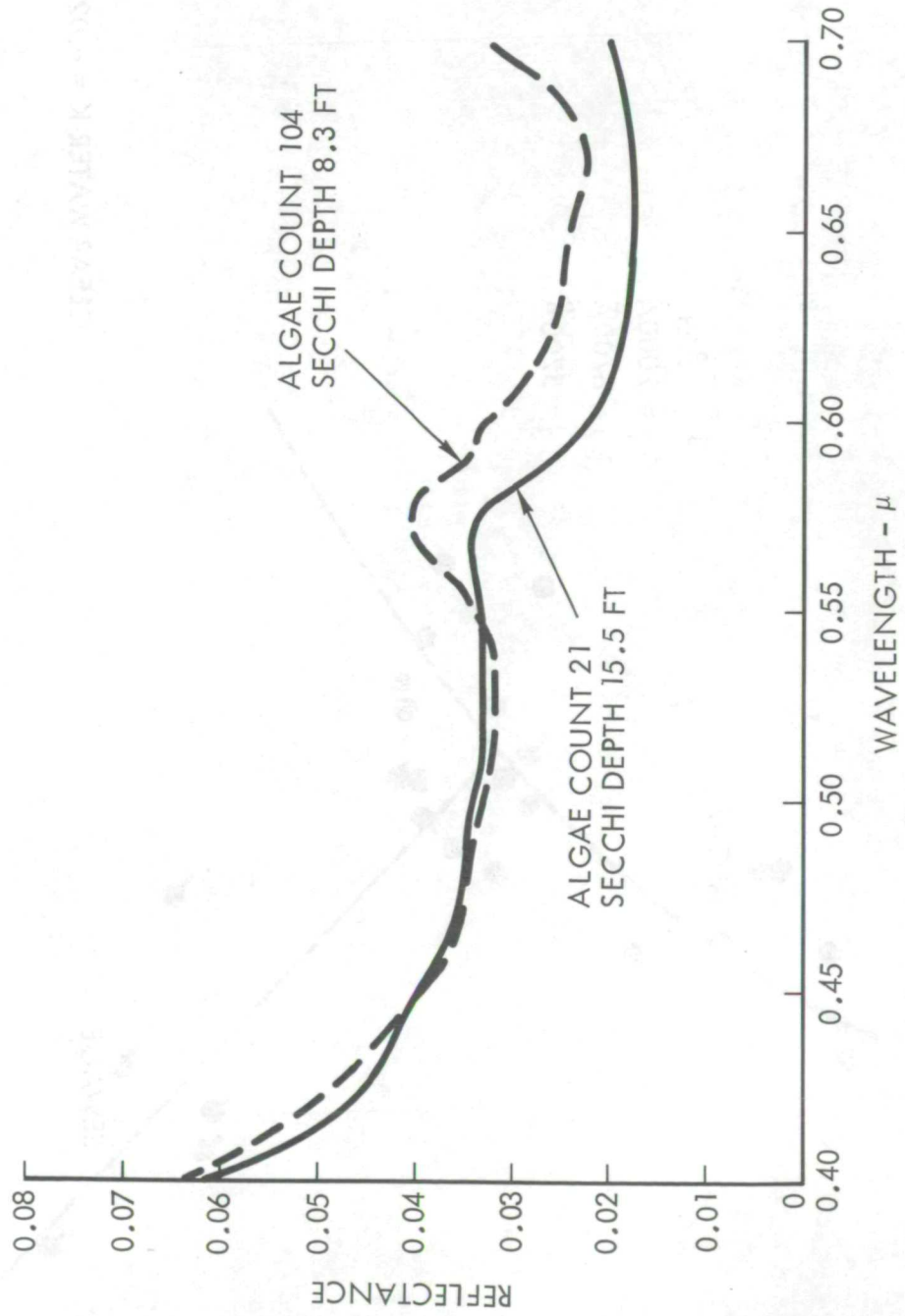


Figure 10 - Spectral reflectance of water containing two concentrations of algae.

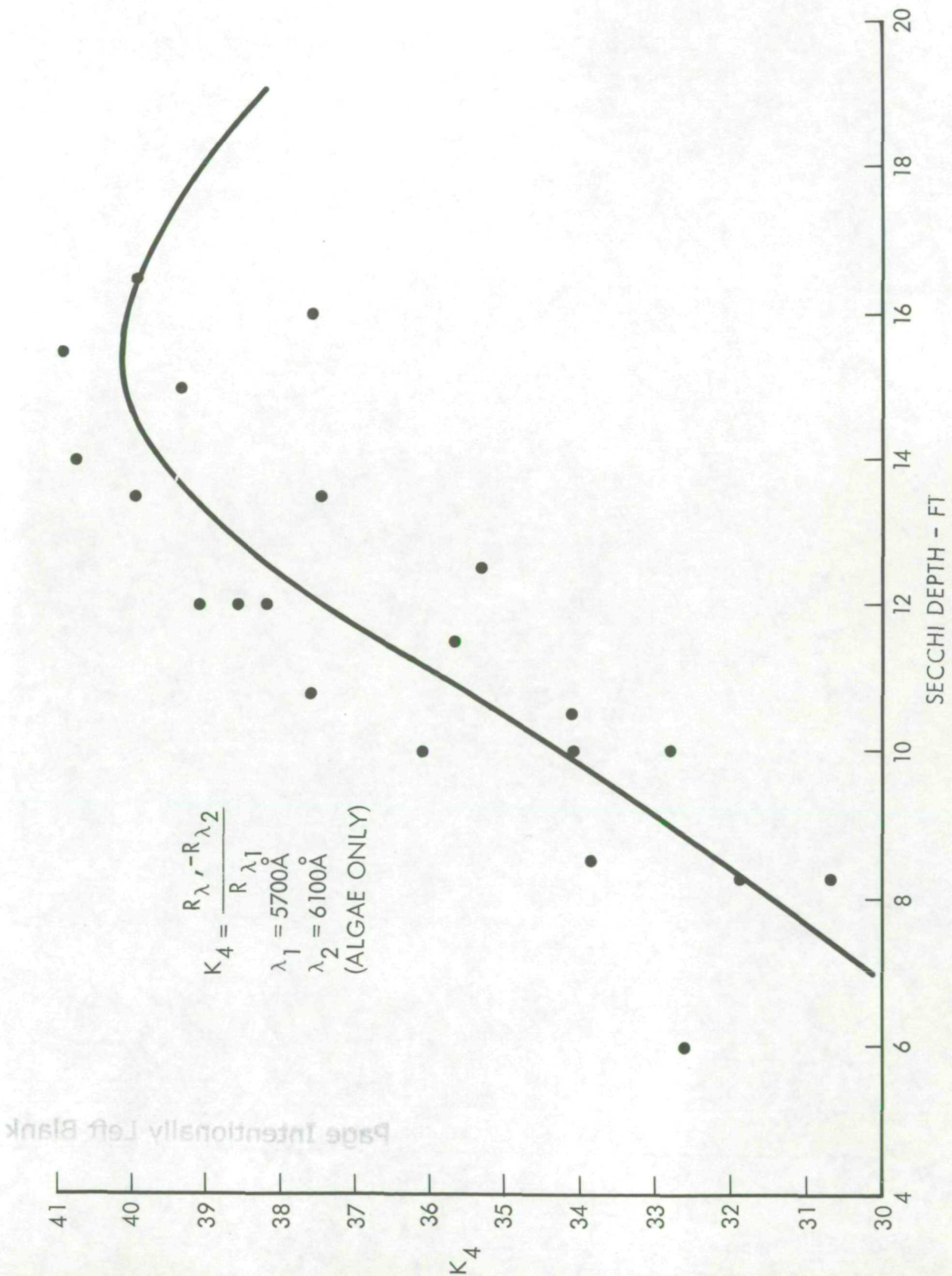


Figure 11 - Parameter K_4 vs. Secchi depth.

Page Intentionally Left Blank

LASER OBSERVATIONS OF WAVE GROWTH AND
FOAM DENSITY FOR FETCH LIMITED 25 M/SEC WINDS

by

Duncan B. Ross
National Oceanic and Atmospheric Administration
Atlantic Oceanographic and Meteorological Laboratories
Sea-Air Interaction Laboratory
Miami, Florida

Vincent Cardone
Department of Oceanography
and Meteorology
New York University

The variability of sea surface conditions has been observed from a low flying aircraft by a laser wave profiling system for fetch limited wind speeds of 25 M/SEC in the North Sea. Wave profiles obtained with the laser system have been analyzed and show that wave growth occurs simultaneously at all frequencies and that an equilibrium value for the higher frequency components is eventually reached, but not before substantially higher (overshoot) values are obtained. Simultaneous photography of the surface has been analyzed and show that 32% of the surface is covered with white caps, foam and streaks. This result is in good agreement with a semi-empirical relationship incorporating both the wind speed and the local wave spectrum which predicts 26% white water for the conditions observed.

INTRODUCTION

For a number of years various scientific organizations have been concerned with developing techniques to remotely observe ocean surface parameters of wave height and wind speed in a quantitative manner. The purpose of these efforts is to provide information about the "state-of-the-sea" in support of operational requirements and to improve environmental forecasts.

During March of 1969, a study of the active and passive microwave characteristics of the ocean surface under the influence of various wind speeds and wave heights was staged out of Shannon, Ireland. This experiment was a cooperative effort of several scientific organizations and included three aircraft and scientists from the Naval Oceanographic Office, NASA Goddard Space Flight Center, NASA Manned Spacecraft Center, NASA AMES Research Center, New York University, and the University of Kansas. The three aircraft were equipped with a variety of remote sensors capable of measuring the microwave brightness temperature, radar backscattering cross section, surface temperature and wave heights.

Between March 6 and March 13, five coordinated flights were conducted over Atlantic weather stations "I" and "J" which are located within about 720 KM of Shannon and are routinely occupied by British and French weather ships. During these flights the highest winds encountered averaged about 16 m/sec, an unfortunate development as the sites were selected due to the high probability of occurrence of winds greater than 20 m/sec and seas greater than 8 meters. The weather situation was particularly interesting to the local Irish meteorologists who marveled at the "mildest weather in twenty years!"

As time was running out a weak meteorological disturbance formed just south of Ireland and moved slowly eastward while a building high pressure system moved eastward from Iceland into Norway between March 12 and March 14. As a result of these developments, the pressure gradient in the North Sea gradually increased and by 2300 GMT, March 13, offshore winds in the North Sea reached 20 m/sec.

By early morning, 14 March, it became apparent that these winds would hold, or increase, during the day and plans were made to conduct a flight experiment between the coast of Denmark and Scotland, the area of highest winds.

The plan of the experiment was to observe the behavior of the microwave signature of the surface under steady state wind conditions, but varying (growing) wave conditions. The NASA AMES Research Center Convair 990, a four engine jet aircraft, equipped with a scanning 19.35GHz microwave radiometer, a laser wave profiler, and a medium resolution infrared radiometer was utilized to obtain data from a distance of 160 kilometers off the coast of Denmark to the vicinity of the Shetland Islands. The NASA MSC P3A aircraft equipped with an active radar scatterometer was utilized to obtain radar cross section data at a point midway between the coasts of Denmark and Scotland. This report describes a portion of the results obtained with the laser wave profiler aboard the Convair 990.

INSTRUMENTATION

The Laser Wave Profiler

The laser wave profiler is a standard model Geodolite 3A airborne altimeter manufactured by Spectra Physics Inc., Mountain View, California (Figure 1). Figure (2) is a schematic diagram of the instrument.¹ The ranging technique consists of amplitude modulating a continuous wave helium-neon laser of red light centered at 6328 Å. The reflected light is collected by an 8 inch Schmidt Cassegrain telescope, detected by a photo multiplier, amplified and phase compared with the modulation frequency of the transmitted beam. The phase difference between these two signals is proportional to the transit time of the light, and hence the range. This range is directly proportional to the wave length of the modulation frequency. The highest modulation frequency available is 49.17MHz with a wave length of 3.048 meters. A total of five modulation frequencies are available yielding range selections of 10^1 , 10^2 , 10^3 , 10^4 and 10^5 feet. By means of a range extender circuit each of these selections may be extended depending on the variability of the terrain. For wave measurements only the full scale increments of 3.048, 6.096 and 30.48 meters are used.*

Static tests of the laser system have been conducted aboard an offshore tower.² Figures 3 and 4 are excerpted from reference (2) and show good agreement with a reference resistance wire wave staff.

Initial flight tests of the system were conducted off Atlantic City, New Jersey, and in the vicinity of ARGUS Island, a U. S. Navy Research Tower located near Bermuda, BWI, in 60 meters of water.

* For more details the reader is referred to reference (1).

Figure 5 is an example of profiles of surface waves as they shoal and break on the beach shown in conjunction with simultaneous strip photography.³ Figure 6 presents a comparison of averaged wave spectra obtained from three two-minute tracks flown near the ARGUS Island Tower with that derived from a twenty-minute sample of wave measurements obtained from the tower's resistance wire wave staff.

Since the aircraft is a moving reference, it is necessary to convert the observed wave spectrum to fixed coordinates. The conversion technique used involves accounting for the speed of the aircraft relative to the phase speed of each wave frequency component and assumes that all waves are traveling in the direction of the wind.⁴ Since this is an approximation, the presence of swell and the spreading of wave energy with distance can lead to errors. In the case presented, little swell was present and the errors associated with directional spreading appear to be minimal for most purposes.

Another source of error is that of aircraft motions of heave, pitch, and roll. Figure 7 depicts the energy spectrum of heave motions, mapped to fixed coordinates, of the type of aircraft involved (a Lockheed Super Constellation) during the ARGUS Island experiment when the surface winds were 12 m/sec. It can be seen that essentially all of the aircraft heave (vertical) motions are concentrated at equivalent wave frequencies of less than .07HZ. The time series of roll angles experienced during this same three-minute track averaged about $\pm 1.5^\circ$. For flight altitudes of 200 M this corresponds to range (wave height) errors on the order of .15 meters. From these data, it can be seen that the majority of range errors associated with aircraft motions are small within the wave frequency pass band. As a result, the most convenient technique for removing these errors is simply high pass filtering, where the low frequency cut off selected depends upon the turbulence and, for most cases, is less than that associated with a true wave frequency of .07HZ. For extremely precise measurements, additional effort must be expended. For the data presented in this paper, the filtering technique was employed with apparently good results.

METEOROLOGICAL SITUATION

As noted in Section I, the general synoptic situation was a result of a weak disturbance moving eastward from Ireland simultaneous to an eastward displacement of a high pressure system located over Iceland. These two events caused a gradual tightening of the gradient in the North Sea and corresponding surface winds increased slowly, but steadily, to a maximum average of 25 m/sec by 1200 GMT, 14 March, as

reported by the German beacon vessel "LHHT", located at 57.7°N, 03°E (Figure 8).

Since only one of the reporting ships shown in Figure 8 was equipped with an anemometer (the rest being Beaufort estimates) it was felt necessary to derive the surface wind field by constructing isotachs of the geostrophic wind from a fine scale analysis of the surface pressure field.

Surface pressure data were obtained from a considerable number of British and continental shore sites and isotachs of the geostrophic wind were drawn relying heavily on the ship reports. Near the ship "LHHT", a ratio of surface (20m) to geostrophic winds of 70% gave good agreement although in nearby regions of large shear, higher geostrophic wind ratios are apparent. This is reasonable considering the effects of lateral turbulent momentum transfer. The above analysis considered the effects of stability after the technique of Cardone.⁶

In order to verify the validity of the inferred surface wind speeds, table 1 was constructed. This table shows wind speeds computed from the Litton model LTN 51 inertial system aboard the aircraft. The flight level winds reported are one minute averages computed approximately every five minutes during the lower altitude tracks. These values were averaged over twenty minutes of flight time (shown in brackets) and reduced to the equivalent twenty meter anemometer height assuming neutral stability and a logarithmic wind profile extending to an altitude of at least 43.3 meters.⁷ The rather consistent agreement between the wind speeds derived by this technique, the geostrophic surface winds and the ship reports, lends considerable confidence to the presumed wind fields.

OBSERVATIONS OF WAVE GROWTH

The intent of the experiment was to begin the downwind flight track as near to the upwind shore as possible and then to fly downwind until the wave spectrum was essentially "fully developed". This was not entirely practical, however, as clearance procedural problems of the aircraft prevented approaching the shoreline within less than about 157 kilometers. Further, due to previous limited success because of relatively low wind speeds, the reported winds were greeted with some scepticism. As a result, the flight track (dashed line of Figure 8) was planned to best accommodate several possible meteorological situations which might be present, and events seem to confirm the final plan selected as a good compromise.

Figure 9 presents plots, at their appropriate fetches, of all available measurements of significant wave height, H_S^* . The fetch was measured as simply the distance from the coastline in the direction of the implied surface wind direction. It is seen that H_S generally increased with fetch to about 370KM but decreased thereafter. As a reference, a theoretical relation (Inoue-Cardone) is plotted for 22 m/sec, a suitable wind speed for much of the data as determined from the analysis of all available wind inputs.⁶ The wind speed for the particular location of each H_S plotted was obtained from the geostrophic analysis and is shown below each value. Up to 370 kilometers the variation of H_S with fetch is in good agreement with the theoretical relation, which applies for infinite duration, fetch limited seas. Beyond 370 KM, the measured wave heights are considerably below the theoretical relation and depart increasingly with fetch. This latter behavior is generally explainable by duration effects, as the latter measurements plotted are from a wind field that exhibited considerable variability in wind duration. In particular, the durations are considerably longer in the near shore (southernmost portion of the first downwind run) area. An inspection of the previous six-hourly sea level pressure analysis indicate no significant variation in the pressure gradient there for the 24 hours preceding the flight. Considering that the winds prior to 24 hours were only slightly lower, these durations are probably sufficient for the seas to be fully developed at their respective fetches. From the vicinity of "LHHT" northwestward, however, the durations are extremely limited. The 3 hourly wind reports at "LHHT", Figure 10, suggest that the duration of 20 m/sec winds was only about 12 hours and that duration of 23 m/sec winds (or higher) was only about 3 hours. Toward the end of the last downwind run, durations were probably more limited, considering the way in which the synoptic scale pressure gradient was changing.

The behavior of the data below 370 KM suggests that these data might be employed to study growth, as the wind field there might be considered to be reasonably steady and homogeneous.

Results

A convenient way to study the gross behavior of a developing sea in this case is presented in Figure 11 which shows the plots of spectral density (M^2 -sec) as a function of frequency (true) and fetch. This contour analysis is based upon spectra computed for 160 KM, 176 KM, 203 KM, 231 KM, 268 KM, and 323 KM fetches. Though this resolution

* H_S is defined as the average value of the highest one third waves.

is not as great, the analysis is conveniently comparable to those obtained in the radar altimeter fetch-limited study at lighter winds by Barnett and Wilkerson.⁸ The analysis in Figure 11 is considerably smoother than those of their study, largely due to the decreased resolution. The major features to be deduced from this figure are:

1. At frequencies above about .13 Hz, the spectral density does not change significantly with fetch. Thus these spectral components are already saturated, or fully developed, and in equilibrium with the wind field.
2. Below about .13 HZ, all spectral components are increasing in intensity with fetch simultaneously.
3. The spectral peak generally moves toward lower frequencies (as indicated by dashed line) with increasing fetch, in general agreement with existing concepts of spectral development. A rather surprising feature, however, is that the magnitude of the spectral density at the peak does not increase markedly with fetch beyond about 185 KM.
4. A given spectral component will overshoot its eventual equilibrium value. That is, if the development of a single frequency component is followed fetchwise, it is seen that the spectral density increases rapidly to a maximum value at a given fetch and then decreases gradually to a lower equilibrium value at greater fetch. The effect is most noticeably between frequencies of .095 and .115. The overshoot effect at higher frequencies is not observed but presumably occurred at shorter fetches (160 KM) as the data suggest that the fetch at which the effect occurs increases with decreasing frequency. This striking feature of the North Sea spectra is perhaps the most remarkable, as it implies the operation of mechanisms in wave generation not yet treated satisfactorily by existing theories. The "overshoot" effect has been reported in wave tank studies and in the field experiment of Barnett and Wilkerson and its appearance here lends support to the fact that this is a "real" phenomena.^{9,10} The magnitude of the overshoot effect observed in the Barnett and Wilkerson study, that is, the ratio of spectral density at eventual equilibrium to that at the peak of the overshoot, was scattered between .35 and .75. For the North Sea mission, this ratio could only be computed for frequencies of .111Hz, .108Hz, and .105Hz where values of .38, .50, and .41 occurred.

Some of the features discussed above are evident if the spectral density is plotted versus fetch for selected frequencies. Thus Figure 12a shows a saturated frequency. Superimposed upon the data

is the spectral behavior for the Inoue-Cardone growth theory which is based upon a modified Miles-Phillips resonance instability growth mechanism and the Pierson-Moskowitz fully developed spectrum.⁶ It is seen that generally in 12 a-f, the equilibrium value observed is 30-40% less than that indicated by theory. This is largely explainable by the different equilibrium range constant of $.52 \times 10^{-2}$ found for the North Sea spectra as compared to $.8 \times 10^{-2}$ used in the Pierson-Moskowitz spectra. The overshoot effect is clearly evident in Figure 12 b-h. The theoretical growth, of course, does not indicate overshoot, as it is based upon the relation (in the early stages of growth)

$$\frac{d(S)}{dt} = A+BS \quad (1)$$

where S is spectral density, t is time, A is the resonance mechanism parameterization and B is the instability mechanism parameterization. Dissipation effects are included by allowing the growth rate to decrease as the fully developed spectral value is approached. For infinite duration limited fetch growth, (1) is written:

$$C_g \frac{ds(f)}{dx} = A+BS(f)$$

where X is the fetch, and C_g is the group velocity of each wave frequency, f. Disregarding the effect of the overshoot, it may be said that the Inoue-Cardone growth (which predicts the variation of H_S fairly well) is too fast for frequencies above .078Hz and too slow for frequencies below .069Hz. The rapid growth of these frequencies is surprising, especially considering that these spectral components should be under the influence of dissipation by bottom friction.

It is possible to quantitatively compute the values of A and B from plots 12, a-o, provided dissipation effects can be considered to be small (not considering bottom friction) if the spectral density is less than 30% of its eventual equilibrium value*. Within this restriction, the computation can be performed on frequencies .087, .083, .078, .074, .069, and .063 Hz and will be performed on spectra recomputed for greater fetchwise resolution.

* After Barnett and Wilkerson

WHITE CAP COVERAGE

A semi-empirical theory for the dependence of foam cover on wind speed and sea conditions has been proposed by Cardone.⁶ An important part of the theory is the model used to describe the growth of the wave spectrum due to energy transferred from a turbulent wind profile - this model is also used in the wave forecasting schemes developed at New York University.

The growth rate of a spectral wave component $S(f)$ in terms of the wind field specified at 19.5 meters above the sea surface, and the friction velocity U_* defined as $\sqrt{\frac{\tau}{\rho}}$, where τ is the surface stress and ρ is the air density, may be described as

$$\frac{dS(f)}{dt} = A(f, U_{19.5}) + B(f, U_*) \cdot S(f) \left(1 - \frac{S(f)^2}{S_{\infty}} \right) \quad (2)$$

where $S(f)$ = spectral intensity at frequency
 A = Phillips Resonance growth term
 B = Miles-Phillips Instability Growth term
 S_{∞} = Pierson Moskowitz Fully Developed Spectrum

The value of the term U_* depends upon the local wind field and the air-sea temperature difference. All non-linear dissipative mechanisms that would act to limit growth are modeled implicitly by the use of the term

$$1 - \left(\frac{S(f)}{S_{\infty}} \right)^2$$

which causes each spectral value to approach its equilibrium or saturated value given by the Pierson-Moskowitz formula. $S(f)$ which is a function of wind speed and frequency and does not take into effect the overshoot phenomena discussed earlier.

The Phillips resonance term can be thought of as an initial excitation mechanism - necessary to start growth for parts of the spectrum with no energy initially - but small in comparison to the instability growth term which is responsible for nearly all the energy transfer.

Energy transfer does not cease after a spectral component reaches its equilibrium value, and the energy thus transferred can be thought of as being dissipated in wave breaking. Whitecaps are a manifestation of wave breaking and thus the whitecap coverage may be closely related

to the energy transfer to the fully developed portion of the spectrum. This energy transfer is given by the expression:

$$E = \rho_w \cdot g \cdot \int_0^{\infty} B \cdot S \cdot \delta \cdot df \quad (3)$$

where $\delta = 1$ when $S = S_{\infty}$
 $\delta = 0$ when $S < S_{\infty}$

This hypothesis was tested with the whitecap data obtained photographically by Monahan¹¹ on the Great Lakes. The spectral growth model was used to hindcast the wave spectrum for each case reported by Monahan from corresponding estimates of stability, wind speed, and fetch (durations were unknown and assumed to be infinite). The energy transferred to the fully developed portion of the spectrum was then correlated with the observed whitecap percentage. The resulting linear regression is shown in equation 4.

$$W_F = - .0185 + .893 \times 10^{-3} \cdot E(\text{ergs/cm}^2/\text{sec}) \quad (4)$$

where W_F = Fresh Water foam density in percent
 E = Energy dissipated in breaking waves.

Salt water whitecaps are apparently more persistent than fresh water whitecaps due to differences in the bubble-size spectra and hence for similar conditions of wave breaking, whitecap coverage should be expected to be greater over the oceans. An approximate salt water correction factor of 1.5 has been suggested by Monahan from results of a laboratory study of comparisons of fresh water and salt water whitecap data.¹²

An example of the computation of percent whitecaps is shown in Figure 13 for a wind speed of 25 m/sec and fetch of 180 n.mi. The dashed line is the fully developed spectrum for 25 m/sec, the solid curve is the hindcasted spectrum for a fetch of 180 n.mi. and the dash-dot line shows the contribution of the factor $B \cdot S$ to the energy dissipation computation. The significant wave height is calculated to be 26 feet. The salt water whitecap cover is computed to be 26%. This result compares favorably with the value of 32% calculated from photography obtained during the North Sea experiment.

Figure 14 is an example of white cap conditions for the 25 m/sec winds observed during this flight. Note the large amount of surface area covered by thin streaks oriented in the direction of the wind. Figure 15 is an example of white-cap density for a 12 m/sec wind speed. The most striking difference between the two is in the amount of streaking evident. This characteristic of the wind driven ocean is important when considering the relationship of remotely obtained micro-wave signatures of the ocean to the surface wind and wave conditions.

CONCLUSIONS

By the use of Photographic and Laser observations of sea surface conditions it has been found:

1. Existing wave theory can be used with good results to predict the rate of growth of the significant wave height with increasing fetch.
2. A migration of the spectral peak toward lower frequencies with increasing fetch is observed.
3. All wave frequencies are receiving energy simultaneously.
4. The spectral density of a particular frequency component will overshoot its eventual equilibrium value by as much as 50%.
5. Semi-empirical calculations of white cap density based on the rate of energy transfer and the state of development of the wave spectrum agree well with observations for the nearly fully developed case.

It should be noted that wave and white cap data such as discussed herein are very difficult to obtain. Thus extension of these results to other conditions of wind speed, fetch, and stability must be done with caution. Experimental efforts are continuing in this area and the emphasis will be on the short fetch and stability criterion and the characteristics of the surface driven by extremely high winds such as associated with hurricanes. These studies will be conducted both in a laboratory wave tank and in the field and should contribute significantly to future theories describing the wind driven seaway.

ACKNOWLEDGEMENTS

The authors are grateful to the many persons who contributed toward this experiment and particularly the scientific and flight crew of the CV990 who responded to extremely short notice and made the North Sea flight possible. Special gratitude is extended Mr. J. W. Sherman, Dr. W. J. Pierson, and Dr. W. Nordberg for their aid and encouragement during all aspects of this effort, and particularly to the Irish Meteorologists at Shannon International Airport whose interest, assistance, and spirit contributed significantly to a successful and memorable experiment.

References

- (1) H. Jensen and K. A. Ruddock, "Applications of a Laser Profiler to Photogrammetric Problems", presented at the American Society of Photogrammetry, Washington, D. C. 1965.
- (2) D. B. Ross, R. A. Peloquin and R. J. Sheil, "Observing Ocean Surface Waves with a Helium Neon Laser", Proceedings of the 5th Symposium on Military Oceanography, Panama City, Florida, May 1968.
- (3) V. E. Noble, R. D. Ketchum and D. B. Ross, "Some Aspects of Remote Sensing as Applied to Oceanography", Proceedings of the IEEE, Vol. 57, No. 4, April 1969.
- (4) M. St. Denis and W. J. Pierson, "On the Motions of Ships in Confused Seas", Trans. Soc. Nav. Arch. and Mar. Eng., 1961.
- (5) C. Catoe, W. Nordberg, P. Thaddeus and G. Ling, "Preliminary Results from Aircraft Flight Tests of an Electrically Scanning Microwave Radiometer", Goddard Space Flight Center Tech. Report No. X-622-67-352, August 1967.
- (6) V. J. Cardone, "Specification of the Wind Field Distribution in the Marine Boundary Layer for Wave Forecasting", Geophysical Science Laboratory, New York University, Report No. TR69-1, December 1969.
- (7) L. Moskowitz, "Reduction of Ocean Wind Data by use of Drag Coefficients with Application to Various Wave Forecasting Techniques", U. S. Naval Oceanographic Office, IMR No. 0-66-64, January 1965.
- (8) T. P. Barnett and J. C. Wilkerson, "On the Generation of Ocean Wind Waves as Inferred from Airborne Radar Measurements of Fetch-limited Spectra," Journal of Marine Research, Vol. 25, Number 3, September 15, 1967, pp 292-328.
- (9) A. J. Sutherland, "Growth of Spectral Components in a Wind-Generated Wave Train", J. Fluid Mech, Vol. 33, 1968.
- (10) H. Mitsuyasu, "On the Growth of the Spectrum of Wind-Generated Waves (II)," Reports, Res. Inst. Appl. Mech., Kyushu University, Vol. XVII, No. 59, 1969.
- (11) Monahan, E. C., "Freshwater Whitecaps", J. Atmos. Sci., Vol. 26, No. 5, 1969.
- (12) Monahan, E. C., "Laboratory Comparisons of Freshwater and Salt Water Whitecaps, J. Geophys. Res., Vol. 74, No. 28, 1969.

TABLE I
 A COMPARISON OF WINDS OBTAINED FROM THE NASA CV990 OVER THE NORTH SEA AND 20-METER LEVEL WINDS
 REDUCED FROM GEOSTROPHIC WINDS BASED UPON THE ANALYSIS SHOWN IN FIG. 3

Time (GMT)	Latitude	Longitude	Altitude (meters)	Flight Level		Reduced Geostrophic	
				Wind Direction	Wind Speed (m/s)	Wind Direction	Wind Speed (m/s)
1338	54°40'N	06°02'E	152	085°	23.7	110°	22.7
1345	55°15'N	06°01'E	152	112°	25.8 [25]	110°	22.7
1350	55°34'N	06°01'E	146	110°	23.1	110°	22.7
1355	55°56'N	06°03'E	116	110°	26.8	110°	22.7
1400	56°07'N	05°24'E	122	110°	22.7	110°	22.7
1407	56°13'N	04°30'E	152	098°	26.8	110°	23.7
1414	56°25'N	03°33'E	152	105°	27.3 [27.3]	110°	24.7
1417	56°28'N	03°12'E	152	107°	22.7	110°	25.8
1420	56°39'N	02°57'E	146	105°	29.9	110°	26.8
1435	57°35'N	02°17'E	152	107°	28.3	110°	25.8
1440	58°02'N	01°32'E	152	105°	25.8 [27.8]	110°	25.2
1445	58°14'N	01°10'E	152	110°	27.3	110°	25.2
1450	58°30'N	00°36'E	152	110°	30.4	110°	24.7
1455	58°48'N	00°01'E	152	108°	25.8	110°	23.7
1500	59°04'N	00°31'W	152	107°	24.7 [24.2]	110°	23.2
1505	59°23'N	01°06'W	152	108°	25.8	110°	22.7
1510	59°46'N	01°27'W	152	112°	21.6	110°	21.6

Note: Flight-level winds averaged over approximately 20-minute legs shown in brackets. The second value italicized is the aircraft value reduced to the 20-meter level after Moskowitz [7].

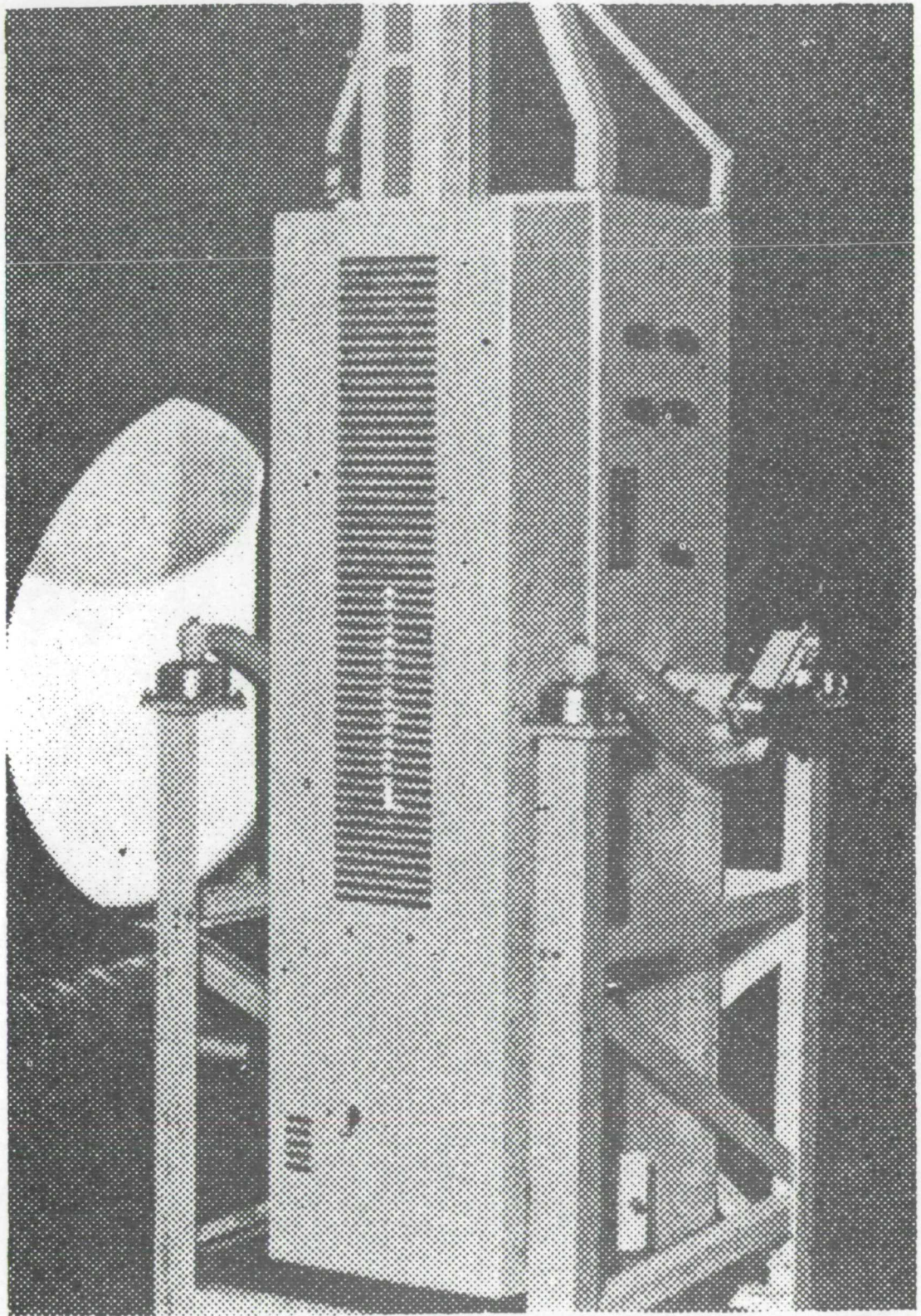


Fig. 1. Geodolite 3A laser profilometer.

GEODOLITE BLOCK DIAGRAM

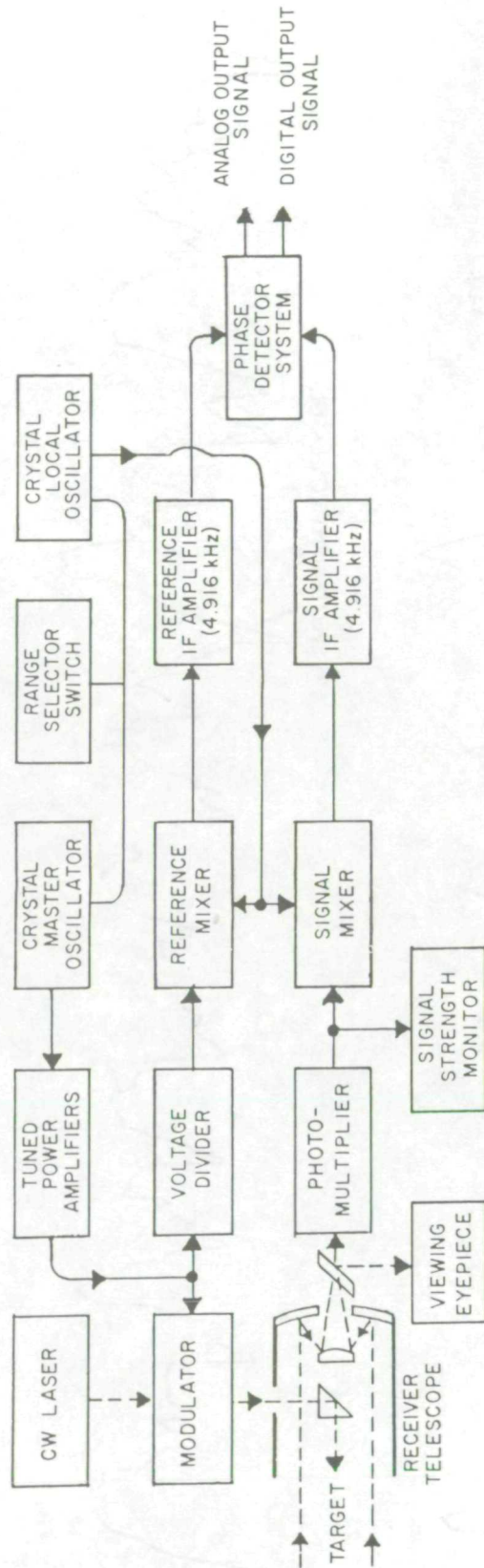


Fig. 2

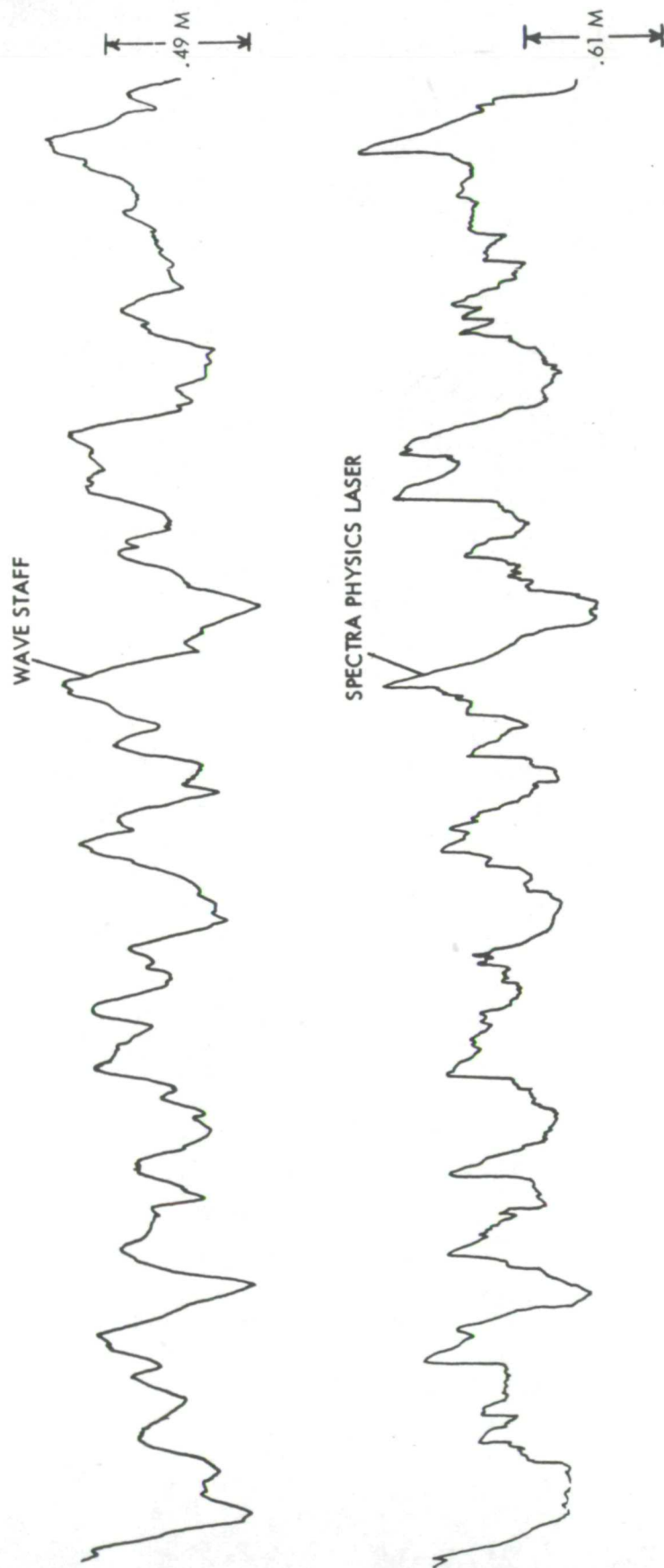


Fig. 3. Comparison of laser and wave-staff recordings of surface waves from a fixed ocean platform.

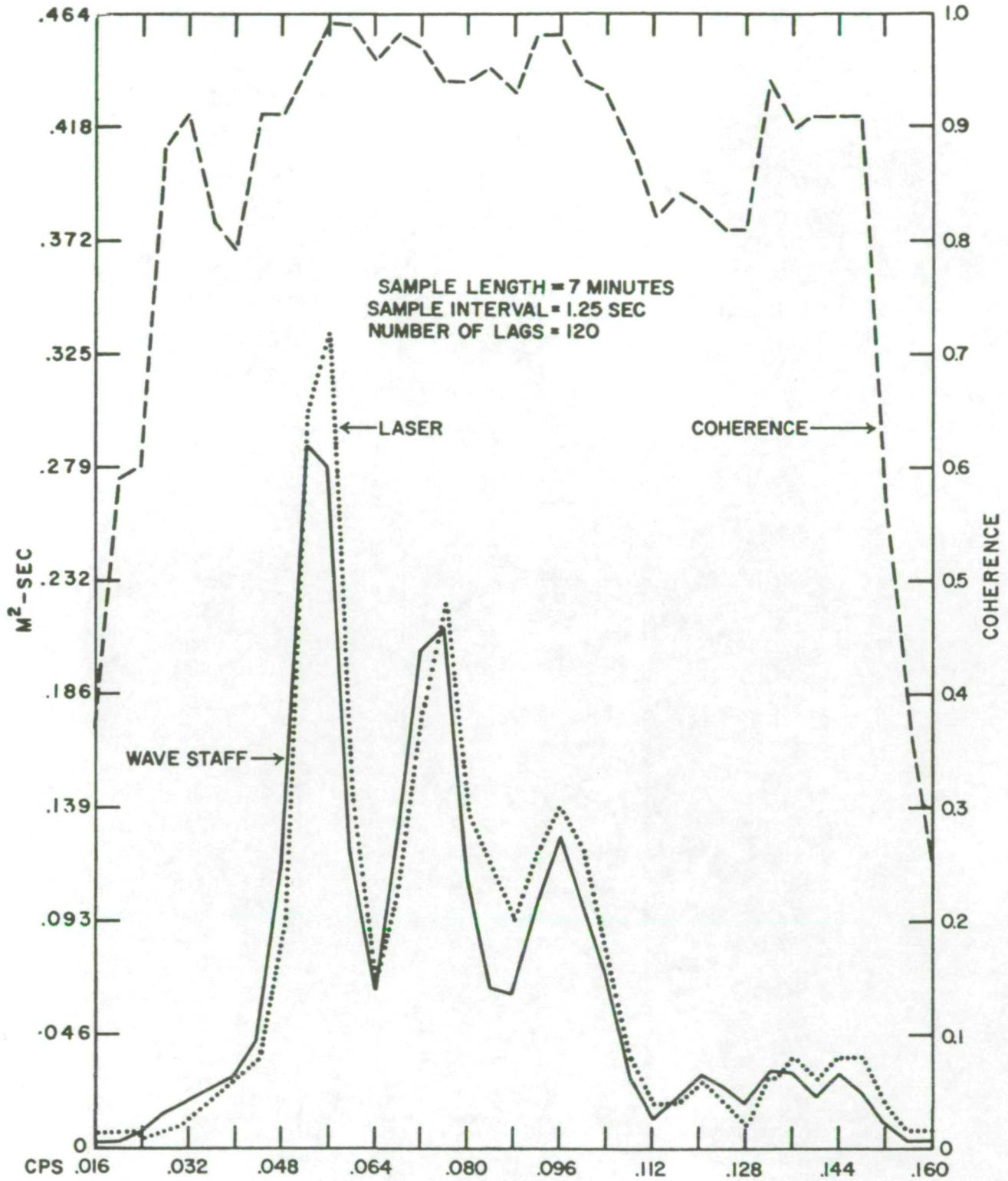


Fig. 4. Comparison of wave-energy spectra derived from laser and wave-staff recordings of surface waves.

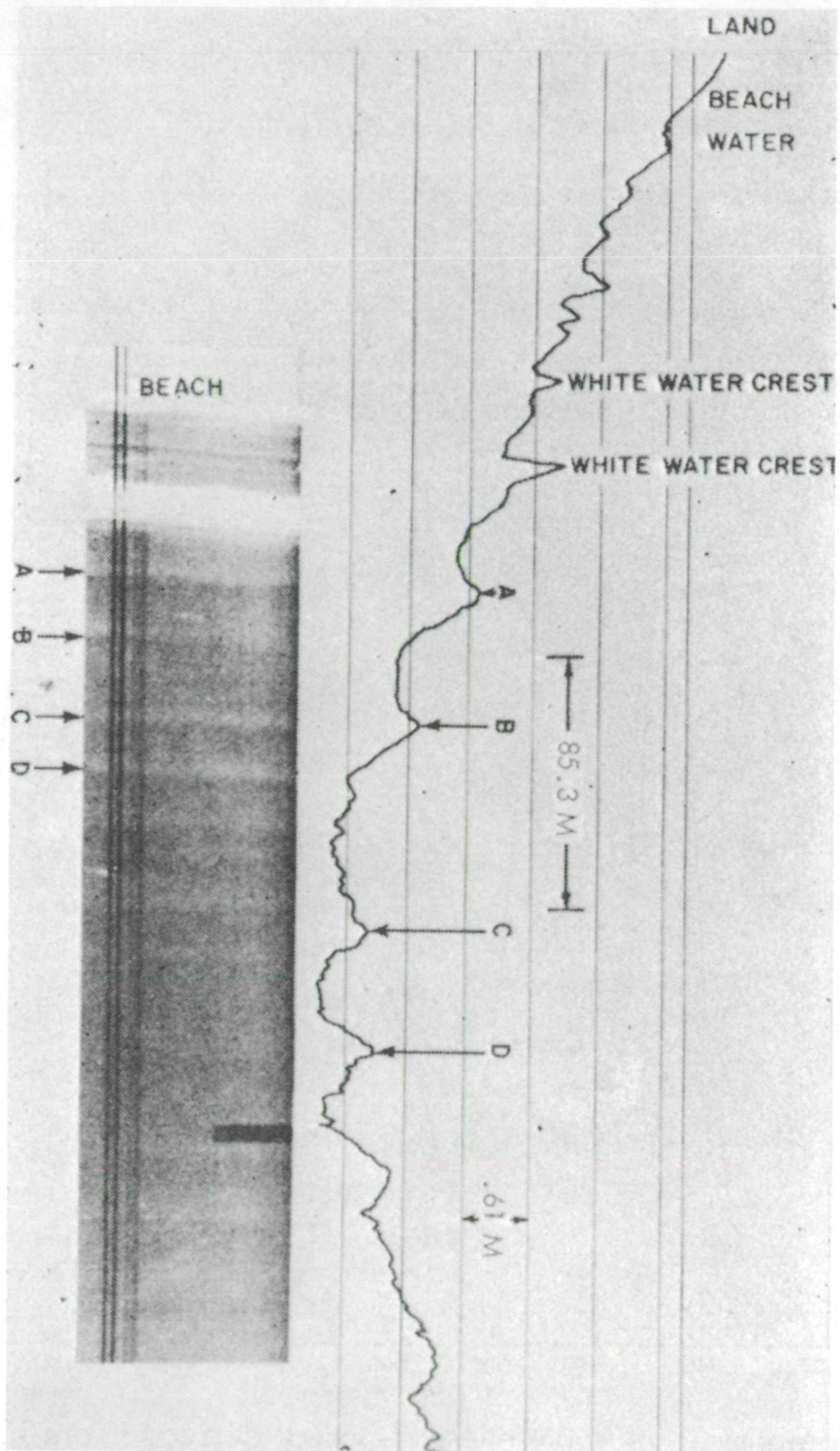


Fig. 5. Airborne laser profiles of surface waves obtained in conjunction with simultaneous continuous strip photography.

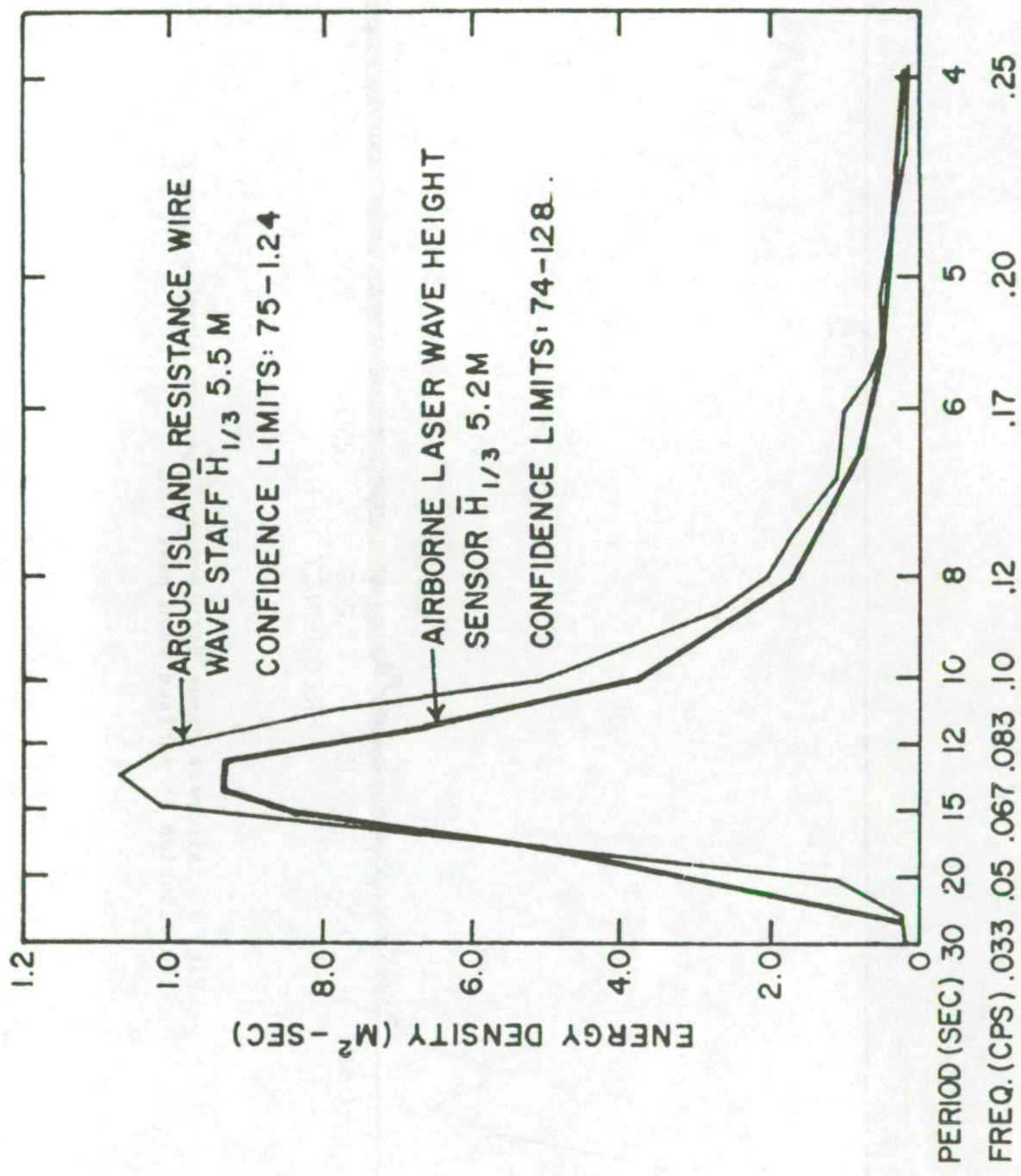


Fig. 6. Comparison of wave-power spectra obtained with the laser profiles aboard a U. S. Navy aircraft with that obtained from an *in-situ* wave staff.

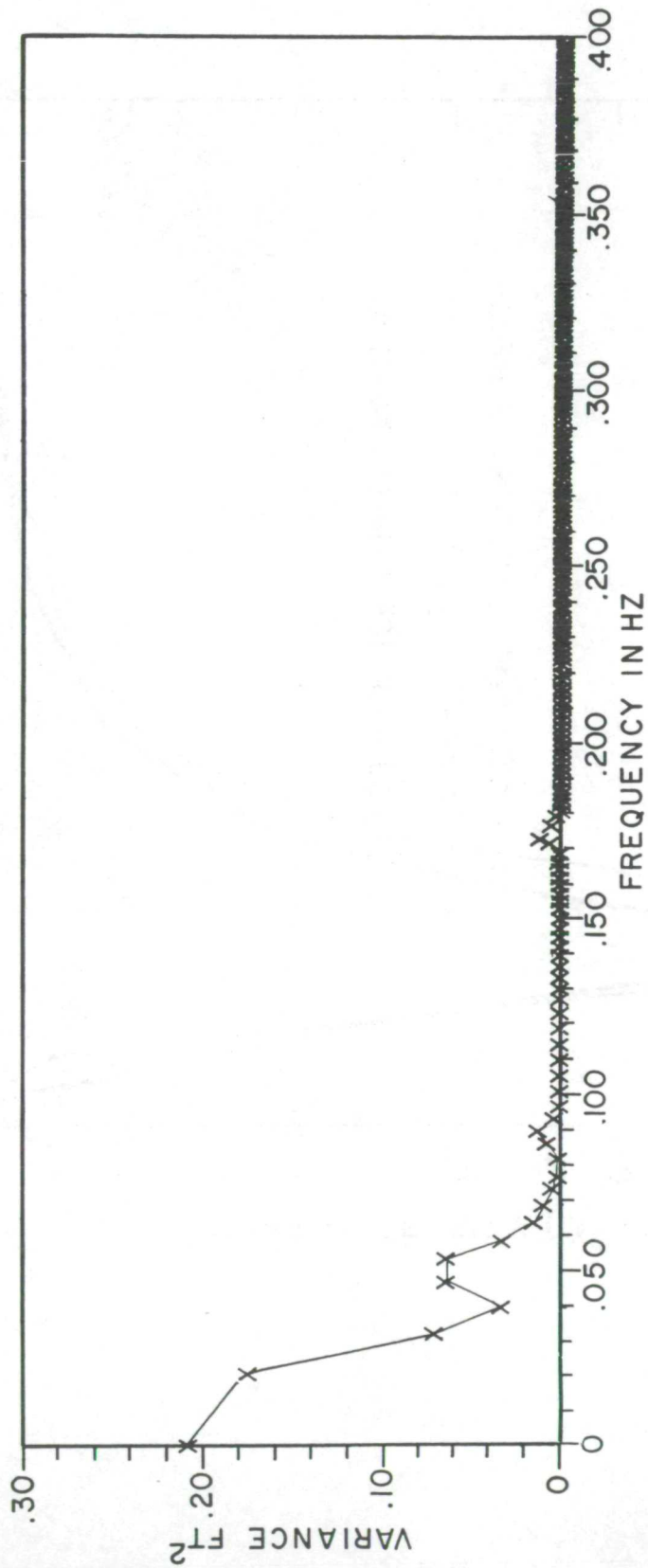


Fig. 7 Aircraft heave displacement spectrum showing energy contribution in surface wave pass band

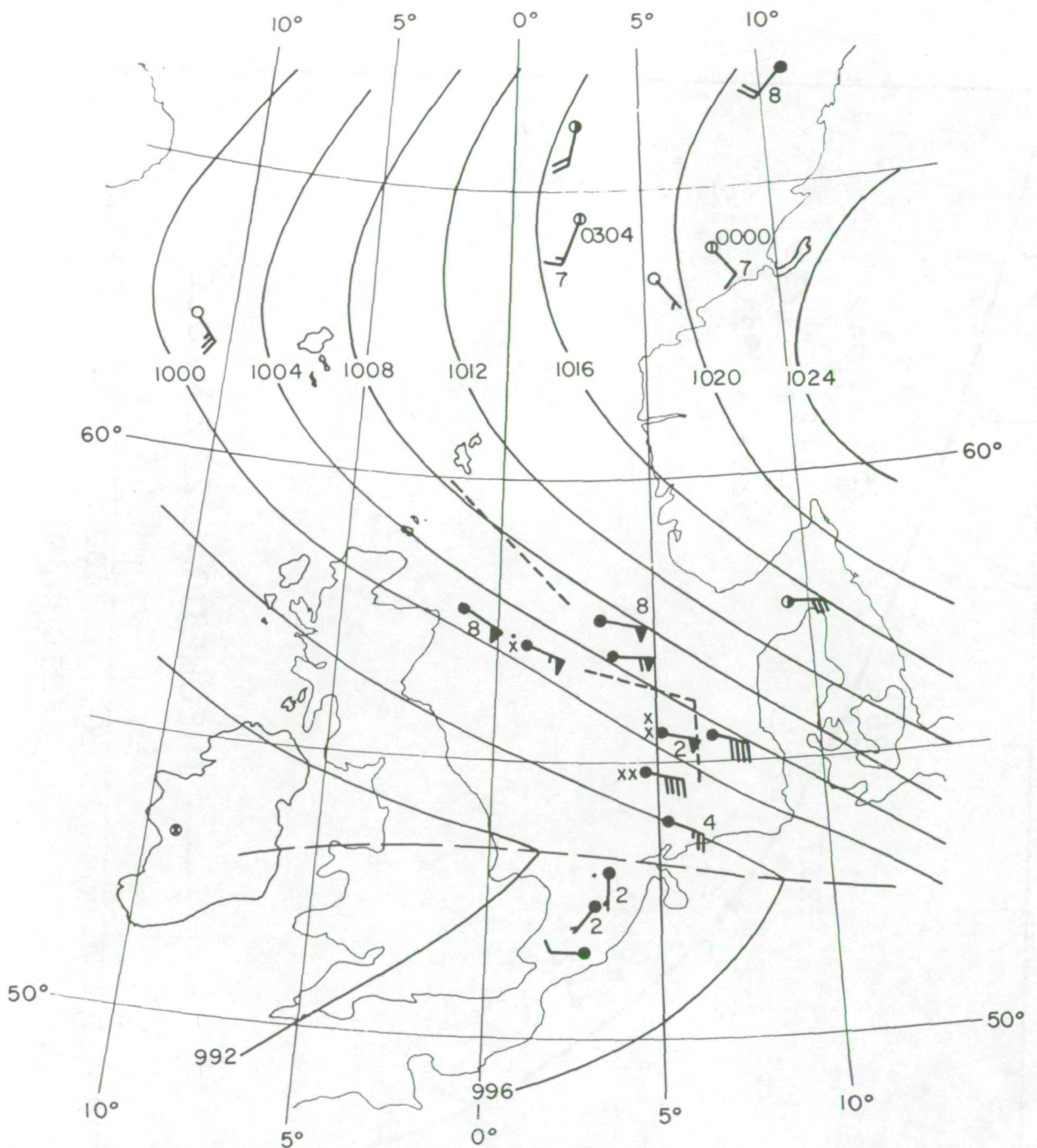


Fig. 8 Ship reports in the North Sea 1200 GMT, March 14, 1969. Dashed line is the flight track of the NASA CV990. The digit adjacent to each report is the wind speed to the nearest knot within the range indicated by the bar or flag.

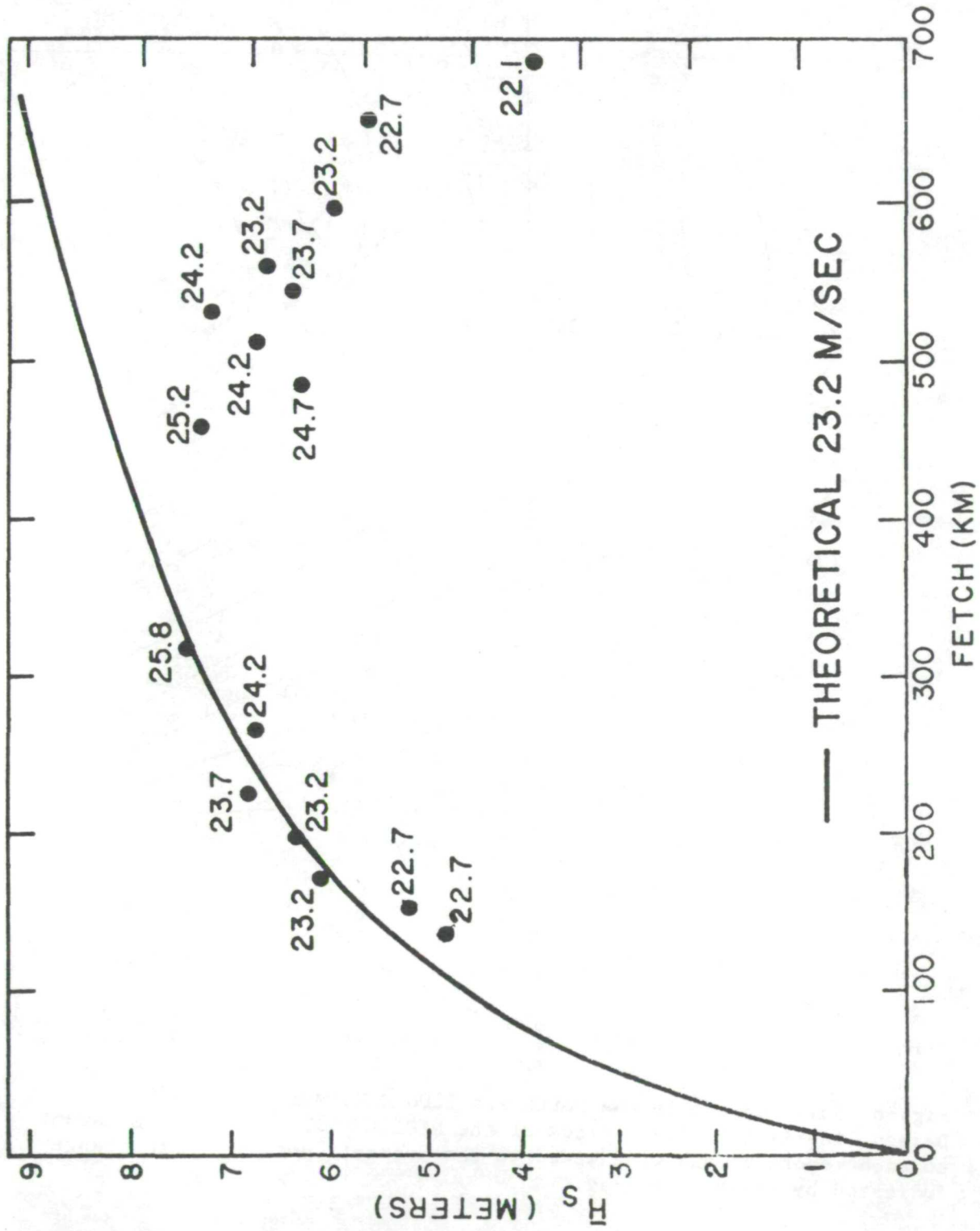
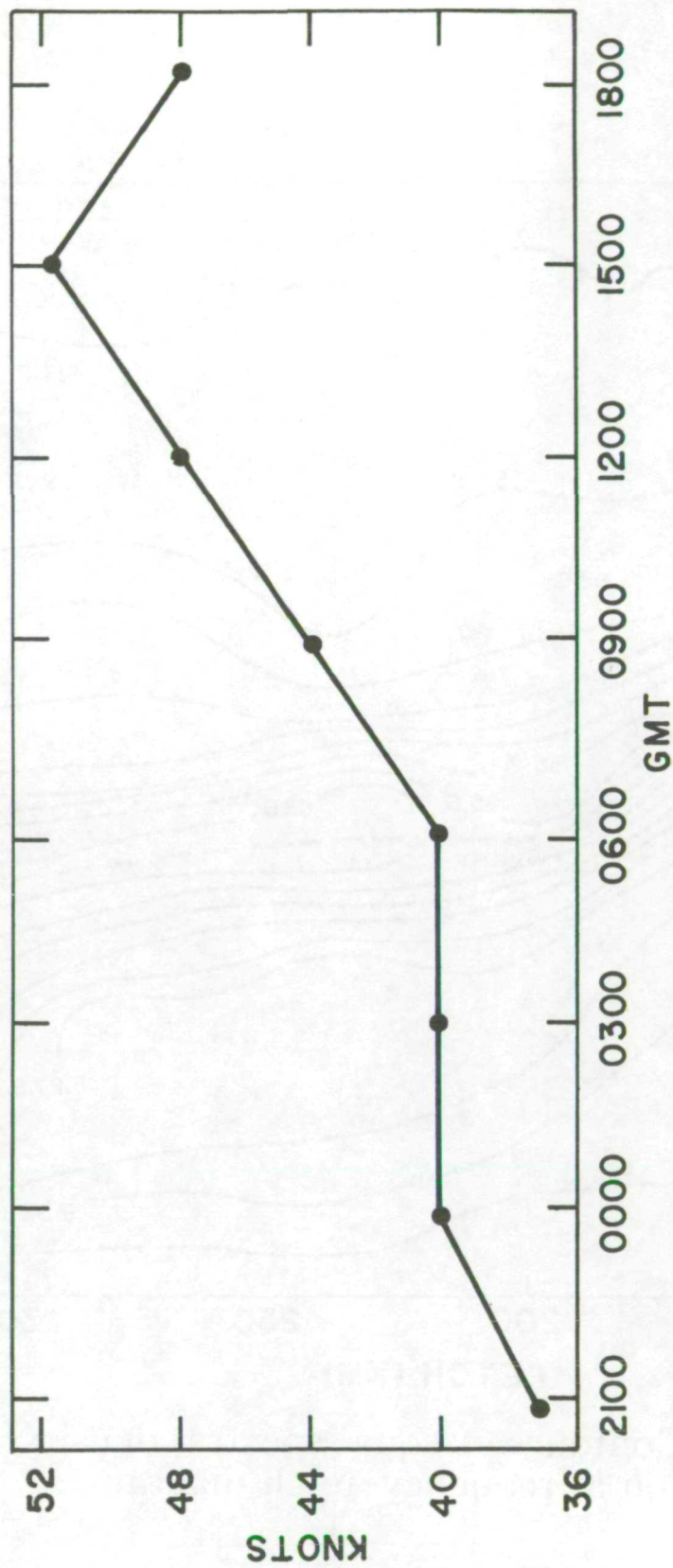


Fig. 9. Observations of significant wave height (\bar{H}_s) as a function of fetch. Wind speeds observed in meters per second are shown next to each value.



WIND SPEEDS REPORTED BY THE GERMAN BEACON SHIP LHHT
(57.5°N, 03°E) ON MARCH 14, 1969 AT 3 HOUR INTERVALS.

Fig. 10

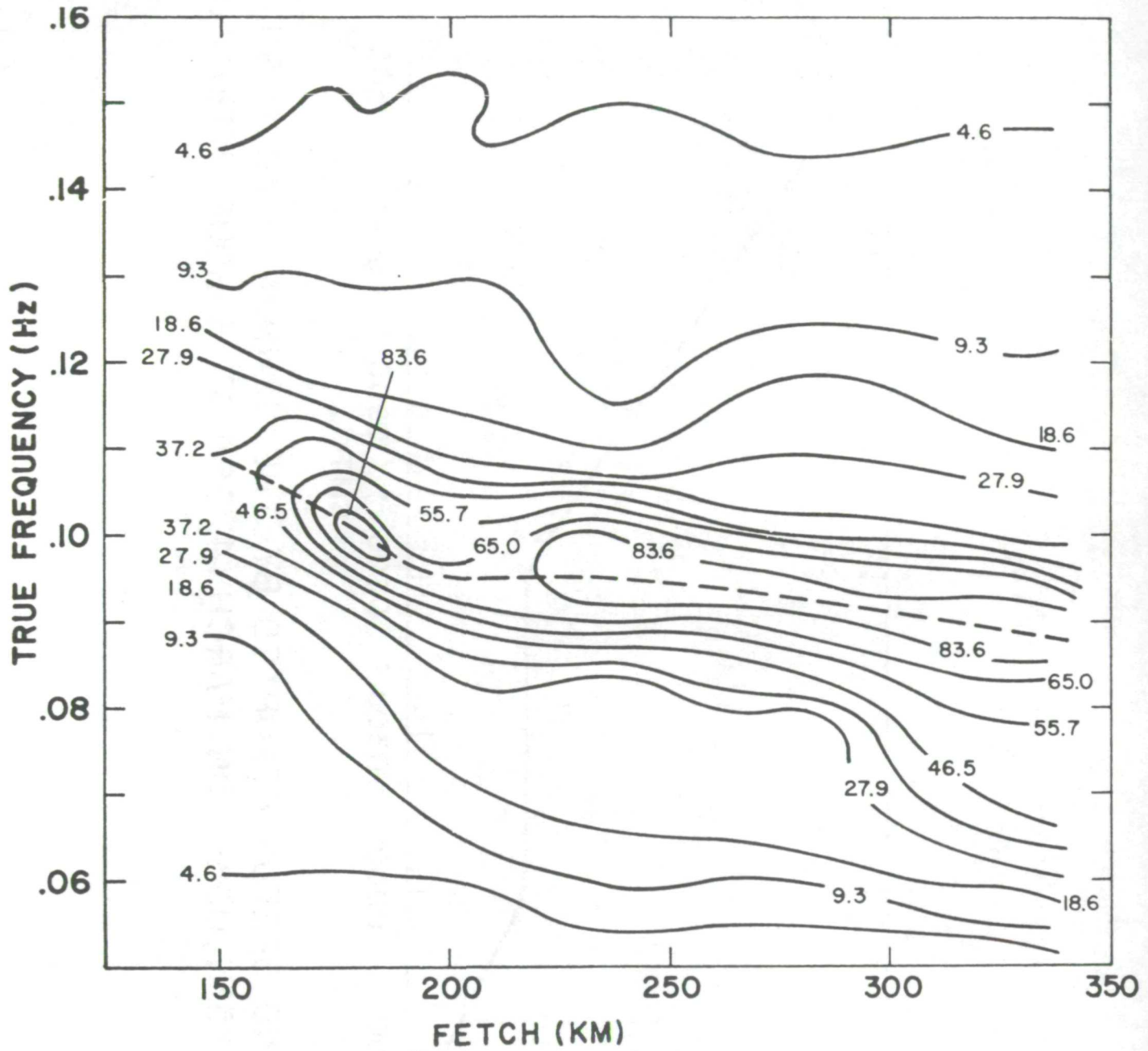


Fig. 11. Contours of equal spectral density ($m^2 \cdot s.$) on a frequency-fetch diagram.

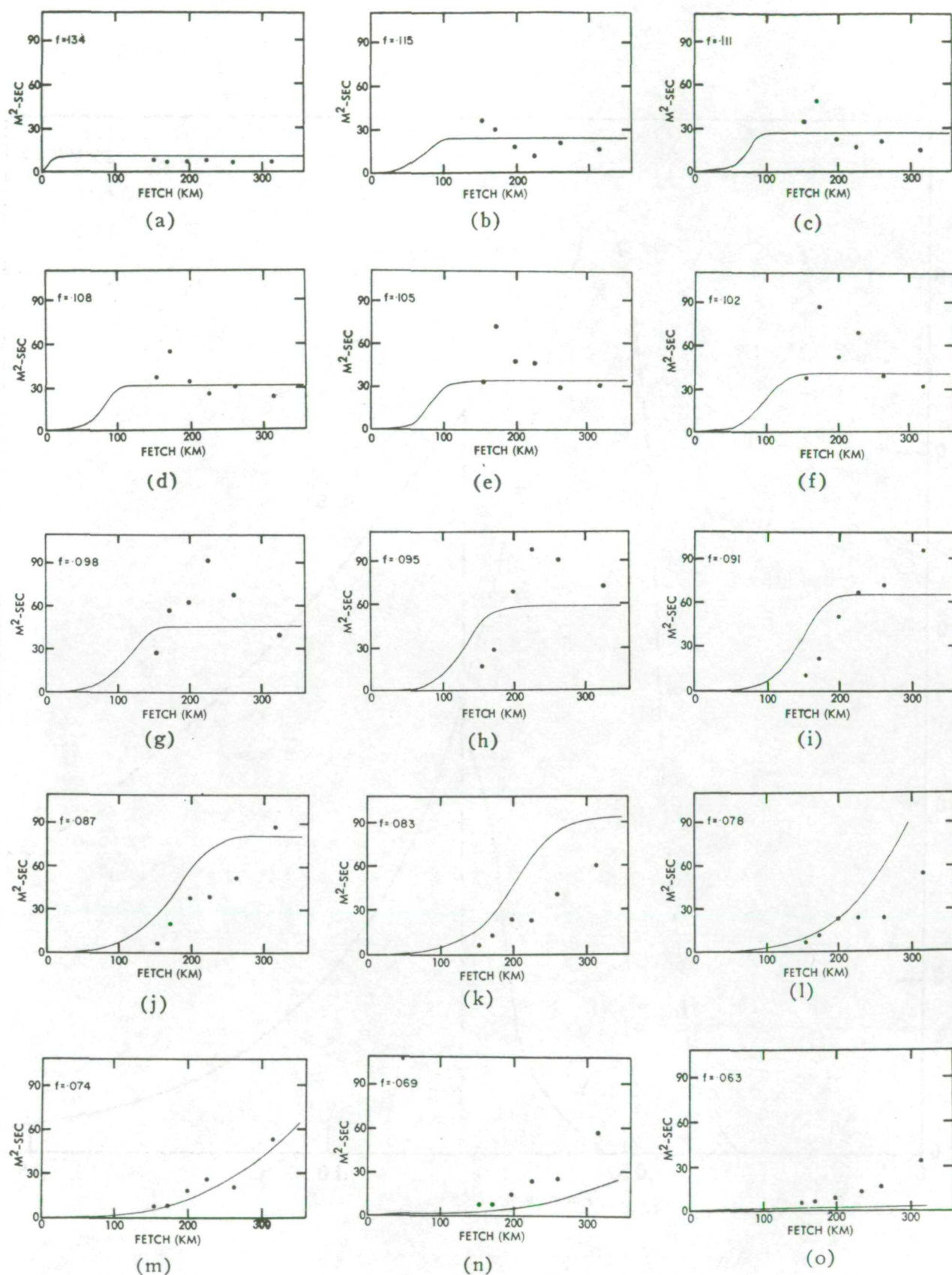


Fig. 12. Plots of spectral density versus fetch for selected frequencies.

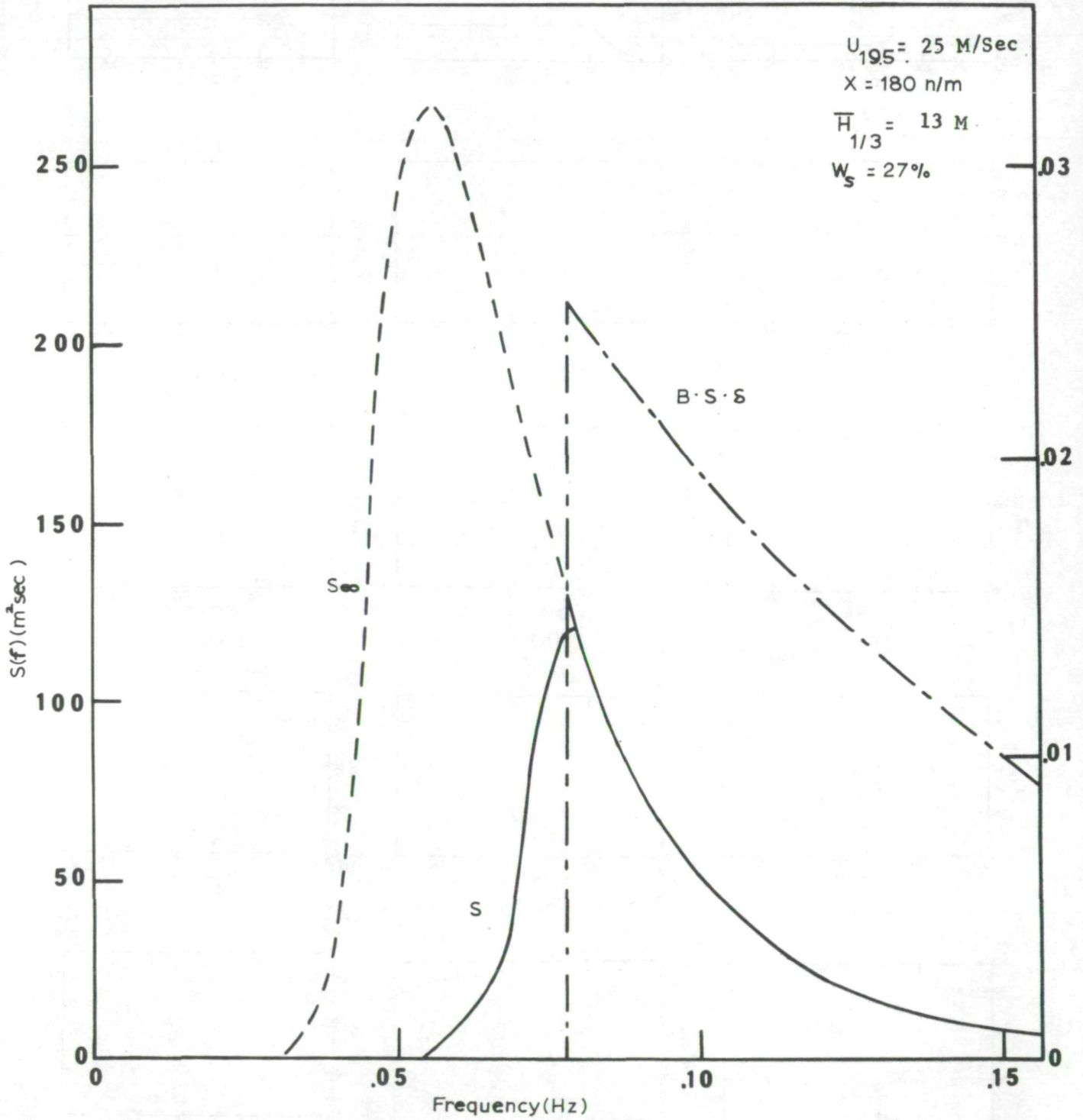


Fig. 13

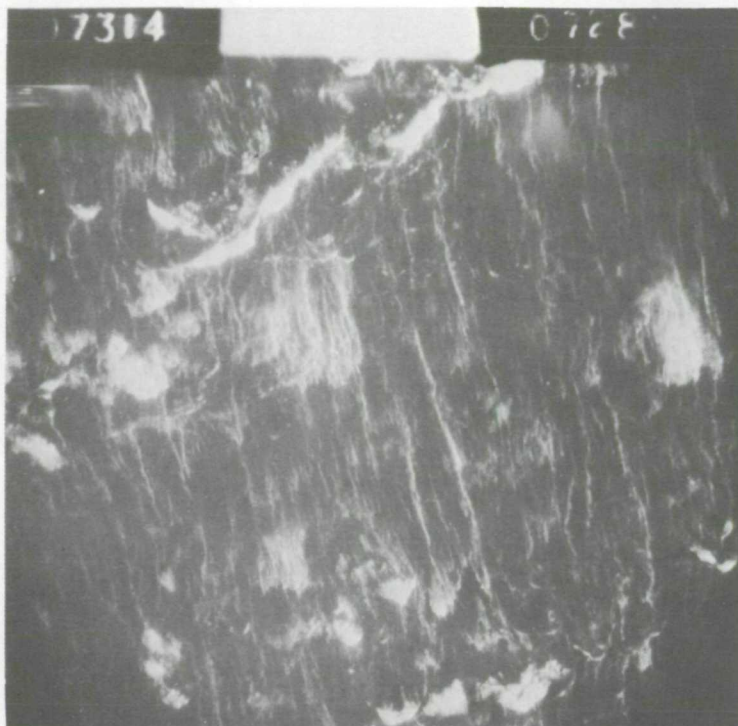


Fig. 14 25 m/sec windspeed.
Note extensive streaking present which
accounts for 27% of the total white water
content of 31%.

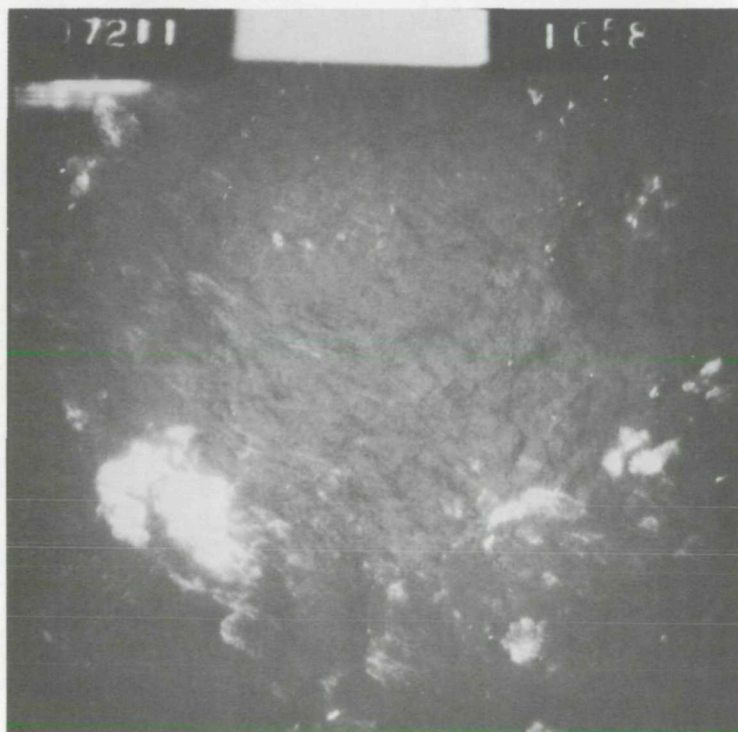


Fig. 15 12 m/sec windspeed.
Note that thin streaks account for
only 3% of the total of 10% white
water.

WHITECAP COVERAGE FROM AERIAL PHOTOGRAPHY

by

Roswell W. Austin
Visibility Laboratory
Scripps Institution of Oceanography
University of California, San Diego
La Jolla, California 92037

INTRODUCTION

This paper describes a portion of the Visibility Laboratory program devoted to determining the feasibility of deriving sea surface wind speeds by remotely sensing ocean surface radiances in the non-glitter regions. With a knowledge of the duration and geographical extent of the wind field, information about the conventional sea state may be derived.

The work has been supported by the Spacecraft Oceanography Project of the Naval Oceanographic Office. The documented aerial photography used was obtained on the Earth Resources Aircraft Project Missions 88, 113, and 119 conducted during 1969 and 1970.

The use of optical techniques for determining sea state has obvious limitations. For example, such means can be used only in daylight and only when a clear path of sight is available between the sensor and the surface. However, sensors and vehicles capable of providing the data needed for such techniques are planned for the near future; therefore, a secondary or backup capability can be provided with little added effort.

In addition to the primary objective of the work noted above, the information currently being sought regarding white water coverage is also of direct interest to those working with passive microwave systems, the study of energy transfer between winds and ocean currents, the aerial estimation of wind speeds, and many others.

DESCRIPTION OF REMOTE SENSING TECHNIQUE

The ocean surface winds and the resulting sea state usually do not need to be known with high spatial resolution. For most purposes, resolution sizes measured in kilometers are sufficient. Low resolution television or scanning radiometer systems can easily supply the needed input data if the radiometric accuracies of the systems are sufficient.

By utilizing the red or near infrared spectral regions, we can minimize the contributions to the observed signal from the light reflected upward by the blue or green ocean water and from the blue skylight returned from the ocean surface by Fresnel reflection. The reflectance of whitecaps and foam in this spectral region remains high. Thus, the effective reflectance of a large resolution element on the ocean surface that includes a mix of areas of essentially black water and whitecaps or foam will depend to a first approximation on the relative fraction of the two which are present in the total area. Unfortunately, this situation is complicated by the fact that in the "black" areas the Fresnel reflectance of the surface will return a portion of the light incident from white clouds and the "white" areas actually will have reflectance varying from a high of 80-90% for new whitecaps to a low of perhaps 10% for the streaks prevalent at the higher wind speeds. It is the effective reflectance and its relationship to the wind speed that is the key to determining wind speed by this remote sensing technique. The full nature of this relationship is the information we are seeking in the present study.

From a knowledge of the local meteorology (i. e., cloud cover) and the solar elevation at the time of observation, the irradiance incident on the ocean surface may be determined with reasonable accuracy. If the sky is clear, the incident irradiance together with the effective reflectance of the resolution element is sufficient to determine the inherent radiance of the surface as viewed from above. If however, the sky contains some clouds (i. e., broken) and the ocean surface is viewed through (large) holes in the clouds, it is necessary to generate an estimate of the distribution of radiance above the reflecting resolution element and to convolve this sky radiance distribution with the angular reflectance functions of both the white and the non-white water area. The angular reflectance properties of the white foam should approximate those of a matte or lambertian surface where-

as the wind roughened non-white areas will have reflectance properties determined by the statistical nature of the wave slopes.

A remote sensor would measure the apparent radiance of the surface. This differs from the inherent radiance just discussed by the spacelight and transmission properties of the intervening path of sight. These optical properties of the air column seem to be sufficiently well coupled to the meteorological properties that a statement of the meteorological regime extant at the time of measurement of the apparent radiance will allow the inherent radiance to be determined. The correlation of optical and meteorological properties of the air mass has been a matter of interest to the Visibility Laboratory for many years and recently the subject of studies specifically directed toward aiding the solution of remote sensing problems. ¹⁻³

It may be noted also that the use of the red or near infrared spectral regions as opposed to the blue or green regions results in a significant reduction in molecular scattering effects in the air column (both spacelight and transmission loss).

Thus we see that the proposed technique allows us to determine ocean surface wind speed from a measurement of apparent radiance providing information is available regarding the local meteorology, the solar elevation and the relationship between effective reflectance of the ocean surface and wind speed.

PROCEDURE FOR WHITECAP COVERAGE DETERMINATION

The concept of using photography to obtain a relationship between wind speed and the fraction of the surface covered by white water is certainly not new. This program, however, has afforded an unusual opportunity to obtain high quality, documented, vertical photography of the ocean surface. The main additional difference between this study and most others is that the analysis of the photography is performed instrumentally, thereby removing the subjective judgement of where the edge of the whitecap lies.

The technique consists of obtaining low altitude aerial photography of the ocean in the vicinity of ocean towers or ships that can provide wind field data by measurement as opposed to estimation. In addition

to that of the ocean surface, photography is also obtained of a gray scale on the ground (see Fig. 1) to provide a calibration for the overall photographic process. Photographic exposures and film processing are carefully controlled to obtain an adequate dynamic range on the film and to assure that the white water areas do not saturate the film. Sensitometric step tablets are printed at the beginning and end of each roll of film to establish the film characteristic and to assist in estimating the uniformity of processing.

The resulting photography is visually screened for exposure, presence of clouds, glitter, processing defects, and for the frame documentation which allows the identification of time, altitude, etc. Selected frames of the most suitable and best quality photography are then scanned in a high speed scanning microdensitometer (Fig. 2). This instrument, an Optronics International Photoscan System P-1000, is directly interfaced with and controlled by an IBM 360/44 computer (Fig. 3). It was especially constructed to accommodate the large format (9-1/2 inch) aerial film acquired with the RC-8 metric cameras. It has scanning apertures of 50, 100, and 200 microns which correspond to ocean surface resolutions of 150, 300, and 600 millimeters at scaling factors of 3000:1. The KA-62 multispectral cameras with 3 inch focal length lenses provide this scale at 750 feet altitude. In the RC-8 cameras with 6 inch focal length, this scale obtains at 1,500 feet. Although the resolution required for remote sensing sea surface wind speeds is of the order of kilometers, resolutions of fractions of a meter allow the examination of the detailed nature of the reflectance function and the separation of some of the experimental artifacts from the desired information.

The scanning speed of the densitometer is such that to build a histogram of the densities of the 1.2 million, 200 micron square picture elements in a 200 by 240 mm field of view takes just over five minutes. Scans at 100 or at 50 microns can be performed at the cost of correspondingly increased scanning times when greater spatial resolution is required. Immediate printouts of tables and plots are obtained of the histogram of picture element densities and the integral of this, the cumulative area in the picture versus photographic density. By scanning the sensitometric step tablets printed on each roll of film and the photographs of the gray scales, film and overall photographic system characteristic curves may be generated from which film densities can be related back to exposure and to the reflectance of the ocean surface (Fig. 4).

RESULTS AND DISCUSSION

Some preliminary results were obtained by scanning some selected Mission 88 photography. Figure 5 is a photograph taken over the North Sea on 14 March 1969 at an altitude of 1,500 feet. The surface wind speeds were 48-50 knots. The large area "A" outlined in white containing most of the frame is approximately 600 meters wide. The large whitecap included within the outline "D" is about the size of a football field (90 m). The four outlined areas were separately scanned and the curves in Figure 6 show cumulative areas having densities equal to or less than the values on the abscissa. Curve A shows the cumulative area-density function for essentially the entire frame; curve B for the small area containing streaks and small whitecaps; curve C for the area having only streaks and background and curve D for the area containing the large whitecap.

The subjective approach for determining a single number for the fraction of the surface covered by white water requires a judgement of where the line separating black and white should be placed. One can appreciate the problems of doing this in photographs such as Figure 5. How, for example, does one properly account for the streaks when using a subjective outlining method? Curve C in Figure 6 shows that in such an area (with the 200 micron aperture used in obtaining the data for these curves) there is essentially no white (low density) area but that the relative amount of the scanned area having densities around 1.0 (10% film transmission) exceeded that of both areas A or B. Thus, the regions containing the streaks are shown instrumentally to have relatively larger amounts of area with intermediate reflectance than the other regions. This is, of course, the result one would anticipate; but we now have the capability of quantitatively describing the observation.

In Figure 7 we see the results of scanning two additional frames taken approximately 10 seconds before and 10 seconds after the previous frame. The spread in the curves is an indication of the variability in the amount of white water present at a given wind speed and shows the necessity of scanning enough frames to obtain a statistically significant functional relationship.

The curves of Figures 6 and 7 show area-film density relationships as opposed to the desired area-surface reflectance functional relationships. The translation from density to reflectance requires both film

characteristic and gray scale calibrations. The Mission 88 films did have step tablets printed on them so that film characteristics could be obtained. However, no gray scale photography was obtained so it is not possible to assign reflectance values to the film densities with the required accuracy. In addition, the film was processed in such a way that the useful dynamic range of exposures was only about 10 to 1 instead of the 100 to 1 or greater which can readily be obtained. Thus, the useful information available from these films was restricted to a narrow range of exposures and the likelihood was great that desired scene information would fall on the shoulder or toe of the film characteristic. Nonetheless, a second abscissa has been placed on the top of Figure 7 which shows what the area-reflectance relationship might be if we assume a value of film density for the 100% reflectance point. Such information properly replotted against a rational reflectance scale would represent the type of output one might expect for a single wind speed.

CONCLUSIONS

In summary, an attempt is being made to obtain quantitative relationships between the effective optical reflectance of the ocean surface and surface wind speeds. Documented photography is being obtained and processed for the study by the Earth Resources Aircraft Program. The photography is being machine analyzed to remove the subjectivity which has existed in previous studies and to extract additional information.

A scanning microdensitometer has been obtained and interfaced directly with an IBM 360/44 computer. Computer programs for the processing of the data have been prepared and are being expanded as the data reduction process proceeds.

Figure 8 presents some results of earlier investigations^{1,4} and shows an apparently tidy result. However, more recent similar analyses of this type show appreciably lower white water areas.^{5,6} Our very preliminary results would appear to be able to embrace both results depending on the white-black demarcation criterion used but generally favor the lower values. We would propose that instead of a single curve it is more completely descriptive of the physical situation to use a family of curves or a surface to describe the wind speed-area-reflectance relationship.

REFERENCES

1. Duntley, S. Q. and Edgerton, C. F., "The Use of Meteorological Satellite Photographs for the Measurement of Sea State," Contract NObs-86012, Lot II, Final Report (June 1966).
2. Edgerton, C. F., "Relationship between Meteorological Conditions and Optical Properties of the Atmosphere," SIO Ref. 67-27 (1967).
3. Duntley, S. Q., Edgerton, C. F. and Petzold, T. J., "Atmospheric Limitations on Remote Sensing of Sea Surface Roughness by Means of Reflected Daylight," SIO Ref. 70-27 (Sept. 1970).
4. Blanchard, D. C., "The Electrification of the Atmosphere by Particles from Bubbles in the Sea," Woods Hole Oceanographic Inst., Ref. 61.9 (April 1961).
5. Rooth, C. and Williams, G. F., "Microwave Radiometry of the Ocean," Contract N62306-69-R-0204, Quarterly Report (Feb. 1970).
6. Monahan, E. C., "Fresh Water Whitecaps," Journal of the Atmospheric Sciences, Vol. 26 (Sept. 1969).

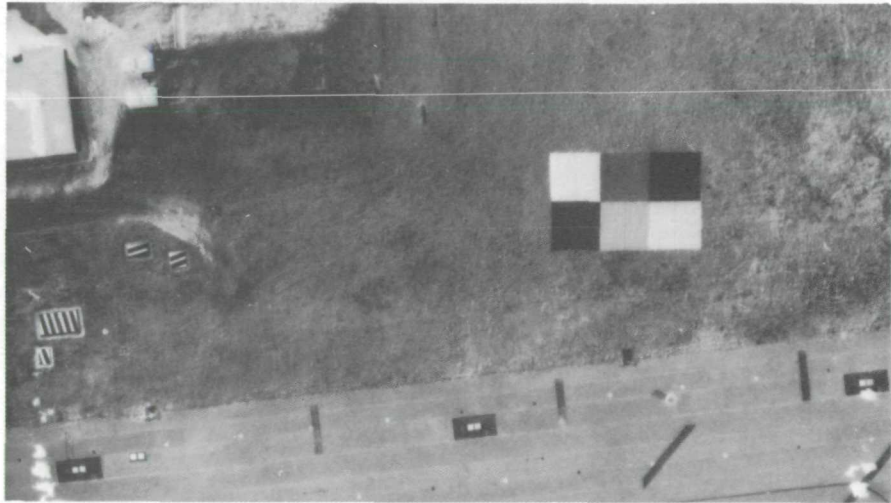


Figure 1. - Canvas Gray Scale deployed next to runway. 20 foot square panels have nominal reflectances of 3, 7, 14, 29, 64, and 83 per cent.



Figure 2. - Scanning Microdensitometer, Optronics International Photoscan System P-1000.

NOT REPRODUCIBLE



Figure 3. - Visibility Laboratory Interactive Image Manipulation Computer Facility. IBM 360/44 in left background. Interactive input-output console in right foreground.

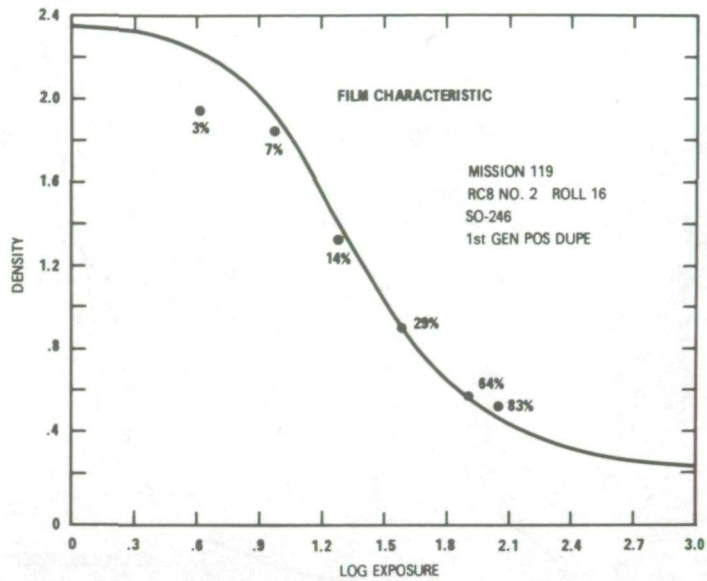


Figure 4. - Typical film characteristic curve with gray scale data superimposed.

NOT REPRODUCIBLE

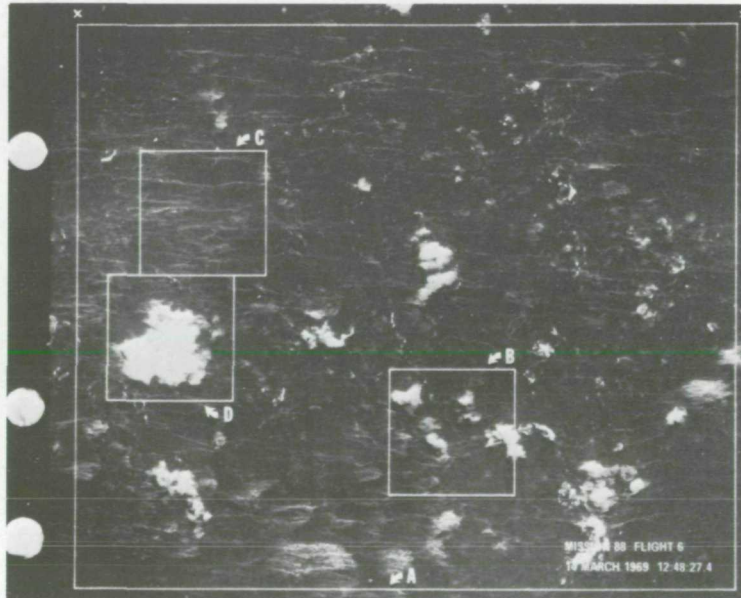


Figure 5. - Frame taken by RC-8 camera on Mission 88 Flight 6 on 14 March 1969 at an altitude of 1500 feet with surface winds of 48 to 50 knots. Large rectangle "A" represents a 500 by 600 meter area on ocean surface. Small squares 110 meters on side show "B" small whitecaps and streaks, "C" streaks only, and "D" large whitecap.

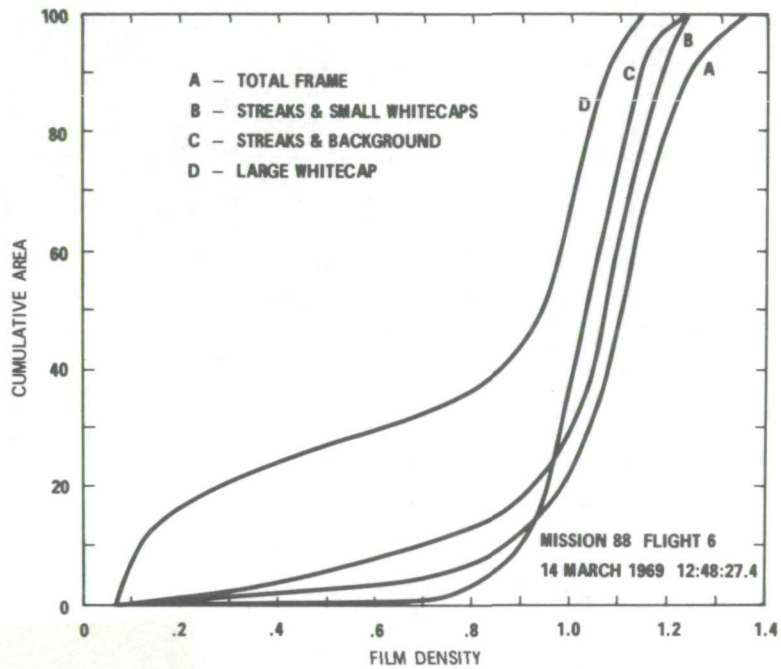


Figure 6. - Cumulative areas (as per cent of total area scanned) versus film density for the four regions outlined in Figure 5.

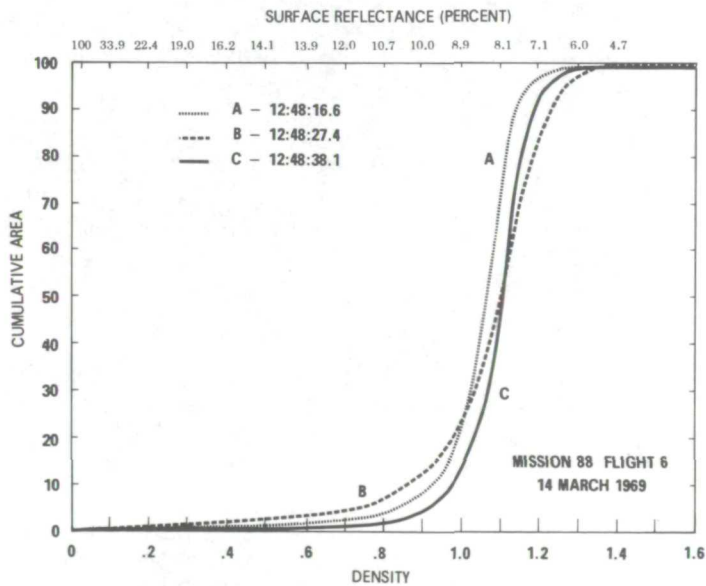


Figure 7. - Cumulative areas for 3 frames of photography taken about 10 seconds apart (no overlap) showing variation occurring in independent areas in the same wind field.

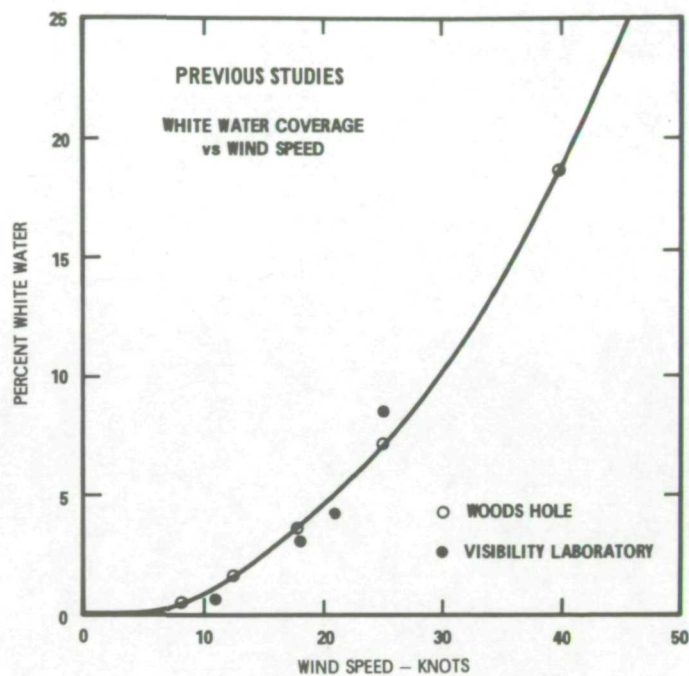


Figure 8. - White water coverage versus wind speed as obtained from earlier studies by Blanchard⁴ (Wood Hole) and by the Visibility Laboratory¹. Present preliminary results are generally lower than those shown in this figure.

ON THE USE OF A SINGLE BLUE BAND IN OCEANOGRAPHY

by

John W. Sherman, III

Abstract

The selection of a single blue band to quantitatively measure ocean chlorophyll is dependent upon the altitude and spectral bandwidth of the filter. These relationships are discussed, and the conclusion made that a blue band from 0.44 to 0.50 microns would best serve this oceanographic application.

INTRODUCTION

The use of multispectral photography and its ensuing adaptation to mechanical and electronic sensors have usually relied on the color-signature differences which are associated with the response of the human eye. Relatively low spectral resolution systems have evolved using high spatial resolution to permit environmental target delineation, while the spectral differences determine the target type and characteristics.

The use of multispectral photography in aircraft and satellite terrestrial applications has required investigators to deal with the perturbing effects of the atmosphere. When used for oceanographic applications, the same techniques are affected by two additional perturbing features: the ocean surface and the water column. Investigators interested in bottom topography and mapping in shallow waters typically require the same spatial resolutions needed overland because the measurement requirements are the same. Surface effects in some applications are noise in the data, while in others (such as pollution) the surface phenomenon itself is the measured parameter. However, in most cases the study of surface effects and phenomena requires a different sun angle relationship to the sensor than when the applications are subsurface. The investigation of the upper hundred feet of the water column is a critical area in synoptic oceanography primarily because life in the sea begins in this upper region where photosynthesis in plant life is possible.

Visible region ocean surface studies (excluding wave phenomena) and water column studies historically have differed from those of bottom topography and mapping studies; namely, in situ measurements of the two former studies have always used high spectral resolution on the order of 20 to 100 Angstroms to detect and measure slight "color" changes in the surface and subsurface characteristics, while a panchromatic approach has been used for bottom studies. The early transition¹ from the in situ to aircraft measurement of the water column has determined the necessity of maintaining high spectral resolution from remote sensors operating above the ocean surface.

The purpose of this discussion is to examine the factors involved in selecting a single blue band for oceanographic applications with prime emphasis on water column measurements related to chlorophyll. The use of a single channel chlorophyll detector from space will serve as a qualitative measurement of chlorophyll in the world's oceans, while a multichannel high spectral resolution sensor will be required before quantitative measurements are possible. Even qualitative data on global chlorophyll are not presently available.

REMOTE MEASUREMENT OF CHLOROPHYLL

The work of Ewing and Clarke² has shown the response of an airborne spectrometer to chlorophyll and to effects of varying altitude. These effects have been combined in Figure 1 (after Ewing and Clarke) in terms of the spectral contrast ratio (SCR) defined as

$$\text{SCR} = \left| \frac{\text{High Chlorophyll-Low Chlorophyll}}{\text{Low Chlorophyll}} \right|$$

where "high chlorophyll" refers to the percent of incident energy at a given wavelength returned to the spectrometer from water containing 0.3 to 0.4 mg/m³ chlorophyll concentration (water typical of the Gulf Stream) and "low chlorophyll" is the same percentage returned from water containing less than 0.1 mg/m³ (this is very sterile water such as might be found in the Sargasso Sea). Thus, a comparison is being made between the most benign waters of the

¹ S. Q. Duntley, "Light in the Sea," Journal of the Optical Society of America, Vol. 53, No. 2, pp 214-233, February 1963.

² G. C. Ewing and G. L. Clarke, "Remote Sensing of Ocean Color from Aircraft"

world's oceans to conditions that are considered to be the threshold for chlorophyll measurement. The range of significant chlorophyll concentrations is from approximately 0.3 to 10 mg/m³.

The data in Figure 1 are repeated in Figure 2 for the 10,000-foot altitude case to delineate the rapid roll-off in response of wavelengths greater than 0.5 microns for filters of 50-Angstrom bandwidths. Using the 10,000-foot altitude data, the SCR has been computed as a function of the short wavelength cutoff for three different bandpass filters of 200, 600, and 1,000 Angstroms (0.02, 0.06, and 0.1 microns, respectively). These results are sketched in Figure 3 which illustrates the following features at 10,000-foot altitude:

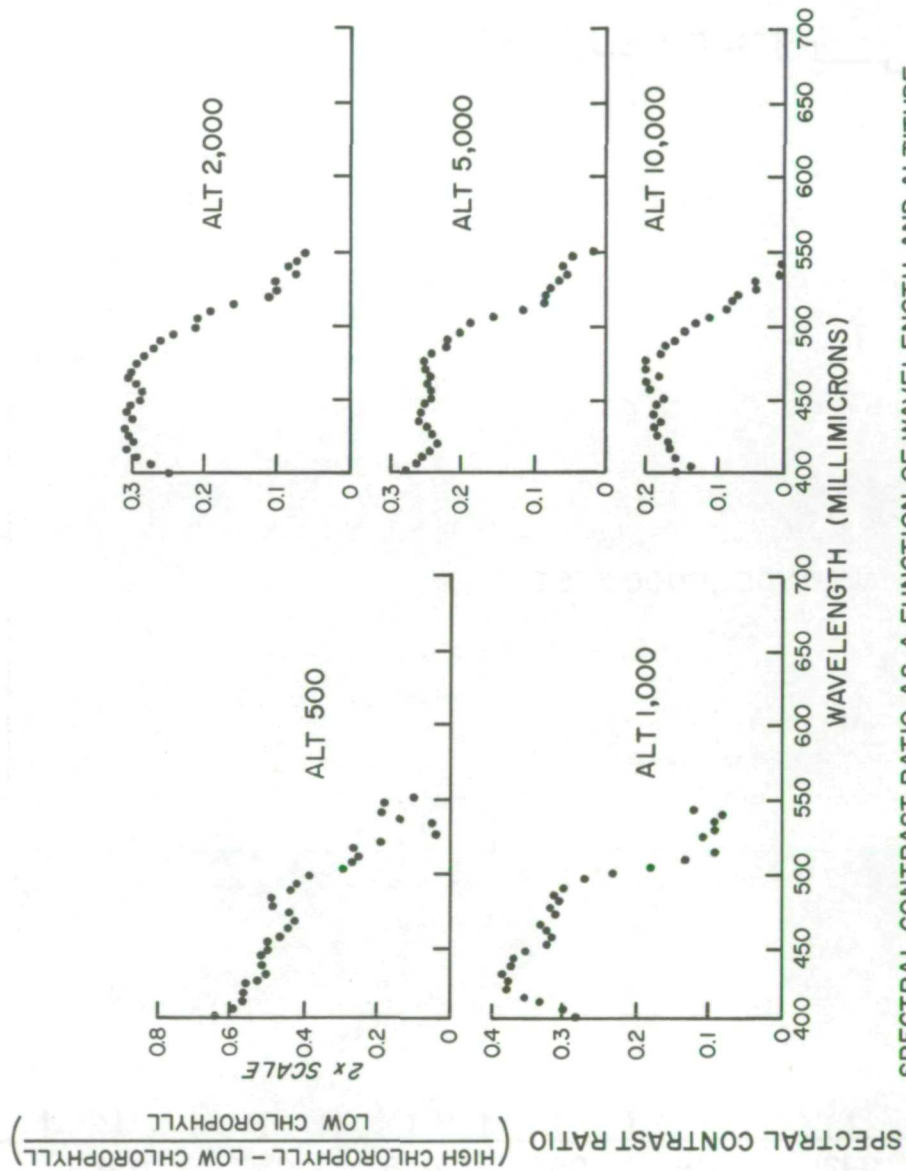
- a. The maximum SCR is a relatively broad function of the short wavelength cutoff within the 0.40- to 0.48-micron region and depends on the filter width.
- b. As the filter width increases, the short wavelength filter cutoff moves deeper into the blue region for maximum SCR.
- c. There is a maximum SCR associated with each of the three filter widths.

Thus, for each filter bandpass, there is a preferred region within the blue region for obtaining the maximum SCR.

The general behavior of the maximum SCR as a function of the filter bandpass width is shown in Figure 4 using the right ordinate. The greater the spectral resolution, the greater the maximum SCR. There is a preferred filter center wavelength which gives the maximum SCR for each filter width which is shown on the left ordinate. The preferred center wavelength moves toward shorter wavelengths as the filter width increases, at least to widths on the order of 600 to 800 Angstroms.

The behavior of the maximum SCR with altitude is illustrated in Figure 5. There is a significant reduction in the maximum SCR as the altitude increases. Also, it should be noted that probably all aerosols and particulate matter and about half the atmosphere are below the 10,000-foot level, and thus, the reduction in the SCR will not continue at the same rate above the 10,000-foot level as measured below that level. Figure 6 shows the preferred center wavelengths with altitude as a function of filter width which

gives the maximum SCR of Figure 5. The general behavior of these data is consistent with that intuitively anticipated. That is, at low altitude with relatively narrow filter widths the preferred center wavelength occurs near the peak absorption for chlorophyll around the 0.42- to 0.44-micron region. As the altitude increases so does the preferred center wavelength increase for the narrow filter widths. However, at broader filter widths there is a convergence of the preferred center wavelengths at around 600- to 800-Angstrom filter widths. Based on this convergence, it appears that the single best channel for chlorophyll measurement is from 0.44 to 0.55 microns for a space system.



SPECTRAL CONTRAST RATIO AS A FUNCTION OF WAVELENGTH AND ALTITUDE

Figure 1.- Spectral contrast ratio as a function of wavelength and altitude.

SPECTRAL CONTRAST RATIO OF CHLOROPHYLL ENRICHED WATER TO STERILE WATER

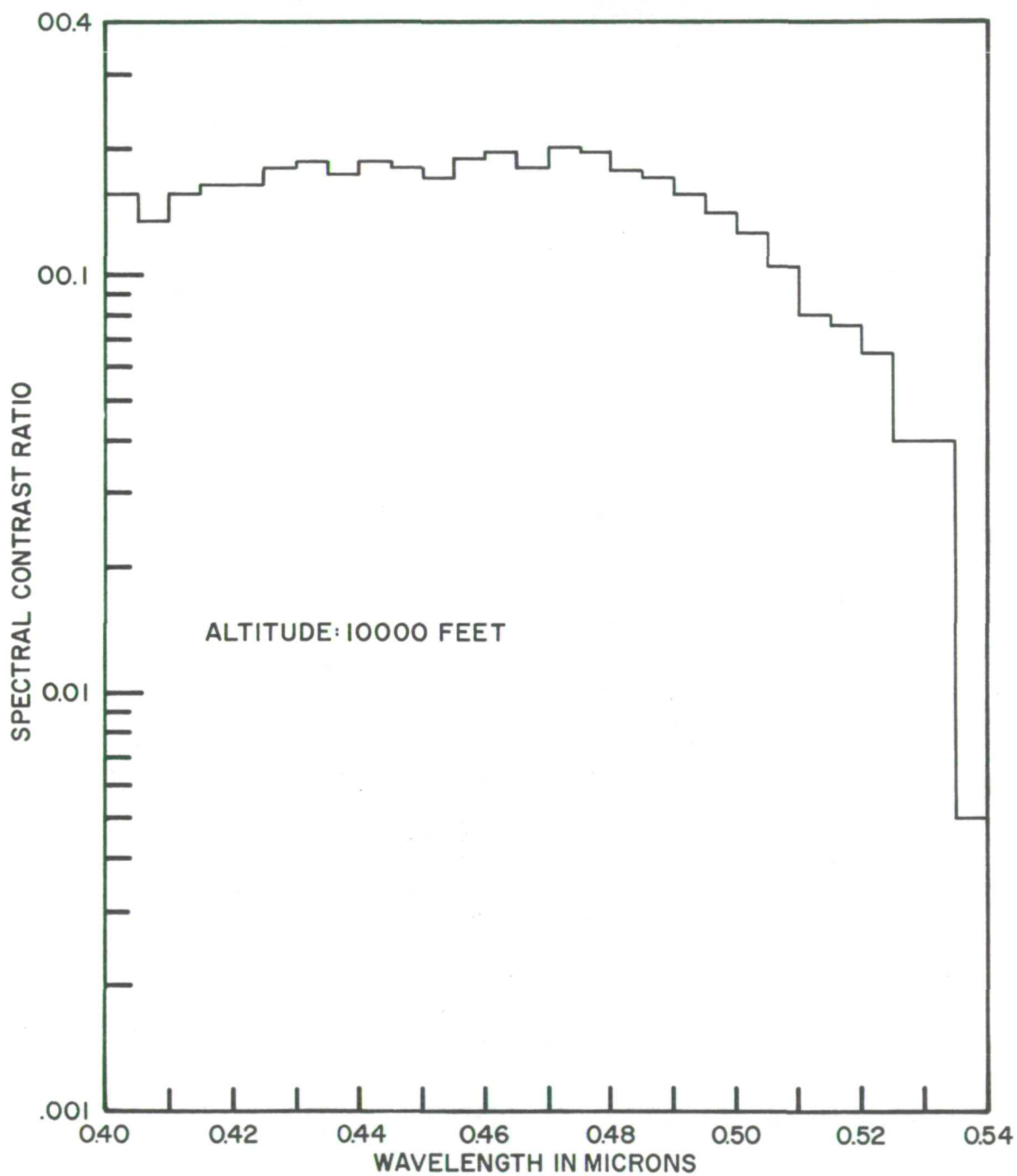


Figure 2.- Spectral contrast ratio of chlorophyll-enriched water to sterile water.

ANALYSIS OF SINGLE BANDPASS CHANNEL FOR CHLOROPHYLL DISCRIMINATION

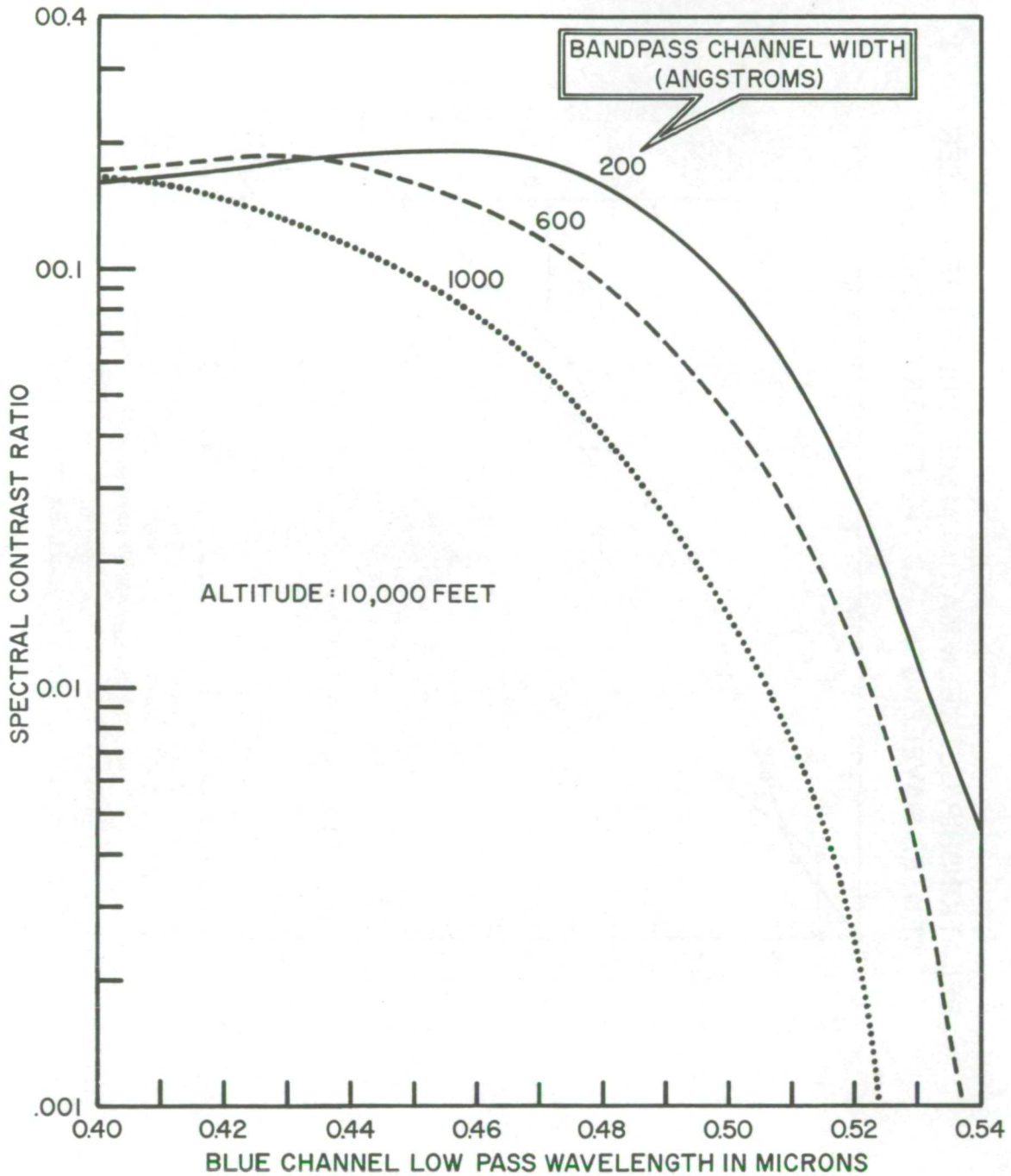


Figure 3.- Analysis of single bandpass channel for chlorophyll discrimination.

RELATIONSHIP BETWEEN MAXIMUM SCR, PREFERRED FILTER CENTER WAVELENGTH AND THE FILTER BANDWIDTH

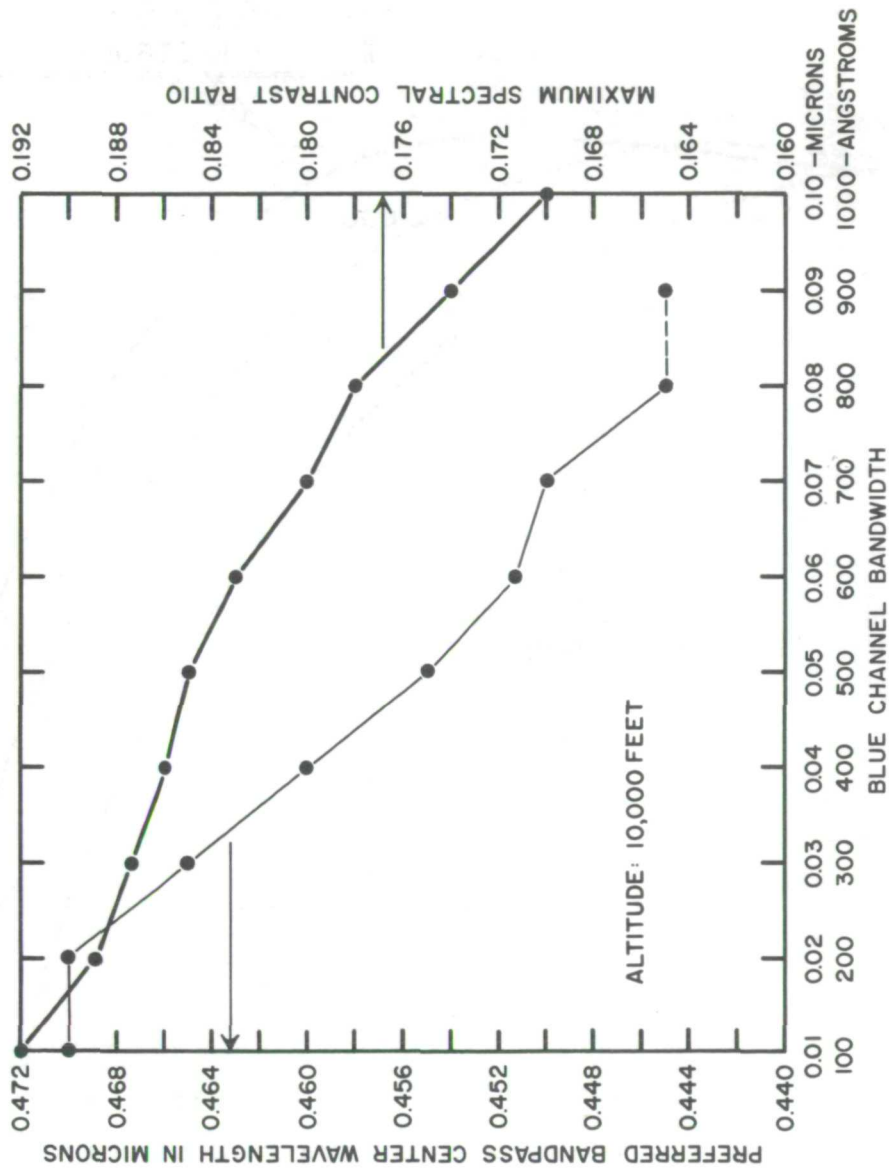


Figure 4.- Relationship between maximum SCR, preferred filter-center wavelength, and the filter bandwidth.

ALTITUDE EFFECTS ON THE MAXIMUM SPECTRAL CONTRAST RATIO

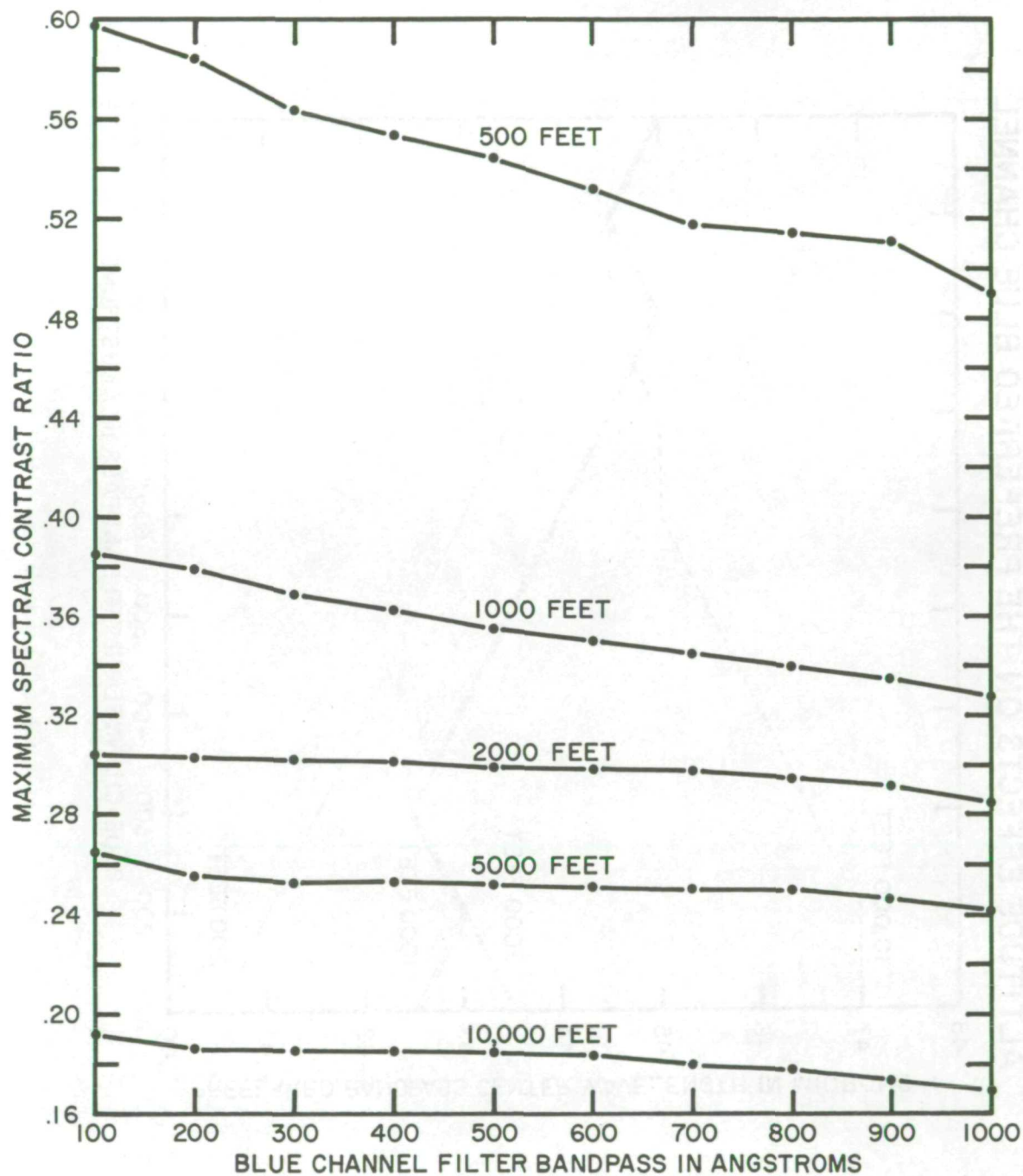


Figure 5.- Altitude effects on the maximum spectral contrast ratio.

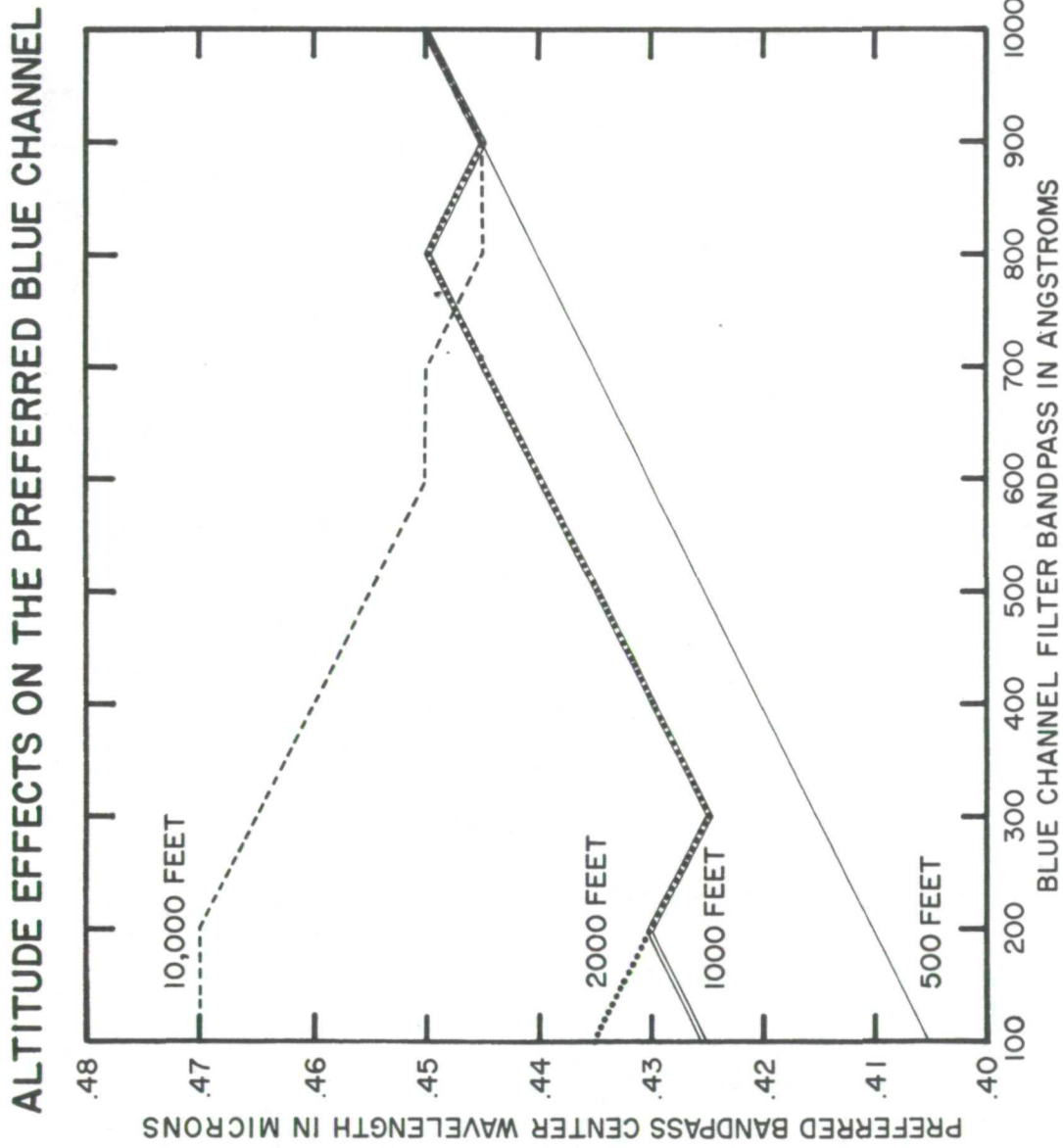


Figure 6.- Altitude effects on the preferred blue channel.

THE VARIATION OF RADAR CROSS SECTION WITH WIND

By N. W. Guinard
Naval Research Laboratory
Washington, D.C. 20390

ABSTRACT

Previous X-band (8910 megahertz) and C-band (4455 megahertz) measurements by the Naval Research Laboratory indicate that two domains exist in the variation of radar cross section with wind at incident angles far from the normal. The first domain for low windspeeds is characterized by a rapid variation of radar cross section with wind and the second domain at higher windspeeds by an asymptotic approach to an upper limit (saturation). The transition between the two domains occurs at a windspeed of approximately 10 knots. Recent Joint Ocean Surface Study I observations tend to confirm this observation and offer additional proof of the validity of the composite surface model developed at the Naval Research Laboratory (and in the USSR) which relates the radar cross section of the sea to the wave-height spectrum. This confirmation was obtained by comparing the radar cross section measured by the four-frequency radar system with the radar cross section calculated from the ocean wave-height spectrum that had been determined by the optical analysis of photographs taken from Argus Island at the same time. A possible explanation for the wind variation of the radar cross section of the open ocean also was evolved, based on radar measurements in a wave tank under various wind conditions and subsequent comparison with optically determined spectra.

NANOSECOND RADAR OBSERVATIONS OF THE OCEAN SURFACE
FROM A STABLE PLATFORM

BY

B. S. Yaplee, A. Shapiro, B. D. Au
D. L. Hammond and E. A. Uliana
E. O. Hulburt Center for Space Research
Naval Research Laboratory
Washington, D. C.

INTRODUCTION

Radar as a remote sensor of ocean surface conditions has been in use for sometime. These radars, using either CW or long pulse modulation require that the measurements be taken at various look angles. The ocean surface conditions are inferred from the steepness of the curves of reflected energy versus angle. However, if one were to reduce the pulse width of the radars until the pulse width resolves the vertical water wave structure and looks only in the direction normal to the ocean surface, an entirely different set of radar returns are available to describe the ocean surface characteristics. This paper will describe some preliminary results obtained by measuring the ocean surface with a nanosecond radar pulse from a fixed platform at vertical incidence.

RADAR SYSTEM DESCRIPTION

A simplified block diagram of the radar system is shown in Figure 1. The transmitted one nanosecond pulse is generated by rapid pulsing of a step recovery diode which is mounted in an x-band waveguide (WR-90). The diode output is amplified by a TWT amplifier and fed to a transmitting antenna. Duplexing is achieved using separate transmitting and receiving antennas which provide adequate isolation. The received pulses are amplified at rf until sufficient signal is available to drive diode detectors with extremely fast response time. The detected signal is

displayed on a sampling scope. The sampling scope stores the information in a manner permitting A-D conversion for recording on magnetic tape. All the synchronization of the rf signals and control signals are programmed by the control unit. The radar system parameters are:

	P_t	=	0.1 W
	PRF	=	70 KHz
	τ	=	1 ns
Antenna Diameter D		=	76 cm
Antenna Beamwidth		=	2°
Receiver Bandwidth		=	10 ⁹ MHz
Antenna Gain		=	35 db

OBSERVATIONAL PLATFORM

The radar system was installed on the Chesapeake Light Tower (Figure 2) which is located about 15 miles east of Virginia Beach, Virginia. The antennas were mounted underneath the catwalk as shown in Figure 3. The antennas are about 70 feet above mean sea level and the radar illuminates a spot on the ocean about one meter in diameter. In order to calibrate the radar system, both in range and amplitude, a corner reflector held on a rigid pole was placed in the center of the antenna beam and mounted about 60 feet from the transmitting antenna (Figure 4). To provide the primary ground truth concerning the waves, three wave poles were placed in a delta configuration surrounding the radar illuminated spot. The electrical output of the three wave poles, using 0.1 second time constant, were recorded simultaneously with the radar data on magnetic tape.

DATA

Figures 5 and 6 are computer plots of the radar data as recorded. These two runs will be used to illustrate two extreme sea conditions that were recorded. Figure 5 represents a calm sea condition with moderate swells. Figure 6 corresponds to a 20 knot wind with wind driven 5-foot waves. Since the wave pole measurements are recorded simultaneously, their output is arbitrarily placed to the left or right of the radar data and their alignment in time is automatic. The plots, as shown, are

an attempt to illustrate, as much as possible with one photograph, a sequence of the time history of the waves passing the radar illuminated spot. Each division of the vertical scale corresponds to one second in time. The horizontal scale measures the time delay of the radar pulse in nanoseconds, where each division corresponds to 5 ns (75 cm).

Figures 7 and 8 are plots of the power spectrum for the data of Figures 5 and 6 respectively. In addition, the wave pole power spectrum is superimposed on the radar spectrum. The agreement is so close that one can truly interchange the two results without serious error.

As mentioned earlier, a corner reflector was placed in the beam so that calibrations may be possible in power and range. The radar returns from the sea of Figures 5 and 6 were calibrated with respect to the radar return of the corner reflector. The power return was averaged for each increment of range resolution so that a plot of reflected power versus depth into the wave height is possible. Figures 9 and 10 show the reflected power versus wave depth for the two examples. The crest is to the left and the trough is to the right. Note that the reflectivity in these two cases is not uniform but increases toward the trough.

If one were to plot the effective amplitude distribution of the returned signals over the vertical water wave structure and normalize the area under the curve, one then obtains the equivalent impulse response for the sea. The returns were plotted in this manner in Figures 11 and 12 with an accompanying photograph of the sea at the time the data were taken. Superimposed is the wave pole amplitude distribution. It is seen that the effective difference between the radar and wave pole distribution is minor, and that the error introduced by the electromagnetic distortion on the derived mean height and wave heights should be small.

SUMMARY

Nanosecond pulse radar systems show promise for measuring the sea and provide information comparable with wave pole measurements. Until further analysis with additional data and thorough comparison with wave pole data, this report is intended as a preliminary discussion of progress to date.

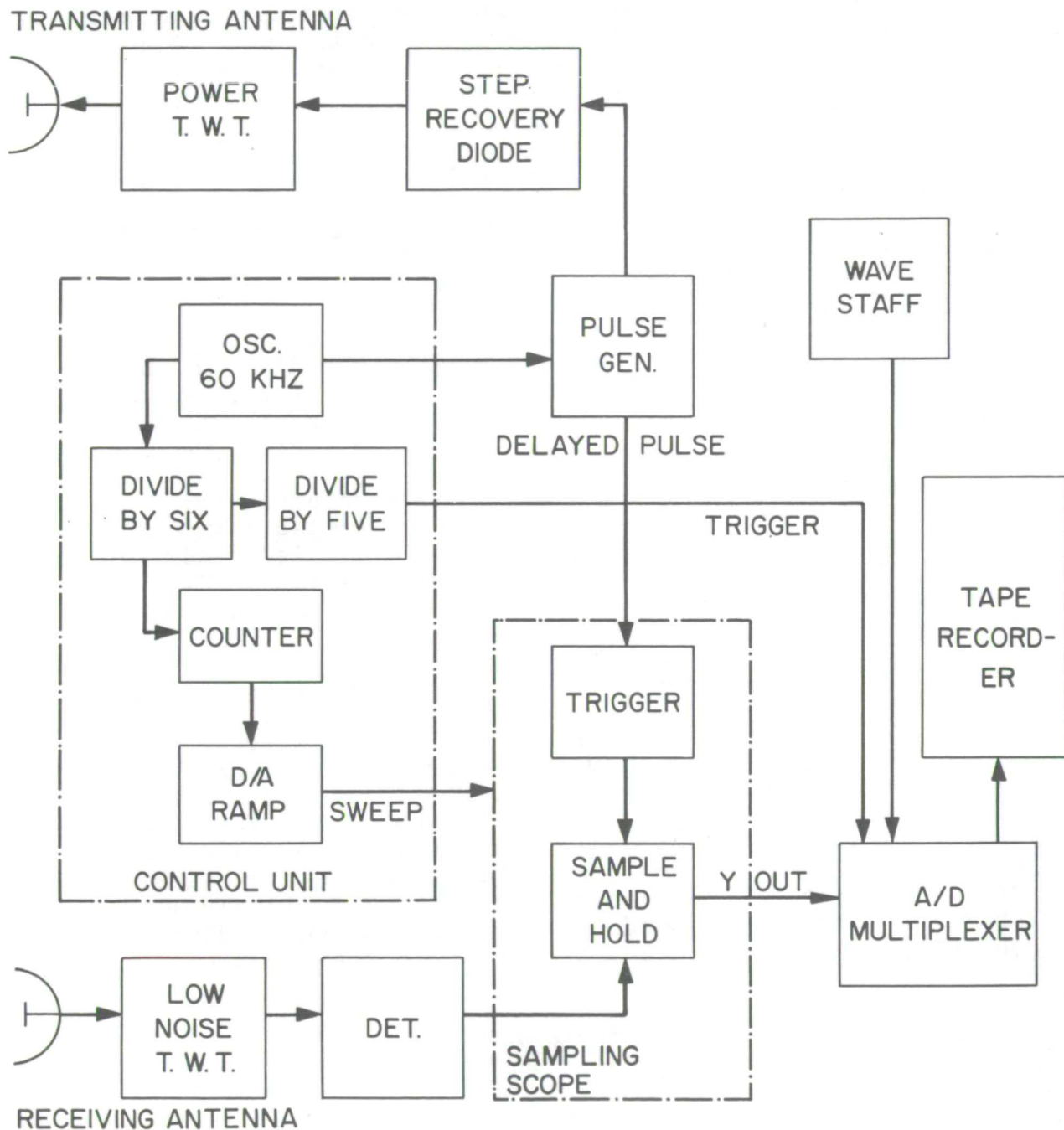


Fig. 1 Radar System



Fig. 2 Chesapeake Light Tower.

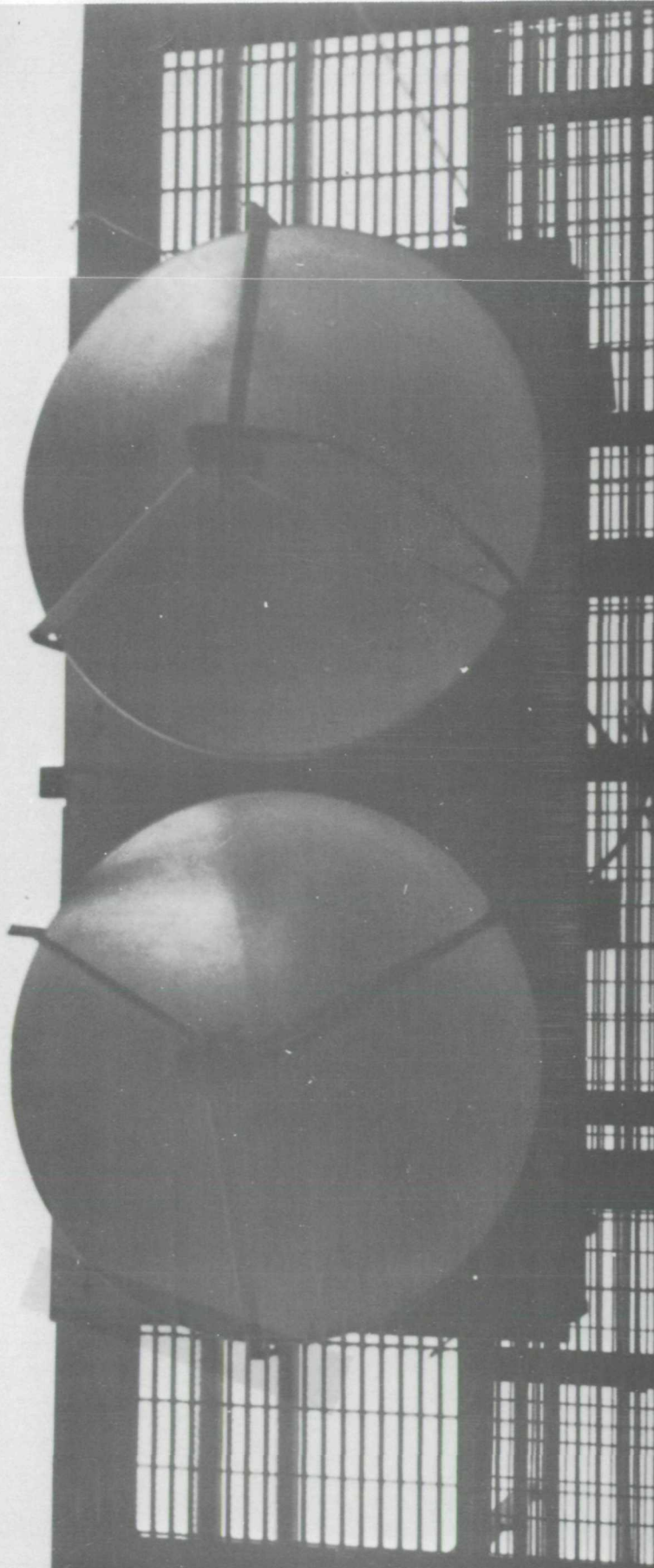


Fig. 3 Antenna Mounting on Catwalk

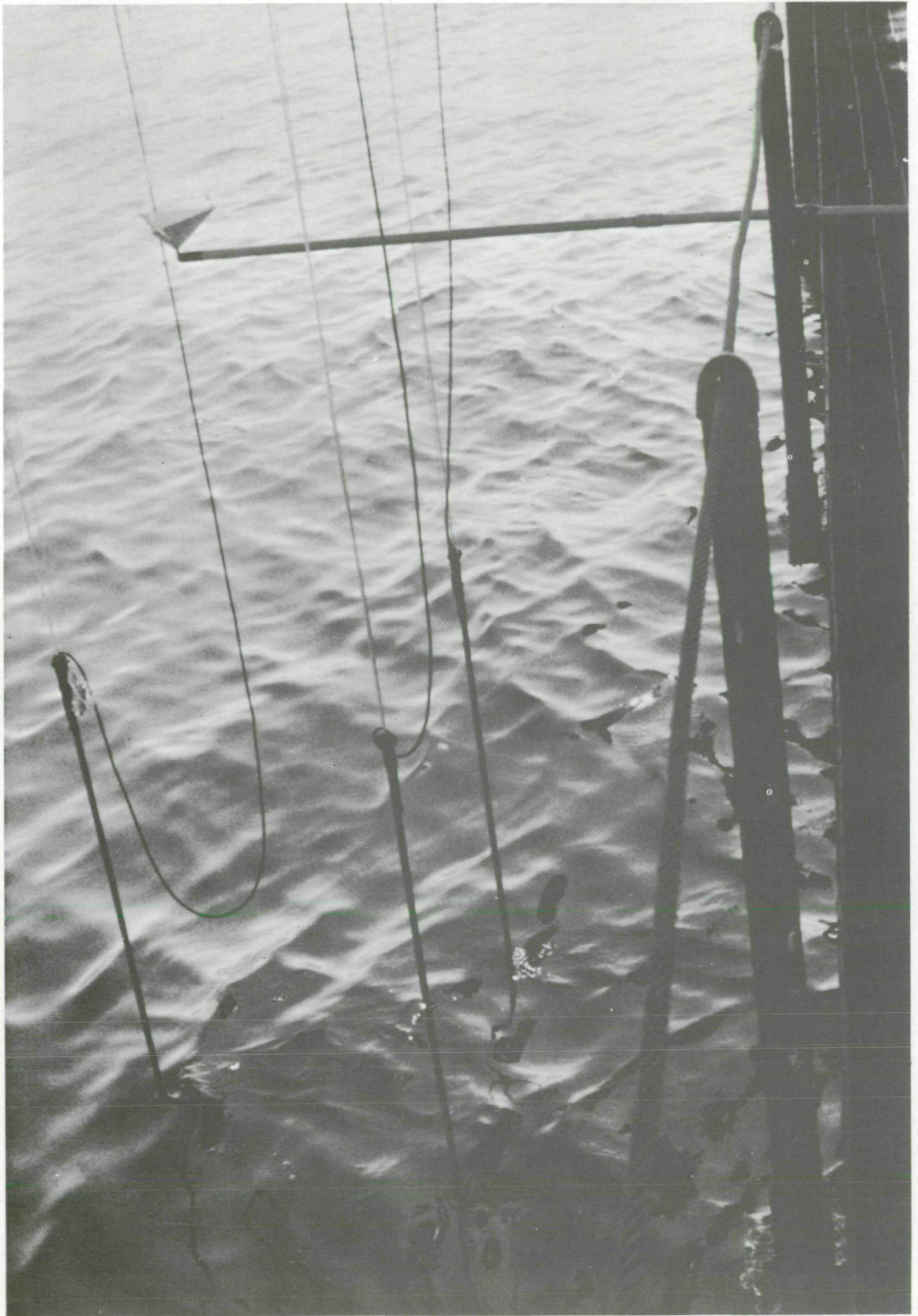


Fig. 4 Wave Pole and Corner Reflector.

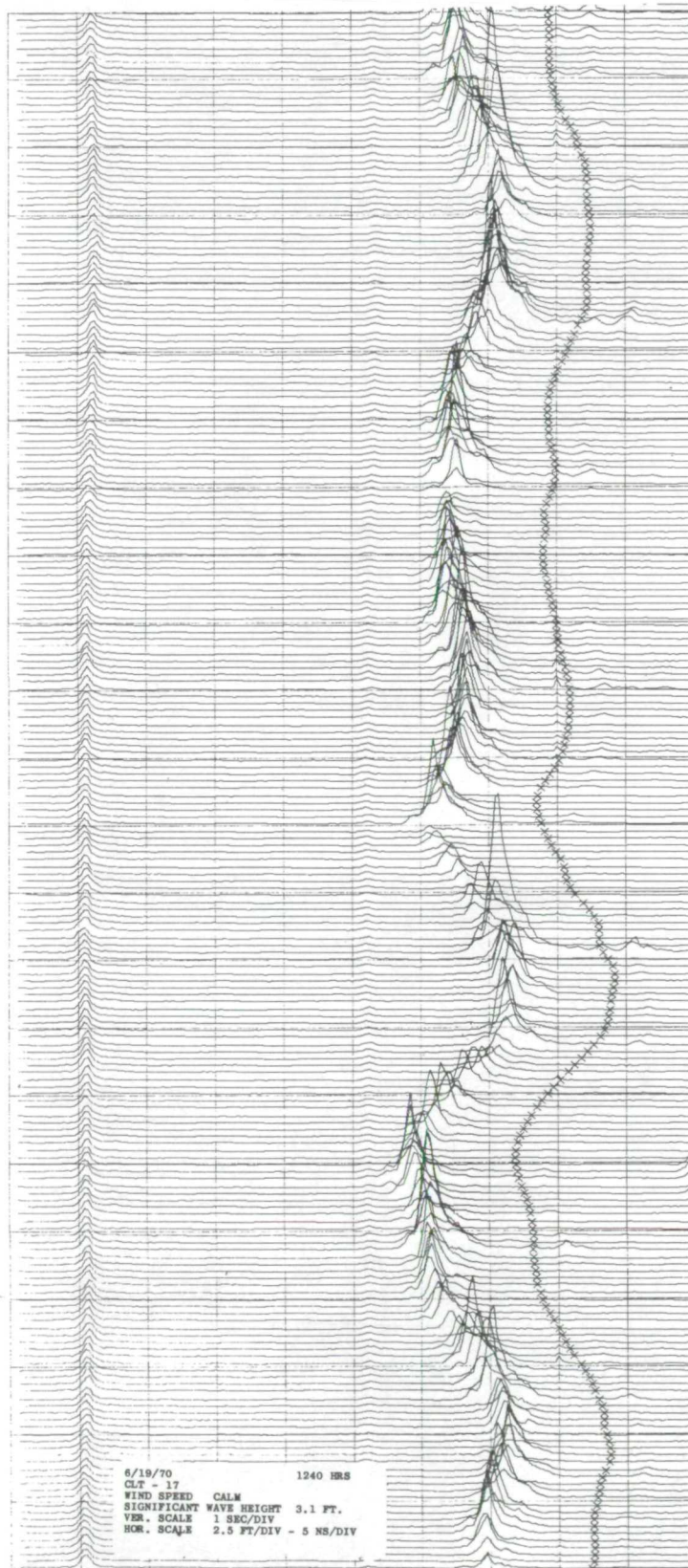


Fig. 5 Computer Plot of Radar Data

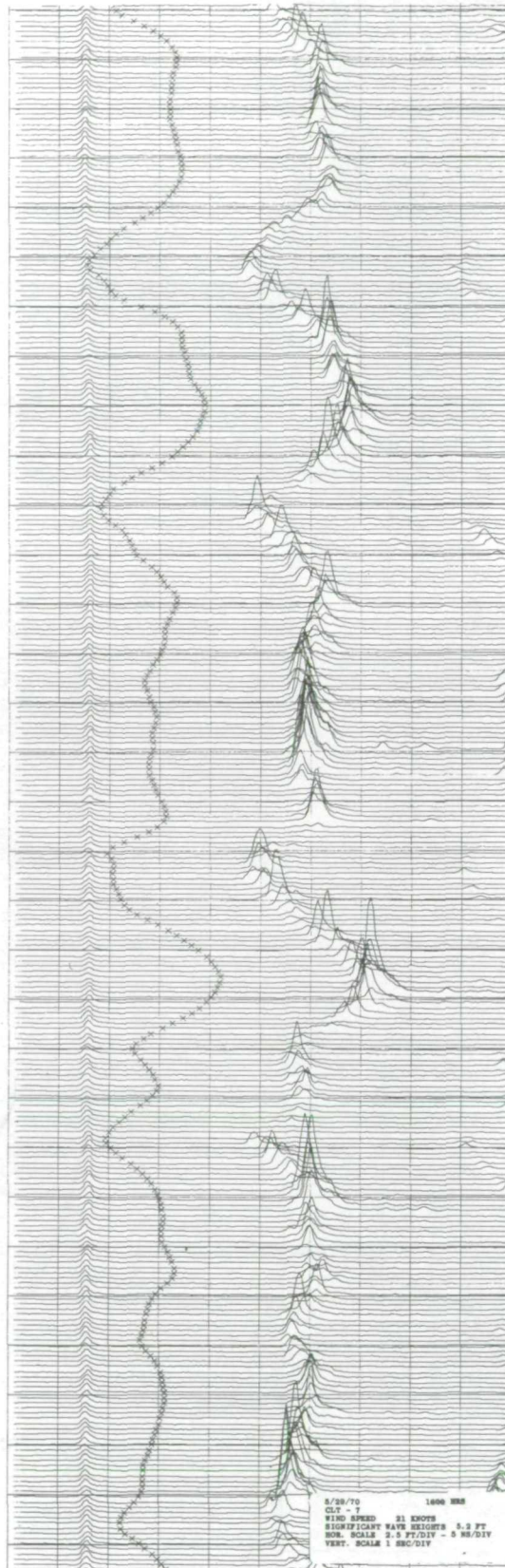


Fig. 6 Computer Plot of Radar Data

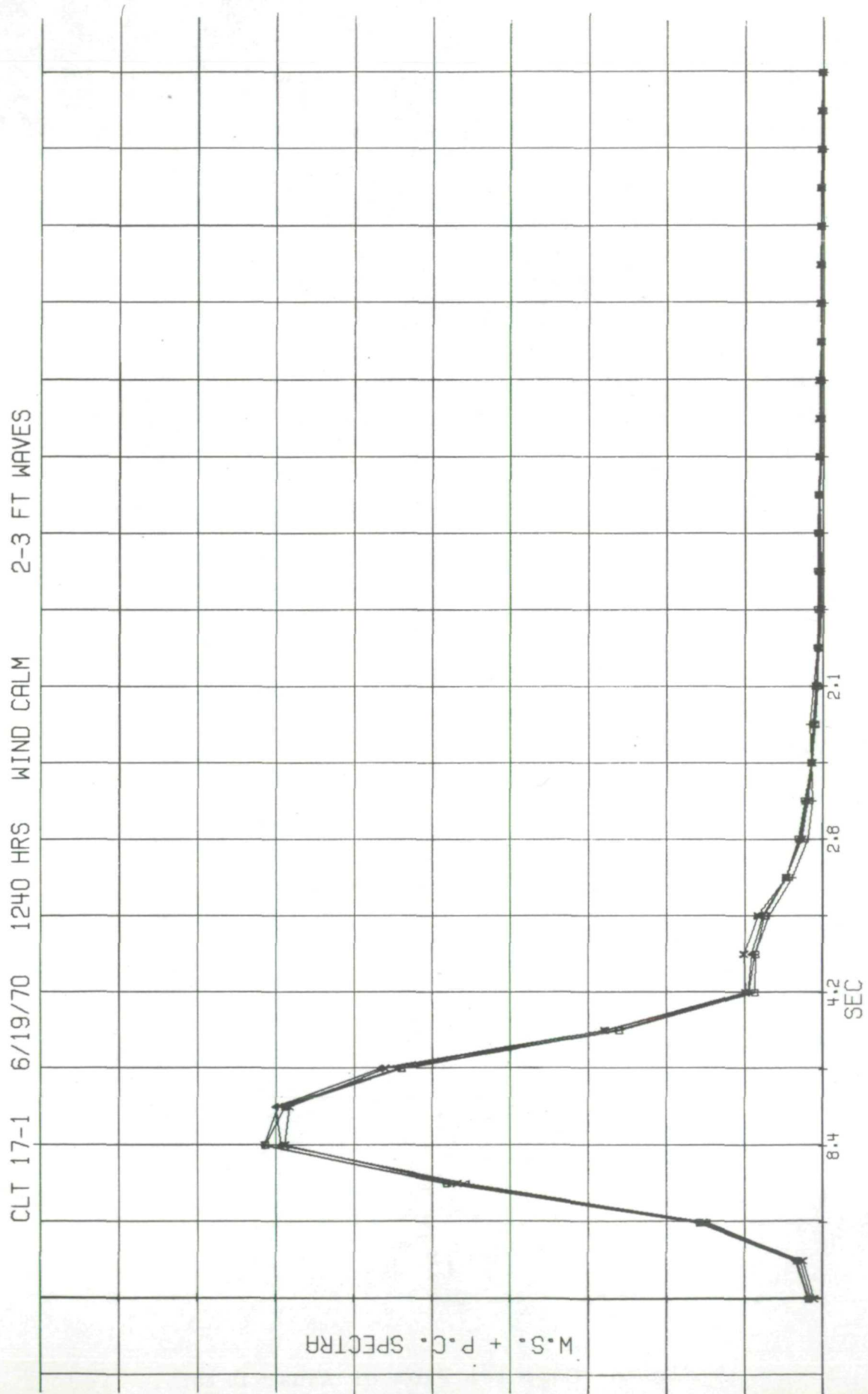


Fig. 7 Power Spectra of Radar and Wave Poles

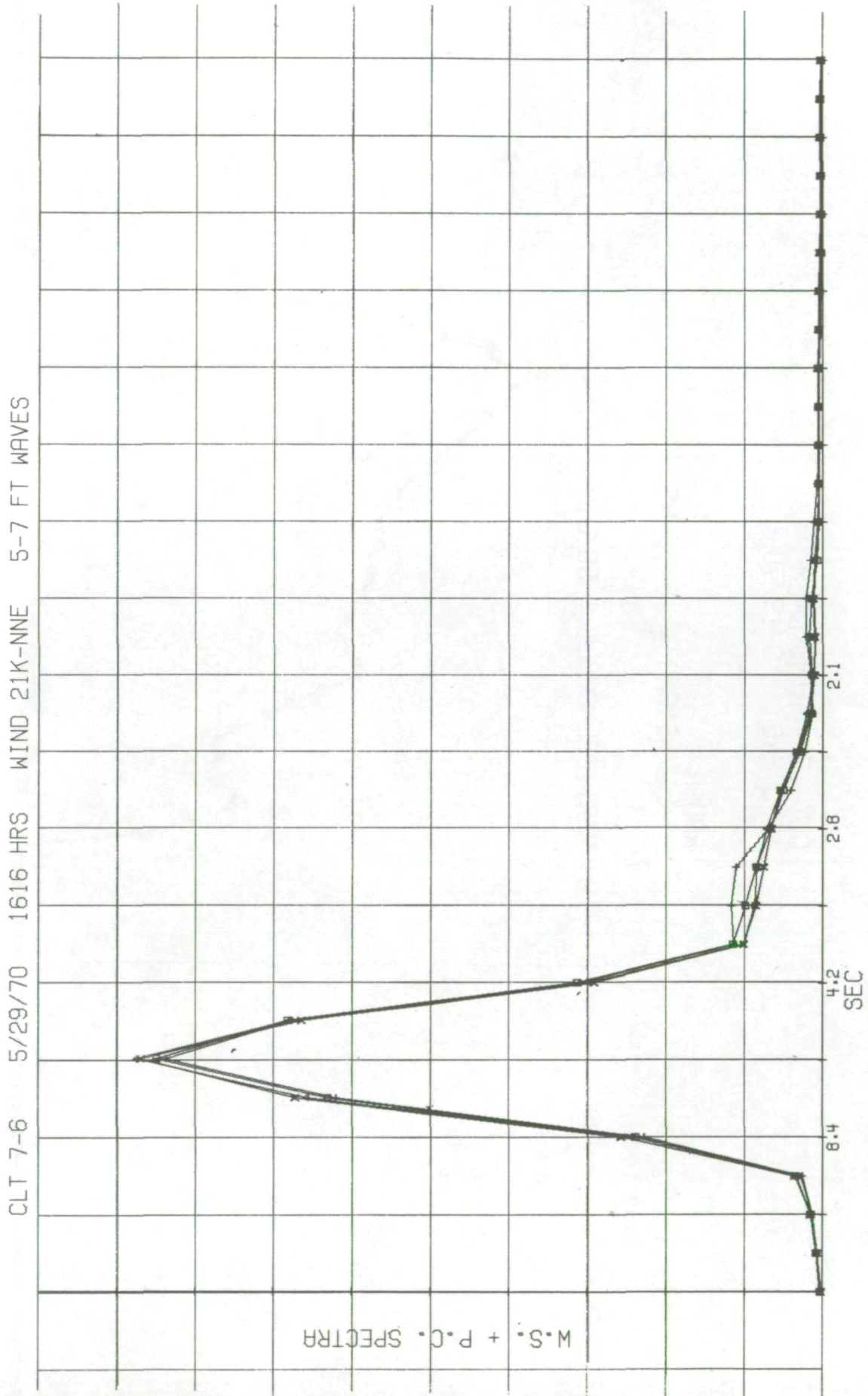


Fig. 8 Power Spectra of Radar and Wave Poles

CLT-17 WIND CALM
1240 HRS 6/19/70

RADAR 2.*SIGMA = 3.46 NS

VERTICAL SCALE = 50/DIV

16 20 24 28 32 36 40

NANO-SEC

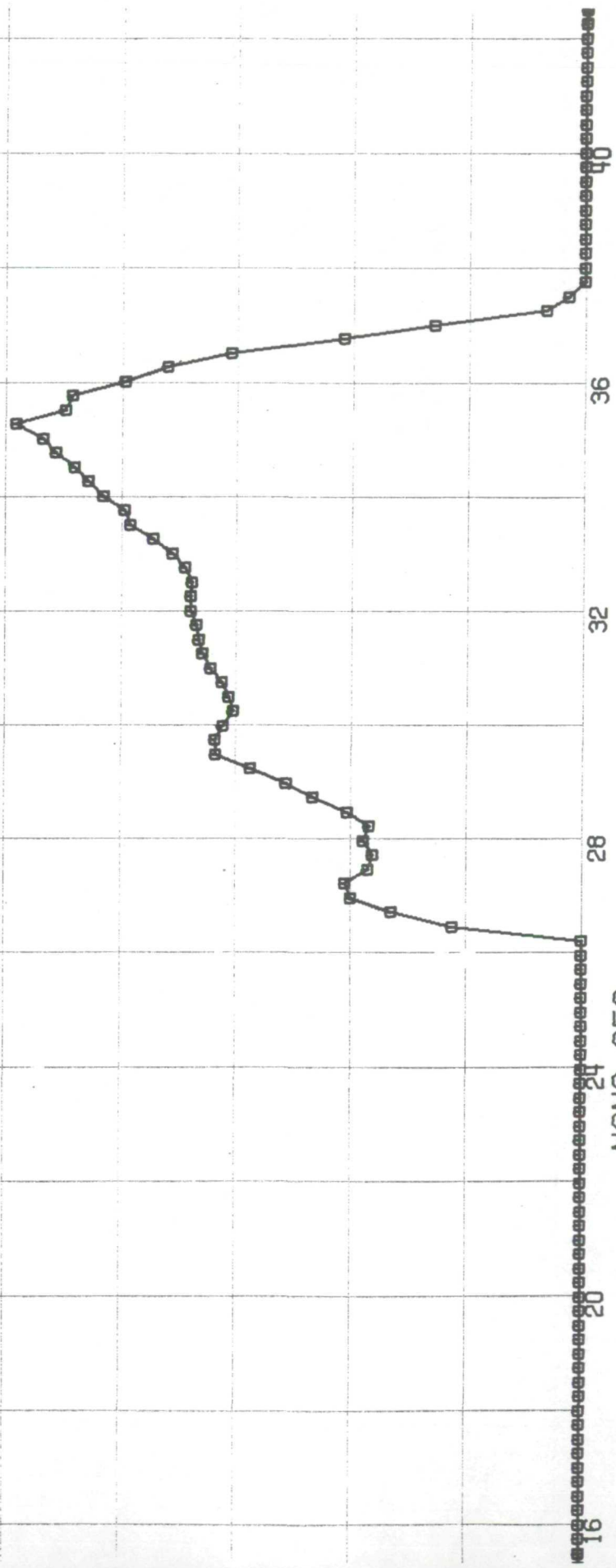


Fig. 9 Reflected Power vs Wave Depth



CLT-7 WIND 21K-NNE
1600 HRS 5/29/70

RADAR 2.*SIGMA = 5.40 NS

VERTICAL SCALE = 50/DIV

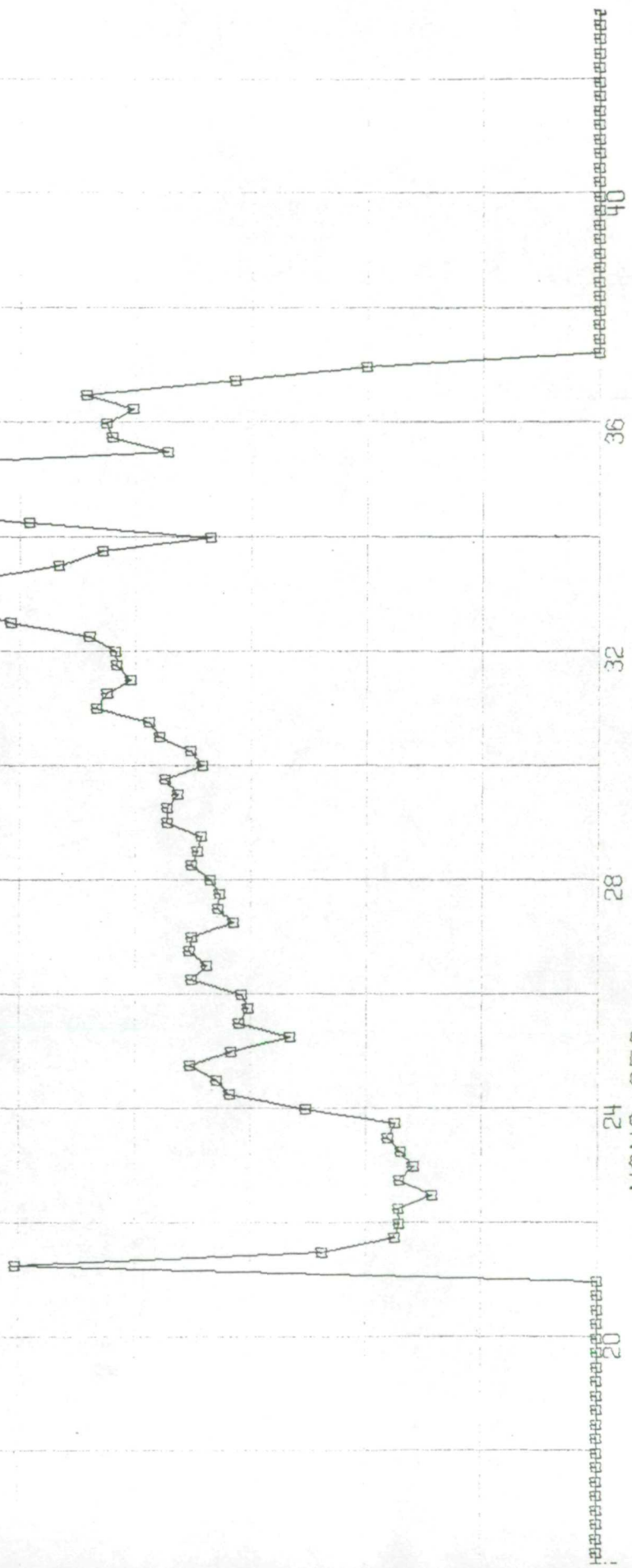


Fig. 10 Reflected Power vs Wave Depth

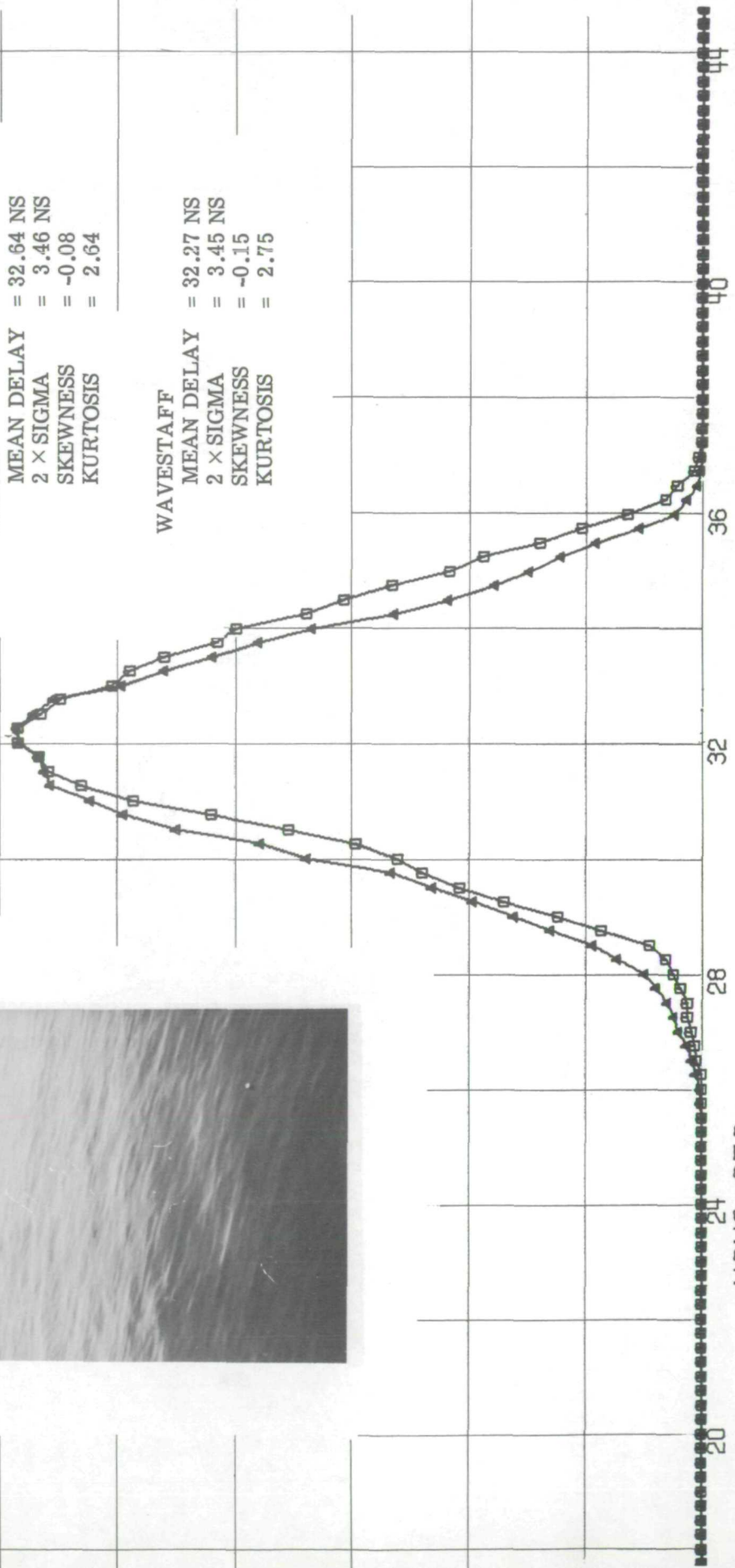
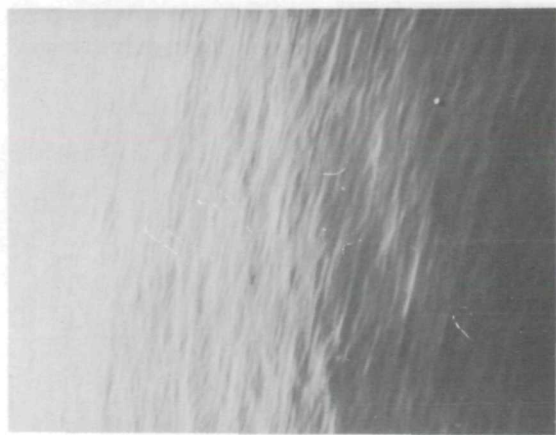
CLT-17 WIND CALM
1240 HRS 6/19/70

RADAR

MEAN DELAY = 32.64 NS
2 x SIGMA = 3.46 NS
SKEWNESS = -0.08
KURTOSIS = 2.64

WAVESTAFF

MEAN DELAY = 32.27 NS
2 x SIGMA = 3.45 NS
SKEWNESS = -0.15
KURTOSIS = 2.75



NANO-SEC



Fig. 11 Equivalent Impulse Response



CLT-7 WIND 21K-NNE
1600 HRS 5/29/70

RADAR

MEAN DELAY = 29.36 NS
2 x SIGMA = 5.40 NS
SKEWNESS = -0.06
KURTOSIS = 2.95

WAVESTAFF Δ

MEAN DELAY = 28.8 NS
2 x SIGMA = 5.84 NS
SKEWNESS = -0.19
KURTOSIS = 3.08

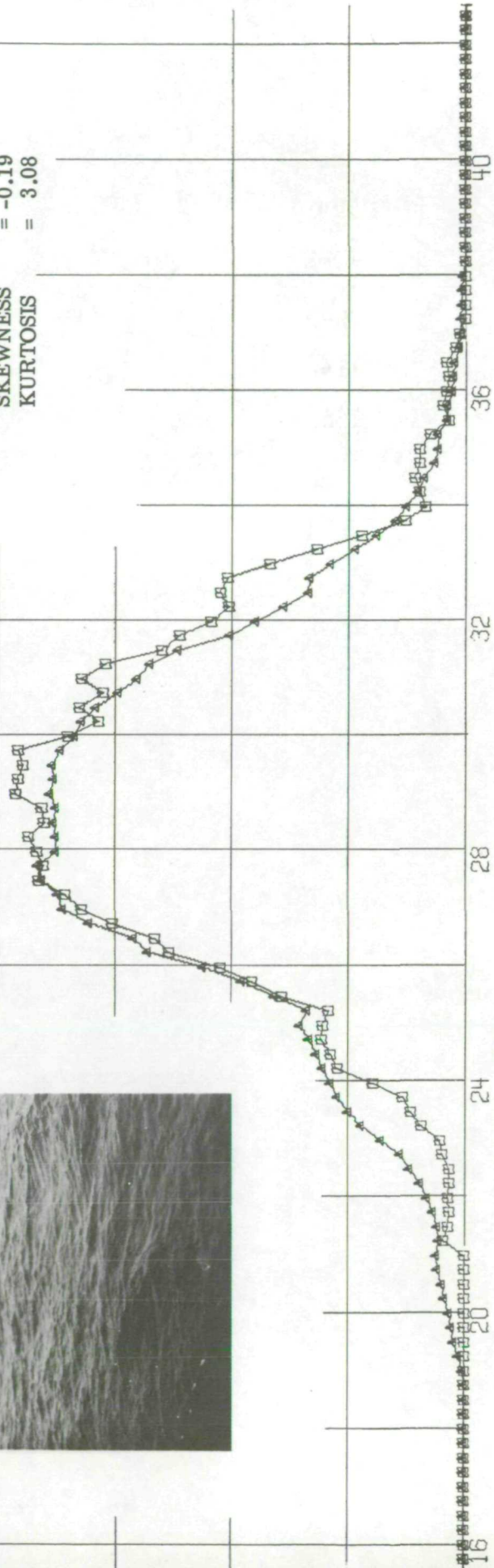
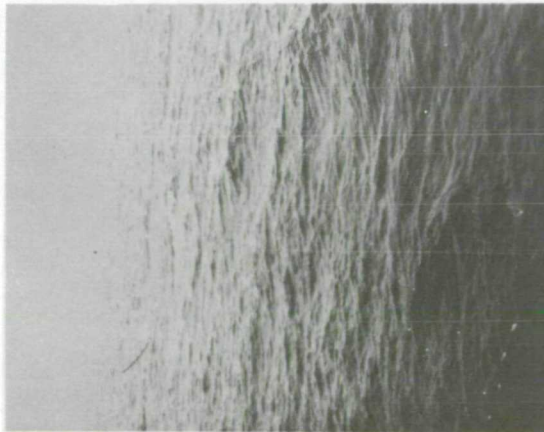


Fig. 12 Equivalent Impulse Response

PASSIVE MICROWAVE STUDIES

by

James P. Hollinger
E. O. Hulburt Center for Space Research
Naval Research Laboratory
Washington, D. C. 20390

INTRODUCTION

The microwave oceanography project is supported by the Spacecraft Oceanography Project Office (SPOC) of the U. S. Naval Oceanographic Office. The objective is to determine, through a measurement program, the optimum system parameters, measurement techniques and understanding of physical phenomena to enable unambiguous all-weather determination of the sea surface properties of sea roughness, surface wind fields, temperature, salinity, sea ice, and pollution by means of remote passive microwave sensing from a satellite. The program is primarily concerned with aircraft-borne observations; however, extensive measurements have also been made from a fixed ocean platform. Both platforms have their own distinct advantages and complimentary information may be obtained by utilizing the special characteristics of each. The aircraft program will be discussed first, and then the results of observations from Argus Island tower will be described.

AIRCRAFT MEASUREMENT PROGRAM

All of our aircraft measurements have been made with the multifrequency microwave radiometer (MFMR) system aboard the NASA MSC P-3 aircraft. The aircraft platform has the advantages, compared to near surface measurements, of spatial resolutions, data acquisition rates, and atmospheric conditions more nearly comparable to those encountered from a satellite. In addition, these properties may be varied to some extent by adjusting the aircraft altitude and the aircraft allows a wide range of sea conditions to be pursued. Since the Earth Resources Review last year, we have participated in four missions. Mission 113 over the Gulf of Mexico in November 1969 was flown primarily to evaluate the MFMR, which had just

been installed in the P-3, and to set up procedures and techniques for the first Joint Ocean Surface Study (JOSS I) as well as to obtain some preliminary sea state data. Extensive sea state measurements were made during Mission 119 off Bermuda in January 1970 as part of JOSS I. Sea ice observations were made as part of Mission 126 off Alaska in April 1970 and salinity effects were studied in the Columbia River plume in August 1970 in connection with Mission 140. Good data were obtained from all of these missions except Mission 126 when poor weather prevented flights over the desired ice conditions. The data from these missions are very nearly reduced but are not yet in final form for analysis and it is not possible to report the results at this meeting. We have worked closely with and had excellent cooperation from the Earth Resources Division in the testing and calibration of the MFMR and in preparing the computer reduction programs. We hope to have the final results in the very near future. In fact a large measure of our program next year will be the analysis and interpretation of the MFMR data taken to date.

TOWER MEASUREMENT PROGRAM

OBJECTIVE

The tower measurements were undertaken to investigate the effects of sea state on the microwave brightness temperature of the sea surface. The fixed ocean platform provides the advantages of high spatial resolution on the sea surface, excellent ground truth, and a relative ease of radiometer calibration and determination of antenna characteristics as compared to an aircraft platform. In addition, there is no correction necessary for radome or atmospheric loss between the antenna and the sea. The microwave brightness temperature dependence on sea state (wind speed) arises from two effects. The first effect results from the increasing roughness of the compact water surface and the second effect from the increasing coverage of white caps and sea foam with increasing wind speed. Although both are properly termed roughness effects, the first will be referred to as the surface roughness effect, and the second as the sea foam effect. The high spatial resolution of the sea surface available from the ocean tower allows these two effects to be studied separately.

Surface roughness has been investigated theoretically using a geometric optics model (1) based on the sea surface slope distribution of Cox and Munk (2) and using a physical optics model (3) which depends upon the correlation function of the surface heights. Multiple-scatter and shadowing effects which become important at large angles of incidence have been investigated using a one dimensional geometric optics model (4). The very high microwave brightness temperature of sea foam compared to the average sea surface, which results in the sea foam effect, was first suggested by Williams (5) and has been supported theoretically on the basis of a physical model for foam (6). Measurements of the microwave brightness temperature of the sea surface (7), (8), (9), (10) indicate a dependence on surface roughness and sea foam which is correlated with wind speed. However more measurements are needed over a wide range of sea conditions with accompanying ground truth and as a function of the observational parameters of frequency, polarization, and incidence angle to understand and interpret the microwave emission of the sea in terms of the properties of the sea surface.

OBSERVATIONS

The measurements to be described were made from Argus Island tower at 1.41, 8.36, and 19.34 GHz in March 1970. Also included are the results of observations at 8.36 and 19.34 GHz made in March-April 1969 (8). Argus Island is located approximately 45 km southwest of Bermuda in 60 meters of water. Each microwave radiometer consists of a parabolic antenna and linearly-polarized feed system followed by a conventional Dicke-type crystal-mixer superheterodyne receiver. The Dicke-switch alternately connects the receiver input to the antenna and to an ambient matched waveguide termination whose temperature is accurately known to allow the absolute antenna temperature of the incident linearly-polarized radiation to be measured. Since the antennas can be rotated about their electrical axes, any plane of linearly polarization may be measured. In practice, the vertical and horizontal components were measured. The rms noise output fluctuations with the 1-sec integration time constant used at 1.41, 8.36, and 19.34 GHz are respectively $1/2$, $1/4$, and $1/2^\circ\text{K}$ and half-power beamwidths are 4.7, 3.4, and 2.7 degrees; this provides a resolution on the sea surface at nadir of about 2.2, 1.2, and 0.9 meters.

Average antenna temperatures were measured by integrating the radiometer output, as successive waves passed through the beam, until a stable value was obtained, usually one to two minutes. Measurements were made at a series of incremented incidence angles. Increments of 5 or 10 degrees were chosen depending on the rate of change of antenna temperature with incidence angle. The relatively high microwave brightness temperature of sea foam compared to the general surface made it easy to recognize the signal produced by a white cap or foam patch of size comparable to or larger than the spatial resolution on the sea surface. These white caps were excluded from the antenna temperature average. Although very thin or small patches could not be individually recognized and removed, it is believed that the majority of white caps were eliminated and that the measured antenna temperature is primarily due to surface roughness effects.

The atmospheric opacity at the time of each sea measurement was determined by atmospheric emission measurements between the zenith and the horizon (11). The measured antenna temperatures were corrected for spurious radiation entering the side and back lobes of the antenna and a partial correction for sky radiation reflected from the sea was made to obtain the brightness temperature of the sea averaged over the main beam of the antenna. In order to correct completely for reflected sky radiation, the differential scattering coefficients of the sea surface must be known (12). Since they are not known, a "first order" correction was made using the average measured emissivity of the sea to obtain the sea reflectivity and assuming specular reflection of the sky radiation. This correction removes the bulk of the reflected sky radiation. However, it is only accurate for smooth seas and becomes poorer as the sea roughens and large angle scattering increases. It also becomes progressively worse at larger incidence angles where the reflected sky radiation is largest and multiple-reflection and shadowing are most severe. Therefore the measured brightness temperature contains a small residual reflected sky component which is dependent upon the atmospheric opacity and sea surface roughness. The absolute errors in antenna temperature and the relative errors in brightness temperature are about $\pm 2^{\circ}\text{K}$. The absolute errors in brightness temperature are about 5 to 10 percent.

The sea states encountered during the measurements ranged from calm to wind speeds of nearly 15 m/sec and

significant wave heights of from 1.2 to 2.3 meters. The sea was never specular nor fully developed. Swell was present even for no wind. In one 24-hour period, the wind direction moved around the compass as the wind speed changed from calm to 14 m/sec. The wind speeds were recorded at a height of 43.3 meters above the sea surface. The sea temperature was $291^{\circ} \pm 1^{\circ}\text{K}$ and the salinity $35^{\circ}/_{\text{oo}} \pm 1^{\circ}/_{\text{oo}}$ for all the observations.

RESULTS AND DISCUSSION

To define the change of brightness temperature with incidence angle and with sea conditions, two groups of data at the upper and lower ends of the wind speeds encountered were selected and averaged together. The two groups represent average wind speeds of 0.5 and 13.5 m/sec. No wind speed for data runs used in either group differs from the average for the group by more than 1 m/sec. Figure 1 shows the brightness temperature of the vertical and horizontal components for these two groups at 1.41, 8.36, and 19.34 GHz as a function of incidence angle. Also shown for comparison purposes are the brightness temperatures calculated for wind speeds of 0 and 15 m/sec using the theoretical geometric optics model developed by Stogryn (1). The dielectric constant of sea water used in the calculations is based on the data of Saxton and Lane (13) and the sky opacity used is the average of the values determined at the time of the observations. The calm sea contribution to the reflected sky radiation has been removed in order that the calculations most nearly correspond to the measured brightness temperatures. The data show that the vertical component is independent of wind speed in the region of 55 degrees incidence angle and increases below and decreases above this angle with increasing wind speed. The horizontal component increases with wind speed over the range of incidence angle from 20 to 70 degrees with a slightly greater increase at the larger incidence angles. The wind speed dependence of the horizontal component generally is greater than that of the vertical component. There is a marked decrease in wind speed dependence with decreasing observational frequency. Except for slight shifts in absolute level which are probably due to errors in absolute calibration, the data is in qualitative agreement with the theoretical calculations. The two biggest differences between the calculations and the measurements are that the theory predicts very little dependence on

observational frequency and a much smaller wind speed dependence of the horizontal component at small incidence angles. This later discrepancy was first pointed out by Nordberg et al. (7) and indicated by previous measurements (8). The failure of the geometric optics model to account for the observational frequency dependence results from the fact that only the dielectric constant of the sea water and the atmospheric opacity are frequency dependent in the model and they primarily affect only the absolute level.

Figure 2 shows the individual measurements of the vertical and horizontal components and the percentage polarization, defined as the ratio of the difference of these two components to their sum, at 55 degrees incidence angle as a function of wind speed. The solid lines are linear least-square solutions fitted to the data. As before, the vertical component is seen to be independent of wind speed and the horizontal component shows a marked decrease in wind speed dependence with decreasing observational frequency. The dependence at 1.41 GHz is only about 1/3 of its value at 19.34 GHz.

To summarize the measurements for all incidence angles most concisely least-square straight lines have been fitted to the data at each incidence angle and the slopes of the lines plotted versus incidence angle in Figure 3. The dotted lines indicate the error in the slope determination. The wind speed independence of the vertical component in the region of 55 degrees incidence angle at all frequencies and the decrease in wind speed dependence of the horizontal component with decreasing incidence angle are apparent. The percentage polarization is dependent on sea surface roughness; decreasing with increasing wind speed. It has the desirable advantage for a spacecraft-borne sensor that it is practically independent of errors in absolute calibration.

Because the atmospheric opacity decreases with decreasing frequency and the measured brightness temperature contains an atmospheric opacity dependent sky reflection component, some decrease in the wind speed dependence of the brightness temperature with frequency is to be expected. In order to estimate what fraction is due to changes in the effective emissivity of the sea and what is due to variations in the reflected sky radiation, the differential scattering coefficients of the sea surface were calculated using the geometric optics model developed by Stogryn (1). This model was chosen because it explicitly contains the wind speed

dependence through the Cox and Munk (2) sea surface slope distribution and is in rough agreement with the data at larger incidence angles. In the calculations the average of the opacities determined during the observations of 0.009, 0.017, and 0.069 nepers at 1.41, 8.36, and 19.34 GHz respectively were used. The range in opacities during the observations was negligible at 1.41 GHz and $\pm 17\%$ and $\pm 33\%$ at 8.36 and 19.34 GHz respectively. These calculations of the differential change in horizontal brightness temperature at 55 degrees incidence angle as a function of wind speed are given in Figure 4. The upper curve is the sum of the calculated wind speed dependence of the radiation emitted by the sea and the wind speed dependent part of the reflected sky radiation. The crosshatched area represents the wind speed dependent reflected sky component. The measured values of the horizontal brightness temperature at 55 degrees incidence angle expressed as differentials above the zero wind speed intercept of the least square line given in Figure 2 are also shown. The calculated sky component is, as expected, greater at higher frequencies. But even at 19.34 GHz, except at low wind speeds, the emitted component is dominant. Thus the geometric optics model indicates that the observed dependence of microwave brightness temperature on wind speed is primarily due to changes in the effective emissivity of the sea surface. The exact separation of the emitted and reflected components is model dependent and a definitive conclusion is not possible until a fully acceptable theory is developed. Depending upon which component is dominant, an observational frequency could be chosen to maximize the wind speed dependent signal. In either case, for remote sensing of sea state, the atmospheric opacity would have to be determined to some degree to allow the received signal to be corrected for the wind speed independent part of reflected sky radiation and the effects of the atmosphere between the sensor and the sea.

The measurements shown in Figure 4 are in fair agreement with the model at 19.34 GHz but the agreement is progressively worse at the two lower frequencies. Since the model calculations depend on the mean square slope of the sea surface, the slope of the calculated curves would be reduced by choosing a smaller value than that given by Cox and Munk. A reasonable fit to the measurements is obtained if mean square slopes of about $1/3$, $1/2$, and $2/3$ of the mean square slope given by Cox and Munk are used at 1.41, 8.36, and 19.34 GHz respectively. Cox and Munk found that the presence of an oil slick reduced the mean

square slope with respect to a clean surface by a factor of two or three which is comparable to the reduction from 19.34 GHz to 1.41 GHz. In addition they calculated (14) that an oil slick damped waves of 0.3 m wavelength by a factor of 10 and that waves shorter than this were essentially eliminated. Thus a possible interpretation of the reduction of mean square slope with decreasing frequency required to fit the observations is that waves shorter than the observational wavelength are unimportant in determining the microwave properties of the sea surface. The adjustment of mean square slope in Stogryn's geometric optics model to fit the observations is analogous to Wright's (15) use of steeper surface tilts with increasing frequency to interpret radar backscatter observations in terms of Bragg scattering. In addition the persistence of the wind speed dependence of the brightness temperature over arbitrary wind and sea directions and wind duration and fetch, as well as the relatively small variation in significant wave height during the observations, implies a close coupling between wind speed and the sea roughness features controlling the microwave properties. This indicates that the very long waves are not of primary importance in determining the microwave properties of the sea. Certainly a frequency dependent model is required to explain the microwave brightness temperature of the rough sea surface.

CONCLUSIONS

Observations of the microwave brightness temperature of the sea show a definite dependence on wind speed. This dependence is due to roughness effects of the compact surface associated with wind-driven waves. The wind speed dependence decreases with observational frequency and any theoretical model used to interpret the microwave characteristics of the sea must be frequency dependent. The frequency dependence may be interpreted on the basis of a geometric optics model (1) as a relative unimportance of surface waves shorter than the observational wavelength in determining the microwave properties of the sea surface.

Surface roughness effects will dominate at the lower wind speeds. But due to the increasing prevalence of sea foam with increasing sea state (16) and the high microwave brightness temperature of foam, the microwave characteristics of the sea will be determined by sea foam at very

high wind speeds (9), (10). The transition wind speed between the two effects is not known but will probably lie in the region between 10 and 15 m/sec.

REFERENCES

- (1) Stogryn, A. IEEE Trans. Antennas and Propagation, vol. AP-15, pp. 278-286, March 1967.
- (2) Cox, C. and Munk, W. J. Opt. Soc. Am., vol. 44, pp. 838-850, November 1954.
- (3) Ulaby, F. T. and Fung, A. K. Southwest IEEE Conf. Proc., pp. 436-440, April 1970.
- (4) Lynch, P. J. and Wagner, R. J. J. Math. Phys., vol. 11, pp. 3032-3042, October 1970.
- (5) Williams, G. F., Jr. J. Geophys. Res., vol. 74, pp. 4591-4594, August 20, 1969.
- (6) Droppleman, J. D. J. Geophys. Res., vol. 75, pp. 696-698, January 20, 1970.
- (7) Nordberg, W., Conaway, J., and Thaddeus, P. Q. J. Royal Met. Soc., vol. 95, pp. 408-413, April 1969.
- (8) Hollinger, J. P. J. Geophys. Res., vol. 75, pp. 5209-5213, September 20, 1970.
- (9) Ross, D. B., Cardone, V., and Conaway, J. IEEE Trans. Geoscience and Electronics, vol. GE-8, (in press) October 1970.
- (10) Nordberg, W., Conaway, J., Ross, D. B., and Wilheit, T. J. Atmos. Sci. (in press).
- (11) Dicke, R. H., Beringer, R., Kyhl, R. L., and Vane, A. B. Phys. Rev., vol. 70, pp. 340-348, September 1 and 15, 1946.
- (12) Peake, W. H. IRE Trans. Antennas and Propagation (Special Suppl.), vol. AP-7, pp. S324-S329, December 1959.

- (13) Saxton, J. A. and Lane, J. A. Wireless Engineer, vol. 29, London: Dorset House, pp. 269-275, October 1952.
- (14) Cox, C. and Munk, W. J. Marine Res., vol. 13, pp. 198-227, 1954.
- (15) Wright, J. W. IEEE Trans. Antennas and Propagation, vol. AP-16, pp. 217-223, March 1968.
- (16) Cardone, V. J. Geophysical Science Laboratory, New York University, Report No. TR 69-1, December 1969.

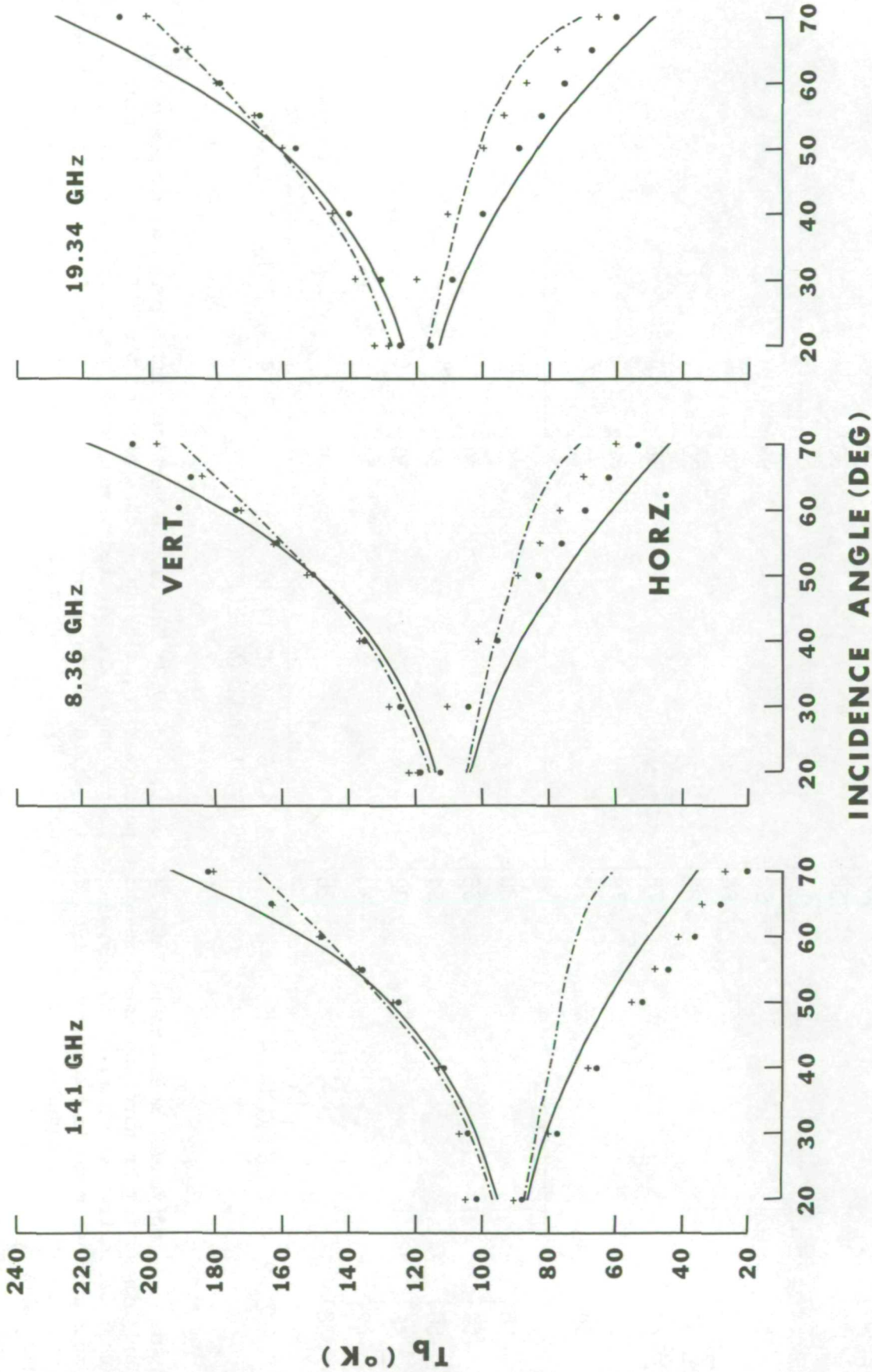


Figure 1.- The vertical and horizontal components of the brightness temperature of the sea at 1.41, 8.36, and 19.34 GHz are plotted as a function of incidence angle for two groups of measurements at the upper and lower ends of the wind speeds encountered. The dots and crosses are average measurements at 0.5 and 13.5 m/sec wind speeds respectively. The solid and dotted curves have been calculated for wind speeds of 0 and 15 m/sec respectively using the geometric optics model developed by Stogryn (1).

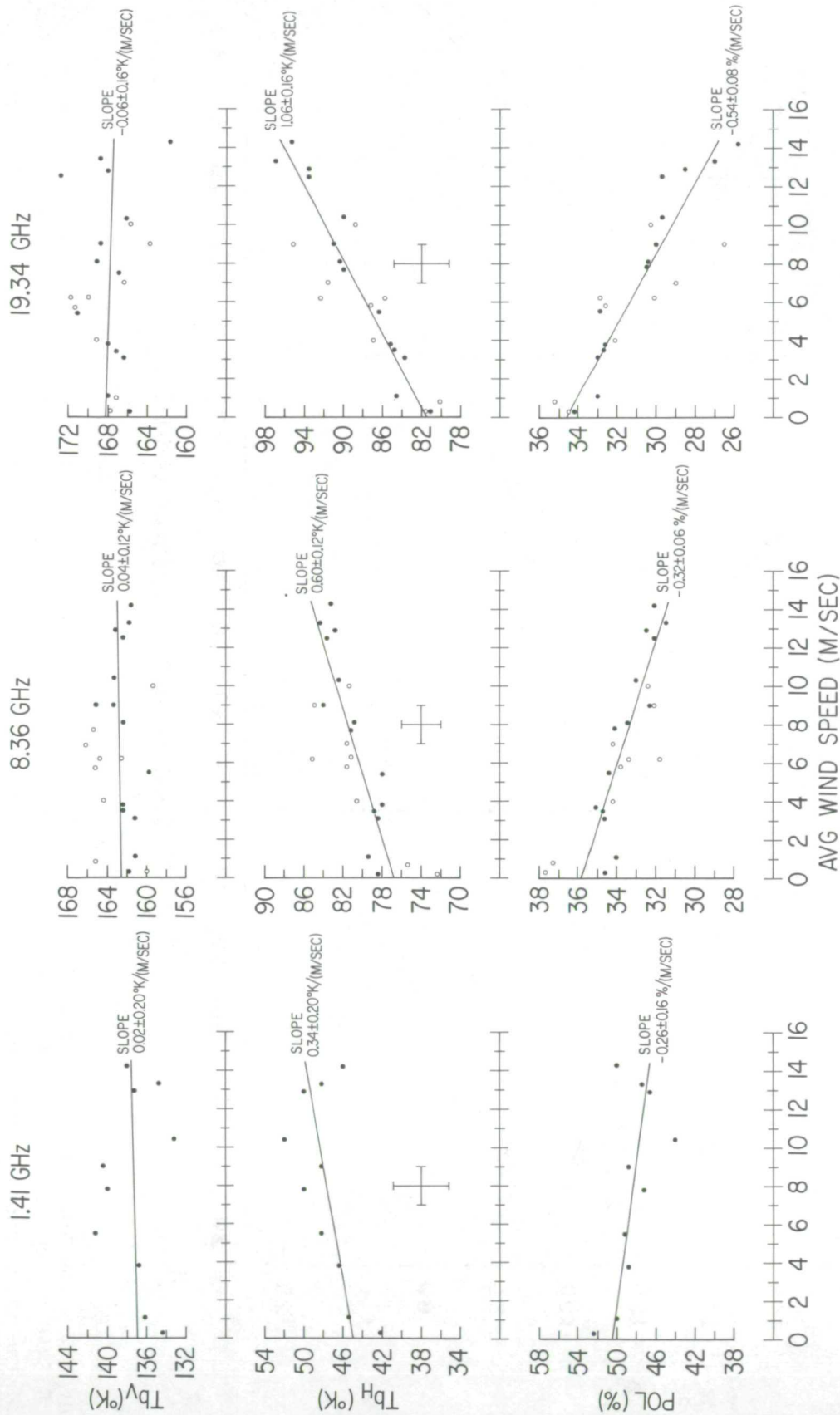


Figure 2.- Individual measurements at 1.41, 8.36, and 19.34 GHz of the vertical and horizontal components of brightness temperature and the percentage polarization, defined as the ratio of the difference of these two components to their sum, at 55 degrees incidence angle are plotted versus wind speed. The open circles are measurements made in March-April 1969 and the solid points observations made in March 1970. The solid lines are linear least-squares solutions to the data. Typical error bars applicable to the individual data points are shown.

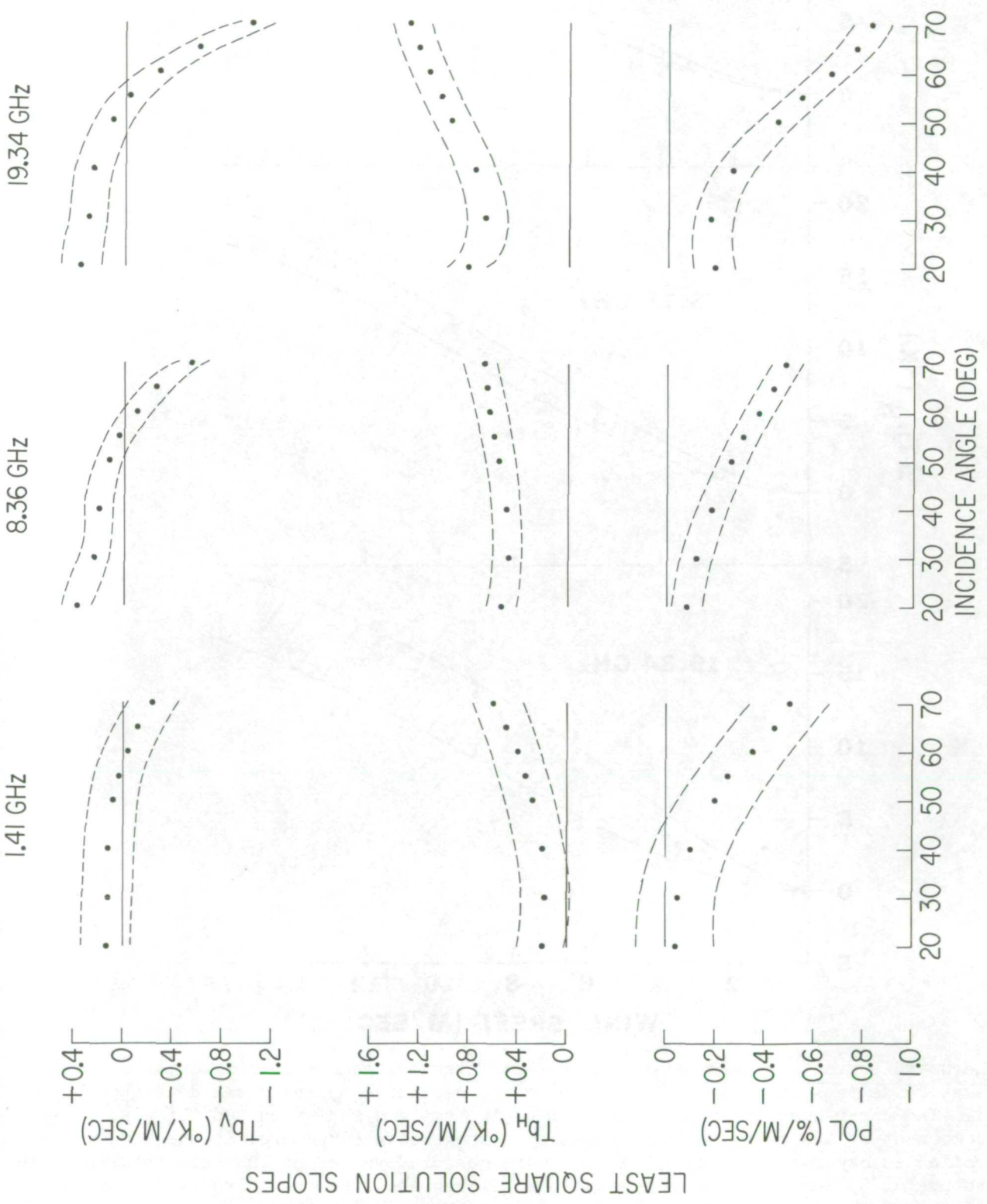


Figure 3.- The slopes of linear least-square solutions fitted to the measurements of the vertical and horizontal components of the brightness temperature and the percentage polarization at each incidence angle are plotted versus incidence angle. The dotted lines indicate the error in the slope determination.

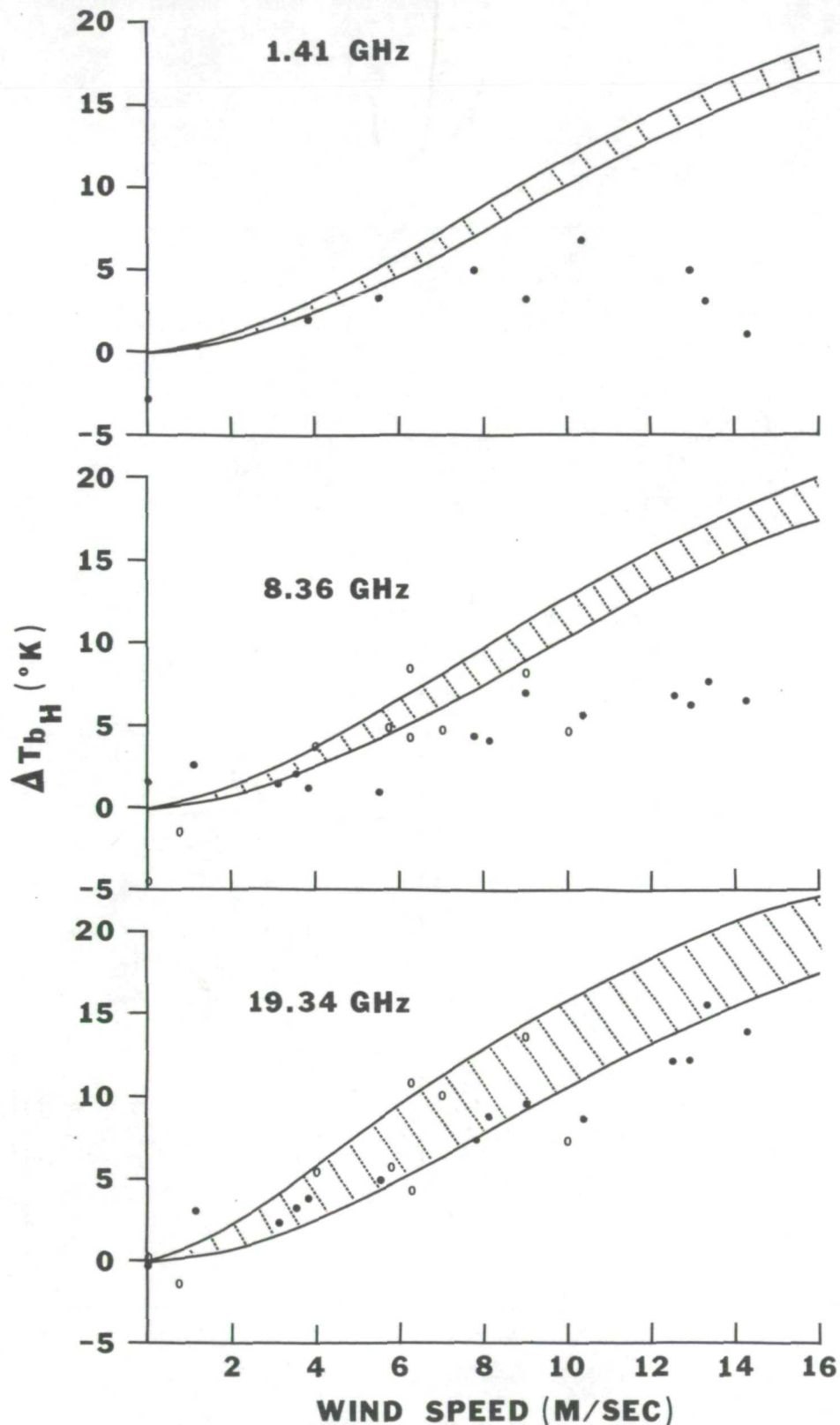


Figure 4.- The solid curves are calculations of the differential change in horizontal brightness temperature at 55 degrees incidence angle based on the geometric optics model developed by Stogryn (1). The upper curve represents the sum of the emitted radiation and the wind speed dependent component of the reflected sky radiation. The crosshatched area is the wind speed dependent reflected sky radiation contribution. The measured values of the horizontal brightness temperature at 55 degrees incidence angle are also shown. The open circles are March-April 1969 data and the solid points are measurements made in March 1970.

THE INTEGRATION OF REMOTE SENSING DATA INTO
GLOBAL WEATHER PREDICTION, WAVE FORECASTING,
AND OCEAN CIRCULATION COMPUTER BASED SYSTEMS

by

Willard J. Pierson, Jr.
Department of Meteorology and Oceanography
School of Engineering and Science
New York University

ABSTRACT

Data from space from infrared imaging systems and SIRS are already providing information of great value in determining sea surface temperature and the atmospheric structure in cloudless areas over the oceans. Although some interpretations differ, it is clear that simultaneous measurements of radar sea return and passive microwave temperature will provide estimates of the wind speed, and perhaps wind direction, over the oceans, especially in cloudless areas, for a wide range of wind speeds. This report is concerned with the problem of integrating the data that would be obtained by a spacecraft, especially one with a combination radar-radiometer, into global analysis procedures for meteorological, wave and oceanographic predictions.

A computer based procedure that defines the mean vector wind as a function of elevation from the sea surface to the gradient wind level using an adequate theory of the structure of the planetary boundary layer has been developed. This procedure employs conventional ship reports, both those transmitted synoptically and those collected climatologically. Examples of the different fields that are produced are given.

A global wave forecasting procedure has been developed. Improved meteorological predictions obtained from the system to be described below would provide high accuracy wave forecasts in the two to four day time frame. Examples of the wave specifications produced for the North Pacific are shown. Data from space can in principle verify the wave heights given by this model as of a given time of observation.

So as to study areas of poor conventional data coverage, the wind analyses have been used to generate data on wind speeds such as would be obtained from a spacecraft. A small fraction of the available ship reports for the North Pacific Ocean have been used to simulate the data density for the South Pacific Ocean. A combined knowledge of low center positions from cloud patterns, coastal and island surface pressures, a few scattered ship reports, and the simulated spacecraft data permit the recovery of the vector wind field over the oceans and the surface atmospheric pressure patterns. The surface pressure pattern is in turn an important parameter in the interpretation of SIRS data. A combined analysis of the surface pressure field and the SIRS data would yield information for the entire atmospheric structure in the initial value problem for a global weather forecast.

The conditions in the interior of the oceans, that is, currents, temperatures, and salinities, are controlled by what happens at the coasts and at the air-sea interface. Fluxes of radiation, heat, momentum and water across the air-sea interface and river runoff and ground water discharge at the coasts can be used as inputs to an ocean circulation model. Presently available data from space and the data that could be obtained by future spacecraft should make it possible both to specify and predict conditions inside the oceans in much the same way as the weather is predicted at present. Efforts to develop such systems are described.

PRESENTLY AVAILABLE DATA FROM SPACE

Quantities of importance to both meteorology and oceanography are presently being sensed from space. Examples are SIRS data, infrared sea surface temperature data, and clouds and cloud patterns. These measurements provide atmospheric soundings, sea surface temperature fields, in which temperature fronts in the oceanic structure can be detected, and information on the location of low centers and fronts.

McClain (1970) has described how sea surface temperature fields can be obtained for four to five day average conditions over both hemispheres, using presently available infrared imagery. The motion of the clouds reveals most of the ocean surface during this period of time, so that realistic fields can be constructed. The sea surface temperature does not vary rapidly so that four or five day averages are permissible for some applications.

The ATS and NOAA imagery of clouds, such as shown in the ATS photograph in Fig. 1, show how fronts and low centers can be located. The surface low pressure centers are undoubtedly located a little to

the east and equatorward of the tips of the spiraling cloud patterns shown in this image. Low centers over the ocean are often missed completely or located poorly on the basis of conventional data, and such images already clearly locate lows as accurately or more accurately, depending on their location, than ship reports. The long arching bands locate fronts. Cold fronts are often carried forward by extrapolation for many days over the ocean on the basis of very poor data in conventional analyses.

SIRS data as described by Wark and Hilleary (1969) can be used to define the constant pressure surfaces for the multi-layer numerical weather prediction models currently in use, as for example described by Shuman and Hovermale (1968). It is important to note that a better definition of the pressure at the surface of the ocean would make the SIRS data even more valuable because it would reduce the error in the specification of the heights of constant pressure surfaces for numerical prediction procedures.

RADAR AND MICROWAVE RESULTS

Results on radar sea return for five different frequencies and on passive microwave emission over a wide range of frequencies lend further support to the concept of using a combination, active radar passive microwave instrument to learn about the winds and waves over the oceans. Ross et al. (1970) have shown that passive microwave emission is sensitive to the presence of whitecaps and that the microwave temperature is related to the foam on the sea surface for high winds and waves. Hollinger (1970) in this third annual review, shows that passive microwave emission at low winds is sensitive both to the structure of the sea surface for high wave numbers and to whitecaps, with the whitecaps being of lesser importance than the sea surface structure for low winds.

The report by Guinard (1970), also in this annual review, indicates that radar sea return is weakly dependent on winds (and waves) for high winds, and that 13.3 gigahertz seems to be a good frequency to study radar sea return. The results of Guinard are not in agreement with the results of Moore and Pierson (1970) for 13.3 gigahertz, where a stronger dependence of radar sea return on wind at higher winds was found, based on a revised analysis of the available radar sea return data from several NASA missions. It is important to note that recent work by Valenzuela et al. (1970), using some of the same radar sea return data reported by Guinard (1970), can be interpreted to indicate a wind speed dependence even for higher winds. Pierson and Moore (1970) have discussed these matters in considerable detail.

The report by Krishen (1970), shows that the problems of calibrating and correcting the 13.3 gigahertz scatterometer of NASA MSC have been solved and that the Mission 119 data and the data from previous missions will form a consistent set of $\sigma^\circ(\theta)$ curves for a wide variety of wind speeds that will be good to $\pm \frac{1}{2}$ db. Some data for Mission 119 has already been prepared and released. A preliminary analysis of these data shows that the value of $\sigma^\circ(\theta)$ agree with previously obtained data, as described by Moore and Pierson (1969), for both the upwind-downwind condition and for the crosswind condition.

One important point about radar sea return is that it is direction dependent with all workers reporting a substantial difference between upwind-downwind and crosswind measurements. In contrast, the passive microwave data do not appear to be sensitive to direction, either the direction of the waves on the sea surface or the direction of the wind that generated the waves. For cloudless conditions, it may be possible to combine sea surface temperature measurements with the infrared, passive microwave emission measurements and radar sea return measurements to obtain both information on the wind speed and partial information on the wind direction.

Radar sea return varies from a maximum in either the upwind or downwind direction to a minimum at the crosswind direction. If the wind speed could be determined from the passive microwave measurements, then if the radar is looking in the upwind or downwind direction, the radar sea return will be a maximum and the wind direction will be known as either the direction χ or the direction $\chi + 180^\circ$. Similarly if the radar sea return is a minimum for the given velocity, then the wind direction is again known with an indeterminacy of 180° . If the radar sea return value lies between the maximum for upwind-downwind and the minimum for crosswind, this implies some angle, say ϕ , between the upwind-downwind direction of the wind and the radar beam. In turn, this implies that there are four possible wind directions that would be given by $\chi \pm \phi$ and $\chi \pm \phi + 180^\circ$. The overall pattern of winds around low centers and a few scattered ship reports should then provide a high quality analysis of the vector wind and the pressures in the planetary boundary layer.

For other conditions such as viewing through stratus clouds with a high liquid water content or rain, the passive microwave signal will be needed to calibrate the radar signal, but it should still be possible to obtain data on the wind speed over the sea surface under these conditions.

COMPUTER BASED PROCEDURES FOR THE USE OF
DATA FROM SPACECRAFT

Once the winds and the pressures in the planetary boundary layer have been determined, they provide the information needed for the planetary boundary layer in numerical weather prediction models. If the pressure field can be determined accurately at the sea surface, it provides a basic input to the SIRS data that then makes it possible to describe the elevations of the constant pressure surfaces throughout the entire troposphere as described by Smith and Fritz (1969). Thus a combination of SIRS data and data from an active radar, passive microwave instrument could almost by itself, along with infrared sea surface temperature data, define the initial value problem for a numerical weather prediction for the entire southern hemisphere, given a few scattered ship reports and cloud imagery. For the northern hemisphere, the spacecraft data will improve the specification of the initial value problem compared to presently available data. This implies improved forecasts of the weather and improved wave forecasts.

It is, however, necessary to develop the computer procedures for utilizing the data that would become available from a combination passive microwave active radar instrument on a spacecraft in a polar orbit. This has been a major effort of our group during the past few years and has resulted in new techniques for analyzing the wind and pressure fields in the planetary boundary layer by means of conventional data. This work has also resulted in the development of a highly superior numerical wave specification and wave forecasting procedure and in the development of a system that simulates the data one might get from a radar radiometer and shows how it can be incorporated into a conventional analysis so as to provide an analysis of the planetary boundary layer in areas of low conventional data coverage. Finally, all of these developments point toward the possibility of computing what occurs and will occur in the interior of the oceans, just as is now done for the atmosphere so as to obtain true oceanographic predictions.

ANALYSIS OF THE PLANETARY BOUNDARY LAYER

If the meteorological and oceanographic data are not obtained in real time, the data density is substantially increased because many ships send in their logs of the weather a month or so late to the National

Weather Records Center. This data base is thus quite complete for most of the Northern Hemisphere, with the amount of ships available, being approximately twice the number that are available on the day-to-day real time teletype services. With this augmented data base, Cardone (1969) has developed a computer based procedure for defining the winds over the surface of the oceans. By means of this analysis, the winds as a function of height from the surface to the gradient wind level can be defined over the Northern Hemisphere oceans. The analysis produces the vector wind at twenty meters, the Monin-Obukov mixing length, the vector friction velocity at the sea surface, which in turn can easily be transformed to the vector wind stress, and the wind at the gradient wind level since the thermal wind is known. Part of the intermediary data needed consists of the air-sea temperature difference field. Examples of the various fields produced by this computer-based procedure are shown in Figs. 2 through 8. Fields such as these are available for the Northern Hemisphere every six hours for more than one year. The printouts are distorted and they should be mentally stretched so that the decimal points would lie on the sides of squares. The title on each figure describes it. The grid is four times the density of the conventional NWP analysis. The analysis has not been smoothed to the same extent as is usual for hemispherical analyses.

The air-sea temperature field as shown in Fig. 6 is an important field for describing the variation of the wind with height in the first meters above the sea surface. This field was obtained from conventional sources. Infrared imagery can supplement the present data sources for determining this field, and SIRS data could give a few data points along the subsatellite track for the air temperature near the sea surface. Above line 105, which is toward the equator, there is not enough information available to specify this field but the values are generally small and have been assumed to be zero.

The field for the inverse Monin-Obukov stability length shown in Fig. 7 provides the required parameter for the computation of the wind profile over the water. If it is zero, the wind profile is logarithmic. Positive values mean a stable atmospheric stratification and a weaker wind stress on the surface for the same wind at anemometer height along with a different variation of the wind with height. Conversely negative values mean an unstable stratification and a greater stress on the sea surface for the same wind at anemometer height.

Fig. 8 shows the magnitude of the friction velocity on the sea surface. The direction of the friction velocity is the same as in Fig. 5 for the wind at 19.5 meters. This stress field, which is directly obtained from this field, is an important field for numerical models of the wind driven ocean circulation.

One of the major purposes of the work by Cardone was to produce wind fields that would yield more accurate wave specifications; that is, a computation given the observed winds for all past times of what the waves are at a particular time, and more accurate wave forecasts, that is, a computation of what the waves will be, given the winds and waves up to a certain time, and forecasts of the winds for a day or so into the future. The growth of the wave spectrum in a given frequency range depends on the wind speed, the atmospheric stability, the fetch, the duration of the wind, and on spectral components that have propagated into an area from other areas. Each of these factors varies from point to point over the ocean. All of these factors are properly included in the wave specification and wave forecasting procedures to be discussed next in this paper in terms of the theories of Phillips (1957), Miles (1957), and Phillips (1966).

There is, however, a part of the wave spectrum that is saturated over a given frequency band. Further input from the wind in adding energy to the wave spectrum for these bands, only causes the production of whitecaps and breakers, so that this energy is eventually dissipated in turbulence. Cardone (1969) developed a way to compute the amount of energy dissipated in this way and called this quantity, the whitecap production index. This whitecap production index was then compared with the measurements of Monahan (1969) and with the measurements in the North Sea described by Ross et al. (1970). The theory for the computation of the whitecap production index is shown in Fig. 9. The computation of this index is a straightforward extension of present results in wave forecasting and specification. There should eventually be a strong interrelationship between the whitecap production index and the work of Austin (1970) as described at this Third Annual Earth Resources Review.

Given the specifications and forecasting procedures to be described in the next section of this paper, and given the sea surface temperature fields as described by McClain, it should not be difficult to remove the effects of fetch, duration, atmospheric stability and sea surface temperature, so as to determine the wind speed simultaneously with radar measurements. This would provide one of the quantities discussed above for obtaining information on the vector wind.

WAVES

Numerical wave specification and numerical wave prediction techniques have been developed. The report by Pierson, Tick and Baer (1966) discusses some of the theory that is used. Bunting (1970) has shown how well the predictions can be expected to verify.

Fig. 10 shows the land-sea table for the North Pacific and Fig. 11 shows the land-sea table for the North Atlantic Ocean that will be used as a basis of printing out such quantities as wave height and wave direction for the hindcasts (and eventually forecasts) that will be produced with this computer program.

The first successful run of this improved and highly sophisticated wave specification and wave forecasting system for the North Pacific was achieved during the week of December 7th, and the week-end of December 12 and 13, 1970. The results, as given in Fig. 12, show what the waves over the North Pacific would have been like if the sea surface had been flat calm and then the winds had started to act on the sea surface and had blown for six hours. After seven more days, or so, the waves over the North Pacific will be quite realistic since the observed winds are used to compute what the waves were like.

The waves are not very high, and the values shown illustrate the problem of start-up time in numerical wave specification models. It is impossible to measure the two dimensional wave spectrum over the whole North Pacific so as to obtain the equivalent of the conditions for a more classical initial value problem. The wave spectra specified by these procedures, after a week or so, given good wind fields, yield significant heights and frequency spectra that verify well against actually measured waves.

It is quite possible that the data from the radar altimeter part of S193 on Skylab A will provide information on wave height that can be compared with the heights predicted by this model. The results of Yaplee et al. (1970) are quite encouraging in this connection as they lend strong support to the assumptions made by Pierson and Mehr (1970) in deriving the theoretical form for an average altimeter pulse being scattered back from the sea surface.

These wave forecasting and wave specification procedures were developed for deep water. Waves near coasts are modified by the effects of refraction over irregular submarine topography. It is important to note here the work of Chao (1970) in which the theory of wave refraction at a caustic was solved and of Chao and Pierson (1970) in which the theory was verified in a wave tank. It should now be possible to predict wave conditions at all important coasts as well as in deep water.

INTEGRATION OF THE DATA FROM A RADAR RADIOMETER INTO A PLANETARY BOUNDARY LAYER ANALYSIS

It is also necessary to develop ways that the data from a radar radiometer can be integrated into conventional data so as to produce useful analyses of the wind and pressure fields in the planetary boundary layer. To study this problem, the data given by the work of Cardone has been assumed to provide an accurate description of the winds over the North Pacific ocean for a particular synoptic map time. Simulated passes of a polar orbiting spacecraft are made over the North Pacific, and it is assumed that the magnitude of the vector wind at 19.5 meters can be determined from the combined radar radiometer data on a grid of points corresponding to repeated cross track scans. This provides a dense field of wind speeds. It is further assumed that the location of low centers can be determined from space photographs of clouds as described above, that conventional coastal data and island data will be available and that a few scattered ship reports will also be available, along with a field of the air-sea temperature difference from, say, SIRS and infrared sea-surface temperature fields. The assumptions simulate what will be available from a combination of spacecraft mounted sensors and conventional data for the Southern Hemisphere, for example, over the South Pacific ocean. Only about twenty or thirty ships from the as many as three hundred to five hundred that actually report for the North Pacific are selected at random from the total list of ships to simulate the Southern Hemisphere conditions.

The results of a computer based procedure developed at New York University by Mr. Leonard Druyan that uses these isolated ships, simulated radar radiometer data reduced to wind magnitudes alone as each grid point, island and coastal data, and cloud data are shown in Fig. 13. The recovery of the pressure field for the limited number of ships used is quite good. Since this figure was prepared added modifications of the computer procedure have led to even better results.

It is planned, once the computer based procedures have been further improved, to compute the pressure fields for a year of data, once per day, so as to produce statistics on how well the system can be expected to operate. The data produced by Cardone, as described above, will also be used to obtain information on the relative frequency of different wind speeds over the Northern Hemisphere oceans, for a further evaluation of the potential accuracies of the proposed radar radiometer system.

Also, the concept that some information on the wind direction can be inferred from the space data has yet to be evaluated in terms

of the use of limited ship data and spacecraft data in the Southern Hemisphere. Limitation of the possible wind directions to either two or four directions at a given point from combined radar radiometer data, can provide enough information when combined with information on the global circulation to define the pressure pattern even more accurately. The simulation described above that uses only wind speed may actually be an overrestriction on the potential system. The root mean square error of the pressure field in Fig. 13 is already low enough to make the pressure field obtained by this method useful in applying SIRS data to the determination of the heights of constant pressure surfaces over the ocean.

PREDICTION OF THE OCEAN CIRCULATION

The time may soon be upon us when it will be necessary to predict conditions inside the ocean, just as weather conditions are now predicted for the atmosphere. The quantities to be predicted at a minimum would be the current speed and direction and the temperature and salinity at a number of levels inside the ocean. The conditions in the interior of the ocean are however, controlled by effects at the ocean atmosphere interface and by runoff at the coasts. Models of the oceans, such as those of Bryan (1969), show clearly that if the fluxes of heat, water, radiation and momentum across the air-sea boundary could be defined over the oceans, and if river runoff could be computed, the motions and conditions in the interior of the ocean would respond realistically to these forcing functions. It would not be necessary to measure the currents, temperatures and salinities in the interior of the ocean in order to predict what goes on in the interior of the ocean, if the conditions at the boundaries are correctly specified throughout past time.

Work toward this goal is also underway. Ways to use space data to compute the solar radiation absorbed at the sea surface are under development and are being correlated with XERB-1 data. The XERB-1 buoy is an experimental buoy located off our east coast that is a prototype of the buoys that may be deployed by the National Data Buoy System of NOAA. There may be many of these buoys deployed in the Northern Hemisphere. They could be the surface truth sites for an eventual combination spacecraft-buoy system. Ways to compute the infrared loss from the sea surface have been developed. The SIRS soundings would be used to define the atmospheric structure over the oceanic points for which the infrared loss would be computed. However, the data density may not be great enough since the method works only along the subsatellite track. The stress fields are known from the work of Cardone, as described above. Other work should make it possible to apply real time forcing boundary

conditions to the finite difference equations of motion for the oceans as given by Friedrich (1970) and Okubo (1970), that will cause a realistic ocean circulation throughout the ocean interior. The motions and conditions in the ocean will then vary in response to the actual weather as it occurred over the ocean surface.

CONCLUSIONS

It seems, therefore, that data from space could play an important role in producing weather forecasts for the Southern Hemisphere of at least the quality now available for the Northern Hemisphere, in producing improved weather forecasts for the Northern Hemisphere by augmenting the data base for the initial value problem in the Northern Hemisphere, in producing forecasts of waves on the global ocean, and in producing forecasts of what is occurring, and will occur in the ocean interior. Some of the necessary computer based procedures for accomplishing these goals have been developed and others are now being developed in our present program.

ACKNOWLEDGEMENTS

The support for most of the research described herein was provided by the Spacecraft Oceanography Project under Contract number N62306-70-A-0075. The work on the prediction of the ocean circulation and on the verification of wave refraction theory at a caustic was supported by the Office of Naval Research under Contract number NO0014-67-A-0467-0012, and the development of the theory of wave refraction was supported by NAVOCEANO under Contract number N62306-70-A-0075. This is Contribution No. 98 of the Geophysical Sciences Laboratory, Department of Meteorology and Oceanography, New York University, Bronx, N. Y.

REFERENCES

- Austin, R. W. (1970): Whitecap coverage from aerial photography. Proceedings of the Third Annual Earth Resources Program Review.
- Bryan, K. (1969): A numerical method for the study of the circulation of the world ocean. J. of Comp. Phys. 4(3), 347-376.
- Bunting, D. C. (1970): Evaluating forecasts of ocean wave spectra. J. Geophys. Res., 75(21) 4131-4143.
- Cardone, V. J. (1969): Specification of the wind field distribution in the marine boundary layer for wave forecasting. Geophysical Sciences Laboratory, New York University No. TR-69-1, December 1969.
- Chao, Y. -Y. (1970): The theory of wave refraction in shoaling water including the effects of caustics and the spherical earth. New York University Geophysical Sciences Laboratory TR-70-7.
- Chao, Y. -Y, and W. J. Pierson (1970): An experimental study of gravity wave behavior near a straight caustic. New York University, Geophysical Sciences Laboratory TR-70-17.
- Friedrich, H. (1970): Preliminary results from a numerical multi-layer model for the circulation of the North Atlantic. Deutsch. Hydrogr. Z. [To appear shortly.]
- Guinard, N. W. (1970): The variation of radar cross section with wind. Proc. Third Annual Earth Resources Program Review.
- Hollinger, J. P. (1970): Passive microwave studies. Proceedings of the Third Annual Earth Resources Program Review.
- Krishen, K. (1970): Results of scatterometer systems analysis for NASA MSC Earth observations sensor evaluation program. Proceedings of the Third Annual Earth Resources Program Review.
- McClain, E. P. (1970): Oceanography studies under the Earth Resources Survey Program. Proceedings of the Third Annual Earth Resources Program Review.

- Miles, J. W. (1957): On the generation of surface waves by shear flow. J. Fluid Mech., Part 1, Vol. 3, 185-204, 1957; Part 2, Vol. 6, 568-582, 1959; Part 3, Vol. 6, 584-598, 1959; Part 4, Vol. 12, 433-448, 1962.
- Monahan, E. C. (1969): Fresh water whitecaps. J. A. S. 26(5) 1026-1029.
- Moore, R. K., and W. J. Pierson (1970): World-wide oceanic wind and wave predictions using a satellite radar radiometer. AIAA Earth Resources Observations and Information Systems Meeting, AIAA Paper No. 70-310.
- Okubo, A. (1970): Some aspects of the New York University mathematical model of the ocean for oceanographic forecasting. New York University Geophysical Sciences Laboratory TR-70-13.
- Phillips, O. M. (1957): On the generation of waves by turbulent wind. J. Fluid Mech. 2, 414-445.
- Phillips, O. M. (1966): The Dynamics of the Upper Ocean. Cambridge University Press.
- Pierson, W. J., L. J. Tick, and L. Baer (1966): Computer based procedures for preparing global wave forecasts and wind field analyses capable of using wave data obtained by a spacecraft. Sixth Symposium Naval Hydrodynamics, ACR-136.
- Pierson, W. J., and E. Mehr (1970): The effects of wind waves and swell on the ranging accuracy of a radar altimeter (Part 1). Distributed by NASA Goddard Meeting on GEOS-C.
- Pierson, W. J., and R. K. Moore (1970): Surface weather and wave conditions. Paper presented at "The Ocean World" conference in Japan. Submitted for publication to Space Aeronautics Magazine.
- Ross, D. B., V. Cardone and J. Conaway (1970): Laser and microwave observations of sea surface conditions for fetch limited 35 to 50 knot winds. Microwave Observations of the Ocean Surface. Analysis of the NASA-NAVY Review 11-12 June 1969. To be published by the U. S. Naval Oceanographic Office.
- Shuman, F. C., and J. B. Hovermale (1968): An operational six layer primitive equation model. J. Appl. Meteor., 7(9) 525-547.

Smith, W. L. , and S. Fritz (1969): On the statistical relation between geopotential height and temperature-pressure profiles. National Environmental Satellite Center ESSA Tech. Memo. NESCTM 18.

Valenzuela, G. K. , M. B. Laing, and J. C. Daley (1970): Ocean spectra for the high frequency waves from airborne measurements. Submitted to J. Marine Research.

Wark, D.Q. , and D. Hilleary (1969): Atmospheric temperature: Successful test of remote probing. Science, 165, 1256-1258.

Yaplee, B.S. , A. Shapiro, D.L. Hammond, and E.A. Vliana (1970): Nanosecond radar observations of the ocean surface from a stable platform. Proceedings of the Third Annual Earth Resources Program Review.



Figure 1. ATIS image showing fronts and low centers near spiral cloud bands over the North Atlantic and South Atlantic Oceans.

Wind speed at 19.5 meters in knots for the portion of the expanded (125 x 125) NWP grid system covering the western half of North Pacific Ocean. Asterisks represent land.
Date: 12/1/66 Time: 0000 GMT

33	34	35	36	37	38	39	40	41	42	43	44	45	46	47	48	49	50	51	52	53	54	55	56	57	58	59	60	61	62	63
125	126	127	128	129	130	131	132	133	134	135	136	137	138	139	140	141	142	143	144	145	146	147	148	149	150	151	152	153	154	155
156	157	158	159	160	161	162	163	164	165	166	167	168	169	170	171	172	173	174	175	176	177	178	179	180	181	182	183	184	185	186
187	188	189	190	191	192	193	194	195	196	197	198	199	200	201	202	203	204	205	206	207	208	209	210	211	212	213	214	215	216	217
218	219	220	221	222	223	224	225	226	227	228	229	230	231	232	233	234	235	236	237	238	239	240	241	242	243	244	245	246	247	248
249	250	251	252	253	254	255	256	257	258	259	260	261	262	263	264	265	266	267	268	269	270	271	272	273	274	275	276	277	278	279
280	281	282	283	284	285	286	287	288	289	290	291	292	293	294	295	296	297	298	299	300	301	302	303	304	305	306	307	308	309	310
311	312	313	314	315	316	317	318	319	320	321	322	323	324	325	326	327	328	329	330	331	332	333	334	335	336	337	338	339	340	341
342	343	344	345	346	347	348	349	350	351	352	353	354	355	356	357	358	359	360	361	362	363	364	365	366	367	368	369	370	371	372
373	374	375	376	377	378	379	380	381	382	383	384	385	386	387	388	389	390	391	392	393	394	395	396	397	398	399	400	401	402	403
404	405	406	407	408	409	410	411	412	413	414	415	416	417	418	419	420	421	422	423	424	425	426	427	428	429	430	431	432	433	434
435	436	437	438	439	440	441	442	443	444	445	446	447	448	449	450	451	452	453	454	455	456	457	458	459	460	461	462	463	464	465
466	467	468	469	470	471	472	473	474	475	476	477	478	479	480	481	482	483	484	485	486	487	488	489	490	491	492	493	494	495	496
497	498	499	500	501	502	503	504	505	506	507	508	509	510	511	512	513	514	515	516	517	518	519	520	521	522	523	524	525	526	527
528	529	530	531	532	533	534	535	536	537	538	539	540	541	542	543	544	545	546	547	548	549	550	551	552	553	554	555	556	557	558
559	560	561	562	563	564	565	566	567	568	569	570	571	572	573	574	575	576	577	578	579	580	581	582	583	584	585	586	587	588	589
590	591	592	593	594	595	596	597	598	599	600	601	602	603	604	605	606	607	608	609	610	611	612	613	614	615	616	617	618	619	620
621	622	623	624	625	626	627	628	629	630	631	632	633	634	635	636	637	638	639	640	641	642	643	644	645	646	647	648	649	650	651
652	653	654	655	656	657	658	659	660	661	662	663	664	665	666	667	668	669	670	671	672	673	674	675	676	677	678	679	680	681	682
683	684	685	686	687	688	689	690	691	692	693	694	695	696	697	698	699	700	701	702	703	704	705	706	707	708	709	710	711	712	713
714	715	716	717	718	719	720	721	722	723	724	725	726	727	728	729	730	731	732	733	734	735	736	737	738	739	740	741	742	743	744
745	746	747	748	749	750	751	752	753	754	755	756	757	758	759	760	761	762	763	764	765	766	767	768	769	770	771	772	773	774	775
776	777	778	779	780	781	782	783	784	785	786	787	788	789	790	791	792	793	794	795	796	797	798	799	800	801	802	803	804	805	806
807	808	809	810	811	812	813	814	815	816	817	818	819	820	821	822	823	824	825	826	827	828	829	830	831	832	833	834	835	836	837
838	839	840	841	842	843	844	845	846	847	848	849	850	851	852	853	854	855	856	857	858	859	860	861	862	863	864	865	866	867	868
869	870	871	872	873	874	875	876	877	878	879	880	881	882	883	884	885	886	887	888	889	890	891	892	893	894	895	896	897	898	899
900	901	902	903	904	905	906	907	908	909	910	911	912	913	914	915	916	917	918	919	920	921	922	923	924	925	926	927	928	929	930
931	932	933	934	935	936	937	938	939	940	941	942	943	944	945	946	947	948	949	950	951	952	953	954	955	956	957	958	959	960	961
962	963	964	965	966	967	968	969	970	971	972	973	974	975	976	977	978	979	980	981	982	983	984	985	986	987	988	989	990	991	992
993	994	995	996	997	998	999	1000	1001	1002	1003	1004	1005	1006	1007	1008	1009	1010	1011	1012	1013	1014	1015	1016	1017	1018	1019	1020	1021	1022	1023
1024	1025	1026	1027	1028	1029	1030	1031	1032	1033	1034	1035	1036	1037	1038	1039	1040	1041	1042	1043	1044	1045	1046	1047	1048	1049	1050	1051	1052	1053	1054
1055	1056	1057	1058	1059	1060	1061	1062	1063	1064	1065	1066	1067	1068	1069	1070	1071	1072	1073	1074	1075	1076	1077	1078	1079	1080	1081	1082	1083	1084	1085
1086	1087	1088	1089	1090	1091	1092	1093	1094	1095	1096	1097	1098	1099	1100	1101	1102	1103	1104	1105	1106	1107	1108	1109	1110	1111	1112	1113	1114	1115	1116
1117	1118	1119	1120	1121	1122	1123	1124	1125	1126	1127	1128	1129	1130	1131	1132	1133	1134	1135	1136	1137	1138	1139	1140	1141	1142	1143	1144	1145	1146	1147
1148	1149	1150	1151	1152	1153	1154	1155	1156	1157	1158	1159	1160	1161	1162	1163	1164	1165	1166	1167	1168	1169	1170	1171	1172	1173	1174	1175	1176	1177	1178
1179	1180	1181	1182	1183	1184	1185	1186	1187	1188	1189	1190	1191	1192	1193	1194	1195	1196	1197	1198	1199	1200	1201	1202	1203	1204	1205	1206	1207	1208	1209
1210	1211	1212	1213	1214	1215	1216	1217	1218	1219	1220	1221	1222	1223	1224	1225	1226	1227	1228	1229	1230	1231	1232	1233	1234	1235	1236	1237	1238	1239	1240
1241	1242	1243	1244	1245	1246	1247	1248	1249	1250	1251	1252	1253	1254	1255	1256	1257	1258	1259	1260	1261	1262	1263	1264	1265	1266	1267	1268	1269	1270	1271
1272	1273	1274	1275	1276	1277	1278	1279	1280	1281	1282	1283	1284	1285	1286	1287	1288	1289	1290	1291	1292	1293	1294	1295	1296	1297	1298	1299	1300	1301	1302
1303	1304	1305	1306	1307	1308	1309	1310	1311	1312	1313	1314	1315	1316	1317	1318	1319	1320	1321	1322	1323	1324	1325	1326	1327	1328	1329	1330	1331	1332	1333
1334	1335	1336	1337	1338	1339	1340	1341	1342	1343	1344	1345	1346	1347	1348	1349	1350	1351	1352	1353	1354	1355	1356	1357	1358	1359	1360	1361	1362	1363	1364
1365	1366	1367	1368	1369	1370	1371	1372	1373	1374	1375	1376	1377	1378	1379	1380	1381	1382	1383	1384	1385	1386	1387	1388	1389	1390	1391	1392	1393	1394	1395
1396	1397	1398	1399	1400	1401	1402	1403	1404	1405	1406	1407	1408	1409	1410	1411	1412	1413	1414	1415	1416	1417	1418	1419	1420	1421	1422	1423	1424	1425	1426
1427	1428	1429	1430	1431	1432	1433	1434	1435	1436	1437	1438	1439	1440	1441	1442	1443	1444	1445	1446	1447	1448	1449	1450	1451	1452	1453	1454	1455	1456	1457
1458	1459	1460	1461	1462	1463	1464	1465	1466	1467	1468	1469	1470	1471	1472	1473	1474	1475	1476	1477	1478	1479	1480	1481	1482	1483	1484	1485	1486	1487	1488
1489	1490	1491	1492	1493	1494	1495	1496	1497	1498	1499	1500	1501	1502	1503	1504	1505	1506	1507	1508	1509	1510	1511	1512	1513	1514	1515	1516	1517	1518	1519
1520	1521	1522	1523	1524	1525	1526	1527	1528																						

Air-sea temperature in degrees Celsius for the portion of the expanded (125 x 125) NWP grid covering the western North Pacific Ocean. Asterisks represent land. Date: 12/1/66 Time: 0000 GMT

	53	54	55	56	57	58	59	60	61	62	63
124
123
122
121
120
119
118
117
116
115
114
113
112
111
110
109
108
107
106
105
104
103
102
101
100
99
98
97
96
95
94
93
92
91
90
89
88
87
86
85
84
83
82
81
80
79
78
77
76
75
74
73
72

Figure 6.

NOT REPRODUCIBLE

SPECTRAL GROWTH MODEL (INOUE-CARDONE)

$$\frac{dS(f)}{dt} = \left[A(f, U_{19.5}) + B(f, U_w) \cdot S(f) \right] \left[1 - \left(\frac{S(f)}{S_\infty} \right)^2 \right]$$

where $S(f)$ = spectral intensity at frequency f

A = Phillips Resonance Growth Parameterization

B = Miles-Phillips Instability Growth Parameterization

S_∞ = Pierson-Moskowitz Fully Developed Spectrum

ENERGY DISSIPATED IN BREAKING WAVES

$$E = \rho_w \cdot g \cdot \int_0^\infty B \cdot S \cdot \delta \cdot df$$

where $\delta = 1$ $S = S_\infty$

$\delta = 0$ $S < S_\infty$

FOAM COVER FRESH WATER

$$W_F = -.0185 + .893 \times 10^{-3} \cdot E \text{ (ergs/cm}^2\text{/sec)}$$

SALT WATER EFFECTS

$$W_S = 1.5 \cdot W_F$$

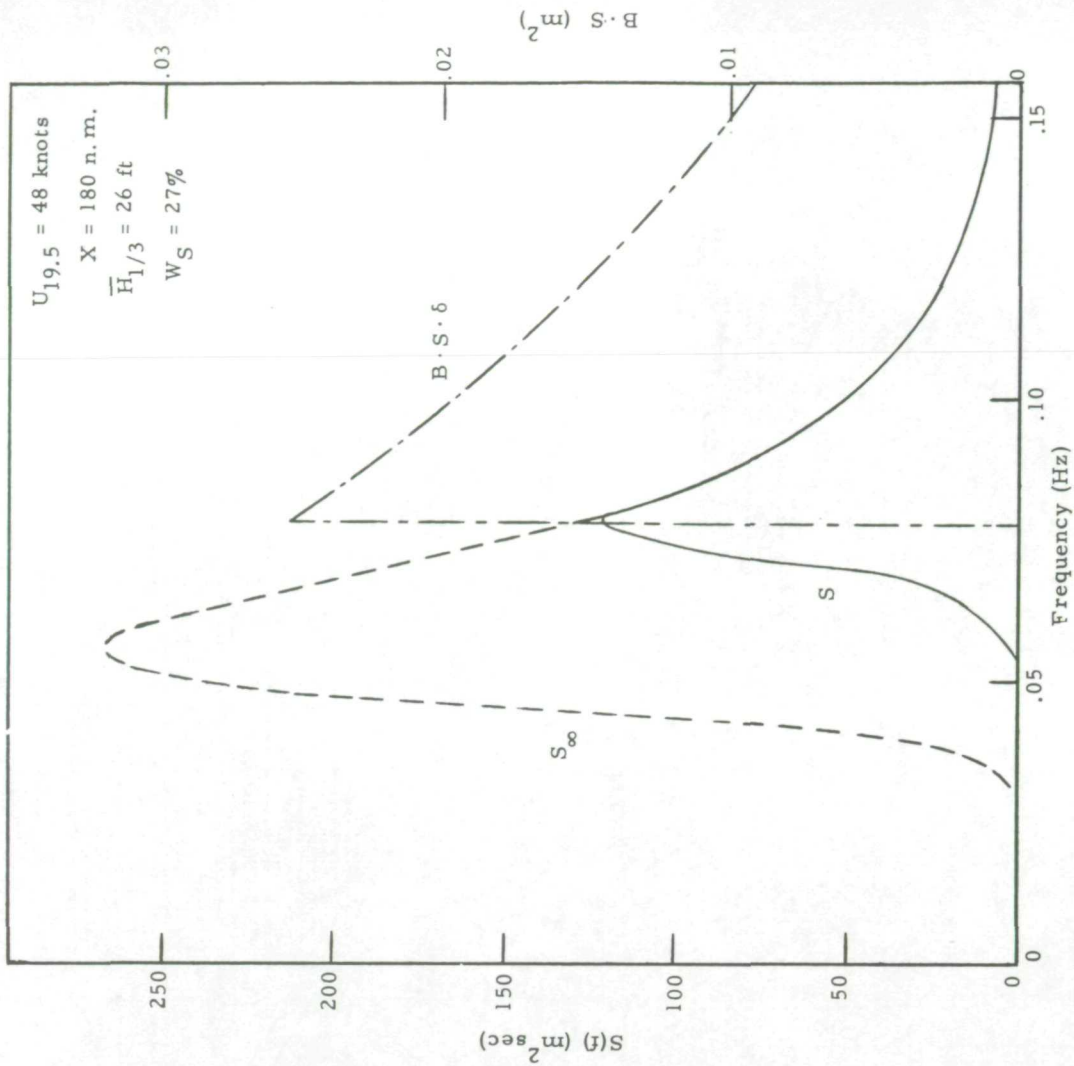


Figure 9. The computation of the whitecap production index.

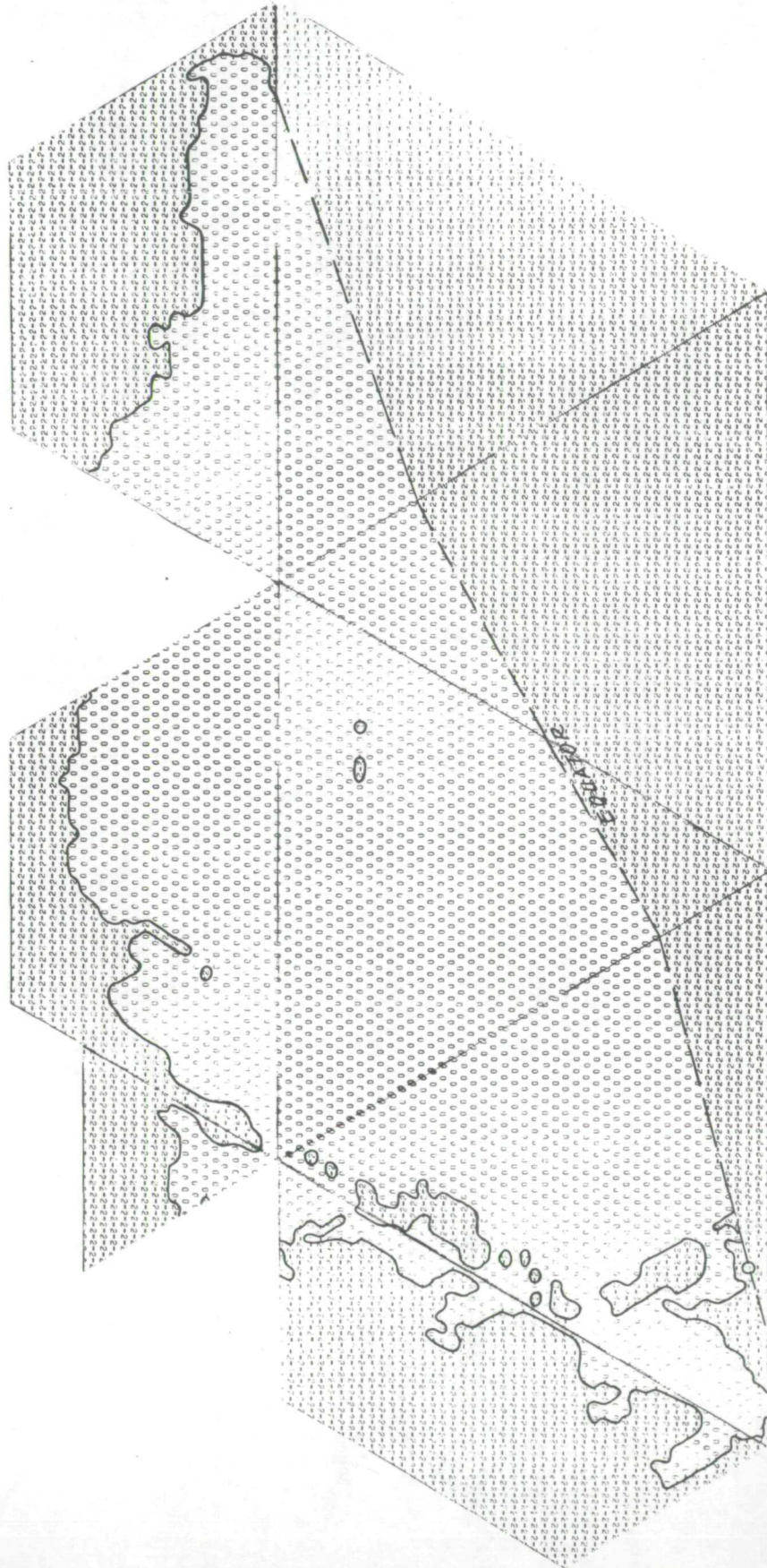


FIG. 10. LAND SEA TABLE FOR WAVE HINDCASTS AT EACH ZERO, 360 NUMBERS TO DESCRIBE THE WAVE SPECTRUM WILL BE COMPUTED

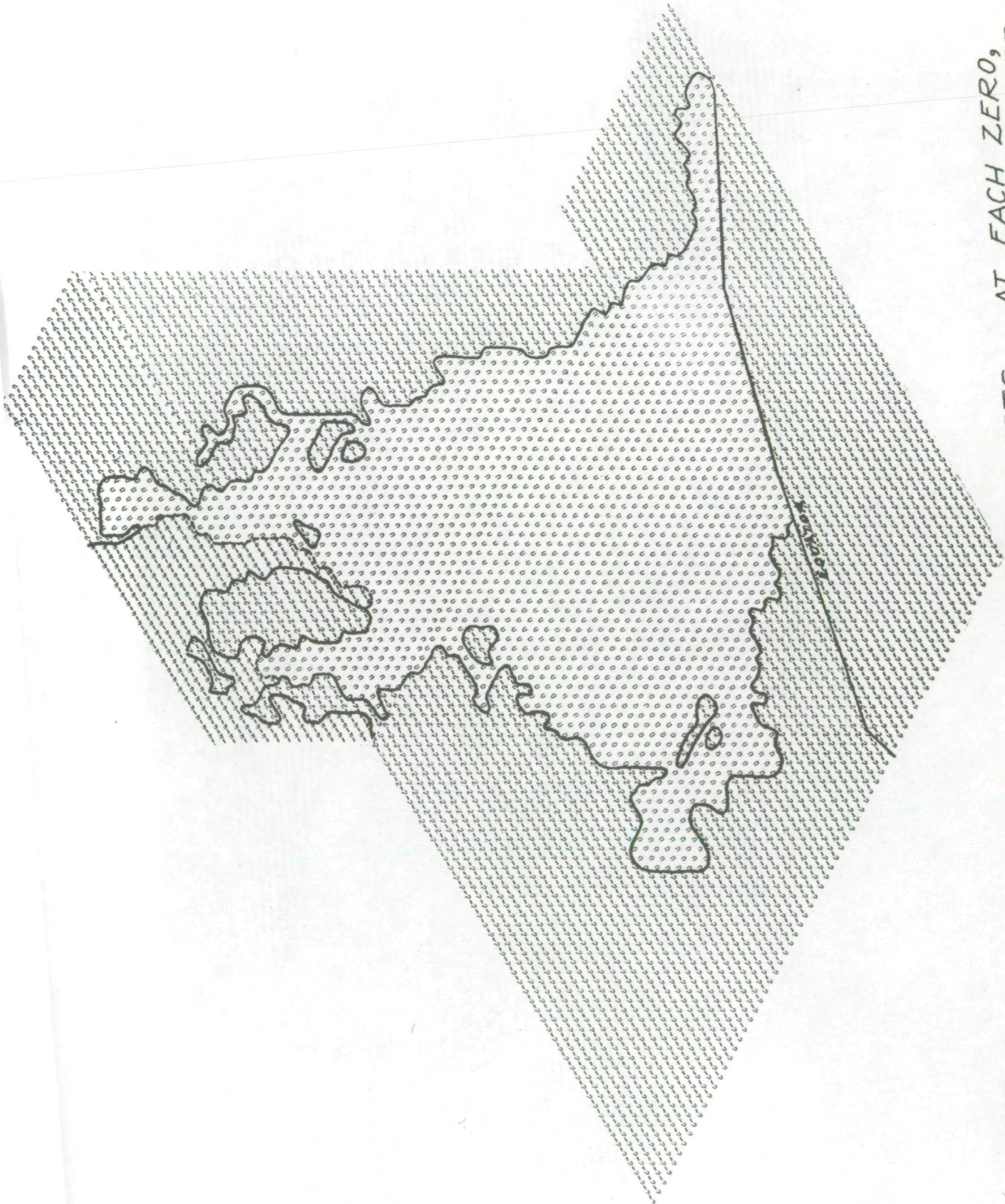


FIGURE 11.
LAND SEA TABLE FOR WAVE HINDCASTS. AT EACH ZERO,
LAND SEA TABLE TO DESCRIBE THE WAVE SPECTRUM WILL BE
360 NUMBERS TO DESCRIBE THE WAVE SPECTRUM WILL BE
COMPUTED (NORTH ATLANTIC)

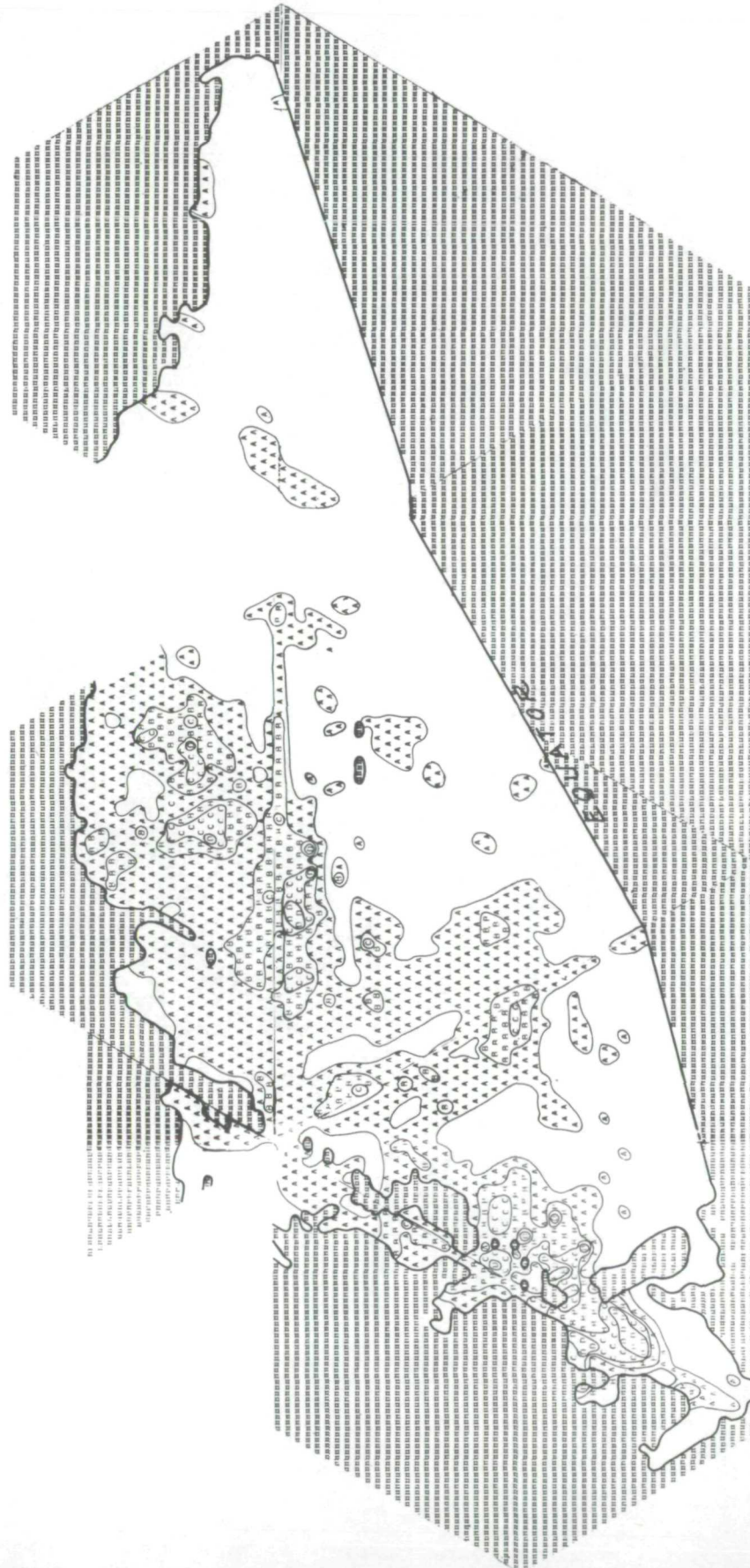


FIG. 12. INITIALIZATION SIGNIFICANT WAVE HEIGHTS FOR NORTH PACIFIC OCEAN. BLANK EQUALS 0 TO 2 FEET, A EQUALS 2 TO 4 FEET AND 50 ON.

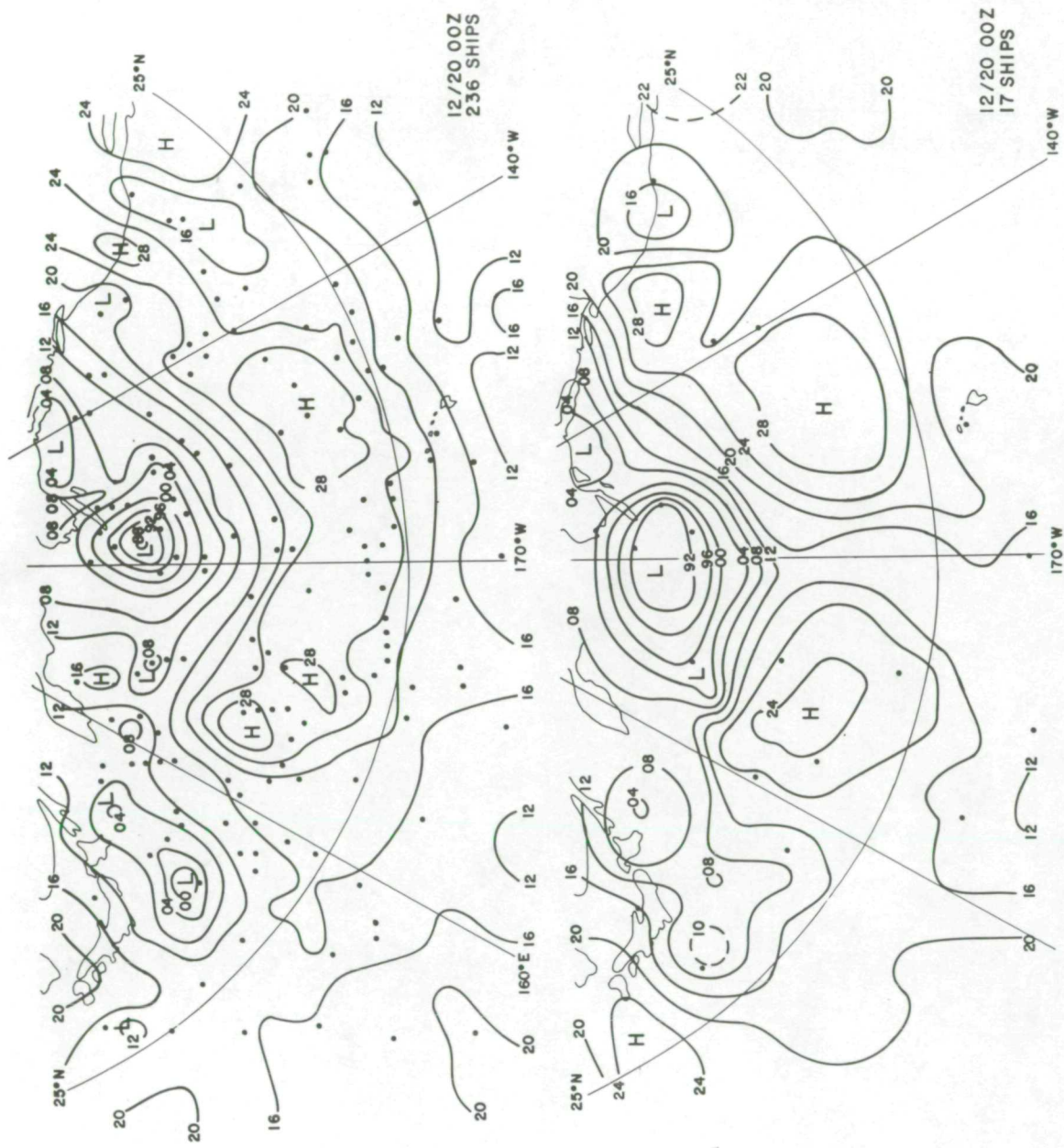


Fig. 13. Top: Pressure field analysis based on all available ships. Bottom: Pressure field analysis based on 17 ships and simulated wind speed information.

Page Informationally Not Blank